DISSERTATION

WINTERTIME AEROSOL IN LAS VEGAS, NEVADA

Submitted by

Steven G. Brown

Department of Atmospheric Science

In partial fulfillment of the requirements

For the Degree of Doctor of Philosophy

Colorado State University

Fort Collins, Colorado

Spring 2014

Doctoral Committee:

Advisor: Jeffrey Collett

Sonia Kreidenweis

Paul Roberts

Colette Heald

Anthony Marchese

ABSTRACT

WINTERTIME AEROSOL IN LAS VEGAS, NEVADA

Numerous studies have found adverse health effects in subjects who live next to major roadways due to air pollution; in particular, there can be severe impacts on lung function and development in children living and/or attending school next to major roadways due to their exposure to air pollutants, including particulate matter (PM) or aerosol. The composition of aerosol at an elementary school next to a major freeway in Las Vegas, Nevada during winter 2008 was measured using a suite of measurements. An Aerodyne High Resolution Aerosol Mass Spectrometer (HR-AMS) was used to quantify the composition of non-refractory PM_1 aerosol, including organic matter (OM); an Aethalometer was used to quantify black carbon (BC); a Sunset OCEC analyzer was used to measure organic and elemental carbon (OC, EC); and a particle-into-liquid system (PILS) coupled to two ion chromatographs (IC) was used to measure fine particle ions. Hi-volume $PM_{2.5}$ samplers were used to collect aerosol on quartz fiber filters at between 2 and 24 hour intervals during the study, a subset of which were analyzed for PAHs and the biomass burning tracer levoglucosan. Data were analyzed by positive matrix factorization (PMF) to determine the amount of fresh, hydrocarbon-like organic aerosol (HOA), more oxidized OA (low-volatility and semi-volatile OA [LV-OOA, SV-OOA]) and biomass burning OA (BBOA).

PM_1 aerosol was predominantly carbonaceous, with OM plus BC accounting for 74% of the overall average 6.9 $\mu g/m^3$ of PM measured. BC had a diurnal pattern similar to traffic volume, while OM was higher in the evening compared to the morning. OM was a mixture of fresh HOA, urban- and regional-scale OOA, and BBOA; in the evening, SV-OOA and BBOA peaked, while HOA concentrations were on average the same in the morning and evening,

similar to BC. OM/OC ratios were low (1.52 ±0.14 on average) during the morning rush hour (average OM = 2.4 $\mu g/m^3$) when vehicular emissions dominate this near-road measurement site, and even lower (1.46 ± 0.10) in the evening (average OM=6.3 $\mu g/m^3$), when a combination of vehicular and fresh residential biomass burning emissions was typically present during a period characterized by strong atmospheric stability. While nitrate and sulfate had size distributions typical of secondary species with a sharp peak in particle diameter between 400 nm and 500 nm, OM had a broader distribution between 100 nm and 400 nm diameter particles, reflecting its combination of fresh, smaller particles and aged, larger particles. OM concentrations were on average similar between periods when the sampling site was upwind and downwind of the freeway, though during the morning OM concentrations were higher under downwind conditions, as was the fraction of HOA.

ACKNOWLEDGEMENTS

This work could not have been done without substantial support from many people. Both Paul Roberts (STI) and my CSU advisor, Jeff Collett, were very encouraging at the onset, when we were initially discussing project ideas and how I could leverage existing STI projects into a PhD project. Hilary Hafner and the Executive Committee at STI helped by allowing me to have a 4/5 time schedule at STI while toiling on my dissertation, and were encouraging over the many years. In addition to the moral and technical support, I deeply appreciate the tuition support from STI, without which this would not have been possible. My good friends Courtney and Tommy Taylor always graciously invited me into their home for many of my visits to CSU. Taehyoung Lee was the mastermind behind the operations during the field study, and was a great sounding board for assorted “don’t these data look odd?” questions. Of course absolutely none of this would have been possible without the loving support of my wonderful wife Anna, who through many years of PhD work always encouraged me to go spend quality time with my data and dissertation.

TABLE OF CONTENTS

LIST OF TABLES

LIST OF FIGURES

Executive Summary

Background

The composition of aerosol next to a major freeway in Las Vegas, Nevada during winter 2008 was examined using a suite of measurements and analyses. Prior studies have found adverse health effects in subjects who live next to major roadways, and in particular, have found severe impact on lung function and development in children living and/or attending school next to major roadways. Concentrations of some pollutants such as ultrafine particles and black carbon (BC) can be up to three times higher next to a roadway compared to urban levels, though particulate matter (PM) concentrations are typically only slightly higher next to a roadway compared to an urban area. However the composition of PM next to a roadway may vary from PM composition elsewhere in the urban area, as next to a roadway fresh vehicular emissions mix with urban PM. In particular, organic aerosol (OA) is of interest as it contains known carcinogens, such as polycyclic aromatic hydrocarbons (PAHs), and oxidative species that can adversely impact lung and cell function. Characterization of OA is important and challenging, as it varies dynamically compared to other aerosol, depending on temperature, meteorology, PM concentrations and PM composition. **Section 1, Introduction**, provides additional details of and discussion on prior published work on near-roadway air pollution and organic aerosol, as well as prior air pollution studies in Las Vegas.

Measurements

In our study, we conducted high time resolution measurements at Fyfe Elementary School, 18 meters from the US 95 freeway soundwall. An Aerodyne High Resolution Aerosol Mass Spectrometer (HR-AMS) was used to quantify the composition of non-refractory aerosol

with a vacuum aerodynamic diameter (v_{da}) of 1 µm (PM_1). These 4-minute measurements included ammonium, nitrate, sulfate and organic matter (OM) concentrations. In addition, individual mass spectrometer fragments were quantified by mass to charge (*m/z*) ratio, including markers of primary, hydrocarbon-like and oxidized organic aerosol (HOA and OOA, respectively) as well as of biomass burning OA (BBOA). Elemental ratios of the OA, e.g., H/C, O/C and OM/OC, and particle size distributions of ammonium, nitrate, sulfate and OM were also determined.

In addition to the HR-AMS measurements, 5-minute averaged BC was measured with an Aethalometer. Semi-continuous measurements of $PM_{2.5}$ organic and elemental carbon (OC, EC) by thermal optical analysis (TOA) were completed using a Sunset OCEC instrument. Semi-continuous measurements of $PM_{2.5}$ K^+, sulfate, nitrate, ammonium and other major ions were made using a particle-into-liquid system (PILS) coupled to two ion chromatographs (IC). Hi-volume $PM_{2.5}$ samplers were used to collect aerosol on quartz fiber filters at between 2 and 24 hour intervals during the study, a subset of which were later analyzed for PAHs and the BBOA tracer levoglucosan. Wind speed and direction were measured at 2 meters above ground level (AGL) at Fyfe. **Section 2, Measurements**, provides additional details on the measurements and associated data processing.

Hypotheses and Results

The overall goal of this work was to characterize aerosol in the near-road environment, how its composition changes with variations in meteorology and by time of day (with the associated changes in traffic patterns and emissions), and the sources of OA. Specific hypotheses included:

1. *Near-road aerosol is predominantly from emissions from vehicles on the freeway, and is carbonaceous and relatively unoxidized.*

OA plus BC accounted for 74% of the overall average 6.9 $\mu g/m^3$ of PM measured. Fresh, unoxidized hydrocarbon-like OA (HOA) accounted for only a quarter of the OA, indicating that fresh vehicular emissions may not be the dominant source of OA next to the freeway. Instead, the OA is a combination of HOA, regional low-volatility, heavily oxidized OA (LV-OOA), and somewhat aged semi-volatile oxidized OA (SV-OOA), which can be from vehicular and other urban-scale emissions. Surprisingly, considering the proximity to the freeway, biomass burning was also a contributor to OA, on average 12% of the OA, despite being present in the evenings only. Analysis of the aerosol composition is shown in **Section 3, Aerosol Composition and Factor Analysis**.

2. *Near-road OA and BC patterns will follow the typical diurnal pattern of traffic, i.e., with peaks of similar magnitude during the morning and evening rush hours.*

Traffic patterns were typical of an urban area, with morning and evening rush hour peaks. BC and CO both peaked in the morning and evening, coincident with the rush hour. OA concentrations peaked in the morning and evening as well; however, concentrations were twice as high, on average, in the evening compared to the morning. The OM/OC ratio was relatively low in both morning and evening, but was lower in the evening (averages of 1.52 and 1.46). These results suggest that while BC and CO are predominantly influenced by primary vehicular emissions, OA is sensitive to a combination of emissions and atmospheric phenomena. During the evening, in addition to fresh vehicle emissions, residential biomass burning contributes to OM; as OM increases, atmospheric stability increases, and

temperature decreases in the evening, more organic compounds can partition to the aerosol phase, further increasing OM and decreasing the OM/OC ratio. Thus, while traffic patterns may be a good predictor of BC and CO variations, OA can be sensitive to a larger combination of influences. Details of diurnal patterns and changing OA composition are shown in **Section 3 and Section 4 Elemental Analyses of Organic Aerosol**.

3. *OA next to the freeway will be similar to vehicle exhaust, as characterized by the OM/OC ratio.*

The OM/OC ratio averaged 1.54, higher than fresh vehicular exhaust (typically 1.2-1.4) and fresh urban aerosol (1.4), but lower than observed OM/OC ratios in other areas (ranging between 1.5-2.2). Day-to-day variability in the fine particle OM/OC ratio was quite large, between 1.44 and 1.73, while daily concentration averages of OM were between 1.1 and 6.6 $\mu g/m^3$. OM/OC ratios were low (1.52 ±0.14, on average) during the morning rush hour (average OM = 2.4 $\mu g/m^3$), when vehicular emissions dominate this near-road measurement site, and even slightly lower (1.46 ± 0.10) in the evening (average OM = 6.3 $\mu g/m^3$), when a combination of vehicular and fresh residential biomass burning emissions was typically present during times with atmospheric stability. Details of OM/OC ratios are discussed in **Section 4, Elemental Analyses of Organic Aerosol**.

4. *Concentrations will be higher when the monitoring site is downwind of the freeway compared to when it is upwind.*

As reported in other work, BC concentrations were two to three times higher during downwind conditions compared to upwind conditions. In contrast, OA concentrations were

not significantly different between downwind and upwind conditions. During the January study, downwind conditions occurred most frequently during the midday, when concentrations were lowest, wind speeds were highest, and traffic low compared to rush hour traffic. Upwind conditions occurred most frequently during the evening, when concentrations were highest, and when vehicular activity and biomass burning emissions peaked. Separating the data by time of day better elucidates the difference between upwind and downwind conditions. In the morning and midday, the downwind concentrations are slightly higher, with higher amounts of primary, less oxidized fragments like *m/z* 43 and 55. In the evening, concentrations during upwind conditions are actually higher for all fragments, as the upwind direction is the direction of arterial roads plus areas of residential biomass burning. Further directionality analyses are shown in **Sections 3 and 4**.

5. *More OA will be contained in smaller particles during downwind conditions and during times of peak traffic compared to upwind conditions and midday/overnight, reflecting the contribution of primary, small particles.*

Fresh vehicular particulate emissions are predominantly small, e.g., a diameter of less than 100 nm, as shown in other studies where concentrations of ultrafine particles, those less than 40 nm in diameter, are much higher downwind of a freeway. While ultrafine particles were not measured in this study, HR-AMS measurements can quantify particles down to 40 nm in diameter. There were only modest differences in OA size distribution by time of day or by upwind/downwind/stagnant conditions, though the larger particles (i.e., aerodynamic diameters greater than 200 nm) were enhanced in heavily oxidized fragments like *m/z* 44. The size distribution of OA was very broad, with most of the OA in particles of 100 – 400

nm diameter, and was quite different compared to the size distribution of inorganic species such as nitrate, which had a sharp peak in the 400 – 500 nm diameter range. This suggests that while there were only modest differences in the OA size distribution between upwind/downwind conditions and time of day, there is a large contribution from primary and less oxidized particles, compared to the secondarily formed inorganic species. Variations in the size distribution of OA and inorganic species are further discussed in **Section 5, Particle Size Analyses**.

6. *At the monitoring site next to the freeway, OA will be comprised of a combination of vehicular emissions, urban-scale OA and regional, oxidized OA.*

During the morning and midday, OA was a combination of local fresh HOA, somewhat oxidized SV-OOA, and more regional, LV-OOA. In the evening, another source was evident, BBOA. A combination of HR-AMS, levoglucosan, Aethalometer BC and PILS potassium ion measurements all confirmed the presence of substantial BBOA. On average, 12% of the OM was apportioned to biomass burning. During the nighttime (5 pm to 5 am), between 25% and 33% of the OM was attributed to biomass burning, depending on the method and data used. The evening occurrence of BBOA and the lack of regional wildfires in this winter period clearly point to local residential wood combustion as the BBOA source. The influence of BBOA is discussed in **Sections 3 through 5**, and the apportionment of BBOA by different measurements and techniques is further explored in **Section 6 Residential Biomass Burning**.

Conclusions

With multiple high-time resolution measurements we have investigated the variability and sources of fine particles next to a major freeway during winter in Las Vegas, Nevada. PM_1 aerosol was predominantly carbonaceous, composed of organic matter and BC. BC had a diurnal pattern similar to traffic volume, while OM was higher in the evening compared to the morning. OM was a mixture of fresh HOA, urban- and regional-scale OOA, and BBOA; in the evening, SV-OOA and BBOA peaked, while HOA concentrations were on average the same in the morning and evening, similar to BC. Variations in O/C, H/C and OM/OC indicated the variable nature of OM day-to-day and hour-to-hour. While nitrate and sulfate had size distributions typical of secondary species with a sharp peak in particle diameter between 400 nm and 500 nm, OM had a broader distribution between 100 nm and 400 nm diameter particles, reflecting its combination of fresh, smaller particles and aged, larger particles. OM concentrations were on average similar between upwind and downwind conditions, though during the morning OM concentrations were higher under downwind conditions, as was the fraction of HOA. These analyses demonstrate the complicated and variable nature of OM, and the influences of meteorology and atmospheric processes on OM that are not as important for other aerosol, such as BC.

1. Introduction

1.1 Near-Roadway Aerosol

A number of epidemiological studies have demonstrated severe health impacts that arise from exposure to particulate matter less than 2.5 microns in aerodynamic diameter ($PM_{2.5}$). $PM_{2.5}$ is comprised of crustal material, trace metals, inorganic species such as sulfate, nitrate and ammonium, plus carbonaceous material. The carbonaceous fraction is composed of black or elemental carbon (BC, EC), which is emitted as a primary emission from combustion and is rather unreactive in the atmosphere, and organic matter (OM). Health effects include increased asthma rates, detrimental fetal development during pregnancy, and decreased lung capacity (Brunekreef et al., 1997; McDonald et al., 2004; Dockery et al., 1993; Dockery and Stone, 2007). Mobile sources, i.e., gasoline and diesel vehicles, are a major source of $PM_{2.5}$, particularly in the western U.S. (Kim et al., 2003; Fine et al., 2004b), and adverse health effects have been strongly associated with proximity to major roadways (Edwards et al., 1994; Nitta et al., 1993; Kim et al., 2004; Finkelstein et al., 2004; Kunzli et al., 2000; Hoek et al., 2002). In additional studies, diesel particulate matter (DPM) was found to be toxic to lung tissue (Mauderly, 1994; Weingartner et al., 1997; Seagrave et al., 2006; Hiura et al., 2000), and both diesel and gasoline vehicle emissions contain polycyclic aromatic hydrocarbons (PAH), which are carcinogenic (Larsen and Baker, 2003; Lobscheid and McKone, 2004; Adonis et al., 2003; Flowers et al., 2002).

Schools heavy in minority or low-income population are disproportionately located near busy freeways (Wu and Batterman, 2006; Reynolds et al., 2004; Green et al., 2004; Schweitzer and Valenzuela, 2004), potentially resulting in higher rates of exposure to near-roadway air

pollution. The causal biological mechanisms of how near-roadway pollution impacts human health are still being examined, but as part of the effort to understand these health effects the near-roadway environment needs to be characterized. This characterization includes understanding the size distribution and composition of near-roadway aerosol, how pollutant concentrations change throughout the day, and the sources of the pollutants.

In previous studies of near-roadway air pollution, significant differences in concentration and relative abundance among species within the first few hundred meters of freeways were observed. In many studies a strong decrease in concentration was observed with increasing distance from the freeway, showing elevated concentrations in the first 50 to 100 meters of black carbon (BC), particle number, and concentrations of gaseous species such as CO and NO_x (Zhu et al., 2002a; Zhu et al., 2002b). Zhu et al. showed that ambient BC concentrations near Interstate 405 in Los Angeles can be approximately three times higher at 30 meters from the roadway compared to 300 meters downwind, where concentrations are similar to urban background levels. BC, along with elemental carbon (EC), is typically used as a surrogate for DPM, which cannot be measured directly. Ultrafine particles, which toxicological studies have associated with health effects (Li et al., 2003), also show a similar pattern to that of BC in near-roadway environments. The extent of elevated ultrafine and EC concentrations near the freeway also depends on fleet mix (Phuleria et al., 2007), where EC concentrations varied near different freeways, commensurate with the level of diesel traffic. Near-roadway concentrations of BC, NO and PAHs generally follow typical traffic patterns, with peaks in the morning and evening rush hour (Fruin et al., 2008), but can vary depending on vehicle speeds, fraction of truck volume, and meteorology.

Concentrations of species also vary by meteorological condition. In Los Angeles, BC, CO and particle number changed with time of day due to changes in source strength and meteorology (Ntziachristos et al., 2007). There can be a large variability in ambient near-roadway pollutant concentrations as wind speed, direction, temperature and relative humidity change (Sardar et al., 2004). In Raleigh, North Carolina, the near-road environment was quite complex and elevated concentrations were found to occur within the first 50 meters from the roadway even when winds did not come directly from the roadway (Baldauf et al., 2008). Many of these near-roadway studies were under persistent winds (i.e., wind speeds often greater than 2 meters/second) or only had measurements during a few days of a week or few hours during the day. We hope to build on these studies and address some of the issues raised by them by examining the near-roadway environment at a school approximately 20 meters from the roadway, throughout the diurnal cycle and under different meteorological conditions during the winter.

1.2 Organic Aerosol

Organic aerosol (OA) can often be the largest component of PM in urban areas, and is typically measured as organic matter (OM) or organic carbon (OC). OM is a complicated mixture of thousands of different molecules, and includes not only particulate OC, but also the hydrogen, oxygen, nitrogen and sulfur that are a part of the thousands of molecules making up OM. OM is a combination of both primary particulate emissions and secondary aerosol formed from gaseous precursors. Combustion is an important source of emissions of OM and its gaseous precursors, while there can also be significant emissions of gaseous precursors from biogenic sources (Kleindienst et al., 2007). Emissions from combustion include fossil fuel combustion such as vehicle exhaust as well as biomass burning (BB), which includes both anthropogenic BB

from wood stoves and fireplaces plus emissions from wildland fires. Combustion emissions include direct emissions of OM and of gaseous precursors that oxidize in the atmosphere to form secondary organic aerosol (Donahue et al., 2012; Kroll et al., 2011).

Jimenez et al. provide an overview of studies throughout the world characterizing fine PM via Aerosol Mass Spectrometers (AMS) (Jimenez et al., 2009), while Hand et al. show composition for fine PM across the U.S. based on measurements from the Interagency Monitoring of Protected Visual Environments (IMPROVE) network and Chemical Speciation Network (CSN) (Hand et al., 2011). Both show that OA often accounts for at least half of the fine PM at multiple locations the western U.S., particularly in urban areas, with an increasing fraction of secondary organic aerosol in rural areas compared to urban areas. In a review of numerous studies, Zhang et al. summarized that in urban areas typically 40% of the OM is primary, while in rural and remote areas only 10%-20% is typically primary(Zhang et al., 2011).

OM is typically high in near-road environments (Phuleria et al., 2007; Riddle et al., 2008; Minguillon et al., 2008; Canagaratna et al., 2010), and is a major component of vehicular exhaust emissions and also includes PAHs, which are carcinogenic (Larsen and Baker, 2003; Lobscheid and McKone, 2004; Adonis et al., 2003; Flowers et al., 2002). As described below, studies using filters have generally focused on characterizing OC (the amount of carbon contained in OM), with typically a time resolution of 2 to 24 hours, while other studies have relied on high resolution aerosol mass spectrometer (HR-AMS) measurements to directly measure OM at high time resolution. Both approaches offer different tradeoffs, and can be used to better understand the near-roadway environment.

Robinson et al and others provide an overview of how vehicular emissions act in the atmosphere (Robinson et al., 2010). Vehicular emissions include a combination of hot gaseous

organic compounds plus particles, such as BC and low volatility organics, though the majority of the emissions are gaseous and semi-volatile (Volkamer et al., 2006; Schauer et al., 1999a; Gundel et al., 1999; Fraser et al., 2000). After exiting the tailpipe into the atmosphere, the vapors rapidly cool and are exposed to sunlight and oxidants, meaning they can quickly oxidize and become less volatile. Depending on the volatility of the resulting secondary aerosol, as well at ambient temperature and aerosol concentration, these secondary products can partition into the particulate phase. Chamber experiments in recent years have shown that the secondary aerosol produced by (predominantly gas phase) combustion emissions can be similar to the amount of primary aerosol generated in combustion (Chirico et al., 2010; Tkacik et al., 2012; Hennigan et al., 2011). This means that OM next to a roadway is an evolving parameter, dependent on not only emissions along the roadway but how these emissions age and interact with the atmosphere as well as with particles and gases from other sources in the area.

1.2.1 Near-roadway Organic Carbon Studies

A number of studies have characterized the composition and sources of organic aerosol, but few have been conducted at schools and only a handful near a roadway. Most studies focusing on organic aerosol have used the chemical mass balance (CMB) receptor model approach to apportion sources of OC using molecular markers (Fraser et al., 2000; Schauer and Cass, 2000; Schauer et al., 2002a; Schauer et al., 1996; Sheesley et al., 2007; Zheng et al., 2007; Zheng et al., 2002). These studies were performed in both urban and rural environments and have shown that mobile sources and wood burning are important sources of OC, but that secondary OC can also be important and is often difficult to characterize. This approach typically only apportions OC, not including the H, O and N associated with the OC, which together make up OM.

In near-roadway environments, molecular marker measurements and CMB analysis have been used to demonstrate that while mobile sources contribute a large fraction of the OC, this can vary with time of day and meteorological condition. In Los Angeles, OC concentrations did not correlate with traffic volume or EC concentrations (Ntziachristos et al., 2007), indicating the complex nature of OC near major freeways. PAH and EC concentrations differed at locations near different freeways, dependent on the relative amount of diesel traffic on the nearby freeway (Phuleria et al., 2007). This work was consistent with previous analyses that showed gasoline vehicles emit higher molecular weight PAHs and diesel vehicles emit lighter PAHs (Miguel et al., 1998; Zielinska et al., 2004a; Zielinska et al., 2004b); these differences in emissions are important both for relating exposure of PAHs to traffic on freeways as well as for conducting receptor modeling. Riddle et al. calculated contributions of gasoline and diesel vehicles to various size fractions smaller than $PM_{2.5}$, showing these sources were most important but that the origin of a significant amount of OC was still unknown (Riddle et al., 2008).

Emissions from mobile sources can vary with season and meteorology, and since mobile sources are an important contributor to OC, these variations can complicate attribution of OC sources. Fine particle EC/OC ratios fell between 0.26 and 1.0 in Pittsburgh in summer and winter (Grieshop et al., 2006), potentially indicating variations in emissions or atmospheric processing of carbonaceous aerosol. Changes in emissions depending on fleet mix and speed have also been shown (Kirchstetter et al., 1999; Zielinska et al., 2004b; Abu-Allaban et al., 2003). Overall, OC in the near-road environment is complex, and understanding its sources under different atmospheric conditions and in different areas is important.

Many of these monitoring campaigns collected and analyzed daily 24-hour samples, analyzed daily filters that were composited into multi-day aggregates, or had samples collected

under persistent winds. Daily samples are extremely useful, since over a 24-hour period sufficient mass is collected to typically ensure low detection limits, and this period complements existing national networks and air quality standards, which are reliant on 24-hour data. However, concentrations of near-roadway carbonaceous aerosol can vary widely throughout the day, dependent on meteorology as well as source strengths (Roberts et al., 2008). In addition, the traditional methods only characterize primary OC, not OM, and have difficulty in apportioning the amount of secondary organic aerosol (SOA) at a monitoring site. Many more recent studies have demonstrated that SOA spans a range of volatility and composition (in terms of oxygen-to-carbon [O/C] ratio), can be quite variable, and is a large fraction of OM (Donahue et al., 2012; Jimenez et al., 2009; Kroll et al., 2011; Robinson et al., 2007). Therefore, it is useful to characterize organic aerosol with higher time resolution than 24-hour filter samples allow, and to understand the nature of OM, not just OC. Characterization of OM rather than OC provides greater information about the total mass contribution of organic matter in fine particles and mass is the most relevant health parameter, at least as assessed in current regulatory schemes.

1.2.2 Aerosol Mass Spectrometer Measurements of Organic Matter

In the past decade, the Aerosol Mass Spectrometer (AMS), and more recently the high resolution AMS (HR-AMS), have been deployed in numerous studies to characterize OM and other particulate species at high time resolution, e.g., at 2-minute resolution (Jimenez et al., 2009; Drewnick et al., 2005; Lanz et al., 2010; Ng et al., 2010; Docherty et al., 2008; DeCarlo et al., 2006; Allan et al., 2003b; Allan et al., 2003a; Sun et al., 2009; Canagaratna et al., 2007; Jimenez et al., 2003; Jayne et al., 2000). The HR-AMS provides measurements of OM, sulfate, nitrate and ammonium, as well as particle size measurements of these species. In contrast to

filter samples analyzed for molecular markers by GC-MS or other approaches, with the HR-AMS, individual molecular marker compounds such as levoglucosan or hopanes are not quantified, but with this loss of molecular specificity we gain high time resolution and a more complete representation of the full organic aerosol fraction. GC/MS, by contrast, typically speciates less than 20% of ambient OC (Williams et al., 2010; Schauer et al., 2002b; Hays et al., 2004). Rather than individual molecules, specific groups of mass-to-charge ratio fragments (*m/z*) can be measured to characterize fine particle OM. Beyond the unit mass resolution (UMR) data where each *m/z* is quantified, individual fragments that comprise each UMR *m/z* can be determined. For example, *m/z* 43 is predominantly composed of the ion $C_3H_7^+$, but also has some contribution from $C_2H_3O^+$ and other minor ions. Where a single ion typically makes up a large fraction of a UMR *m/z*, both the *m/z* and the ion will be referenced, e.g., *m/z* 43 ($C_3H_7^+$), *m/z* 44 (COO^+), *m/z* 57 ($C_4H_9^+$). In addition to identifying individual ions in each *m/z*, the elemental composition of the OM can be determined, allowing for direct measure of H/C, O/C and OM/OC ratios.

Jimenez et al, Zhang et al, and Ng et al, among others, provide summaries of ambient studies using AMS data and how OA evolves in the atmosphere (Jimenez et al., 2009; Zhang et al., 2011; Ng et al., 2010). AMS data are often evaluated with positive matrix factorization (PMF) or other mathematical methods (Zhang et al., 2004a; Zhang et al., 2005a; Zhang et al., 2005b) to decompose the mass spectra and identify differences between fresh, hydrocarbon-like organic aerosol (HOA), and more aged, oxygenated organic aerosol (OOA), as well as biomass burning OA (BBOA). A pattern of saturated hydrocarbon fragments such as *m/z* 43 ($C_3H_7^+$) and *m/z* 57 (i.e., $C_4H_9^+$) were found to be typical of HOA. Two types of OOA spectra are often observed (Docherty et al., 2008; Huffman et al., 2009; Jimenez et al., 2009), one typical of low

volatility OOA comprised of *m/z* 44 (i.e., CO_2^+), LV-OOA, and one that represents less processed and less oxidized OOA. This spectrum has also been observed in chamber experiments with diesel exhaust and termed semi-volatile OOA (SV-OOA). Figure 1-1 shows example HOA, LV-OOA and SV-OOA spectra, compiled over multiple studies as reported in Ng et al, 2011. The HOA spectra is typical of long-chain hydrocarbons, such as those emitted in vehicle exhaust or in lubricating oils, and is similar throughout many ambient studies. The LV-OOA spectra has a high fraction of the total signal from *m/z* 44, while SV-OOA is less aged and is somewhere between LV-OOA and HOA spectra, with a modest fraction of its spectra from both *m/z* 44 and *m/z* 43.

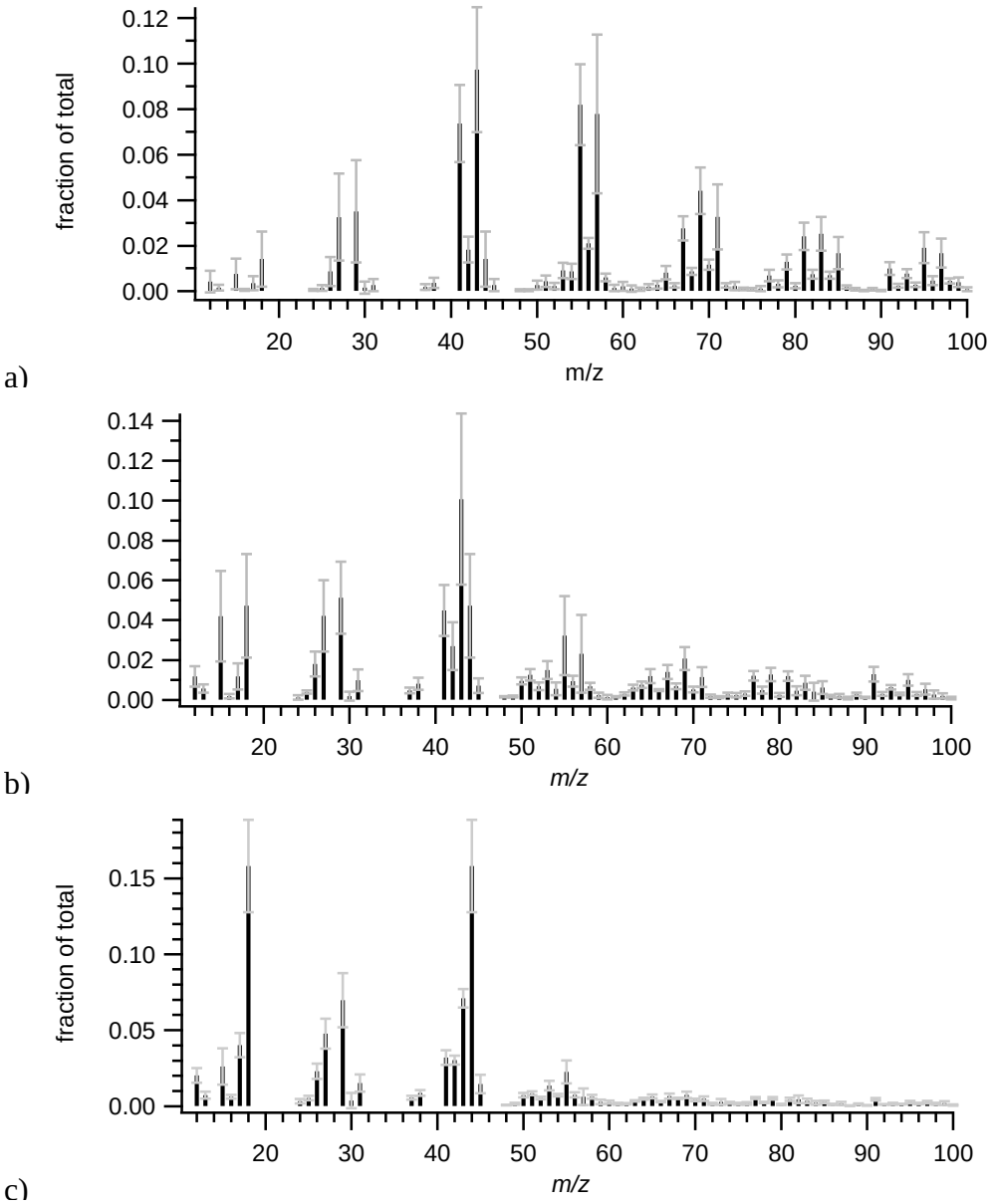

Figure 1-1. Example spectra compiled over multiple studies by Ng et al., (Ng et al., 2011), for a) HOA; b) SV-OOA; c) LV-OOA. Grey error bars represent the standard deviation across the data sets used.

Ambient studies across the world have found that urban sites have higher amounts of HOA(characterized by hyrdrocarbon fragments) relative to downwind, rural and remote sites, consistent with the conceptual model of fresh HOA and associated gaseous emissions in urban areas aging to OOA at sites further away from emission sources (de Gouw et al., 2005; de Gouw et al., 2008; Jimenez et al., 2009). On average for urban sites reported in Zhang et al, 45% of the

AMS PM_1 was OM, of which 42% was determined to be of primary origin, i.e., HOA, BBOA and/or cooking OA(Zhang et al., 2011). In contrast, downwind and rural sites had on average 82%-90% of the OM as OOA, even though the fraction of PM_1 that was OM was similar to urban sites (43%-52%).

Next to a roadway, Canagaratna et al used an AMS aboard a mobile laboratory for a short period of time (less than an hour) at locations next to a roadway in Somerville, MA (Canagaratna et al., 2010). They found that HOA was highest next to the roadway and decreased by a factor of four 300 meters downwind, similar to CO_2, while OOA concentrations were comparable next to the freeway and 300 m downwind, suggesting rapid dilution or reaction of HOA next to the roadway, while OOA is likely more urban-scale. Vehicle chase experiments have also been done with the AMS and other instrumentation in New York (Canagaratna et al., 2004). Measuring individual plumes from trucks and buses, they found a bimodal size distribution of OM, with maxima at 80-110 nm aerodynamic diameter d_{va} and in the 500 nm d_{va} range, consistent with other studies showing a wealth of smaller particles in fresh vehicular emissions (Kittelson et al., 2004); the presence of an OM peak in this smaller size range was also observed to vary with traffic activity near the sampling site (Drewnick et al., 2004a). The chemical composition of the average diesel exhaust plumes sampled in Canagaratna et al. was more similar to lubricating oil than with pure diesel fuel.

1.2.3 Elemental Analysis and OM/OC Ratio Measurements

A significant advantage of the HR-AMS is that it can directly determine (with some assumptions) OM and H/C, O/C and OM/OC ratios, instead of simply OC. National-scale, routine $PM_{2.5}$ networks such as the Interagency Monitoring of Protected Visual Environments (IMPROVE) and CSN programs typically measure OC, but not OM. OM must be inferred from

these OC measurements using an assumed OM/OC ratio. However, the OM/OC ratio can vary widely depending on source influences, monitoring location, season, and meteorology (Turpin and Lim, 2001; Bae et al., 2004a; Aiken et al., 2008; Chan et al., 2010; Simon et al., 2011). Aerosol containing more aliphatic hydrocarbons tends to have a lower OM/OC ratio (Russell, 2003; Turpin and Lim, 2001; Maria et al., 2003), while aerosol dominated by secondary formation is typically more oxygenated and thus has a higher OM/OC ratio (Aiken et al., 2008). Even with high-resolution molecular speciation, typically only 10% of the OM can be quantified (Rogge et al., 1993; Volkamer et al., 2006). An accurate OM/OC ratio is necessary to achieve mass closure between gravimetric PM measurements and collocated measurements of PM constituents; to properly reflect the role of OM in regional and local air quality management plans; and to improve model predictions of OM (Polidori et al., 2004; 2008). The OM/OC ratio has also been used to characterize the relative level of oxidation of the organic material in the atmospheric aerosol as an estimate of the degree of chemical processing in the atmosphere (de Gouw et al., 2005; 2008; Aiken et al., 2009).

The OM/OC ratio in ambient air has been measured directly using high-resolution aerosol mass spectrometer (HR-AMS) measurements, as well as inferred via calculations using OC and other data. Chan et al. (2010) provided a review of key studies of OM/OC. For southern California, White and Roberts (1977) estimated an OM/OC ratio of 1.4, based on calculations of missing particulate mass that could not be explained by other measurements. This ratio of 1.4 has historically been used as a default OM/OC value—for example, in the IMPROVE program (Malm et al., 1994). Turpin and Lim (2001) estimated OM/OC to be between 1.6 for urban aerosol and 2.1 for rural/aged aerosol, based on a survey of published speciated organic molecular marker data from multiple sites in the U.S. Russell (2003) used Fourier Transform

Infrared (FTIR) spectroscopy analysis of particulates on quartz fiber filters (QFF) and determined OM/OC to be on average 1.4, with a range of 1.2 to 1.6. Using 3 years of QFF analysis of organic molecular markers at an urban and rural site in the Midwest, Bae et al. (2006) estimated that OM/OC was between 1.5 and 1.9 at the rural site and between 1.3 and 1.6 at the urban site. Recently, Simon et al. (2011) developed a calculation of OM/OC by applying multi-linear regression techniques and using many years of filter data collected from over 100 sites in the U.S., predominantly in rural areas, as part of the IMPROVE program. They estimated OM/OC ratios to be on average between 1.37 and 1.94, with lower ratios in the western U.S. and during winter. Together, these studies provide a consistent range of estimates for OM/OC, though they are based on indirect measurements of OM and typically use 24-hour averaged samples.

With the development of the high-resolution AMS (HR-AMS) instrument (DeCarlo et al., 2006; Jayne et al., 2000; Jimenez et al., 2003) and associated data analysis techniques (Aiken et al., 2007), direct, high-time-resolution measurements of the elemental composition of non-refractory aerosol are possible. This means that the H/C, O/C, and N/C ratios of OM can be directly quantified, so a total OM concentration and an OM/OC ratio is obtained at high time resolution, e.g., at 2-minute intervals. The OM/OC ratio is calculated from AMS data [69, 83, 84] as $\frac{\left[12+1*\left(\frac{H}{C}\right)+16*\left(\frac{O}{C}\right)+14*\left(\frac{N}{C}\right)\right]}{12}$. The OM/OC ratio is largely driven by the extent of oxygenation in the organic aerosol, i.e., the more oxygens associated with carbon in the aerosol the higher the OM/OC ratio. For example, a PAH like pyrene ($C_{16}H_{10}$) has a very low OM/OC of 1.05, and a long chain alkane such as triacontane ($C_{30}H_{62}$) has an OM/OC ratio of 1.17. More oxidized species have higher OM/OC ratios. A carboxylic acid like azealic acid ($(CH_2)_7(CO_2H)_2$) has a ratio of 1.75, and a compound with multiple hydroxyl groups such as

levoglucosan ($C_6H_{10}O_5$) has an OM/OC of 2.25. Contributions from other elements occasionally included in organic molecules, such as sulfur, are not included. Based on OM/OC and OM values, AMS-inferred OC concentrations can also be determined. Gilardoni et al. (2009) and Aiken et al. (2009) found that OM/OC ratios in the Mexico City area were between 1.6 and 1.8 in the urban area and between 1.8 and 2.1 aloft. In Riverside (eastern Los Angeles area) during the winter, Williams et al. (2010) determined OM/OC to be on average 1.8. At a remote site in British Columbia, Sun et al. (2009) determined OM/OC to be 2.28 (+/- 0.23). Chan et al. (2010) determined that OM/OC ratio values at a rural site in Ontario, Canada, were between 1.9 and 2.5.

OM/OC ratios have also been determined for a number of specific sources, and in particular for vehicular emissions. Using an HR-AMS, Chirico et al. (2010) found that the OM/OC ratio from vehicular emissions can vary between 1.26 at warm idle and 1.40 at cold idle, with other variations depending on the type of engine and operating condition. After 5 hours of photochemical aging in a chamber, warm-idle and cold-idle OM/OC ratios increased to 1.45 and 1.63, respectively. Using a bottom-up approach in the development of a national-scale emission inventory, Reff et al. (2009) estimated OM/OC ratios to be about 1.25 for vehicle exhaust. The OM/OC ratio of general laboratory-generated secondary organic aerosol (SOA) ranges from 1.4 to 2.7 (e.g., Kleindienst et al., 2007).

OM/OC is directly related to the hydrogen-to-carbon (H/C) and oxygen-to-carbon (O/C) ratios of organic aerosol; higher O/C translates to higher OM/OC (Aiken et al., 2008). The ambient OM/OC depends not only on the emission ratio of OM sources and subsequent aging, but also on the volatility of the OM and how it partitions between the gas and particle phases (Kroll et al., 2011; Donahue et al., 2012). Higher OM concentrations lead to increased SOA yields from gaseous precursors (Donahue et al., 2012). Sage et al. (2008) noted that under high

OM conditions, semi-volatile and relatively unoxidized species can quickly contribute to OM concentrations via partitioning from the gas phase. The semi-volatile material can also move into the particle phase via oxidation, leading to lower vapor pressures and subsequent partitioning; decreases in temperature and higher OM concentrations can also lead to increased gas-to-particle conversion of less oxidized species (Cappa and Jimenez, 2010).

Many of the ambient experiments described in the literature occurred at locations where a significant portion of the organic aerosol is transported some distance from emission sources to the monitoring location, resulting in more aged, more oxidized organic aerosol and a higher observed OM/OC. Extensive work has also been done in chemical aging chambers to understand the initial OM/OC ratio of vehicular and other emissions and the process by which they may change over time in a controlled environment, but little work has been done to characterize the OM/OC ratio of vehicular emissions in the ambient near-roadway environment. In the short time from the emission of organic aerosol and semi-volatile vapors from the tailpipe to their impact at a nearby receptor, nucleation, dilution, condensation, evaporation, and oxidation can all affect the gas/aerosol organic mixture and its phase partitioning.

1.2.4 Residential Biomass Burning: A Source of Wintertime OM

Though the focus of this work was on characterizing the near-roadway environment, biomass burning can be a significant source of OM as well. Biomass burning can include both residential, home heating biomass burning during the wintertime, as well as transport from wildfires or prescribed burns. In the winter, wildfire and prescribed burns in the Las Vegas area are minimal, so the main biomass burning influence is from residential burning. Understanding the impact of residential biomass burning on $PM_{2.5}$ concentrations in urban areas is of particular interest, since emissions are potentially controllable through burn-prevention or fireplace

change-out programs (Bergauff et al., 2009; Ward and Noonan, 2008), and because of specific health effects associated with inhalation of biomass burning PM (Freeman et al., 1992; Seagrave et al., 2006; Travis et al., 1985; Naeher et al., 2007). Residential biomass burning can lead to high concentrations during the evening and overnight, when emissions are trapped in a shallow boundary layer (Allen et al., 2011; Wang et al., 2011), and these short, high concentration events can have acute health impacts (Lighty et al., 2000; Barregard et al., 2007). Biomass burning emissions include not just BC and OM, but also carcinogens including benzene and polycyclic aromatic hydrocarbons (PAHs).

Levoglucosan and potassium are commonly used tracers for apportioning biomass burning. Levoglucosan is an anhydrous sugar produced in the combustion of cellulose (Simoneit et al., 1999; Simoneit, 2002; Engling et al., 2006; Schauer et al., 2001; Sullivan et al., 2008). It is typically quantified from extractions of aerosol collected on quartz fiber filters and subsequent chemical analysis by GC-MS or other analytical techniques. While levoglucosan is a good tracer for biomass burning, Sullivan et al and others have found that the relationship of levoglucosan with organic aerosol in biomass burning emissions can vary widely by fuel type and burning conditions(Sullivan et al., 2008). Levoglucosan can also be quantified on a semi-continuous basis using the HR-AMS, where the ion $C_2H_4O_2^+$ at *m/z* 60 is a commonly used indicator for biomass burning and is proportional to the amount of levoglucosan in the sampled aerosol (Alfarra et al., 2007; Weimer et al., 2008; Schneider et al., 2006; Lee et al., 2010), though levoglucosan is not the only source of this ion, as other organic species, such as other anhydrosugars and organic acids, also contribute to its mass.

While levoglucosan is unique to biomass burning, making it a good tracer, its atmospheric lifetime can vary from ~ 1 to 10 days (Cubison et al., 2011), meaning that it may not

be fully conserved between source and receptor. In addition, as emissions age, gas/particle partitioning of semivolatile material may mean that the relationship of levoglucosan to OM emitted changes over time, as organic material is either condensed into the particle phase or partitioned in the vapor phase (Hennigan et al., 2011; Cubison et al., 2011; Oja and Suuberg, 1999). In laboratory experiments, Heringa et al found OM from woodstoves could increase by a factor of 3 to 4 due to SOA formation, and dependent on the type of burning apparatus and flaming/smoldering conditions(Heringa et al., 2011). They also found that the $C_2H_4O_2^+$ fragment at *m/z* 60 increased in concentration due to SOA contributions and possibly increased gas-to-particle partitioning, which can overcompensate for the degradation of primary levoglucosan, thus potentially leading to an overestimation of biomass burning based on source emissions measurements of the $C_2H_4O_2^+$ fragment. In Spain, Minguillon et al found that filter levoglucosan-apportioned biomass burning was less than from AMS-based apportionment, possibly due to the contribution of SOA captured by the AMS measurements (Minguillon et al., 2011). Based on data from seven field studies, the SOA formation averages 25% of the primary OA (Cubison et al., 2011), so based on emissions source profiles alone, OA from biomass burning could be underestimated. Mohr et al., Takegawa et al. and others have found that the additional signal at *m/*z 60 is likely from long chain alkanoic acids or other acid compounds(Mohr et al., 2009; Takegawa et al., 2007). Cubison et al 2011 further demonstrated that without biomass burning influence, in ambient aerosol there is a background level of *m/z* 60 of ~ 0.3% of OM, likely due to acids and other compounds (Cubison et al., 2011). Lee et al 2010 suggest that increases/decreases in levoglucosan yield in biomass burning smoke may be offset to some extent by corresponding decreases/increases in other molecules that also yield $C_2H_4O_2^+$ ions, resulting in a fairly stable OA/$C_2H_4O_2^+$ ratio across fuel and burn types (Lee et al., 2010).

Thus, a combination of filter-based levoglucosan plus higher time resolution AMS $C_2H_4O_2^+$ measurements should effectively bound the contribution of biomass burning to OA.

Potassium is also produced from the combustion of wood lignin. Elemental potassium (K) and soluble potassium (K^+) are commonly used as tracers when using data from XRF and IC analysis of Teflon and nylon filters, respectively (Kim et al., 2003; Poirot, 1998; Liu et al., 2005; Brown et al., 2007). There are other prevalent sources of potassium, such as dust, sea salt or cooking aerosol, which can confound use of this tracer (Aiken et al., 2010; Zhang et al., 2010; Schauer et al., 1999b). In experiments of different biomass fuels Sullivan et al found poor correlation between K^+ and levoglucosan among the fuel types, while Lee et al. showed that emissions of K^+ were higher under flaming conditions compared to smoldering conditions; AMS $C_2H_4O_2^+$ emissions were comparable between conditions (both K^+ and AMS $C_2H_4O_2^+$ were reported in terms of ratio to total PM) (Lee et al., 2010; Sullivan et al., 2008). These results are consistent with other studies suggesting that K^+ may have only a modest correlation at best with organic tracers of biomass burning. during Zhang et al 2010 found an r^2=0.59 using 24-hour filter data during wintertime in the Southeastern U.S., but a much lower correlation in summer, and that K had a lower spatial variability compared to levoglucosan(Zhang et al., 2010). In Mexico City, Aiken et al. found levoglucosan had a modest correlation with $PM_{2.5}$ K (r^2=0.67), and that non-biomass burning sources accounted for typically two-thirds of K concentrations(Aiken et al., 2010). In source profiles, the ratio between K and levoglucosan can be quite variable, ranging between 0.03-0.16 (Fine et al., 2004a, 2002b, 2002a; Fine et al., 2001; Lee et al., 2010). In part because of this variability and confounding alternative potassium sources, Minguillon et al suggested that, based on K from 24-hr filter measurements compared

to AMS, levoglucosan, and other measurements, K was an unreliable tracer for their sites in Barcelona and rural Spain due to the influence of other sources (Minguillon et al., 2011).

1.3 Study Area: Las Vegas

1.3.1 Prior Studies

Las Vegas is the focus of our study, and in a shallow bowl area, with mountains to the west and north, and is a relatively isolated, large urban area with a 2010 population of over 1.9 million in the greater metropolitan area of Clark County (http://quickfacts.census.gov/qfd/states/32/32003.html). For a city of its large size, there have been relatively few detailed studies to assess sources of PM in the area. A key study, Green et al (Green et al., 2002), focused on about 50 24-hour filter samples collected in 2000-2001. The major components of $PM_{2.5}$ were BC, OM and crustal elements, with carbonaceous material contributing over 50% of the total mass at an urban site (East Charleston). Ammonium sulfate and nitrate concentrations were generally quite low, about 12% of the total $PM_{2.5}$ mass. Though no formal apportionment was done, based on extensive data analysis they surmised that gasoline and diesel vehicle emissions are likely an important source, but that other sources such as residential biomass burning may also be a significant contributor. Another study, the Southern Nevada Air Quality Study (SNAQS) (Watson et al., 2007), used 10-12 filter samples at 4 sites from January 2003 to apportion $PM_{2.5}$. 80% of the mass was from carbonaceous aerosol, and 38%-49% of the $PM_{2.5}$ was attributed to mobile sources. Biomass burning contributed 11%-21% of the mass. Dust, ammonium sulfate and ammonium nitrate comprised the remainder of the mass. These apportionments were based on a standard suite of filter analyses, and included OC and EC by thermal optical reflectance (TOR), sulfate and nitrate by IC, and metals by XRF. No continuous data were used, nor were specific tracers for biomass burning available, other than K,

which has additional, significant non-BB sources. Without more specific tracers or higher time resolution data, the apportionment of OC has a high uncertainty. In addition, the temporal pattern of OC could not be examined, since only 24-hour filters on a handful of days were collected.

1.3.2 Study area specifics

Measurements were made next to a classroom and playground in Las Vegas, Nevada, during January 2008 at Fyfe Elementary School, directly adjacent to and 18 meters from the US 95 highway soundwall (Figure 1-2 and 1-3); it is 60 m from the middle of the first set of lanes, and 90 m to the middle of the farthest set of lanes. The US 95 freeway has six lanes in each direction, with an annual average daily traffic (AADT) volume of 203,000 vehicles a day (http://www.nevadadot.com/reports_pubs/traffic_report). Though US 95 is a north/south freeway, it is oriented east/west next to Fyfe. Assuming half the medium size vehicles (21-40 feet in length) and all the large (greater than 40 feet in length) are diesel trucks, diesel truck traffic is 6% of the traffic on average (Brown et al., 2012). The monitoring site is on the north side of the freeway, so the site is directly downwind of the freeway when winds blow from the south. North of the site is a residential area; the homes in the immediate neighborhood were built starting in the 1960s, and many have wood-burning fireplaces. There is little heavy industry in Las Vegas, with most $PM_{2.5}$ emissions coming from dust, miscellaneous sources, and off-road vehicle emissions (e.g., http://www.epa.gov/air/emissions/pm.htm#pmloc); mobile sources comprise 9% of the emissions, but they account for 36% of the emissions if dust is excluded. A major electricity generation source listed in the most recent (2005) national emission inventory (NEI) has since closed. In the wintertime, nighttime low temperatures are usually between 0 – 5 degrees C, with shallow inversion layers occurring in the evenings.

Figure 1-2. Map of Las Vegas area, with monitoring location at Fyfe Elementary School.

Figure 1-3. Close-up view of Fyfe Elementary, outlined in orange. The monitoring site, indicated by the red circle, is 18 m from the soundwall, 60 m from the middle of the first set of lanes, and 90 m to the middle of the farthest set of lanes.

1.4 Document Overview and Study Objectives

This document presents analyses focused on aerosol measurements taken at the Fyfe Elementary School in January 2008. Objectives for this study were:

a) Complete high quality measurements of aerosol, and in particular, of organic aerosol, during a month-long intensive measurement campaign;

b) Characterize aerosol concentrations and composition next to a roadway, and how concentration levels and composition vary with changes in meteorology and traffic patterns;

c) Assess sources of organic aerosol, and how these vary with time of day and meteorology;

d) Utilize HR-AMS measurements to describe the OM/OC and elemental ratios of organic aerosol and to characterize the size distribution of non-refractory aerosol next to a roadway.

Specific hypotheses tested include:

1. Near-road aerosol is predominantly from emissions from vehicles on the freeway, and is carbonaceous and relatively unoxidized.
2. Near-road OA and BC patterns will follow the typical diurnal pattern of traffic, i.e., with peaks of similar magnitude during the morning and evening rush hours.
3. OA next to the freeway will be similar to vehicle exhaust, as characterized by the OM/OC ratio.
4. Concentrations will be higher when the monitoring site is downwind of the freeway compared to when it is upwind.
5. More OA will be contained in smaller particles during downwind conditions and during times of peak traffic compared to upwind conditions and midday/overnight, reflecting the contribution of primary, small particles.
6. At the monitoring site next to the freeway, OA will be comprised of a combination of vehicular emissions, urban-scale OA and regional, oxidized OA.

Section 1, this section, provides introductory material on near-road air pollution, organic aerosol and its sources, and the Las Vegas area. **Section 2** describes the instruments and methodologies used. **Section 3** presents an overview of the measured aerosol composition, a

comparison between collocated aerosol measurements, and an in-depth view of the organic aerosol measurements using the receptor model positive matrix factorization. **Section 4** discusses elemental analyses of the organic aerosol, focusing on how the OM/OC varies by time of day and meteorology. **Section 5** presents size distribution analyses, to better understand how the aerosol size distribution varies diurnally and with changes in meteorology. **Section 6** covers additional apportionment of the fraction of organic aerosol from residential biomass burning, using multiple techniques.

2. Methods and Data

2.1 Summary of Measurements

The focus of this work is on measurements taken at Fyfe Elementary School in Las Vegas, Nevada during January 2008. A summary of measurements used in these analyses is shown in Table 2-1. An Aerodyne High Resolution Aerosol Mass Spectrometer (HR-AMS) was used to quantify PM_1 aerosol at 2 minute averages: OM, sulfate, nitrate and ammonium concentrations and particle size distribution, as well as elemental ratios (OM/OC, H/C, O/C) of the OM and OM composition by *m/z*. Total particulate black carbon (BC) was determined with 5-minute averages using a Magee Scientific Aethalometer. A Sunset Labs OCEC instrument provided hourly measurements of $PM_{2.5}$ OC and EC. 20-minute averaged $PM_{2.5}$ ion concentrations (sulfate, nitrate, potassium, plus other ions) were found using a particle-into-liquid sampler (PILS). Gaseous measurements of CO, NO_x, NO and NO_2 were also made, at 5-minute resolution. Hi-volume $PM_{2.5}$ samplers were used to collect PM on 8 x 10 inch quartz fiber filters at varying intervals (24-hours, morning rush hour, late morning, midday/afternoon, and overnight). Wind speed and direction data were taken at 1-minute resolution, and vector-averaged to 2-minute, 5-minute and hourly averages. Temperature was measured at 2 m and 10 m.

Table 2-1. Summary of Measurements at Fyfe Elementary.

Instrument	Frequency	Details
HR-AMS	2-minute	OM, SO_4, NO_3, NH_4; OM composition by *m/z*; elemental ratios (O/C, H/C, OM/OC); particle size distribution of OM, SO_4, NO_3, NH_4 and individual *m/z*
Magee Scientific Aethalometer	5-minute	Black carbon at 880 nm and 370 nm (termed "BC" and "UV" respectively)
Thermo Scientific 48i	5-minute	CO
Thermo Scientific 42i	5-minute	NO, NO_2, NO_x
Sunset OCEC	1-hour	OC, EC; detection limit ~ 0.3 µg/m^3
Hi-volume $PM_{2.5}$ sampler	Multiple intervals: 0500-0900; 0900-1100; 1100-1700 1700-0500 LST	Quartz fiber filters extracted for levoglucosan quantification via GC-MS; 17 selected filters analyzed, 12 during 1700-0500 LST
PILS	20-minute, averaged to 1-hour	SO_4^{2-}, NO_3^-, NH_4^+, K^+, Cl^-, Ca^{2+}, Na^+ ions
Wavetronix	1-hour	Traffic speed, volume by three vehicle sizes: small (less than 21 feet in length), medium (21-40 feet) and large (greater than 40 feet); located 0.5 km west of Fyfe Elementary on US 95
RM Young AQ 5305-L	1-minute	Wind speed, direction
Campbell Scientific 41382VC	1-minute	Temperature at 2 m and 10 m

2.2 High Resolution Aerosol Mass Spectrometer Description and Operation

The Aerodyne HR-AMS was operated in the CSU mobile laboratory at Fyfe Elementary during January 5 – 28, 2008. Details can be found in the very thorough introduction of the instrument of DeCarlo et al., 2006. Earlier versions of the instrument had a quadrupole mass spectrometer (Q-AMS), instead of a time-of-flight mass spectrometer (ToF MS), and are described in earlier manuscripts (Jayne et al., 2000; Jimenez et al., 2003), and a review of the instruments can be found in Canagaratna et al . There are three main sections in the HR-AMS (Figure 2-1): aerosol inlet and aerodynamic lens; particle flight and sizing region; and the time-of-flight mass spectrometer (ToF MS). In the first part, ambient air is drawn through a URG

cyclone (D_{50} = 2.5 µm, 3 lpm) followed by a critical orifice (approximately 0.1 lpm flow) and a series of apertures and vacuum chambers, focusing the aerosol into a narrow beam under high vacuum (approximately 10^{-5} Pa). Canagaratna et al, Sun et al. and Takegawa et al. report that there is 100% transmission of particles with aerodynamic diameter (d_{va}) of 70-500 nm, with approximately 50% transmission at 1 µm d_{va}, implying that the AMS measures PM_1(Canagaratna et al., 2007; Sun et al., 2009; Takegawa et al., 2009). Since the particles are under vacuum, the term d_{va} is used. Larger particles may have too much inertia to be consistently focused in the beam (Zhang et al., 2004b), so the transmission begins to decline with 500 nm d_{va} particles, reaching 50% at 1 µm d_{va}.

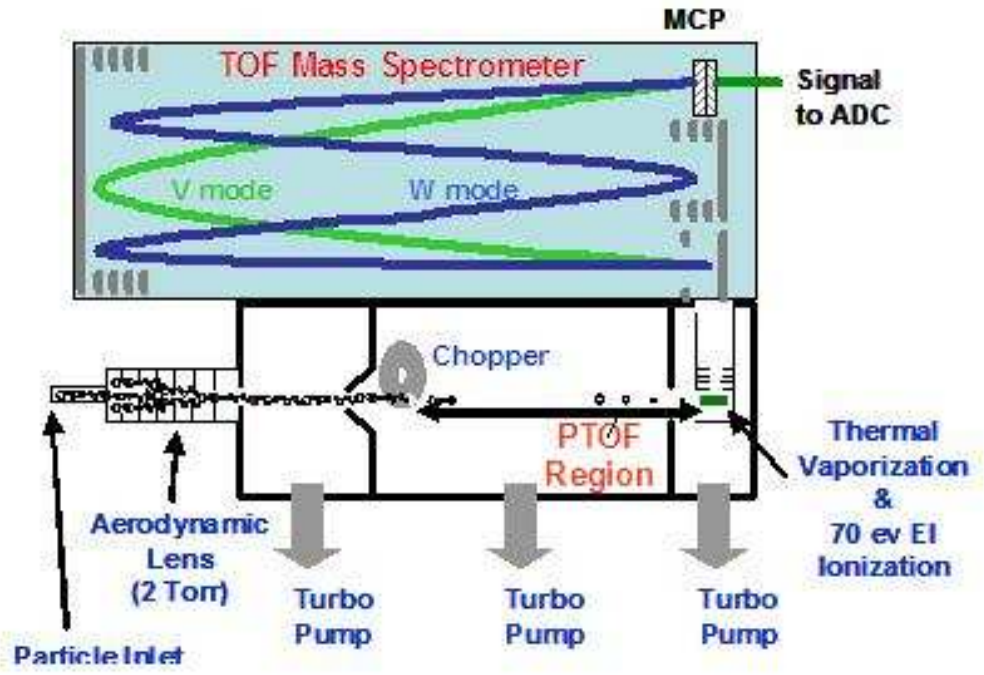

Figure 2-1. Schematic of the HR-AMS, from http://cires.colorado.edu/jimenez-group/wiki/index.php/File:WToF.jpg.

Next particles enter the particle time of flight (PToF) region. Here a mechanical chopper regulates the aerosol introduced into the PToF region, operating at ~ 100 Hz. The chopper operates among three positions: "closed", when the beam is blocked; "open" with full transmission of the beam; and "chop", where the aerosol beam is modulated with a 1% duty

cycle via a slit in the chopper. The open mode allows for mass spectra of the aerosol in the beam to be found. The closed mode is used to track baseline concentrations of residual gases, such as oxygen and nitrogen, when no aerosol are present; thus the difference in the mass spectra between the open and closed mode yields the mass spectra of the aerosol in the beam. During chop mode, the aerosol beam is chopped, so that only packets of individual particles are transmitted through the PToF region. The time it takes to travel through the PToF region is dependent on the d_{va} of a given particle; larger particles take longer than smaller particles. A mass spectra is then found for the continuum of particle sizes that travel through the PToF region, enabling for quantification of individual *m/z* by d_{va} range.

Once particles are transmitted through the PToF region, they are vaporized and ionized for analysis by mass spectrometry. The AMS is designed so that under a range of aerosol compositions concentrations of specific components like organic matter and sulfate can be quantified. Thus a vaporization/ionization scheme is needed that introduces the aerosol in the MS region in a characteristic pattern. Canagaratna et al., DeCarlo et al. and others have reviewed the numerous schemes available (Canagaratna et al., 2007; DeCarlo et al., 2006). Here, particles are flash vaporized on a resistively heated tungsten surface at 600 degrees C coupled with a 70 eV electron impaction (EI) ionizer. While this setup means that molecules are ionized in a reproducible and characteristic manner, it means that only non-refractory species such as sulfate, nitrate and OM are quantified. Crustal species, metals, sea salt and elemental carbon cannot be quantified, since they do not evaporate fast enough at this temperature under high vacuum conditions. Using this standard ionization technique means that spectra are generally comparable to standards developed by National Institute of Standards and Technology (NIST) (Canagaratna et al., 2007; Dzepina et al., 2007), which may use other mass spectrometry

techniques such as GC-MS. Differences between NIST spectra and AMS spectra may arise since species are vaporized at a high temperature in the AMS before ionization, resulting in more fragmentation compared to NIST spectra (Alfarra et al., 2006). Dzepina et al., report that this is particularly true for species with strong structures, such as PAHs (Dzepina et al., 2007).

Particles may bounce, meaning that the collection efficiency (CE) of particles is not necessarily 100%. Prior studies have used a CE of between 0.5 and 1 (Drewnick et al., 2004b; Drewnick et al., 2005; Takegawa et al., 2005; Zhang et al., 2005b; Drewnick et al., 2004a). Matthew et al. and Middlebrook et al. report that the CE approaches 1 for aerosol with low sulfate content and with higher nitrate content, i.e., nitrate higher than sulfate (Matthew et al., 2008; Middlebrook et al., 2012). Matthew et al. report that with higher organic content CE approaches 1, though in areas dominated by secondary organic aerosol, where LV-OOA is the majority of the OA, the CE is lower than 1, as found in Middlebrook et al. when they reviewed 3 field campaigns (Middlebrook et al., 2012). CE is still an area of ongoing research, and the validity of this assumed CE can be assessed by comparing the AMS measurements to collocated PILS measurements for sulfate, nitrate and ammonium, and collocated Sunset OC measurements for OM. The correlations between these collocated measurements are very high, and are detailed in Section 3.

After vaporization and ionization, ions enter into a ToF MS. In a ToF MS, ions are accelerated by a pulse extractor from the source region into a field free drift region where ions are separated by time of flight. After ionization, all ions ideally have the same nominal kinetic energy, so ions of different m/z will obtain different velocities before reaching a detector. Low *m/z* ions achieve higher velocities and therefore reach the detector first, while larger m/z ions achieve lower velocities and impact the detector later. The time it takes for a given ion to reach

the detector is proportional to m/z and the tube length, and inversely proportional to the applied acceleration voltage from the pulse extractor. Since there is no scanning involved, an entire mass spectrum can be obtained very quickly. The ToF MS is operated in two modes, "V" and "W". These modes refer to the geometry of the ion flight paths (see Fig. 2-1) V mode, with its shorter flight path, is best used for quantification, and enables quantification of ions with a resolution better than than 0.01 m/z. W mode has a longer path length than V mode, thus increasing the resolution but decreasing the sensitivity for quantification due to ion loss. V mode is used in this work to quantify the concentration of each individual *m/z* and therefore the total sulfate, nitrate, ammonium and OM, while W mode is used to determine elemental ratios of the OM. V and W mode were set to alternate every 2 minutes, resulting in a V mode spectra and corresponding W mode spectra every 4 minutes.

Jimenez et al., Alfarra et al., Canagaratna et al., DeCarlo et al., and others have laid out the details behind converting ion signals from the ToF MS into mass concentrations (Jimenez et al., 2003; Canagaratna et al., 2007; Alfarra et al., 2004; DeCarlo et al., 2006). For a given *m/z*, the concentration can be found as detailed in equation 1 from Jimenez et al, assuming a CE of 1 (Jimenez et al., 2003):

$$C = \frac{10^{12}}{IE}\frac{1}{Q}\frac{MW}{N_A}I \qquad (1)$$

where IE is the ionization efficiency, 10^{12} is used to convert units to µg m^{-3}, Q is the volumetric flow rate (cm^3 s^{-1}), MW is the molecular weight for the fragment of the given *m/z*, N_A is Avogadro's number, and I is the detected ion rate (counts per second). IE is a dimensionless quantity that represents the number of ions detected per parent molecule, and is dependent on the efficiency of the vaporization and ionization of the parent molecule, as well as the detection

efficiency of the daughter ions in the MS. Laboratory studies have shown that IE is different for organic and inorganic species (Jimenez et al., 2003; Alfarra et al., 2004), but for inorganic or organic species IE varies linearly with MW. Since nitrate particles are used to calibrate the HR-AMS, as described later, the mass generated from equation 1 is in nitrate-equivalent concentration. To convert this to actual concentration, the species-specific relative IE (RIE) is used, as documented in Jimenez et al, where RIEs are 1.4 for OM and 1.15 for sulfate. This then modifies equation 1 to the following for a given species *s*, relative to nitrate:

$$C_S = \frac{10^{12}}{RIE_s IE_{NO3}} \frac{1}{Q} \frac{MW_{NO3}}{N_A} I_s \qquad (2)$$

To calculate total mass concentrations of "bulk" species such as sulfate, nitrate, ammonium and OM, the concentrations over all *m/z* originating from the parent molecules is summed. Equation 2 may be further modified if the collection efficiency (CE) differs from 1. Often a CE of 0.5 is used, in sulfate-rich or sulfate–dominated environments. CE may be less than 1 because of inefficient focusing in the aerosol beam if sampled aerosol particles are not very close to spherical, particle bounce off of the vaporizer, or transmission losses through the inlet. In addition, Allan et al showed that there can be some temperature dependence of the CE when the inlet temperature is close to the ambient dewpoint (Allan et al., 2004). CE can be assessed by comparing HR-AMS measurements to PILS (or other independent) measurements of nitrate. As shown in Section 3, the agreement between the instruments was extremely high (r^2=0.95, PILS/AMS ratio =1.3) with only a small bias, some of which may be due to the different size ranges effectively measured by the two instruments ($PM_{2.5}$ for PILS, PM_1 for the AMS) so a CE of 1 was used.

2.2.1 HR-AMS calibration

Nitrate particles are used for AMS calibration since they are vaporized in the AMS with nearly 100% efficiency, are commonly found in the atmosphere, and are relatively straightforward to generate. Ammonium nitrate particles were generated by a particle generator and size-selected via a differential mobility analyzer (DMA) for 350 nm aerodynamic diameter particles, for three different mass concentration levels: approximately 2 $\mu g/m^3$, 8 $\mu g/m^3$, and 15 $\mu g/m^3$. Particles are also fed to a condensation particle counter (CPC), so that calculated mass between the HR-AMS and CPC can be compared. As shown in Figure 2-2, the HR-AMS and CPC measurements agreed quite well for the calibrations during the field study.

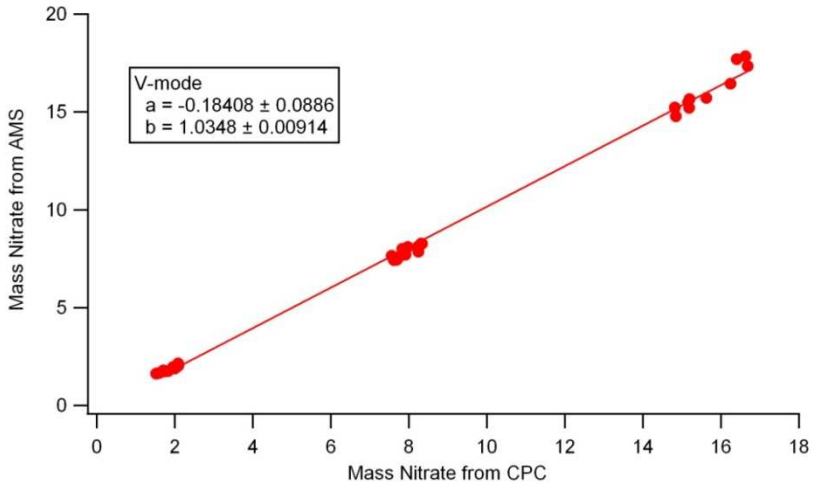

Figure 2-2. Comparison of HR-AMS and CPC nitrate mass measurements as part of calibration during Las Vegas field operations set up. The "*a*" value is the intercept of the red linear regression line, and the "*b*" value indicates the slope of the line. For a good comparison, *a* should be close to zero and *b* close to 1.

2.2.2 Particle Size Calibrations

For calibration of the particle size measurements, polystyrene spheres (PSLs) were used and four different d_{va} were fed to the HR-AMS via a size selecting DMA: 100 nm, 200 nm, 350

nm and 500 nm. In addition, ammonium nitrate particles were generated as described above and fed to the HR-AMS via the DMA for the following d_{va}: 50 nm, 60 nm, 70 nm, 80 nm, 90 nm, 100 nm, 150 nm, 250 nm, 350 nm, 500 nm and 600 nm. The particle velocity for each of these calibration d_{va} is then found and the relationship between velocity and d_{va} determined via the equation:

$$\text{Velocity} = Vgas_{lens} + [Vgas_{exit} - Vgas_{lens}] / [1 + (Daero/D^*)^b] \quad (3)$$

where $Vgas_{lens}$ is the velocity of the gas in the lens, $Vgas_{exit}$ is the gas velocity at the lens exit, D* is an effective scaling diameter and b is the power dependence. The Vgas terms provide limits to the particle velocity for small and large size particles. A small particle cannot travel faster than the expanding gas ($Vgas_{exit}$) and a very large particle cannot go slower than the velocity of the gas in the lens ($Vgas_{lens}$). Figure 2-3 summarizes the calibration with the combined PSL and ammonium nitrate datasets.

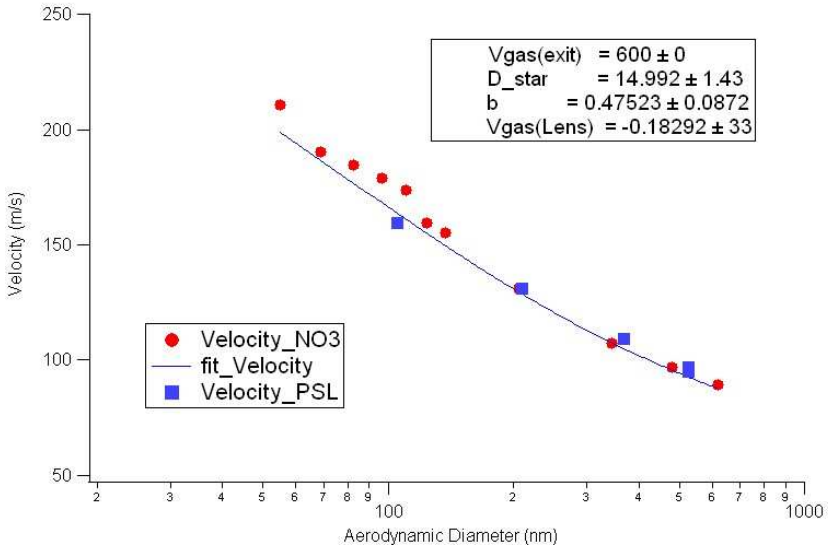

Figure 2-3. Relationship of particle velocity (y axis, m/s) with vacuum aerodynamic diameter (nm, x-axis) using PSL and ammonium nitrate particles. PSL (red dots) and ammonium nitrate (blue dots) particles of known d_{va} were sampled by the AMS, and the velocity of each particle type was measured by the AMS; the line is the non-linear least squares fit to determine the relationship between the velocity measured by the AMS and d_{va}. $Vgas_{lens}$ is the velocity of gases (e.g., N_2) in the lens, $Vgas_{exit}$ is the gas velocity at the lens exit, D* is an effective scaling diameter and b is the power dependence.

DeCarlo et al, Jimenez et al, and others have shown that a particle's d_{va} can be different than its volume equivalent diameter d_{ve}, which is the particle diameter if it was "melted" into a sphere, or mobility diameter d_m, which is the diameter determined by instruments such as the DMA (Jimenez et al., 2003; DeCarlo et al., 2004). As described in DeCarlo et al 2004 , the relationship between d_{va} and d_{ve} is dependent on a particle's density as well as shape (i.e., the degree of deviation from a sphere):

$$d_{va} = \frac{\rho_p}{\rho_o}\frac{d_{ve}}{X_v} \quad (4)$$

Where ρ_p is the particle density, ρ_o is standard density (1 g/cm^3), and X_v is the shape factor, or the ratio of the drag experienced by a non-spherical particle compared to a spherical particle.

2.2.3 Summary of HR-AMS Field Operations

Diagnostics during set up are described above. During field operations, diagnostic parameters were continuously logged. This includes checking for consistent flowrate, ionization efficiency, voltages for the heater, duty cycle and *m/z* calibration peak position. Figure 2-4 summarizes these diagnostics during the study. Diagnostics were within acceptable ranges. The three instances of sudden changes of flowrate were excluded from analysis (i.e., these samples were "blacklisted" within Squirrel); these occurred during set up of calibrations. The airbeam signal intensity and IE may change if the ionization and transmission efficiency changes during the field study; a slow decrease over weeks can be typical, and large, sudden aberrations can indicate an issue with the instrument (Takegawa et al., 2005). Both of these, as well as the heater bias, were relatively constant throughout the campaign. Other diagnostics were also relatively constant throughout the field study.

Operations began at 2300 LST on January 5, after set up calibrations described earlier. Additional calibrations with ammonium nitrate particles were done weekly, on January 8, January 15, and January 23. The air beam and flow rates were consistent throughout the study period. Daily, a filter was placed on the inlet so that particle free air was sampled for 10 minutes, to ensure the baseline is fairly constant and to check for leaks so that there is no false particle signal (i.e., the spectra when sampling filtered air should reflect only gaseous species). At the end of the study, size calibrations were repeated, and showed that there was little change since the beginning of the study.

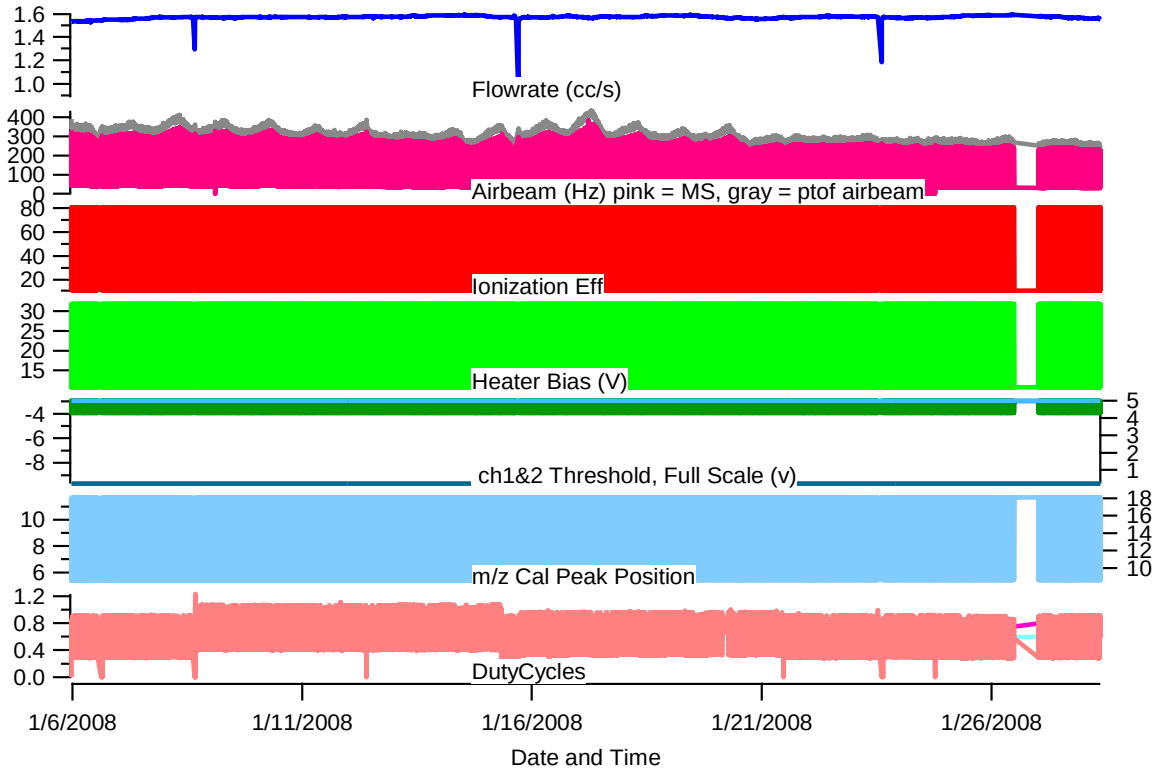

Figure 2-4. AMS diagnostic values during the Las Vegas field study.

2.3 HR-AMS Data Processing

Data were acquired via the standard HR-AMS data acquisition (DAQ) software available from http://cires.colorado.edu/jimenez-group/ToFAMSResources/ToFSoftware/index.html. The *m/z* range was 0-600, though in data analysis (described later) only *m/z* less than 300 were utilized. Data were processed using the ToF-AMS Analysis Toolkit version 1.51 (termed "Squirrel") and the ToF-AMS HR Analyais Toolkit version 1.10 (termed "Pika"), available from the Colorado.edu AMS wiki page (Figure 2-5). Both toolkits are implemented in Igor Pro software; here Igor version 6.22A was used. HDF files acquired via the DAQ were imported into an Igor experiment via Squirrel. This imports and processes raw data and diagnostic data. Details are provided in Appendix A.

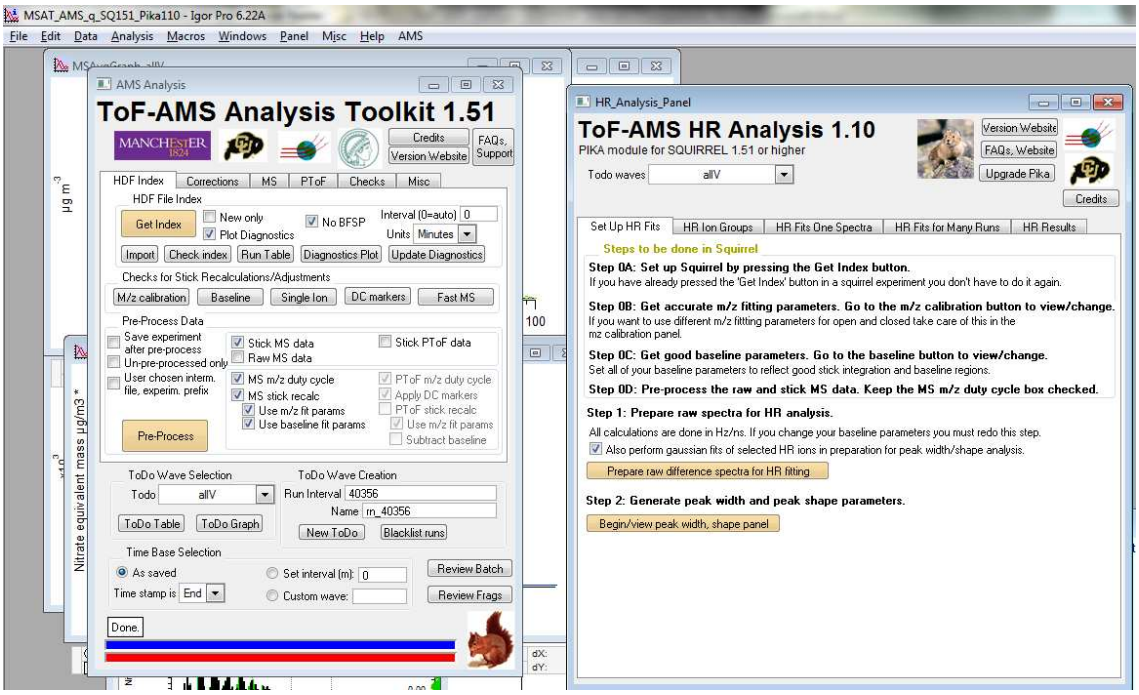

Figure 2-5. Squirrel and Pika dashboards in Igor.

Mass calibrations were done using fragments from abundant background gases such as Ar, O_2 and N_2, plus fragments from tungsten (atomic symbol W) or phthalates which are found

in the AMS, providing a stable set of background ions to use to ensure that the peaks from the mass spectrometer are assigned to the correct *m/z*. Using fragments from these background species in the "closed" mode, i.e., when no particles are present, the relationship between individual *m/z* ions' time of flight and their exact *m/z* are determined, and a curve describing this relationship determined, which is then used to determine all *m/z* for the "open" mode, when particles are present.

For unit mass resolution (UMR) data, the standard fragmentation table described in Allen et al. was used, to correct for interferences from gaseous species and to correctly allocate individual *m/z* among different aerosol types, i.e., organic, nitrate, sulfate, etc (Allan et al., 2004). For example, the signal at *m/z* 64 could be from SO_2^+ ion (from a sulfate aerosol) or from organic fragments (e.g., $C_5H_4^+$). At this *m/z* the organic fraction is calculated based on the signal at the *m/*z where an alkyl group (CH_2^+) is subtracted or added to the *m/z* 64 ion (in this case *m/z* 50 and 78), since organic aerosol are usually comprised of long chain hydrocarbons and the vaporization/ionization scheme used in the AMS results in a series of C_nH_{2n+1} fragments. Since inorganic species like sulfate, nitrate and ammonium have characteristic fragmentation patterns, and only occur at a handful of *m/*z, these patterns can be taken into account and the mass at each *m/*z from other species, namely organic aerosol, can be determined for the *m/*z values that have both an inorganic and organic component. Other *m/z* may have only organic signals, so the full signal is assigned to organics.

Particle size distributions were determined with PToF mode data. When in PToF mode, the aerosol beam is chopped, and particles that make it through the chopper enter a particle time of flight (PToF) region, where larger particles take longer to travel through than smaller particles. The time it takes to travel through the PToF region for selected size particles is

determined with particles of known diameter, as described earlier. As part of the post-processing, a baseline of the time it takes before particles make it through the PToF region needs to be determined. To do this we examine individual runs to find the time it takes before aerosol signal is found, and the time at which there are no more particles being transmitted through the AMS.

High resolution (HR) data were determined using the "PIKA" module of the AMS software, using standard practices. Via PIKA, individual unit mass resolution (UMR) *m/z* can be deconvolved into ions of higher resolution, e.g., from *m/z* 43 to the ions $C_3H_7^+$ (mass 43.05478) and $C_2H_3O^+$ (mass 43.01839), using a Gaussian fit for each HR ion peak width and shape. In PIKA, *m/z* calibration and baseline from Squirrel were used, and were well fit, as described above. Next, peak width and shape were determined. Similar to *m/z* calibration, the Gaussian fits for selected calibration ions were generated to develop a relationship between peak width and *m/z*. CH^+, OH^+, H_2O^+, C_2H^+, N_2^+, O_2^+, Ar^+, SO^+, $C_4H_2^+$, SO^+, and $C_6H_5^+$ gave the best fitting statistics for peak width. Peak shape was determined using O_2^+ and CH^+. The goal is to use the fitting ions to develop a smooth peak shape, which PIKA will then use as the shape for all ion peaks. Details are provided in Appendix A.

2.4 Aethalometer Black Carbon Measurements

2-channel black carbon (BC) data were collected using a Magee Scientific Aethalometer model AE-22 with a $PM_{2.5}$ inlet at 5 L/min. Flow was monitored with a NIST-traceable flow meter; if flows were outside of 10% of the target rate, a flow calibration using the instrument's firmware was done to regain target flow. Flow checks were done every one to three months; the

instrument passed an audit by an outside firm conducted in April 2008. The Aethalometer has a manufacturer-specified lower quantifiable limit (LQL) of 0.05 $\mu g/m^3$ and precision of 4%. Aerosol is collected on a quartz fiber filter tape continuously for 5 minutes, and then the amount of optical attenuation through the filter is analyzed using LED light sources at 880 nm and 370 nm (Park et al., 2010; Hansen, 2002; Hansen, 1998). Every 5 minutes, the amount of light transmitted through a 0.95 cm^2 spot on the filter where aerosol is collected is measured. A beam also measures the transmission through a portion of the filter where aerosol is not collected, in order to correct variations in lamp brightness and changes in the electronic response of the sensor. The attenuation (ATN) of light through the collecting part of the filter is defined as:

$$ATN = 100 * \ln (I_0 / I) \quad (5)$$

where I_0 is the intensity through the part of the filter not collecting aerosol, and I is the intensity through the collecting part of the filter. Therefore, a value of 1 would be from a blank, while a value of 100 would be extremely dark. To obtain the attenuation for the 5 minute interval, the attenuation of a reading is subtracted from the previous reading, yielding the amount of attenuation due to the increase in aerosol deposited in the last 5 minute sampling period. From this attenuation value, the Aethalometer then calculates the amount of black carbon present based on the manufacturer's calibration curves relating black carbon concentration and optical attenuation.

Time-stamp and filter tape spot saturation corrections were done using the Washington University Air Quality Lab AethDataMasher Version 6.0e. With the Aethalometer, optical absorption at 880 nm (BC channel) and 370 nm (UVC channel) are obtained. There is enhanced absorption from biomass burning-associated organic compounds in the UVC channel compared

to the BC channel (Kirchstetter et al., 2004; Sandradewi J. et al., 2008; Jeong et al., 2004); in contrast, there is little difference in absorption of diesel exhaust between the two channels. Thus, the difference between the UVC and BC channels can be used as an indicator of the presence of biomass burning BC.

2.5 Sunset Organic and Elemental Carbon (OC, EC) Measurements

A Sunset OCEC instrument (Bae et al., 2004b; Jeong et al., 2004; Bauer et al., 2009; Rattigan et al., 2010) measured organic and elemental carbon on an hourly basis. The Sunset OCEC instrument uses a thermal optical method similar to NIOSH 5040 (Chow et al., 2001; Sin et al., 2004) and has a limit of detection of 0.3 $\mu g/m^3$ for OC and 0.01 $\mu g/m^3$ for EC (Bauer et al., 2009). Aerosol is drawn through a $PM_{2.5}$ cyclone inlet with a mass flow controller and a carbon denuder at 8 L/min, and deposited on a quartz fiber filter for 47 minutes. Aerosol is then analyzed during an 8-minute cycle by heating the filter to 840°C for 5 minutes to quantify OC, and then by introducing an oxidizing carrier gas (He with 10% O_2) at 850°C for 3 minutes to quantify EC. The remaining 5 minutes is used for cooling down the oven. During the filter heating, carbonaceous material evolves off the filter as CO_2, which is quantified using a non-dispersive infrared (NDIR) detector. EC is determined as any carbon evolved off the filter after the introduction of He/O_2 once the laser-monitored filter absorbance matches the initial absorbance measured when the filter was first heated. After each hourly analytical cycle, calibration gas of 5% CH_4 with He flushes the system. Instrument response is calibrated using a 99.9% reagent grade sucrose solution and a 5% CH_4/He calibration standard. Filters were changed nominally every five days, and independent flow checks every two weeks.

2.6 Levoglucosan Measurements

Quartz fiber filters (8”x10”, Pall Life Sciences, TISSUQUARTZ 2500QAT-UP) in Tisch 231 $PM_{2.5}$ plates were used in hi-volume samplers (nominal flow rate 68 m^3/hr) to collect aerosol for later chemical analysis. Filters were pre-baked at 550 degrees C for at least 12 hours in order to remove any organic material. After baking, filters were individually wrapped in aluminum foil and kept in a freezer when not in use. Samplers were run on automated timers for five samples daily: 1) 0500-0900 (local time), to capture morning rush hour conditions; 2) 0900-1100, to have measurements in parallel with gaseous VOC and carbonyl measurements, reported elsewhere (McCarthy et al., 2013); 3) 1100-1700, to capture midday conditions; 4) 1700-0500, to capture overnight conditions; and 5) 24-hr filters, from 0900-0900. The 24-hour filters were operated 0900-0900 in order to fully capture the nighttime period when concentrations are highest, instead of the more typical operation starting/stopping at midnight. The midnight to midnight schedule would have resulted in a given filter capturing parts of two nighttime periods, even though the concentrations may be quite different, thus making that sample difficult to interpret. In addition, the same sampler was used for all 24-hour measurements, so a time when site operators were on site (0900) was required to facilitate filter changes. In addition to the collected filters, a trip or field blank filter was nominally collected daily. Flow checks were done in the morning and evening (e.g., 0900 and 1700).

Filters were stored at the Colorado State University Atmospheric Science chemistry lab until use. Half of 17 selected filters was cut and wrapped in aluminum foil for extraction and chemical analysis by EPA ORD labs. Only a limited number of samples could be analyzed, so 12 overnight samples were selected since this is the period of highest OM concentrations. In addition, morning and midday filter samples were also extracted for comparison (Olson et al.,

2012). Quartz filters were extracted in a solvent mixture of hexane, methanol, and dichloromethane (1:1:1) (GC2 grade, Burdick and Jackson) using a Dionex ASE 200 Accelerated Solvent Extractor. Chromatographic grade nitrogen was used to concentrate samples to a final volume of 300 mL. A gas chromatograph (GC, Hewlett-Packard 6890N) and inert mass selective detector (MSD, HP5973N) was used and chromatographic separation was completed using a 30-m, 0.25-mm i.d. with 0.25-mm film thickness capillary column (DB-5MS, Part No. 122-5532, J&W Scientific). The GC was operated as follows: injector temperature of 315 degree C; column flow of 1 mL/min; pressure pulse of 25 psi for 0.5 min; initial GC oven temperature initially set at 35 C, ramped at 20 C/min until reaching 160 C, ramped at 2 C/min until reaching 315 C. The MSD was operated under selective ion monitoring (SIM) mode. Recovery, precision, limits of detection and quantitation, blank levels, calibration linearity, and agreement with certified reference materials for compounds analyzed in this study are given elsewhere (Turlington et al., 2010). External calibration curves (5-500 pg/mL) using authentic standards (Absolute Standards, Accustandards, and Chiron) were determined for all analytes. Deuterated surrogate standards (50-200 pg/mL) (n-C26-d54, n-C30-d62, n-C36-d74, chrysened12, benz(b)fluoranthene-d12, indeno(1,2,3-cd)pyrene-d12 and coronene-d12) and deuterated internal standards (1000 pg/mL) (n-C20-d42, n-C25-d52, n-C28-d58, n-C32-d66, benz(a)anthracene-d12, benzo(e)pyrene-d12, dibenzo(a,h)anthracened14 and dibenzo(a,i)pyrene-d14) were used for all samples.

2.7 Other Ambient Measurements

Wind speed and direction were measured with an RM Young AQ 5305-L at 2 meters above ground level (AGL) at Fyfe. Semi-continuous measurements of $PM_{2.5}$ K^+, sulfate, nitrate, ammonium and other major ions were made using a PILS system coupled to two ion

chromatographs (IC). The detailed design and operation of the PILS is described elsewhere (Orsini et al., 2003; Weber et al., 2001; Weber et al., 2003; Sorooshian et al., 2006) and is briefly summarized here. The PILS nucleates aerosol particles to form water droplets by mixing a denuded aerosol stream with supersaturated steam. The nucleated droplets are collected into a flowing liquid stream by inertial impaction. The liquid stream, containing an internal LiBr standard to determine dilution by condensed water vapor, is split into two streams which are injected every 15 minutes to two ion chromatographs (Dionex, DX-500) for measurement of major inorganic ion (Cl^-, SO_4^{2-}, NO_3^-, Na^+, NH_4^+, K^+, Mg^{2+} and Ca^{2+}) concentrations. Each IC system consisted of a 6-port valve injector fitted with a 200µL sample loop, a pump (Dionex GP40 or IP20), Dionex CD20 conductivity detector, an analytical separation column, and a suppressor. The cation eluent was 20 mM MSA (methanesulfonic acid) at a flow rate of 1.0 mL/min (Dionex CG12A/CS12A column and CSRS-ULTRA II suppressor). The anion system used a Dionex AS4A-SC/AG4A-SC column pair (1.8mM Na_2CO_3/1.7mM $NaHCO_3$ eluent) or a Dionex AS14A column (8mM Na_2CO_3/ 7mM $NaHCO_3$ eluent), depending on the campaign, with an ASRS-ULTRA II suppressor.

A $PM_{2.5}$ cyclone (16.7 LPM, URG-2000-30EH) and two URG annular denuders (URG-2000-30X242-3CSS) were used upstream of the PILS/IC. The first denuder was coated with Na_2CO_3 for removal of acidic gases and the second denuder was coated with phosphorous acid to remove basic gases. Denuders were exchanged every 5-6 days after calibration and blank checks. Blanks were taken by sampling particle-free air, drawn through a HEPA capsule filter (12144, Pall Corporation), through the PILS/IC system after a calibration check standard (NO_3^-, SO_4^{2-} and NH_4^+ concentrations of 20 µN and Cl^-, Na^+, K^+, Ca^{2+} and Mg^{2+} concentrations of 10 µN) was injected. Approximately every 10 days the PILS was cleaned and the ion chromatographs

recalibrated. A sample flow rate of 16.7 L/min for the PILS/IC was controlled by a critical orifice with a vacuum regulator. 20-minute data were aggregated into hourly concentrations, where all three 20-minute measurements within an hour were required to complete an hourly average.

2.8 EPA PMF Methods

Positive matrix factorization (PMF) is a common analysis which decompose a matrix of speciated sample data into two matrices — factor contributions and factor profiles – in order to understand the factors or sources impacting the speciated sample data (Poirot et al., 2001; Reff et al., 2007; Norris et al., 2008; Engel-Cox and Weber, 2007; Ke et al., 2008; Brown et al., 2012; Ulbrich et al., 2009a; Kim and Hopke, 2007). The two most common programs are PMF2 and ME2, in addition to a freely available graphical user interface (GUI) developed by EPA, EPA PMF, which uses the ME2 program. Ulbrich et al., and others have also expanded on the details of PMF application to AMS data, including a PMF analysis package in Igor Pro (Lanz et al., 2007; Lanz et al., 2010; Ng et al., 2010; Ulbrich et al., 2009a). The detailed methods of these programs have been documented elsewhere (Paatero, 1997; Paatero and Tapper, 1994), and are summarized below.

A speciated data set can be viewed as a data matrix **X** of dimensions *n* by *m*, in which *n* samples and *m* chemical species were measured. Rows and columns of **X** and of related matrices are indexed by *i* and *j*, respectively. The goal of multivariate receptor modeling, for example with PMF, is to identify the number of factors *p*, the species profile *f* of each source, and the amount of mass *g* contributed by each factor to each individual sample:

$$x_{ij} = \sum_{k=1}^{p} g_{ik} f_{kj} + e_{ij} = c_{ij} + e_{ij} \quad (6)$$

where e_{ij} is the residual for each sample/species. Notation is as follows. Entire matrices are denoted by capital bold-face letters. Columns of the source contribution matrix **G** may be denoted by $\mathbf{g}_k$, and similarly rows of source profile matrix **F** denoted by $\mathbf{f}_k$. Matrix **C** represents the *modeled* part of matrix **X**.

In PMF factor elements are constrained so that no sample can have a significantly negative source contribution. PMF allows each data value to be individually weighted. This feature allows analysts to adjust the influence of each data point, depending on the confidence in the measurement. The PMF solution minimizes the object function *Q* (Equation 7), based upon the estimated data uncertainties (or adjusted data uncertainties) u_{ij}.

$$Q = \sum_{i=1}^{n} \sum_{j=1}^{m} \left[\frac{x_{ij} - \sum_{k=1}^{p} g_{ik} f_{kj}}{u_{ij}} \right]^2 \qquad (7)$$

ME-2 is the underlying program used to solve the PMF problem in the program of EPA PMF (Norris et al., 2008), the user interface that feeds the data and user specifications to ME-2. ME-2 then performs the iterations via the conjugate gradient algorithm until convergence to a minimum Q value. The minimum Q may be global or local; users can attempt to determine which by using different starting points for the iterative process and comparing the minimum Q values reached. Output from ME-2 is then fed back through EPA PMF and formatted for users to interpret.

Variability in the PMF solution has traditionally been assessed via bootstrapping (BS), where PMF solutions using a series of data sets that are resampled versions of the original data set are generated. EPA PMF performs bootstrapping by randomly selecting non-overlapping

blocks of samples (consecutive samples, block size supplied by user) and creating a new input data file of the selected samples, with the same dimensions as the original data set. PMF is then run on the new data set, and each bootstrap factor is mapped to a base run factor by comparing the contributions of each factor. The bootstrap factor is assigned to the base factor with which the bootstrap factor has the highest uncentered correlation, above a user-specified threshold. If no base factors have a correlation above the threshold for a given bootstrap factor, that factor is considered "unmapped". If more than one bootstrap factor from the same run is correlated with the same base factor, they will all be mapped to that base factor. This process is repeated for as many bootstrap runs as the user specifies.

EPA PMF was used in this application (Norris et al., 2008; Brown et al., 2012). New features within EPA PMF v5.0 allow the user to take advantage of rotational tools available in ME-2(Paatero and Hopke, 2008; Paatero et al., 2002). In general, the non-negativity constraint alone in PMF analysis is not always sufficient to produce a unique solution. To reduce the number of solutions, additional information such as known source contributions and/or source compositions can be used. This additional information can be incorporated into the PMF solution by "pulling" parts of a PMF solution, such as a factor profile or contribution. For example, if a source type has a typical ratio among elements in its source profile, a PMF-resolved factor profile could be pulled toward that ratio if the user has good confidence that the factor is related to such a source. The strength of each pull is controlled by specifying a limit on the change in the goodness-of-fit parameter *Q*, *dQ*. If the user wishes to perform a weak pull, a small limit on *dQ* would be allowed. For a stronger pull, a large limit *dQ* would be allowed. These pulls are activated in ME-2 by the use of an optional control file called "moreparams.txt", which is generated by EPA PMF when a user specifies a pull, or can be generated as a text file

by a user outside of EPA PMF and ME-2. When the moreparams file is present, ME-2 generates a solution where the base solution is pulled as indicated in the moreparams file. Additional details are available elsewhere (Paatero et al., 2002; Paatero, 2007; Norris et al., 2009).

3. Analysis of Aerosol Composition and Factor Analysis

3.1 Chapter Summary

Ambient non-refractory PM_1 aerosol particles were measured with an Aerodyne High Resolution Time-of-Flight Aerosol Mass Spectrometer (HR-AMS) at an elementary school 18 meters from the US 95 freeway soundwall in Las Vegas, Nevada, during January 2008. Additional collocated continuous measurements of black carbon (BC), carbon monoxide (CO), nitrogen oxides (NO_x), and meteorological data were collected. The U.S. Environmental Protection Agency's (EPA) positive matrix factorization (PMF) data analysis tool was used to apportion organic matter (OM) as measured by HR-AMS, and rotational tools in EPA PMF were used to better characterize the solution space and pull resolved factors toward known source profiles. Three- to six-factor solutions were resolved. The four-factor solution was the most interpretable, with the typical AMS PMF factors of hydrocarbon-like organic aerosol (HOA), low-volatility oxygenated organic aerosol (LV-OOA), biomass burning organic aerosol (BBOA), and semi-volatile oxygenated organic aerosol (SV-OOA). When the measurement site was downwind of the freeway, HOA composed about half the OM, with SV-OOA and LV-OOA accounting for the rest. Attempts to pull the PMF factor profiles toward source profiles were successful but did not qualitatively change the results, indicating that these factors are very stable. Oblique edges were present in G-space plots, suggesting that the obtained rotation may not be the most plausible one. However, solutions found by pulling the profiles or using Fpeak retained these oblique edges, indicating the base solution is likely a best fit, even with rotational ambiguity. On average, HOA made up 26% of the OM, while LV-OOA was highest in the afternoon and accounted for 26% of the OM. BBOA occurred in the evening hours, was

predominantly from the residential area to the north, and on average constituted 12% of the OM; SV-OOA accounted for the remaining third of the OM.

3.2 Overview of Aerosol Concentrations During Study

OM averaged 3.3 $\mu g/m^3$ during the January intensive campaign, and with BC accounted for 74% of the AMS measured mass (Figure 3-1). The average organic mass spectra (Figure 3-2) was mostly composed of less oxidized, hydrocarbon-like fragments. OM was typically highest during the evening hours (i.e., 1900 through 2100 LST) with a secondary peak in the morning (i.e., 0600-0900 LST, during rush hour commute) as shown in Figure 3-3. In contrast, concentrations of other species such as BC, CO, and NO_x had peaks in the early morning and overnight (Figure 3-3b shows BC as an example). AMS fragments associated with HOA, such as *m/z* 57 ($C_4H_9^+$) and *m/z* 43 ($C_3H_7^+$), showed a similar diurnal pattern. AMS fragments associated with OOA, such as *m/z* 44 (COO^+), showed only minor fluctuations throughout the day, while those used as tracers of biomass burning, such as *m/z* 60 ($C_2H_4O_2^+$), were evident only during the evening and overnight hours (Figure 3-4).

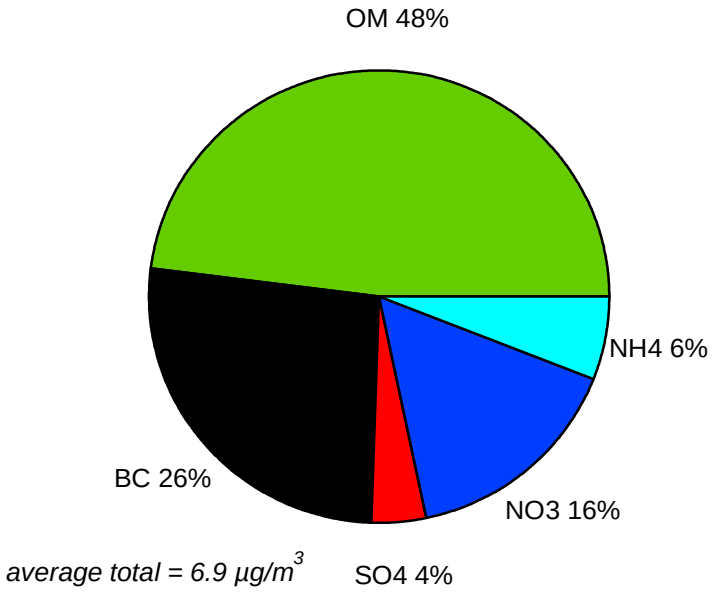

Figure 3-1. Average composition of PM_1 at Fyfe Elementary School in January 2008. All measurements except for BC are from HR-AMS, and BC is from Aethalometer (no size cut).

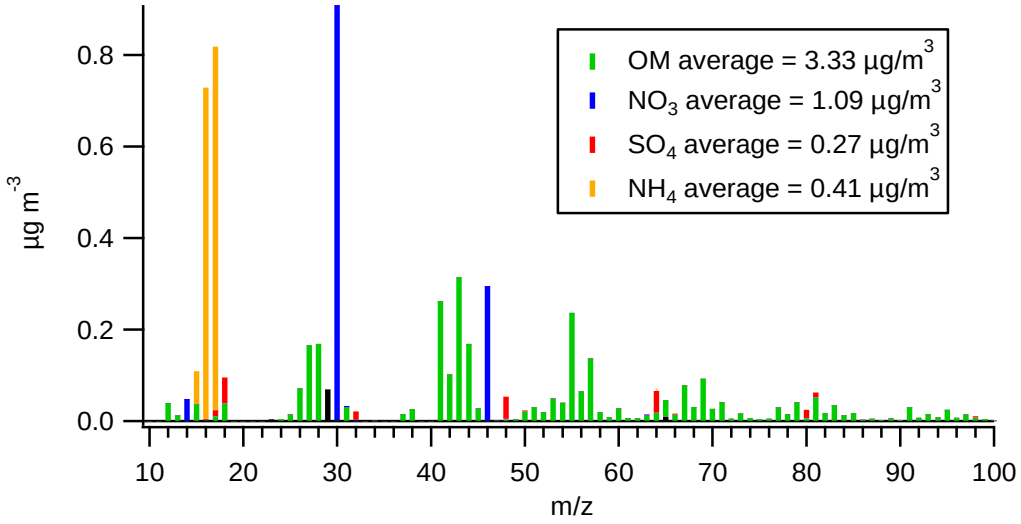

Figure 3-2. Average mass spectra during the study.

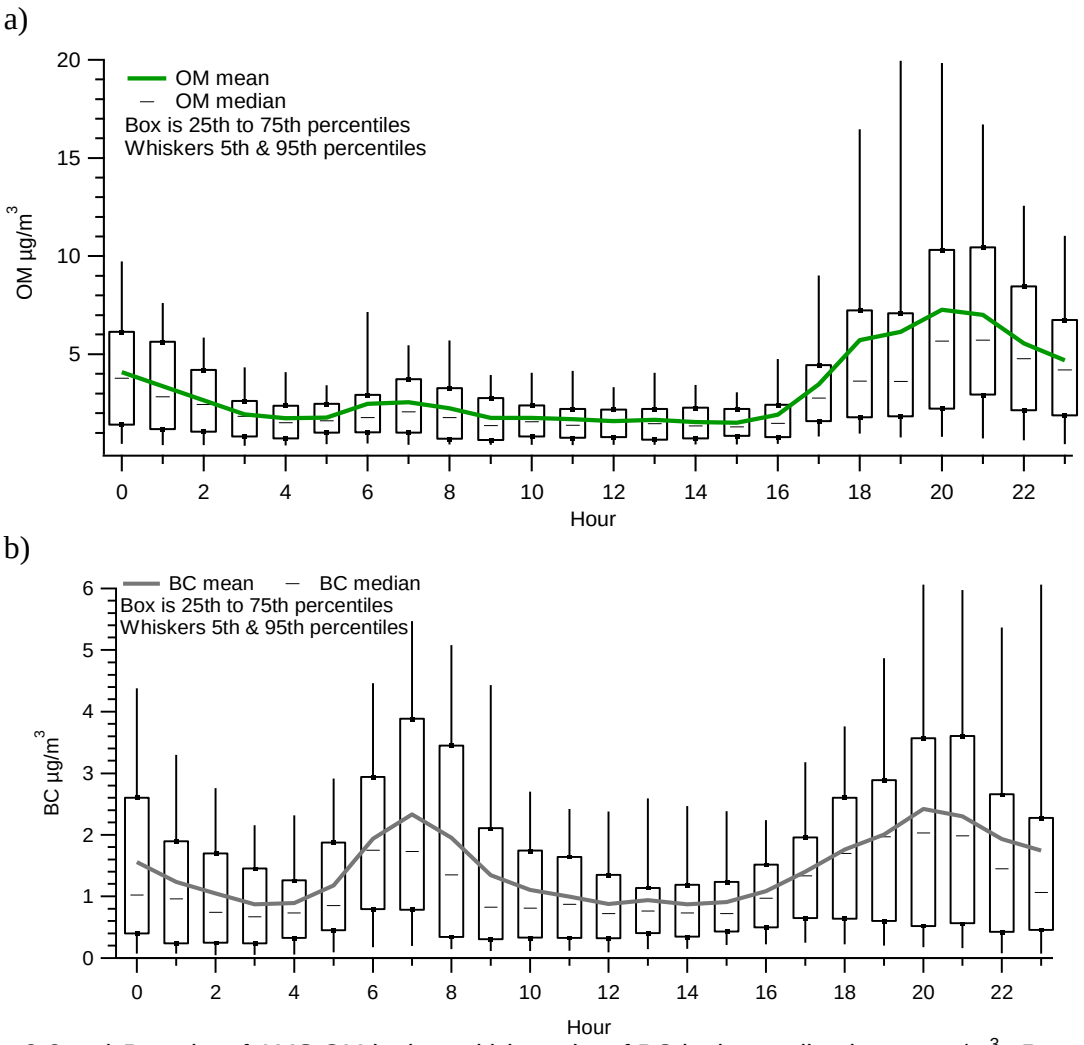

Figure 3-3. a) Box plot of AMS OM by hour, b) box plot of BC by hour; all units are µg/m^3. Panel a) is reproduced under Creative Commons Attribution 3.0, originally published in Brown et al., 2012.

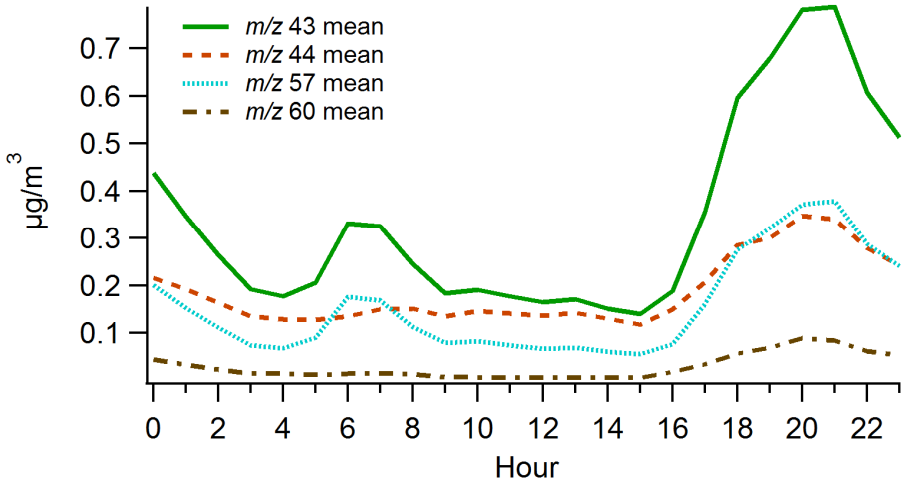

Figure 3-4. Average concentrations of selected *m/z* (43, 44, 57, and 60) by hour; units are µg/m^3. Figure is reproduced under Creative Commons Attribution 3.0, originally published in Brown et al., 2012.

There was only modest correlation (i.e., r^2 of 0.40 to 0.60) of OM and fragments such as *m/z* 43, 44, 57, and 60 with BC, CO, and NO_x. Since BC and CO are from primary emissions and OM is a mixture of primary emissions and secondary products of atmospheric reactions, the modest correlations among these parameters suggest that a large fraction of the OM may be secondary in nature. OM concentrations were similar between upwind (relative to the highway) and downwind conditions (medians of 2.0 $\mu g/m^3$ and 1.6 $\mu g/m^3$, respectively); there was a higher median OM concentration during upwind conditions since these occurred during the evening, when wind speeds were lower and the boundary layer shallower than during the daytime, when downwind conditions prevailed and higher wind speeds and more dispersion occurred. OM was highest during stagnant, low-wind conditions, with an average of 3.7 $\mu g/m^3$. In contrast, some other pollutants showed sharper differences between upwind and downwind conditions; for example, concentrations of primary emission pollutants such as BC were more than three times higher under downwind conditions than under upwind conditions (Roberts et al., 2010). BC had a median concentration of 1.24 $\mu g/m^3$. BC is more than twice as high at this site compared to a site 2 km away in the urban center but away from freeways (Hancock Elementary School), where BC was, on average, 0.5 $\mu g/m^3$. This difference (~ 0.74 $\mu g/m^3$) between the near-road site at Fyfe and the urban background site at Hancock suggests that emissions from the freeway are a large contributor to the BC at Fyfe, but may not be as large a contributor to OM or other aerosol species.

While OM did have a distinctive diurnal pattern in general, it was episodic during the intensive. A multi-day OM episode occurred with relatively high, sustained concentrations in the first week (Figure 3-5). The episode ended around midnight on January 12 when a storm front came through the area. During the episode, OM concentrations were relatively high during

the overnight periods under a stable boundary layer. A short-duration but very high OM concentration episode occurred the evening of January 19, with the highest 2-minute and hourly averaged OM concentrations of the entire intensive. Although sampling took place over four weekends, the meteorological conditions during those weekends were quite different, with drizzle and rain on the first weekend (Sunday, January 6), a front with high winds and rain on the second (Saturday night January 12), a stagnation episode on the third (Saturday January 19), and windy conditions on the last weekend. With the low number of weekends and the wide range of meteorological conditions, comparing weekday to weekend concentrations may not be as useful here compared to data sets that comprise many weekends.

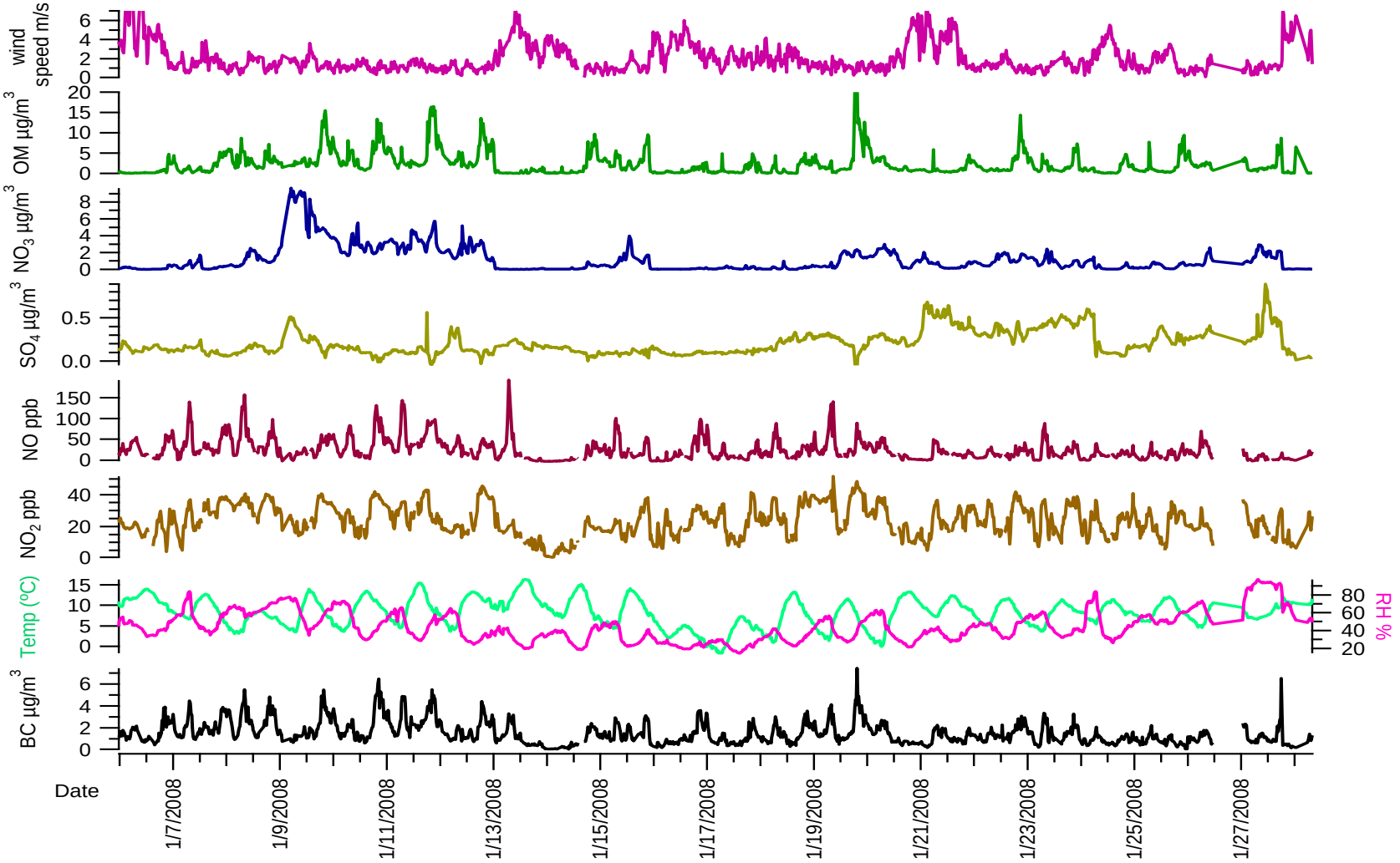

Figure 3-5. Time series of Aethalometer BC (µg/m^3), temperature (degrees C), relative humidity (%), NO_2 (ppb), NO (ppb), AMS sulfate (µg/m^3), AMS nitrate (µg/m^3), AMS OM (µg/m^3), and wind speed (m/s). Major tick marks indicate midnight local time for each day.

3.2.1 Inorganic Aerosol Patterns

Temporal patterns for both sulfate and nitrate differed from the temporal pattern for OM. Sulfate concentrations were low throughout the study, with an average concentration of 0.27 $\mu g/m^3$, and a maximum 20-minute average of 0.88 $\mu g/m^3$. These sulfate levels are quite low compared to many other areas in the U.S., though typical of the western U.S., as there is minimal transport of sulfate into Las Vegas and no major sources of SO_2 or sulfate upwind of the urban area.

Nitrate concentrations were episodic but were also typically low, with a median concentration of 0.54 $\mu g/m^3$ and average of 1.09 $\mu g/m^3$. The nitrate concentrations are lower than is typical in western urban areas. Nitrate concentrations had little relationship with OM or concentrations of other measured pollutants. In a one-day episode, nitrate peaked above 8 $\mu g/m^3$ for three hours, after which it decreased to approximately 2 $\mu g/m^3$ for the next two days (Figure 3-6). Figure 3-7 shows nitrate concentrations with respect to relative humidity and temperature. The nitrate episode occurred after a 24-hour period when winds were stagnant, temperatures were low (less than 8°C), and relative humidity was relatively high (greater than 55%), including during the midday, which was atypical. Nitrate was greater than 1 $\mu g/m^3$ on a few other days, but these periods typically lasted only a few hours. These higher concentrations occurred during the day and night, with no distinct, consistent diurnal pattern, unlike OM, BC, CO, and other pollutants, which peaked in the evening and early morning hours.

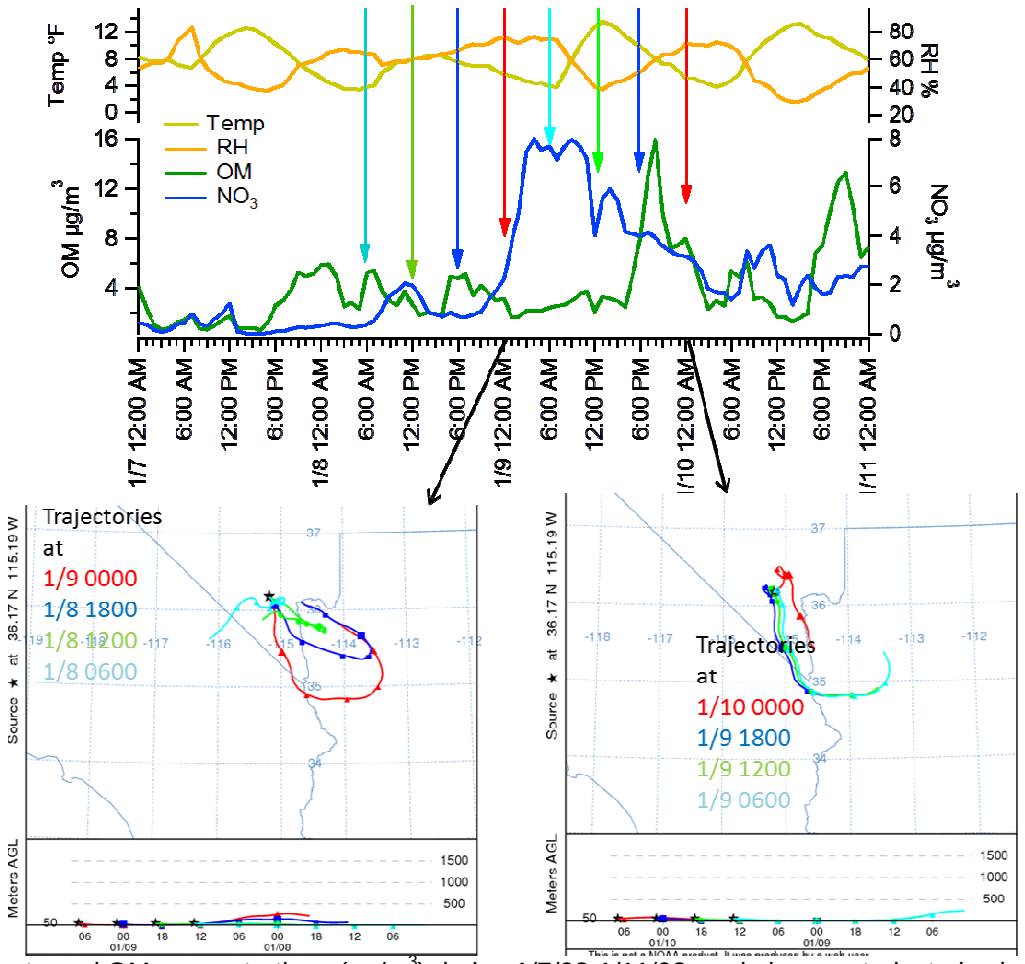

Figure 3-6. Time series of nitrate and OM concentrations (µg/m^3) during 1/7/08-1/11/08, and air mass trajectories backwards every 6 hours during 1/8 0600 LST - 1/10 0000 LST. Arrows indicate the trajectory color for each start time.

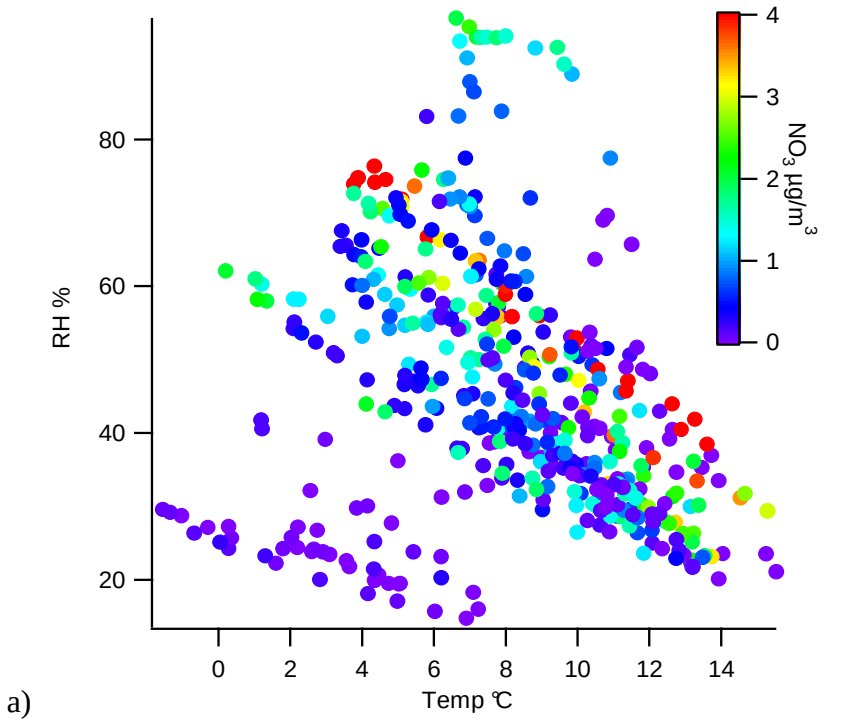

a)

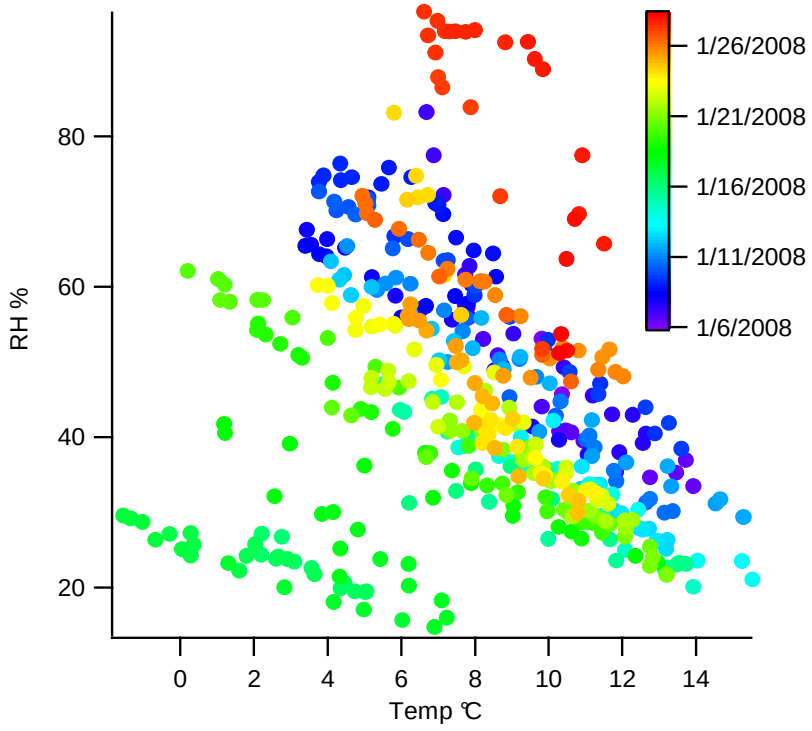

b)

Figure 3-7. Temperature and % relative humidity colored by a) nitrate concentrations; b) date time.

There have been limited studies of speciated $PM_{2.5}$ in Las Vegas, with the 2000-2001 Las Vegas Valley Visibility/$PM_{2.5}$ study the one with the most data (Green et al., 2002). Here they found wintertime sulfate concentrations, on average, lower than 0.5 $\mu g/m^3$, and average nitrate concentrations between 0.2 and 0.6 $\mu g/m^3$ at three sites. Though no formal apportionment was done, based on extensive data analysis they surmised that gasoline and diesel vehicle emissions are likely an important source, but that other sources such as residential biomass burning may also be a significant contributor. Another study, the Southern Nevada Air Quality Study (SNAQS) (Watson et al., 2007), used 10-12 filter samples at 4 sites from January 2003 to apportion $PM_{2.5}$. 80% of the mass was from carbonaceous aerosol, and 38%-49% of the $PM_{2.5}$ was attributed to mobile sources. Biomass burning was 11%-21% of the mass. These apportionments were based on a standard suite of filter analyses, and included OC and EC by TOR, sulfate and nitrate by IC, and metals by XRF; since only 24-hour filters on a handful of days were collected there was limited opportunity for temporal analyses (time of day, day-to-day variation, etc).

There are very few major sources immediately upwind of Las Vegas, so the amount of transported secondary organic carbon and ammonium sulfate is generally low, though there can be transport from California. Some speciated $PM_{2.5}$ data have been collected as part of EPA's chemical speciation network (CSN) from 2002 to 2007. Using the data from this 5-year period, average sulfate concentrations are 1 $\mu g/m^3$, and average nitrate concentrations are 0.89 $\mu g/m^3$, though sulfate is lower and nitrate is higher in the winter. These low values are corroborated by Chapter 2 of the IMPROVE network annual report (Hand et al., 2011), which shows that sulfate and nitrate concentrations are extremely low in Las Vegas compared to other areas in the U.S. and are lower than 1 $\mu g/m^3$, on average. Unlike most of the U.S. or much of Europe, there is

very little coal-fired power production upwind of Las Vegas, so SO_2 (and sulfate) levels are low. In many prior studies elsewhere, sulfate concentrations are higher and are correlated with LV-OOA concentrations; however, as the sulfate levels are so low in Las Vegas, it is unlikely that LV-OOA will correlate with sulfate. As Las Vegas is in an arid desert environment with little agriculture in the area, ammonia emissions are relatively low (e.g., http://nadp.sws.uiuc.edu/nh3net/) , so ammonium nitrate formation may be limited by the availability of ammonia. Nitrate has been observed to often correlate with SV-OOA, as both may be associated with similar transport and formation mechanisms. When nitrate formation is limited by ammonia availability, however, there is little reason to expect it to correlate with SV-OOA.

3.2.2 Variations with Meteorology

Nitrate was episodic and sulfate was very low, so much of the analysis presented here focuses on OM and BC. The monitoring site is located adjacent to the freeway, such that the site is downwind of the freeway at angles between 120 and 250 degrees. However, upwind/downwind comparisons are not straightforward here. Hours with downwind conditions occurred 16% of the time, of which 45% of these were during the midday (0900-1700 LST) when wind speeds are highest and in between peak traffic periods (Figure 3-8). During peak traffic periods in the morning (0500-0900 LST) and evening (1700-2000 LST), the site was downwind of the freeway only 20% of the time.

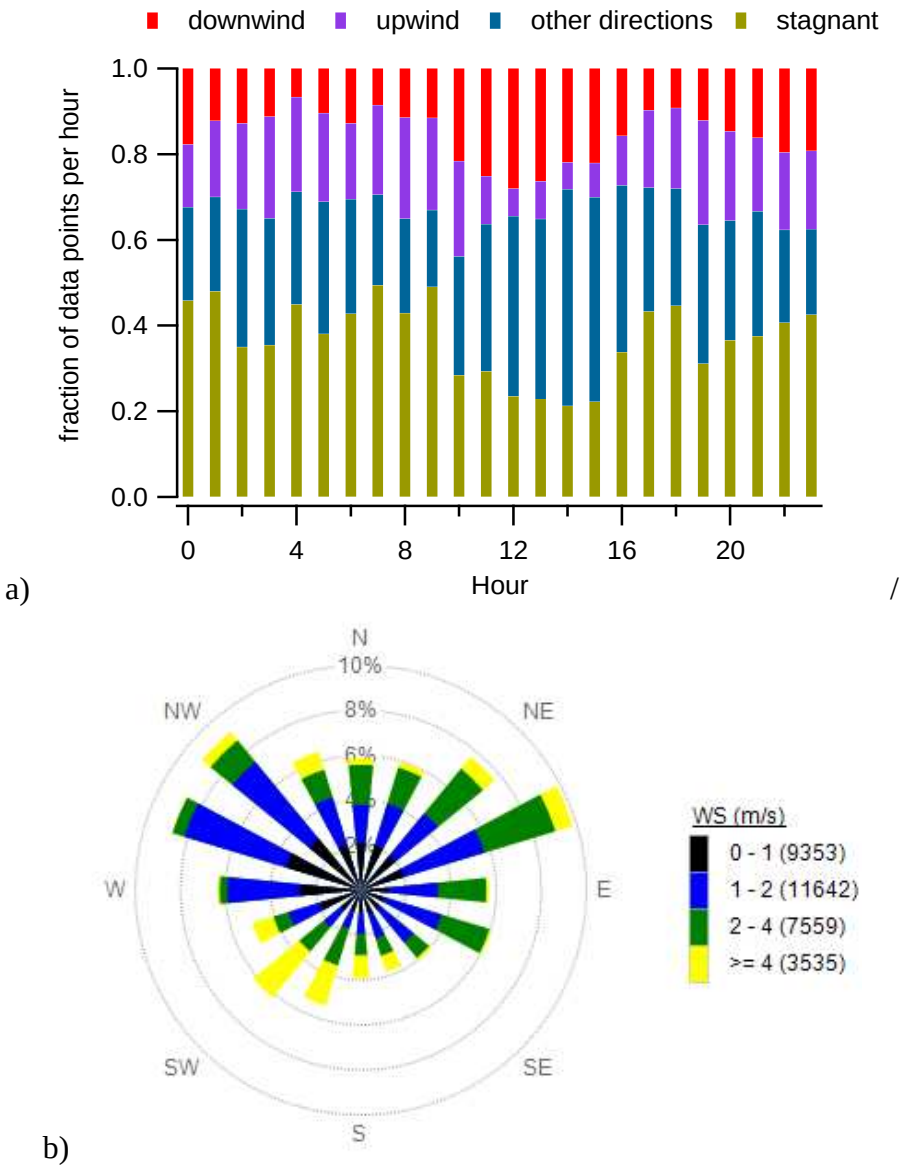

Figure 3-8. Wind summary during January 5-28 2008: a) fraction of 2-minute AMS data points per hour by wind condition (downwind of freeway, upwind of freeway, parallel to freeway [other directions], or stagnant [wind speed less than 1 m/s]); and b) wind rose. Panel b) is reproduced under Creative Commons Attribution 3.0, originally published in Brown et al., 2012.

Since downwind conditions occur mostly in the midday and upwind conditions occur mostly in the morning and evening, a simple downwind/upwind analysis could be biased since concentrations are lower in the midday compared to morning and evening. Therefore, upwind/downwind analysis was done for different times of day. Since stagnant conditions occur

37% of the time and are when concentrations are highest, stagnant conditions were also included in the analysis in a separate bin. OM concentrations were generally similar whether our monitoring site was upwind or downwind of the freeway (Figure 3-9). This differs for other pollutants such as BC, where downwind concentrations were, on average, more than two times higher during downwind conditions. This shows that the enhancement of being next to the roadway is not nearly as large for OM as for BC, since OM is a mixture of primary, semi-volatile, and more oxidized material, whereas BC is primary material that, in a near-roadway environment, predominantly originates from emissions along the roadway. Like BC, OM was higher during stagnant conditions (those with winds less than 0.5 m/s), as a shallow boundary layer and minimal dispersion quickly led to the buildup of pollutants. During the daytime when emissions from the freeway may be most prominent, concentrations during downwind conditions were higher than during upwind conditions. Only during the evening hours (1700-2300 LST) when other, non-mobile emission sources become important, were upwind concentrations higher than downwind. This increase is likely due to contributions from residential biomass burning, as explored further with PMF.

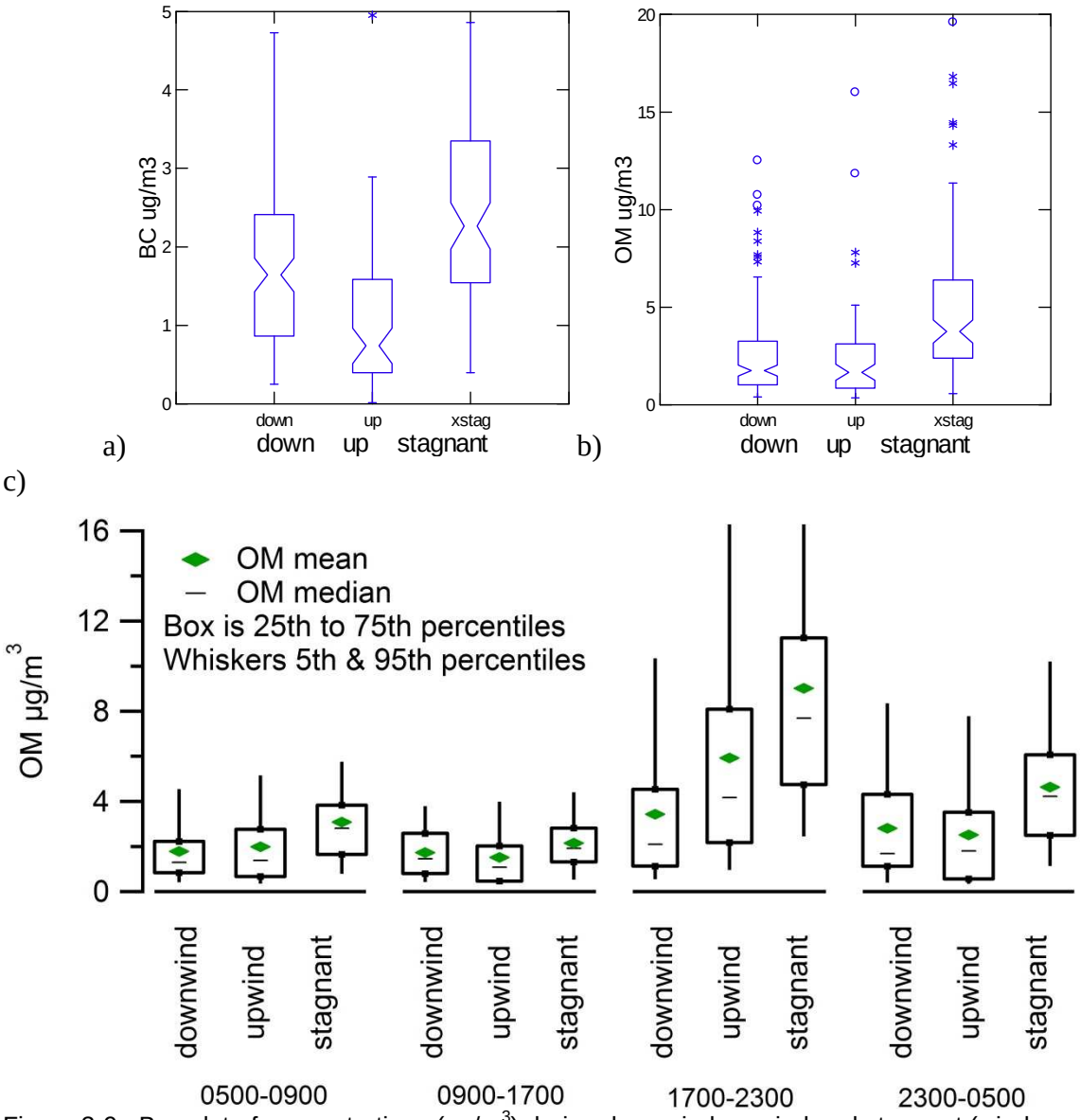

Figure 3-9. Box plot of concentrations (µg/m^3) during downwind, upwind and stagnant (wind speed less than 0.5 m/s) conditions for a) OM; b) BC, and c) OM, grouped by time of day.

OM was also examined by wind direction and speed, to examine the individual data points comprising the box plots in the above figure. Figure 3-10 shows hourly averaged OM by wind direction, with each hour of the day indicated by the number; colors indicate wind speed in (a), and indicate concentrations of *m/z* 60 in (b). Figure 3-11 shows how OM and BC vary with wind speed; Figure 3-12 shows the average mass spectra during upwind, downwind and stagnant

conditions. BC and OM both have a similar pattern in relation to wind speed, with a steep drop off in concentration once winds are greater than 1.5 m/s. OM is similar on average when the monitoring site is downwind or upwind of the freeway, but that is due to the diurnal pattern of winds, where upwind conditions occur more in the evening when wind speeds are low, while downwind conditions occur in the midday, when wind speeds are higher. The high concentrations during low wind speeds from the 280-310 degree sector are in the evening when residential biomass burning occurs, as indicated by the relatively high concentrations of *m/z* 60. The mass spectrum changed throughout the day, with more oxidized fragments like *m/z* 44 higher in the midday compared to the morning or evening, and biomass burning-related fragments like *m/z* 60 higher in the evening. Upwind/downwind differences varied by times of day, as seen in Figure 3-13, which shows the difference between the upwind and downwind mass spectrum by time of day. In the morning and midday, the downwind concentrations are slightly higher, with higher amount of primary, less oxidized fragments like *m/z* 43 and 55. In the evening, concentrations during upwind conditions are actually higher for all fragments, as the upwind direction is the direction of arterial roads plus areas of residential biomass burning.

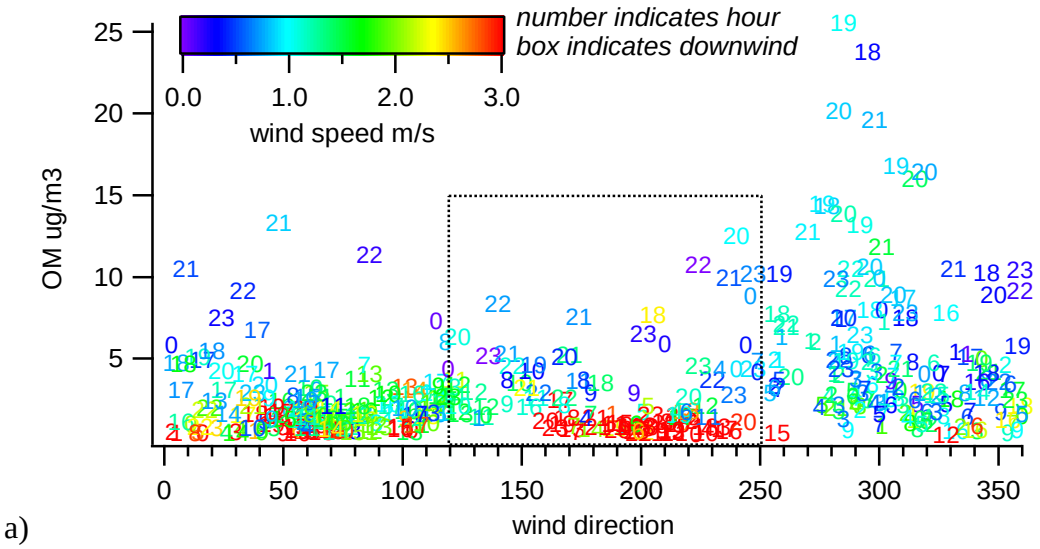

a)

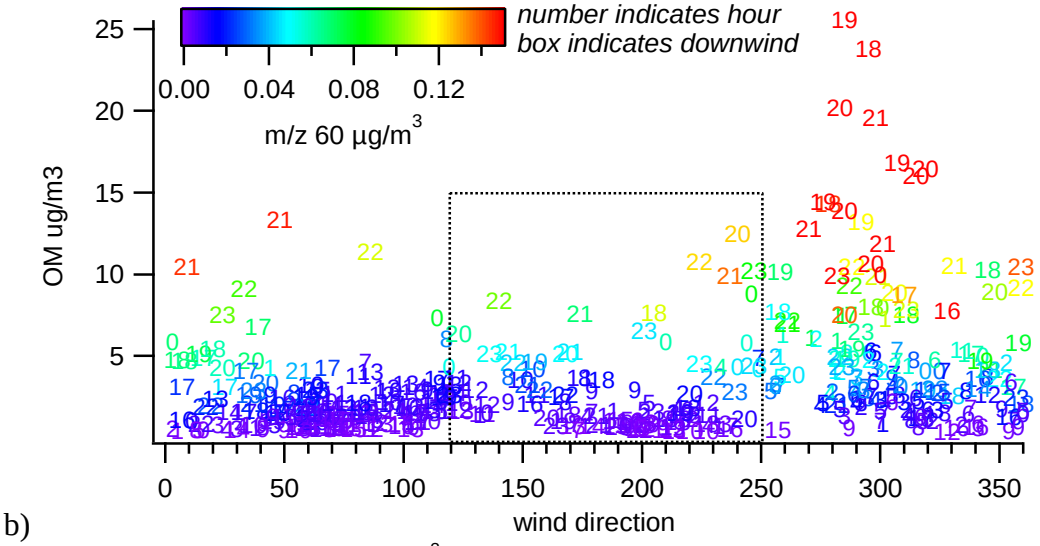

b)

Figure 3-10. OM concentrations (µg/m^3) versus wind direction, where number indicates hour of day and a) color indicates wind speed (m/s) and b) color indicates *m/z* 60 concentrations (µg/m^3). The box shows the angle when the monitoring site is downwind of the freeway.

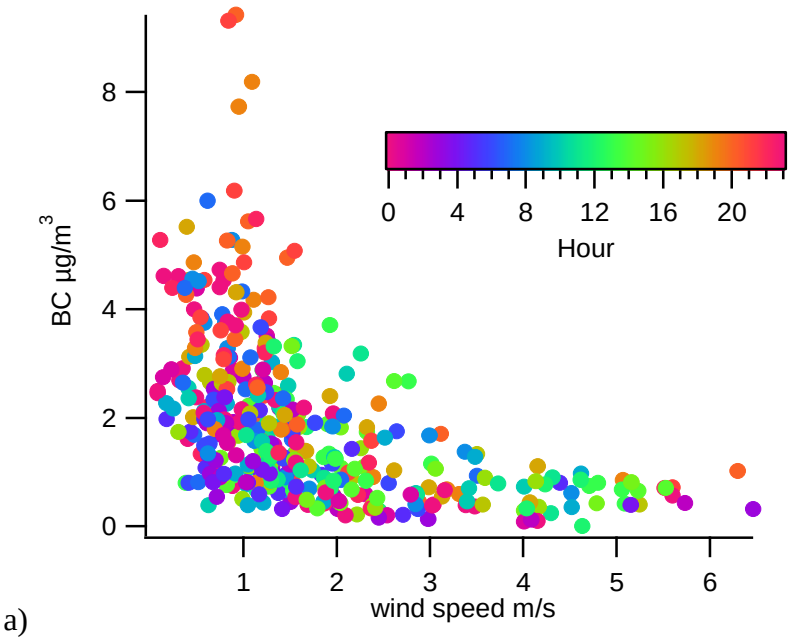

a)

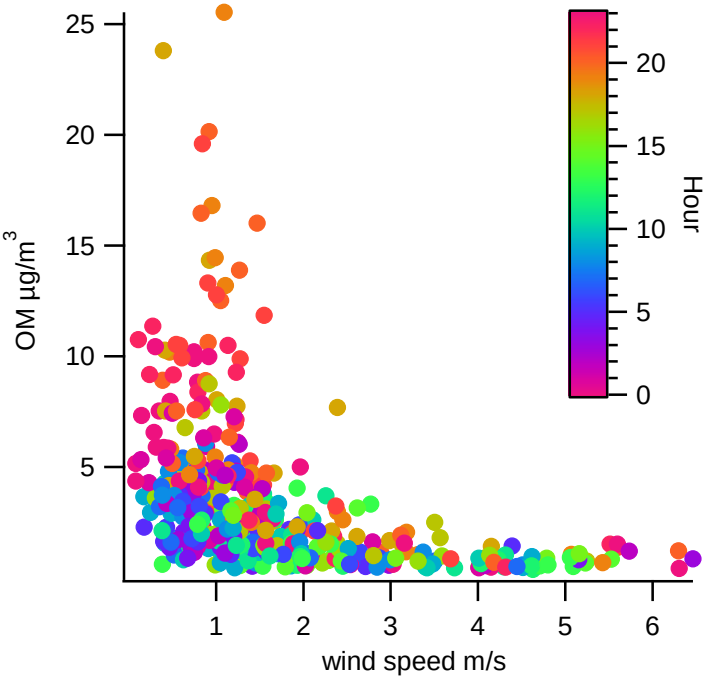

b)

Figure 3-11. Concentrations (µg/m^3) with relation to wind speed (m/s), colored by hour: a) of BC; and b) of OM.

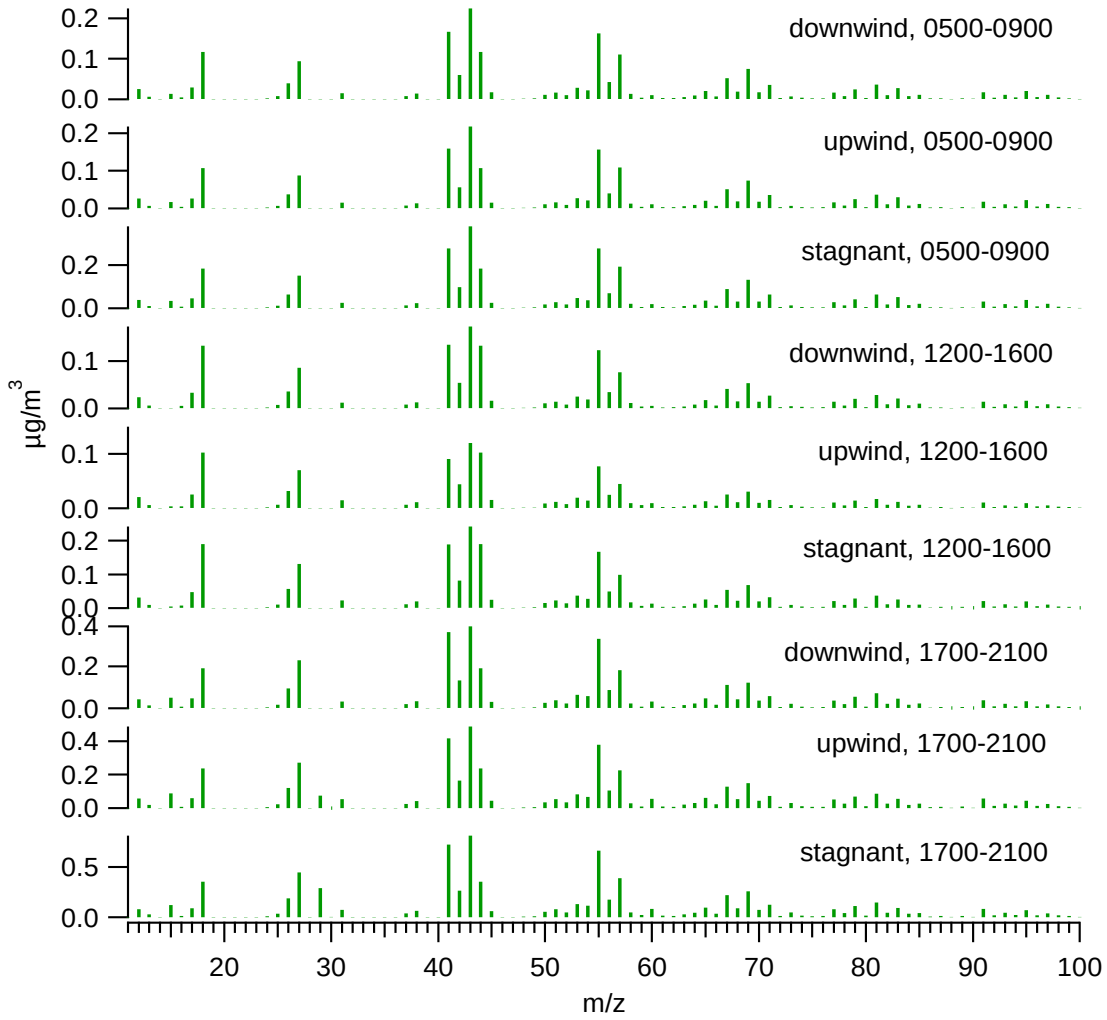

Figure 3-12. Average organic mass spectra (µg/m^3) during upwind, downwind and stagnant conditions in the morning (0500-0900 LST), midday (1200-1600 LST) and evening (1700-2100 LST).

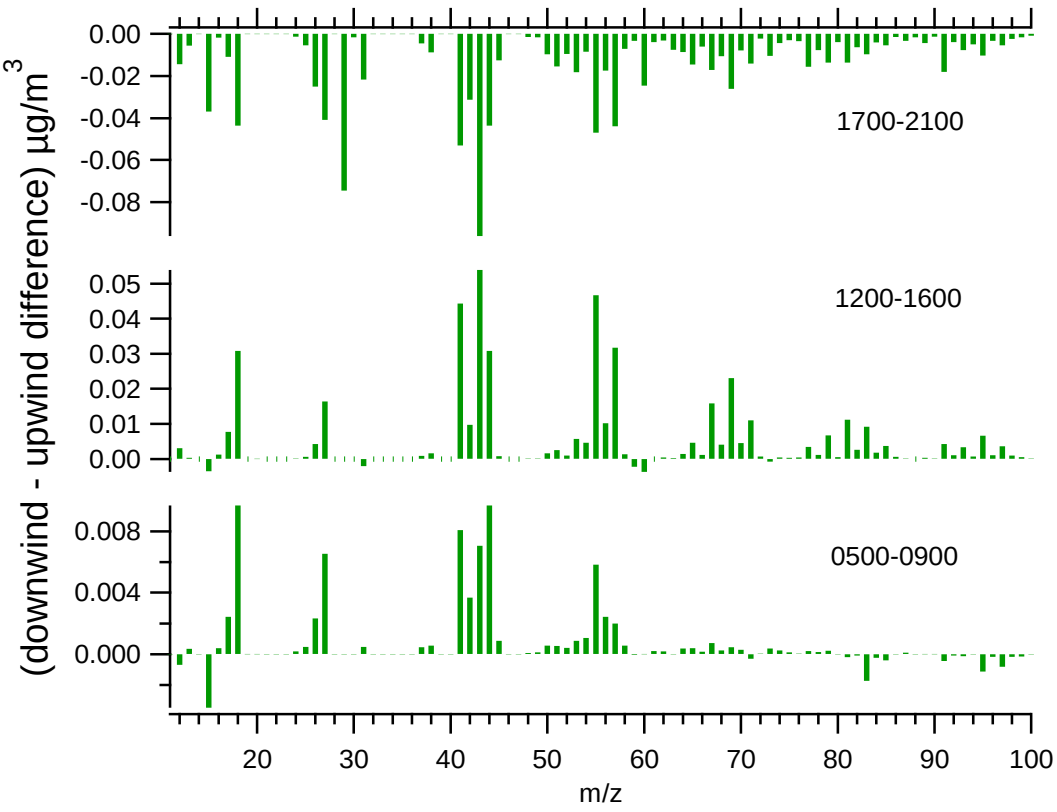

Figure 3-13. Difference between the mass spectrum (µg/m^3) during downwind and upwind conditions in the morning (0500-0900 LST), midday (1200-1600 LST) and evening (1700-2100 LST). Positive values indicate higher concentrations downwind.

In addition to wind direction and speed, temperature can also influence OM concentrations; gas-to-particle partitioning increases with lower temperatures. Figure 3-14 shows the relationship of OM with temperature; numbers indicate the hour of the day, and colors indicate the concentrations of the biomass burning indicator *m/z* 60. There was no clear relationship between temperature and OM, as OM was highest during modest temperatures (6-12 degrees C), though the coldest temperatures (i.e., below 4 degrees C) typically occurred during the very early morning and when wind speeds were higher, and thus when OM is generally low.

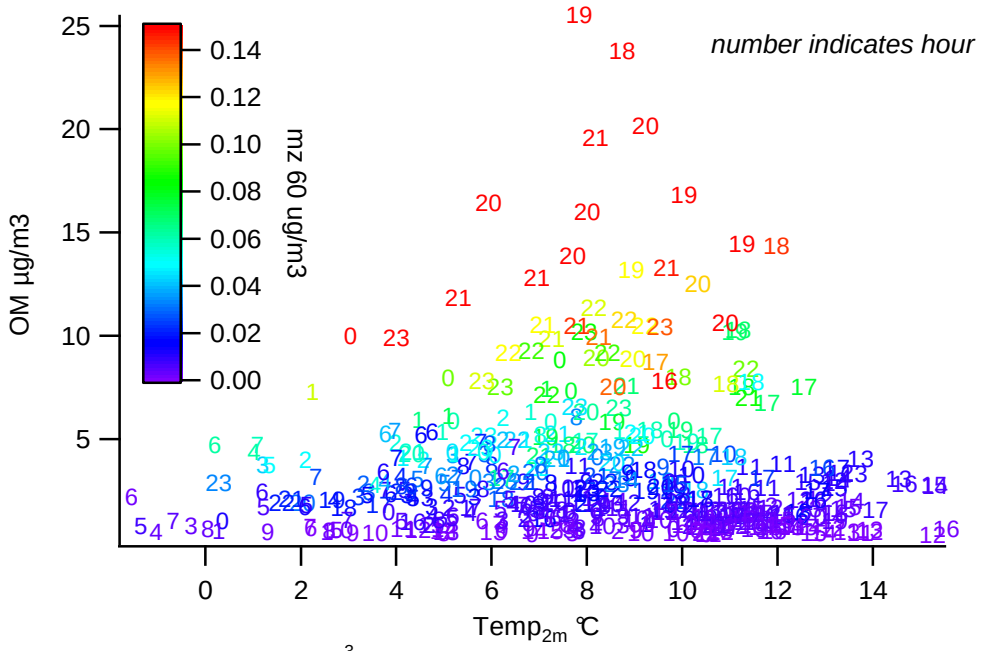

Figure 3-14. OM concentrations (µg/m^3) by temperature (degrees C). The number indicates the hour of the day, and color shows the concentration (µg/m^3) of *m/z* 60.

3.3 Comparisons Between Measurements of Aerosol Species

A number of collocated measurements were made during the study. Measurements of sulfate and nitrate were made via both HR-AMS and PILS, though sulfate concentrations (median via AMS of 0.16 µg/m^3) were generally below PILS lower limit of quantification (e.g., http://eosweb.larc.nasa.gov/PRODOCS/narsto/document/STL_Supersite_QAFR_v1.pdf) so a comparison is not shown. A Sunset OCEC measured $PM_{2.5}$ OC and EC, which can be compared to HR-AMS OM or derived-OC and Aethalometer BC, respectively. Scatter plots between measurements for these species are shown in figure 3-15. Nitrate comparisons between AMS and PILS shows very good agreement (r^2=0.95), though with some modest bias towards the PILS (median PILS/AMS ratio = 1.3); this bias is most evident at lower concentrations below 2 µg/m^3. Aethalometer BC and Sunset EC also compared very well (r^2=0.95), but with a significant bias, with average BC/EC ratio equal to 1.83. This bias was consistent across all levels of concentration, and had no relationship with OM concentration or time of day.

AMS-inferred OC data were averaged for comparison to the hourly Sunset OC data. AMS PM_1 OC concentrations and Sunset $PM_{2.5}$ OC concentrations compared well (median difference = 0.05 $\mu g/m^3$, r^2=0.89, slope = 0.91; assuming y-intercept=0) across all times of day, with the poorest relationship occurring when OC concentrations were less than 0.5 $\mu g/ m^3$ (Figure 3-15). The average and median hourly OC_{ams} concentrations during the study were 2.3 and 1.5 $\mu g/m^3$, while the average and median Sunset OC concentrations were 2.4 and 1.5 $\mu g/m^3$. The correlation between the AMS and Sunset measurements is similar to or stronger than other studies, such as in Tokyo (Takegawa et al., 2005) or in Riverside (Docherty et al., 2011), perhaps because in the Las Vegas study the source mixture is less variable than in other studies.

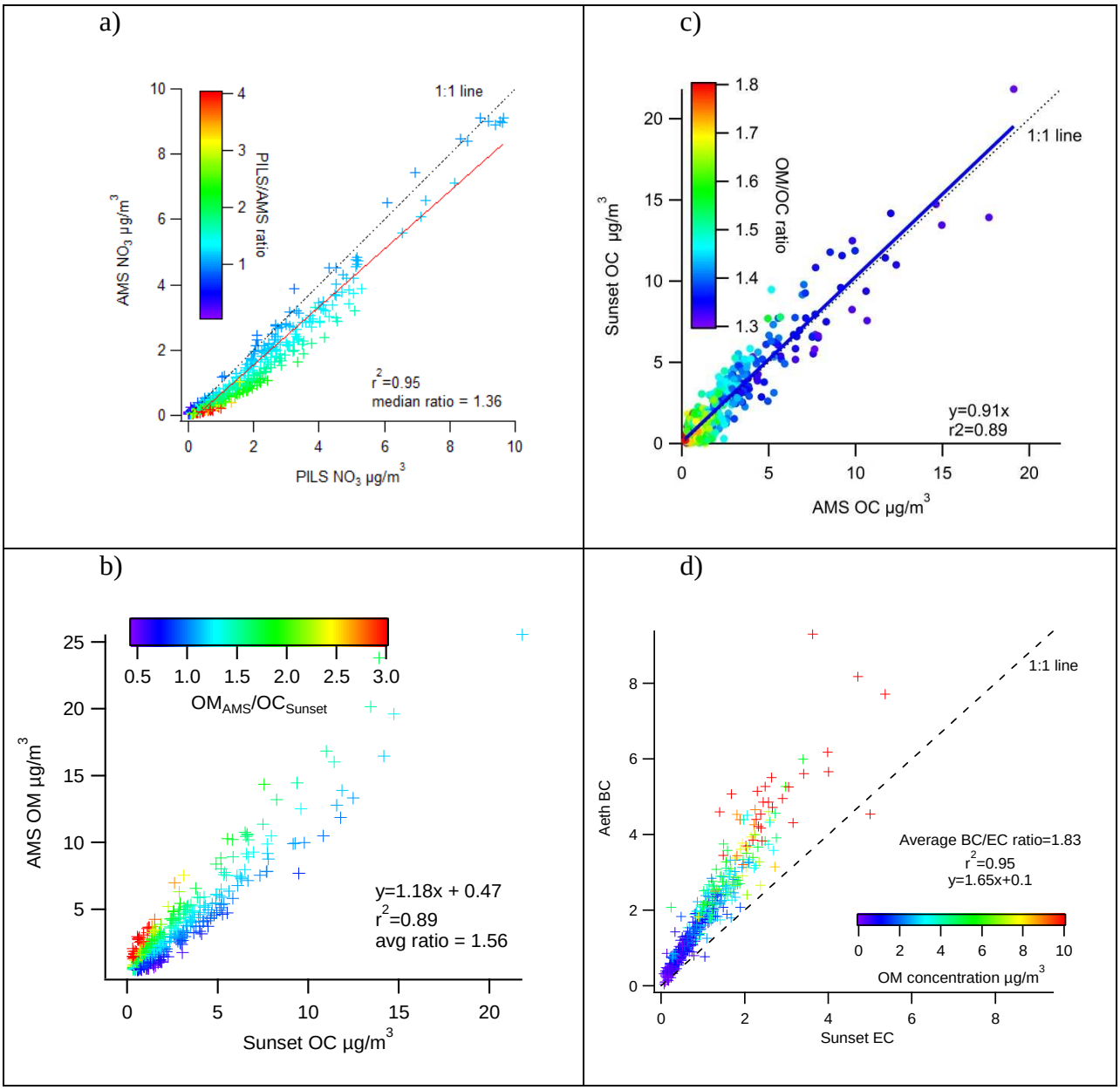

Figure 3-15. Comparison between measurements: a) hourly averaged AMS and PILS NO_3; b) hourly averaged AMS OM and Sunset OC; c) AMS-derived OC and Sunset OC; and d) Aethalometer BC with Sunset EC. All units are µg/m^3.

3.4 Factor Analysis via PMF

3.4.1 Data

A matrix of 7,455 2-minute HR-AMS V-mode observations of 198 unit mass resolution (UMR) fragments made every 4 minutes during January 2008 at Fyfe was used in EPA PMF analysis. Fragments predominantly from inorganic species such as nitrate and sulfate were not retained for EPA PMF analysis. Fragments *m/z* 15, 18, 19, 20, 29, and 30 were excluded from EPA PMF analysis because of potential interference with nitrogen and oxygen. While data up to *m/z* 700 are available, many fragments above *m/z* 200 had low signal-to-noise (S/N) ratios (i.e., less than 6), made a minimal contribution to total OM, and were collinear with a number of other fragments. Fragments up to *m/z* 240 were retained for EPA PMF, a total of 198 fragments. Fragments with low S/N may bias the results (Paatero and Hopke, 2003), so the uncertainties of a given fragment were multiplied by 3 if the S/N for the fragment was less than 6; this reduces the fragment's influence on the solution. A global 10% uncertainty was also applied to account for additional modeling uncertainty (Norris et al., 2008). EPA PMF was run in the robust mode, which reduces the influence of outliers.

Each observation was also classified as downwind (wind speed greater than 2 m/s and wind direction between 90 and 270 degrees; N=1,360); upwind (wind speed greater than 2 m/s and wind direction between 310 and 60 degrees; N=949); other (wind speed greater than 2 m/s and wind direction between 60 and 90 degrees or between 270 and 310 degrees; N=461); or calm (wind speed less than 2 m/s; N=4,907). As an additional set of runs, EPA PMF was also applied to downwind-only data to examine whether factor profiles change, and how factor contributions change. Since downwind-only data are more heavily influenced by the freeway, we may expect

that a downwind-only HOA factor would be more similar to vehicle exhaust source profiles than when all data are used.

The AMS PMF results were averaged up to 20-minute intervals to allow for matching with the collocated 5-minute data, which were also averaged up to 20-minute intervals. The 20-minute averaged AMS data (N=1491) were also re-analyzed with EPA PMF to evaluate the impact of high-mass transient events; profiles and contributions were then compared to the results using 2-minute data. Factor profiles were compared to PMF factor profiles from earlier ambient studies (Lanz et al., 2008; Lanz et al., 2007; Ulbrich et al., 2009a; Ulbrich et al., 2009b) as well as to source profiles (Mohr et al., 2009; Sage et al., 2008; Weimer et al., 2008) originating from a publicly available online database of reference spectra hosted by University of Colorado (Ulbrich et al., 2009a; Ulbrich et al., 2009b). Specifically, source profiles of Honda gasoline exhaust and diesel exhaust (Mohr et al., 2009), PMF-resolved OOA and HOA factor profiles from Pittsburgh (Zhang et al., 2005a; Zhang et al., 2005b), BBOA factor profiles from Switzerland (Lanz et al., 2010; Lanz et al., 2008; Lanz et al., 2007), aged diesel exhaust profile from chamber experiments (Sage et al., 2008), and burning and smoldering oak and chestnut wood source profiles (Weimer et al., 2008) were used.

3.4.2 PMF Analysis Summary

Three- to six-factor solutions were explored with EPA PMF. Initially, 50 runs from a random seed were performed for each number of factors. Random starting seeds were used to increase the likelihood of finding a global minimum of the goodness-of-fit parameter, *Q*. The stability of *Q* over these runs, the ratio of *Q* to expected (theoretical) *Q*, scaled residuals, the $Q/Q_{expected}$ by fragment and sample, and factor independence (G-space plots) were examined. If these parameters are not stable for a given number of factors, it indicates that a global minimum

was not consistently achieved, and that a solution may not be stable (Norris et al., 2008; Reff et al., 2007). In all solutions, the total OM was well apportioned (i.e., slope equal to 1.0±0.10) and r^2 was greater than 0.95 between apportioned and total OM.

PMF factors were classified by their temporal pattern and the comparison of their profile with source profiles and profiles from previous studies. The typical AMS PMF factors of HOA, LV-OOA, and BBOA were resolved in every solution with three or more factors, and the identification of each factor profile was based on its similarity to profiles available in the literature, the abundance of key fragments in each profile, and each factor's temporal pattern. For example, the LV-OOA factors displayed a significant amount of *m/z* 44 and were similar to the OOA factor identified in Pittsburgh and elsewhere. BBOA factors had typical tracer fragments of *m/z* 60 and 73, which are produced during AMS analysis of levoglucosan and related anhydrosugars produced during biomass combustion (Lee et al., 2010; Lanz et al., 2008; Sandradewi et al., 2008; Schneider et al., 2006). The HOA factors were similar to the HOA factor from Pittsburgh and a diesel exhaust source profile.

With more than three factors, semi-volatile OOA (SV-OOA) was also resolved. This factor's profile was similar to that of aged diesel exhaust and was more episodic than HOA or LV-OOA profiles. With five and six factors, additional factors that occurred during the nighttime were resolved. The additional nighttime factors occurred nearly every night coincident with BBOA between 1700 and 0200 LST, and contributions were higher with low wind speed conditions and with winds from the north (upwind). With peaks of *m/z* 41, 43, 55, and 91, it is unclear what these "night OA" factors may represent. The change in the BBOA between the four- and five-factor solutions and its temporal variability suggest the additional fifth factor may be related to biomass burning, but the lack of known tracer fragments and correlation with source

profiles makes this link difficult to prove. We focused the remainder of the analyses on the four-factor solution. Figure 3-16 summarizes the amount of OM apportioned by factor and a comparison of measured and apportioned OM. In the 4 factor solution, PMF on average under-apportioned the OM, with an average difference between the sum of PMF factors and the measured OM of 0.18 $\mu g/m^3$. Table 3-1 summarizes the correlation of factor profiles with selected source, aged source, and PMF factor profiles from other studies.

a)

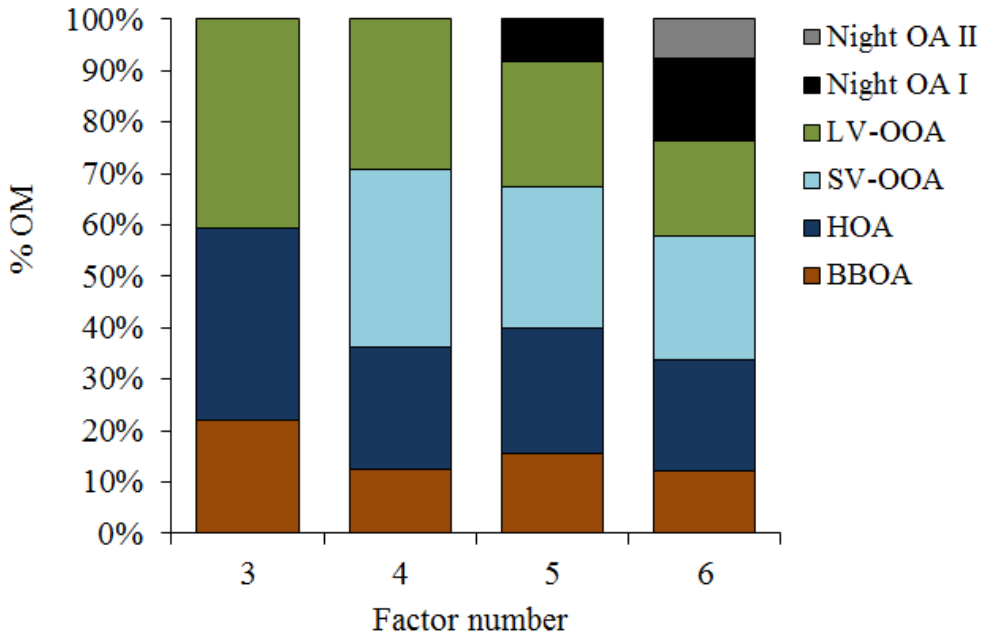

b)

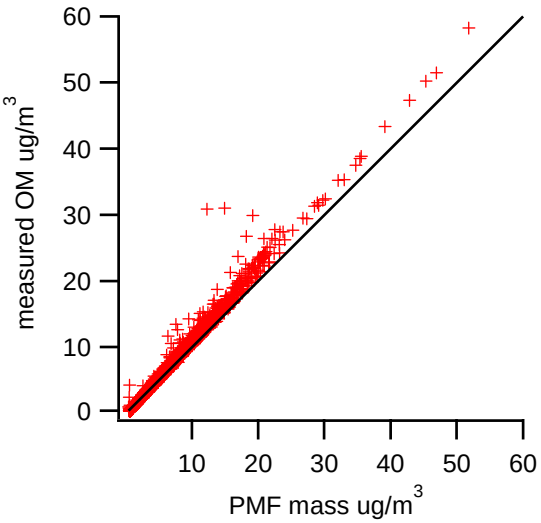

Figure 3-16. a) OM apportioned by factor number, and b) comparison of measured and apportioned OM, with a 1:1 line. Figures are reproduced under Creative Commons Attribution 3.0, originally published in Brown et al., 2012.

Table 3-1. Correlation (r^2) of PMF factor profiles with Pittsburgh OOA PMF profile (Zhang et al., 2005a), Pittsburgh HOA PMF profile, gasoline and diesel exhaust source profiles (Mohr et al., 2009), aged diesel exhaust profile (Sage et al., 2008), charbroil source profile(Lanz et al., 2007), oak-flame source profile (Weimer et al., 2008), oak-smolder source profile, chestnut-flame source profile, chestnut-smolder source profile, and levoglucosan profile (Schneider et al., 2006). Correlations from 0.80 to 0.90 are denoted in italics, and those greater than 0.90 are denoted in bold.

N	Factor	Pitt HOA	gas-oline	Diesel	Pitt OOA	Aged diesel	charbroil	Oak smolder	Oak flame	levo-glucosan	Chestnut flame	Chestnut smolder
3	LV-OOA	0.59	0.58	0.58	**0.98**	**0.95**	0.26	*0.88*	**0.91**	0.74	*0.83*	*0.89*
	HOA	**0.97**	**0.92**	**0.95**	0.46	0.75	0.57	0.29	0.71	0.49	0.50	0.62
	BBOA	*0.80*	0.73	0.76	0.67	*0.82*	0.40	0.44	*0.89*	0.77	0.77	*0.85*
4	LV-OOA	0.38	0.39	0.38	**0.99**	*0.87*	0.13	**0.93**	*0.83*	0.70	0.80	*0.84*
	HOA	**0.99**	**0.96**	**0.98**	0.48	0.77	0.60	0.32	0.69	0.48	0.50	0.62
	BBOA	0.47	0.41	0.44	0.59	0.64	0.20	0.39	0.75	*0.80*	0.77	*0.80*
	SV-OOA	**0.91**	*0.84*	*0.87*	0.57	0.79	0.49	0.37	0.80	0.58	0.60	0.71
5	LV-OOA	0.46	0.46	0.46	**0.99**	**0.90**	0.18	**0.91**	*0.88*	0.72	*0.82*	*0.87*
	HOA	**0.99**	**0.97**	**0.98**	0.47	0.78	0.61	0.32	0.68	0.49	0.50	0.62
	BBOA	0.71	0.69	0.69	*0.86*	**0.91**	0.37	0.69	**0.95**	*0.89*	**0.91**	**0.97**
	SV-OOA	*0.90*	*0.82*	*0.85*	0.56	0.78	0.47	0.37	0.79	0.56	0.58	0.69
	Night OA I	0.60	0.51	0.59	0.42	0.61	0.27	0.26	0.57	0.30	0.35	0.45
6	LV-OOA	0.13	0.16	0.15	0.59	0.46	0.05	0.54	0.47	0.44	0.51	0.51
	HOA	0.12	0.17	0.14	0.55	0.38	0.11	0.60	0.42	0.43	0.49	0.48
	BBOA	0.24	0.26	0.24	0.72	0.57	0.13	0.66	0.59	0.56	0.63	0.64
	SV-OOA	0.24	0.28	0.25	0.61	0.48	0.12	0.60	0.54	0.54	0.59	0.61
	Night OA I	0.33	0.36	0.34	0.54	0.48	0.16	0.47	0.53	0.55	0.56	0.61
	Night OA II	0.14	0.16	0.15	0.49	0.35	0.03	0.47	0.42	0.42	0.44	0.47

3.4.3 Factor Analysis Details

The factors in the four-factor solution were HOA, LV-OOA, and BBOA factors, plus a semi-volatile OOA (SV-OOA) factor. The HOA and LV-OOA factors were better resolved than in the three-factor solution. Profiles of each factor, the average factor concentration plus other species' concentrations by hour, and a time series of concentrations are provided in Figures 3-17 to 3-21. Figure 3-22 provides scatter plots of factor contributions with selected collocated measurements: HOA with BC, HOA with CO, SV-OOA with nitrate, and LV-OOA with sulfate. Factor profiles were compared to profiles available in the literature to help confirm identification; regression statistics were reported using Pearson correlation values, and each scatter plot associated with the regression statistics was examined to ensure that the correlation was not biased by the large range of concentrations of the individual *m/z* fragments. Bootstrapping, in which many runs are used to gauge the uncertainty of the base solution (in this case 300 runs with an r^2 of 0.60), showed good reproducibility of the factors. All factors were reproduced at least 98% of the time, demonstrating that these factors are stable and characterize the solution space well.

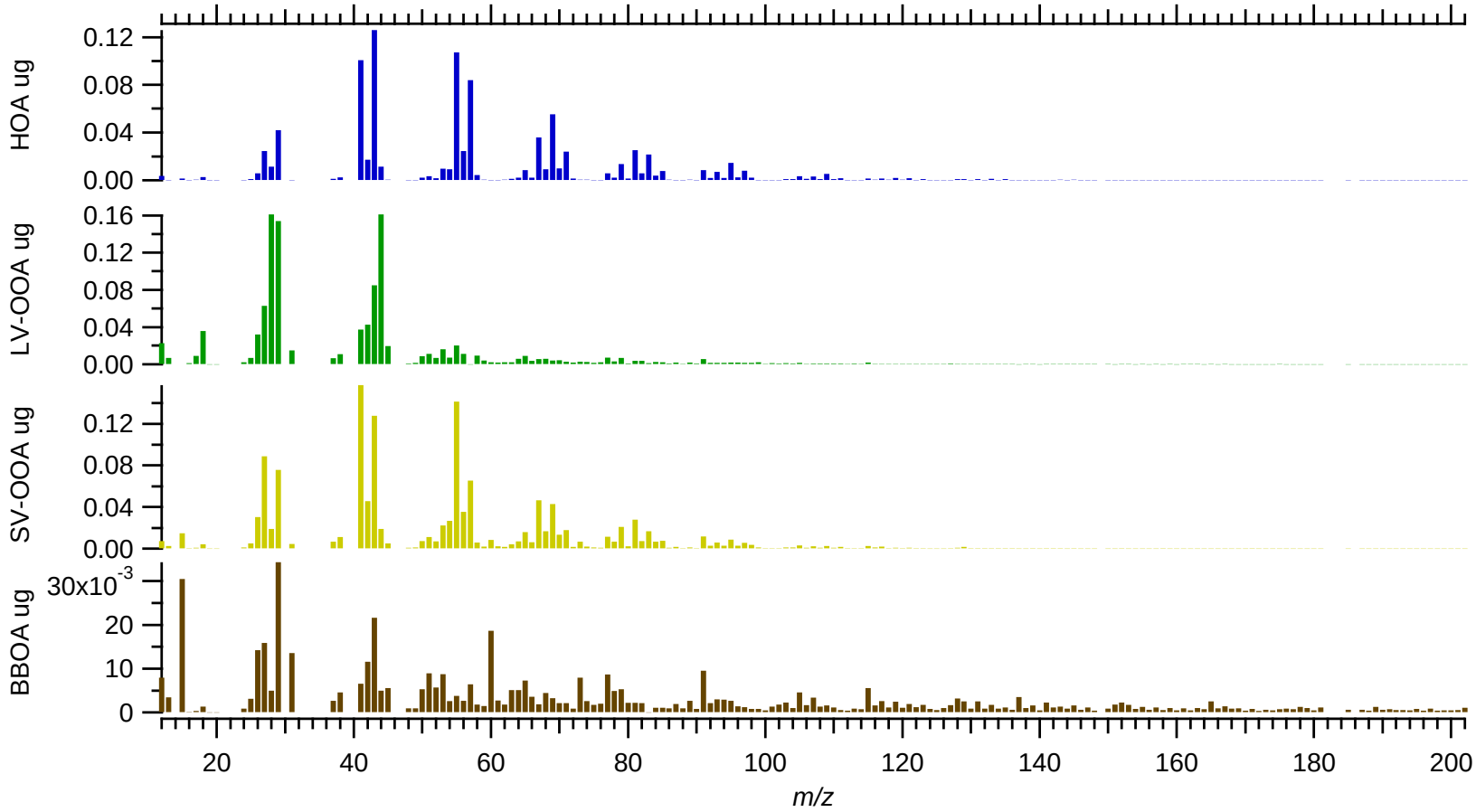

Figure 3-17. PMF factor profiles through *m/z* 200 for the four-factor solution. Figure is reproduced under Creative Commons Attribution 3.0, originally published in Brown et al., 2012.

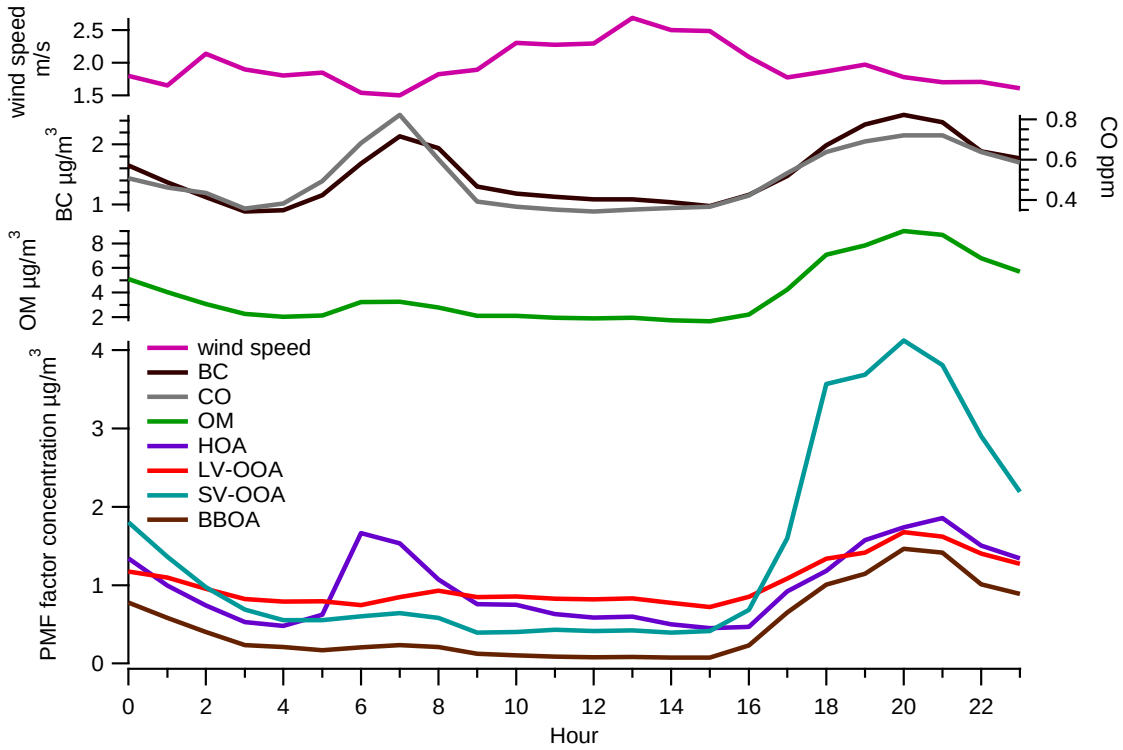

Figure 3-18. PMF factor contributions, OM, BC, CO, and wind speed averaged by hour. Figure is reproduced under Creative Commons Attribution 3.0, originally published in Brown et al., 2012.

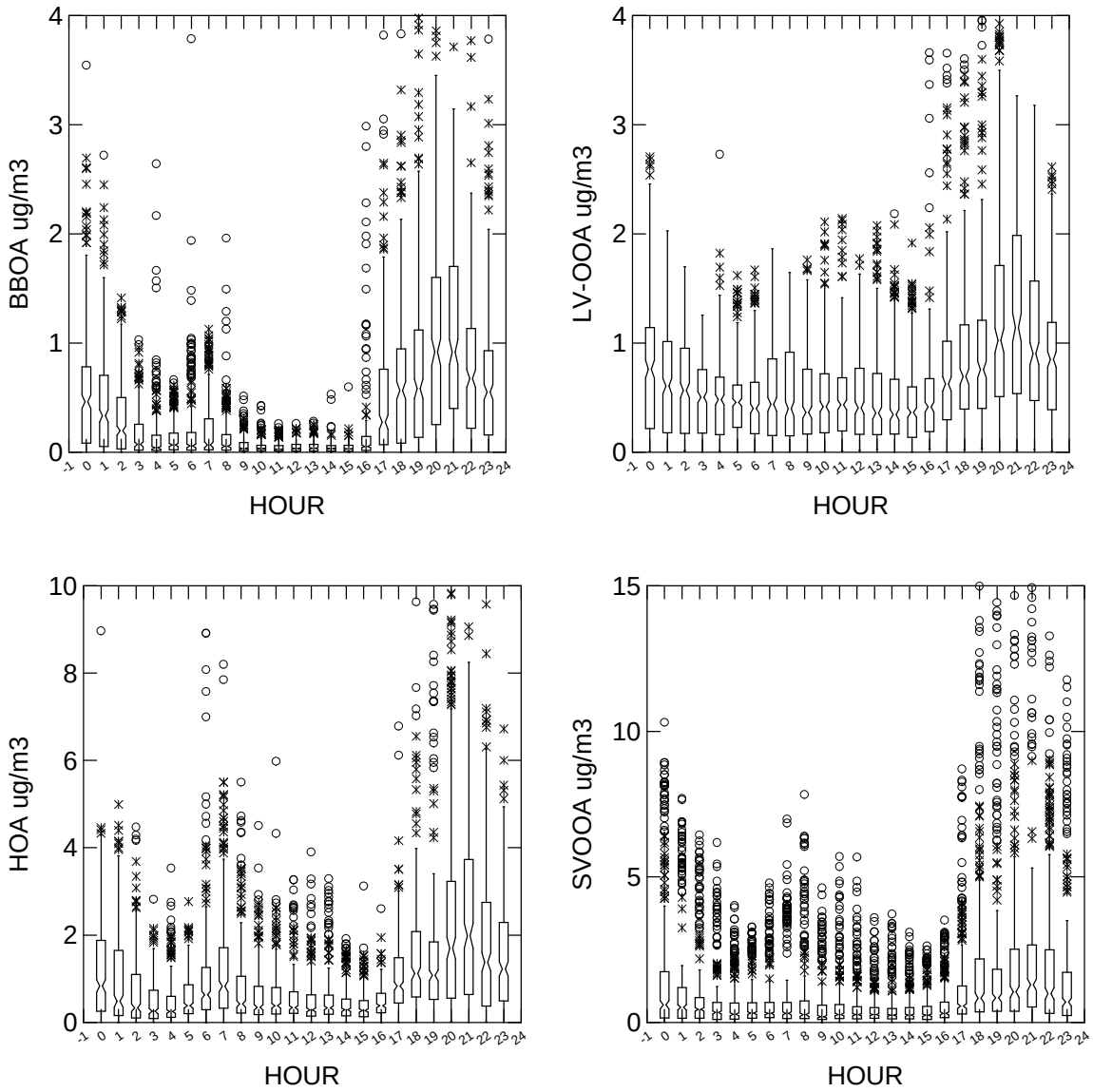

Figure 3-19. Notched box plots of factor contributions (μg/m^3) by hour in the four-factor solution for BBOA, LV-OOA, HOA, and SV-OOA (μg/m^3). Notches indicate median, the boxes the interquartile range (IQR), the whiskers 1.5*IQR, and the points beyond the 1.5*IQR are plotted individually. Figures are reproduced under Creative Commons Attribution 3.0, originally published in Brown et al., 2012.

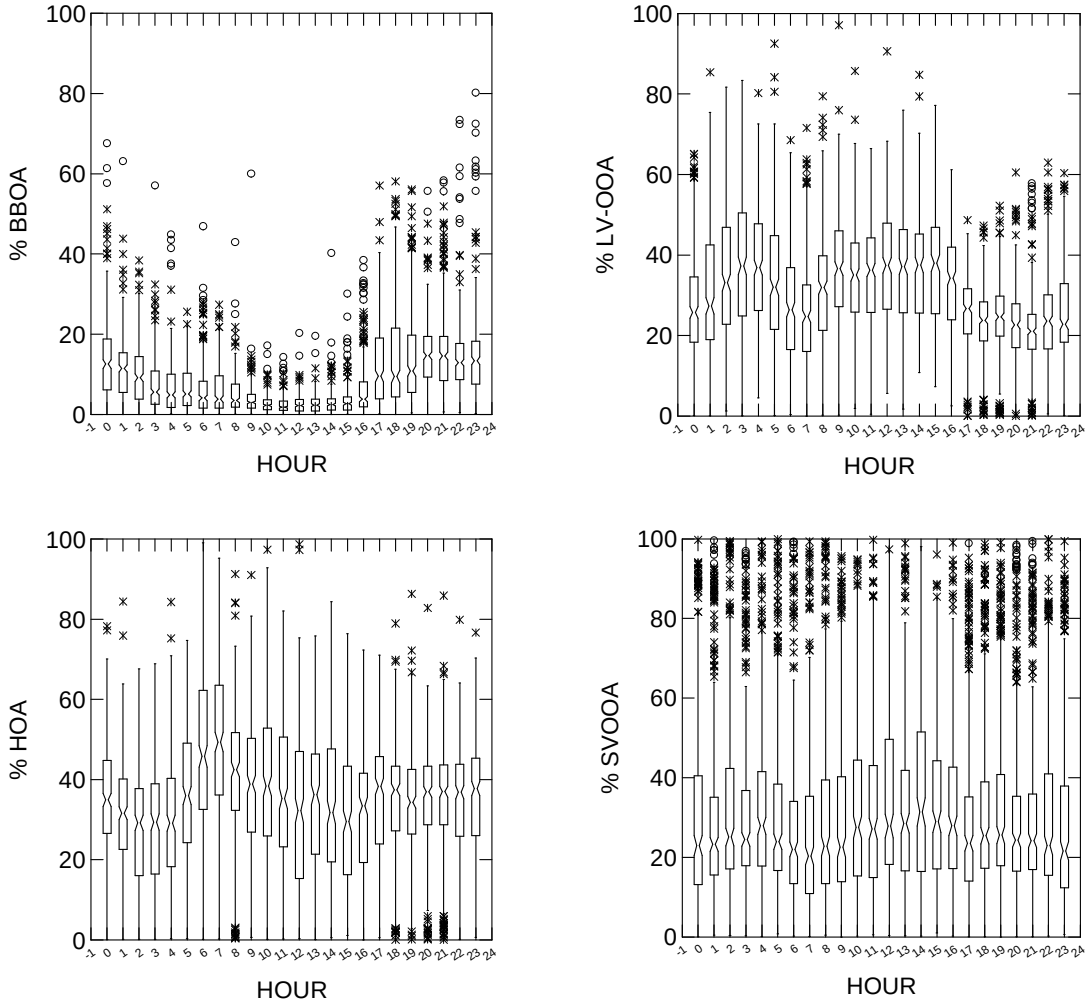

Figure 3-20. Notched box plots of factor contributions (% of total OM) by hour in the four-factor solution for BBOA, LV-OOA, HOA, and SV-OOA (μg/m^3). Notches indicate median, the boxes the interquartile range (IQR), the whiskers 1.5*IQR, and the points beyond the 1.5*IQR are plotted individually. Figures are reproduced under Creative Commons Attribution 3.0, originally published in Brown et al., 2012.

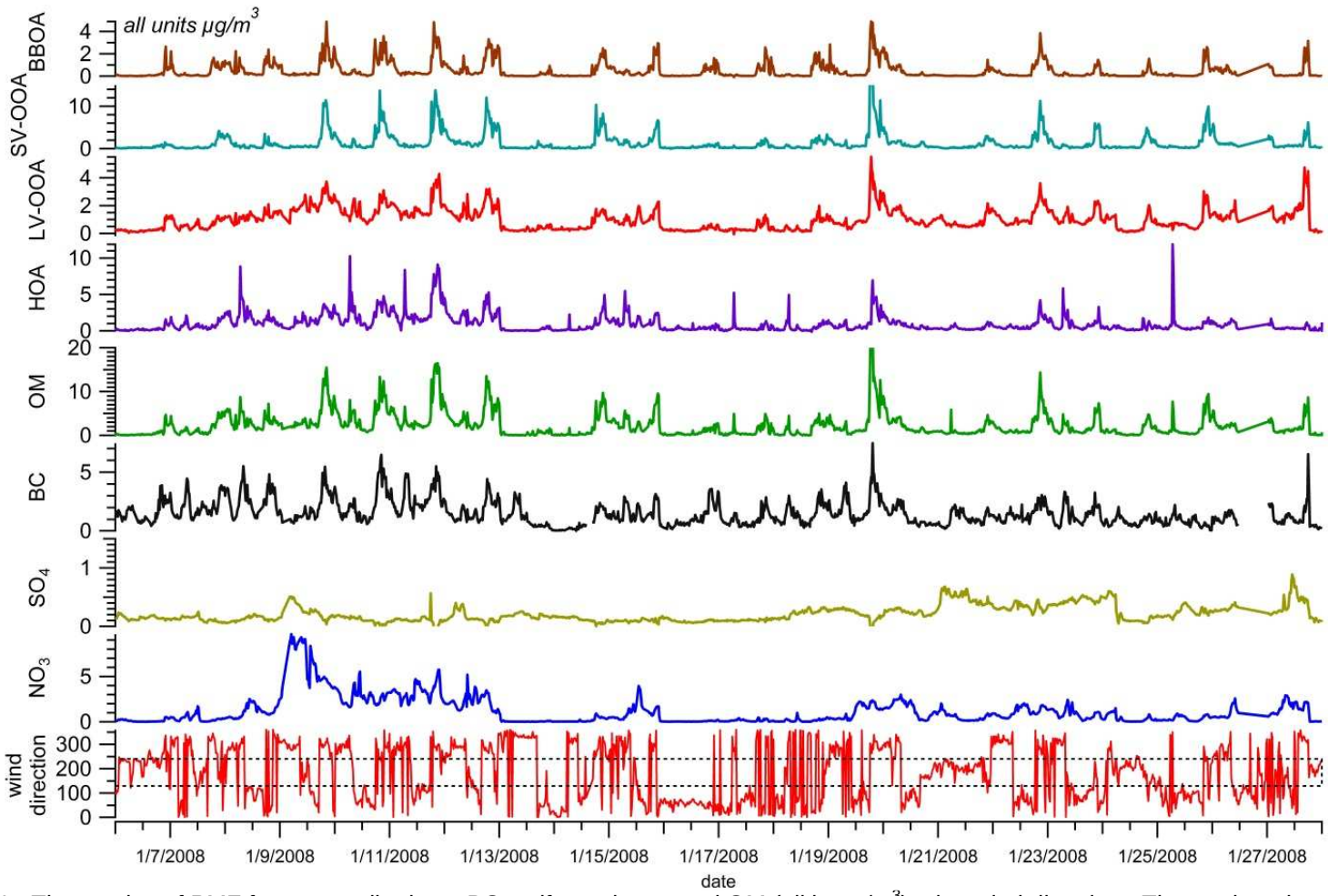

Figure 3-21. Time series of PMF factor contributions, BC, sulfate, nitrate, and OM (all in µg/m^3), plus wind direction. Times when the monitoring site is downwind are outlined by the dashed box. Figure is reproduced under Creative Commons Attribution 3.0, originally published in Brown et al., 2012.

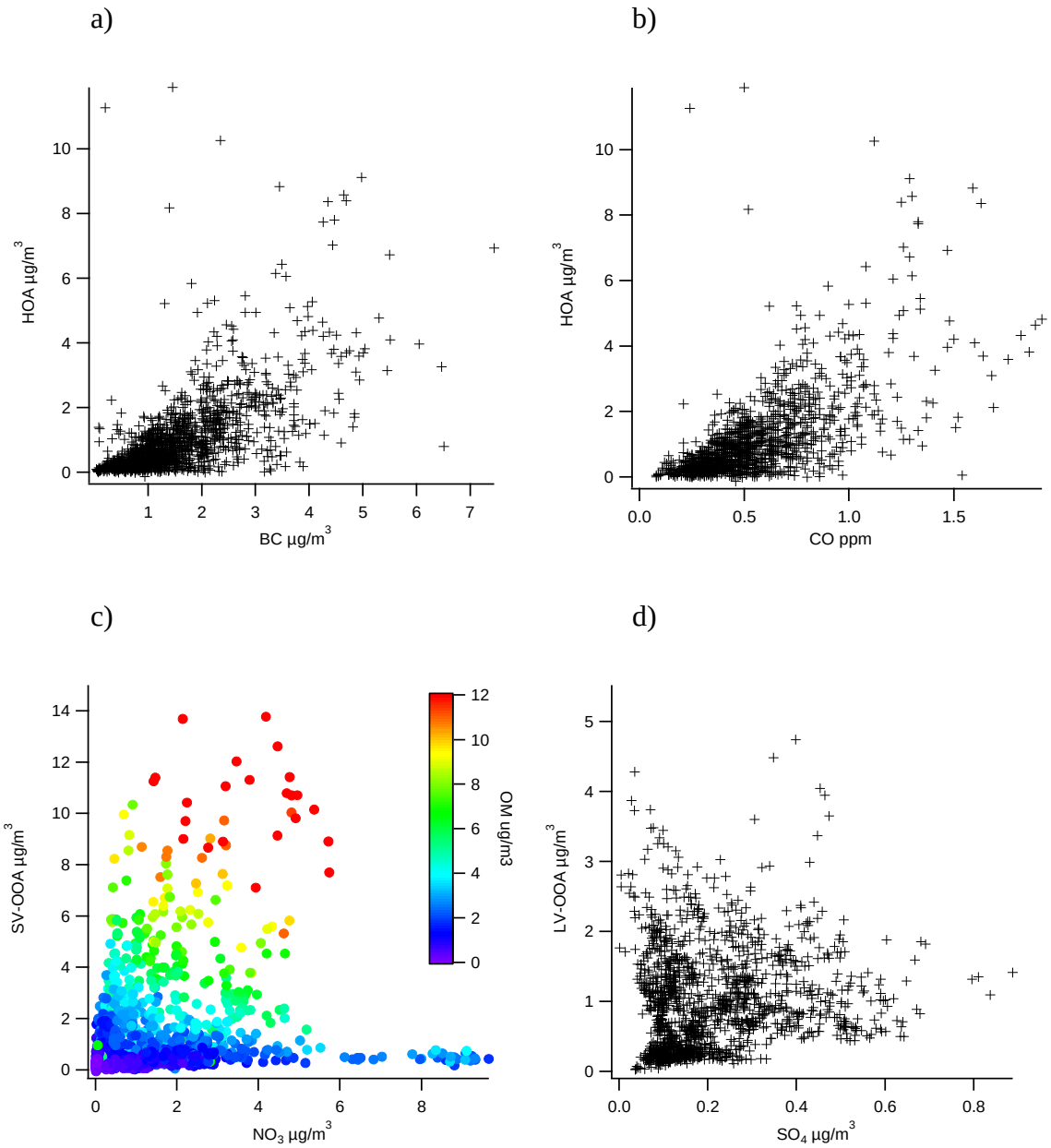

Figure 3-22. Scatter plot comparisons of PMF factor contributions for: a) HOA and BC; b) HOA and CO; c) SV-OOA and nitrate; and d) LV-OOA and sulfate. Figure is reproduced under Creative Commons Attribution 3.0, originally published in Brown et al., 2012.

The LV-OOA factor displayed the typical high amount of *m/z* 44 but with a lower amount of *m/z* 43 than in the three-factor solution, and it showed a high correlation with the

Pittsburgh OOA factor profile (r^2 of 0.99; Table 3-1). LV-OOA accounted for 26% of the OM with four factors and showed only small diurnal variability in its concentration, though it was a much greater percentage of the OM during the daytime than at other times. Similar to other factors and total OM, LV-OOA concentrations were lower at higher wind speeds, though it was a higher percentage of OM at higher wind speeds. LV-OOA showed little correlation with other pollutants; ozone, which often showed a moderate correlation with LV-OOA in other studies, was not measured here. Sulfate is also often correlated with LV-OOA, but during this study sulfate levels were extremely low, with a median of 0.16 $\mu g/m^3$. LV-OOA is heavily oxidized and likely part of a background OM, and it may be transported into Las Vegas. In addition, there are very few SO_2 sources upwind of Las Vegas, so there is very little sulfate transported into the area. Thus, we may not expect LV-OOA concentrations to be correlated with sulfate here.

The BBOA factor accounted for 12% of OM, on average, and was similar to the BBOA factor found in the three-factor solution. This factor had 64% of the *m/z* 60 fragment, which is associated with levoglucosan and related anhydrosugars (Schneider et al., 2006; Lee et al., 2010; Lanz et al., 2007); the contribution from BBOA was well correlated with *m/z* 60 ($r^2 = 0.86$). The remainder of the *m/z* 60 was in SV-OOA (28%) and LV-OOA (8%). This portion of *m/z* 60 is likely from carboxylic acids rather than anhydrosugars. This BBOA factor is most likely from residential wood burning in the evenings rather than wildfire emissions since there was little regional wildfire activity in the winter; furthermore, the contribution was nearly zero during the daytime, with a sharp rise in concentrations nearly every evening after 1700 LST that peaked around 2100 LST. While the BBOA factor concentration began to decrease after around 2100 LST, its relative contribution to OM remained above 15% until after midnight. The factor was highest in terms of both concentration and relative contribution to OM under low wind speed

conditions (i.e., less than 2 m/s). This profile is similar to a smoldering Chestnut profile (r^2=0.80) and the levoglucosan combustion profile (r^2=0.80) (Schneider et al., 2006). This BBOA factor is mostly associated with winds from the north and west—the direction of a large residential neighborhood upwind of the freeway. When using five factors, the BBOA factor profile has even better correlations with both of these profiles (r^2 of 0.89 and 0.91), plus an r^2 of 0.95 with an oak flaming profile. However, since the fifth factor is unidentified, we have focused on the four-factor solution.

The HOA factor accounted for 26% of the OM and had peaks of *m/z* 41, 43, 55, 57, and other fragments typical of hydrocarbon-like fragments. HOA concentrations were highest during the early morning and overnight periods and, as a percent of total OM, the factor's contributions were highest during the early morning (0600-0800 LST). The HOA factor profile has a high correlation with diesel exhaust (r^2=0.98) and gasoline exhaust (r^2=0.96) source profiles (Mohr et al., 2009). The HOA profile here was very similar to that observed in Pittsburgh (r^2=0.99). This factor is likely heavily influenced by the mobile emissions on the adjacent freeway but may also have originated in part from other sources. Similar to concentrations of BBOA and other pollutants such as BC, HOA concentrations rapidly decreased with increases in wind speed, though on a relative basis there was no significant difference in its contribution. With sustained winds (i.e., greater than 2 m/s), HOA concentrations were significantly higher under downwind conditions. HOA had modest correlation with collocated measurements of CO (r^2=0.66), NO_x (r^2=0.64), and BC (r^2=0.68). This may be in part because BC, CO, and NO_x have large differences between upwind and downwind conditions. For example, BC is twice as high under downwind conditions (average 2.3 $\mu g/m^3$) than upwind conditions (average 1.2 $\mu g/m^3$), while OM (and HOA) do not have as large a difference.

The last factor resolved was designated as semi-volatile OOA (SV-OOA), which accounted for 35% of the OM. It showed strong peaks of *m/z* 41, 43, 55, 57, 67, 69, and 71 but also had some contribution from *m/z* 44, with a 43/44 ratio of 6, almost half the value for HOA (11). The SV-OOA factor profile had a moderate correlation with Pittsburgh HOA and with chamber-aged diesel exhaust (r^2 of 0.91 and 0.79, respectively), and lower correlation with Pittsburgh OOA (r^2=0.59). SV-OOA contributions were highest in the evening and overnight hours, though on a relative basis its contributions were generally very consistent across all hours. Like HOA, SV-OOA factor contributions decreased with higher wind speeds, but its relative contribution was not significantly different among wind speed ranges. In other studies, this factor sometimes has a modest correlation with nitrate. Here, nitrate was extremely episodic, in that its concentrations were less than 0.5 $\mu g/m^3$ half the time, with a day-long episode of concentrations greater than 4 $\mu g/m^3$ and a few hours during which concentrations intermittently exceeded 2 $\mu g/m^3$. In contrast, SV-OOA was present during nearly the entire study and had a modest diurnal pattern similar to other factors where it was highest in evening hours.

It is also possible that the SV-OOA factor contains some contribution from cooking organic aerosol (COA), as the SV-OOA factor shows similarities in both profile and temporal patterns to a COA factor found in London and Manchester (Allan et al., 2010). Similar to the COA profile, the largest peaks in the SV-OOA profile are at *m/z* 41 and *m/z* 55, and in both profiles *m/z* 41 is greater than *m/z* 43 and *m/z* 55 is more than twice *m/z* 57; this is in contrast to HOA, where *m/z* 43 is greater than *m/z* 41, and *m/z* 55 is only slightly higher than *m/z* 57. Similar to the COA factor, our SV-OOA factor peaks, on average, in the evening, again in contrast to HOA, which peaks in the morning and evening hours associated with rush hour. There are, however, times when the SV-OOA factor is high that are not likely periods of high

cooking emissions, such as late morning or midday. Expanding to five factors was inconclusive, since the fifth factor was similar to SV-OOA and COA but was generally collinear with BBOA; it was unclear what this fifth factor represented, so we have retained the SV-OOA label for this factor, with the caveat that there is likely some COA influence.

To help confirm factor identification and understand the OM composition difference between upwind and downwind conditions, we examined the factor contributions during downwind (N=1360) and upwind (N=949) conditions and compared them to the average over the study period. We also examined the OM composition under downwind conditions (N=195) from 0500 to 0900 LST, when the impact from emissions on the freeway is expected to be highest. Results are summarized in Figure 3-23. As expected, HOA contributions are higher under downwind conditions; during morning downwind conditions, HOA accounts for 49% of the OM. SV-OOA was, on average, similar during upwind, downwind, and stagnant conditions, except during morning downwind situations when it was only 23% of the OM. The minimal difference with different wind directions suggests that SV-OOA is a slightly aged factor that is not characteristic of direct, primary emissions. BBOA contributions were low, on average, under downwind conditions and higher (16% on average) during upwind conditions. LV-OOA contributions were relatively lower during morning downwind conditions and relatively highest during midday periods, regardless of wind direction.

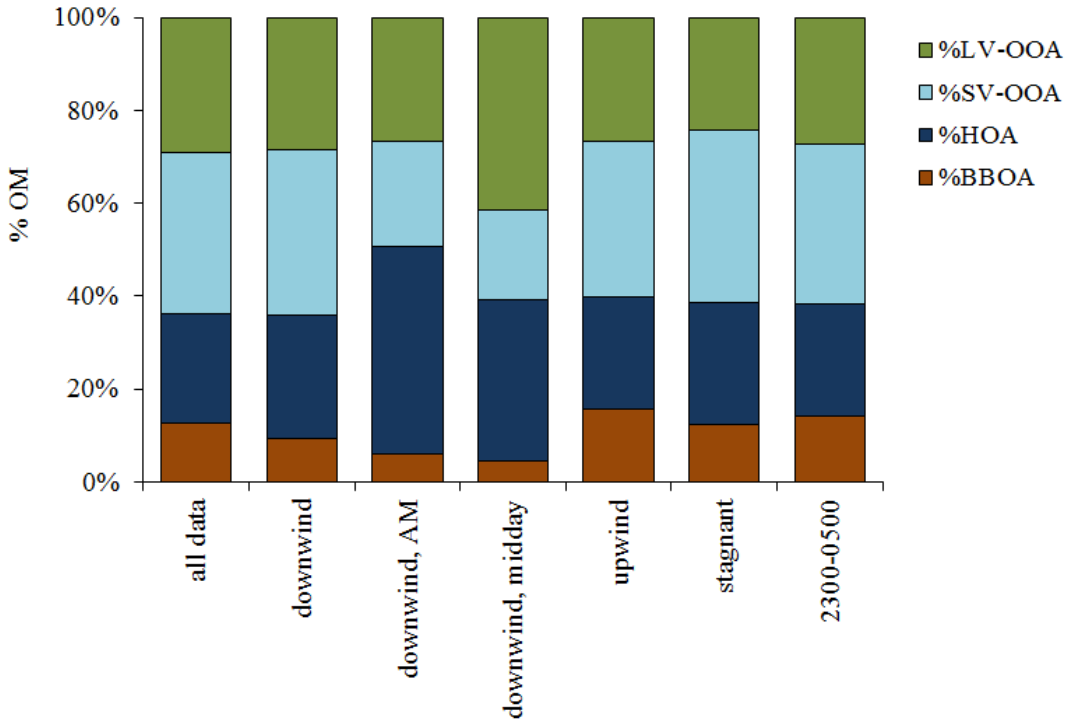

Figure 3-23. Attribution of OM by factor in the four-factor solution over all data, during downwind conditions only, during downwind conditions between 0500 and 0900 LST only, during downwind conditions midday, during upwind conditions only, during stagnant conditions, and during 2300-0500 LST only. Figure is reproduced under Creative Commons Attribution 3.0, originally published in Brown et al., 2012.

3.4.4 Further Analysis of PMF Solution Space

Fpeak is a parameter available in PMF to rotate the entire solution, a process that can help indicate if there is rotational freedom in the solution. G-space plots of the base solution show distinct edges, indicating some factor interdependence. The four-factor solution had the least number of edges (Figure 3-24). An edge between LV-OOA and BBOA occurs in the four-factor solution when BBOA is low but LV-OOA is present. This may be due to the difficulty in finding a "fixed" profile that accounts for BBOA, which likely changes over the course of an evening as the emission rate from biomass burning decreases and the emissions become more processed in the atmosphere. This idea is supported by the six-factor solution, in which additional factors better separate out and apportion BBOA and other sources.

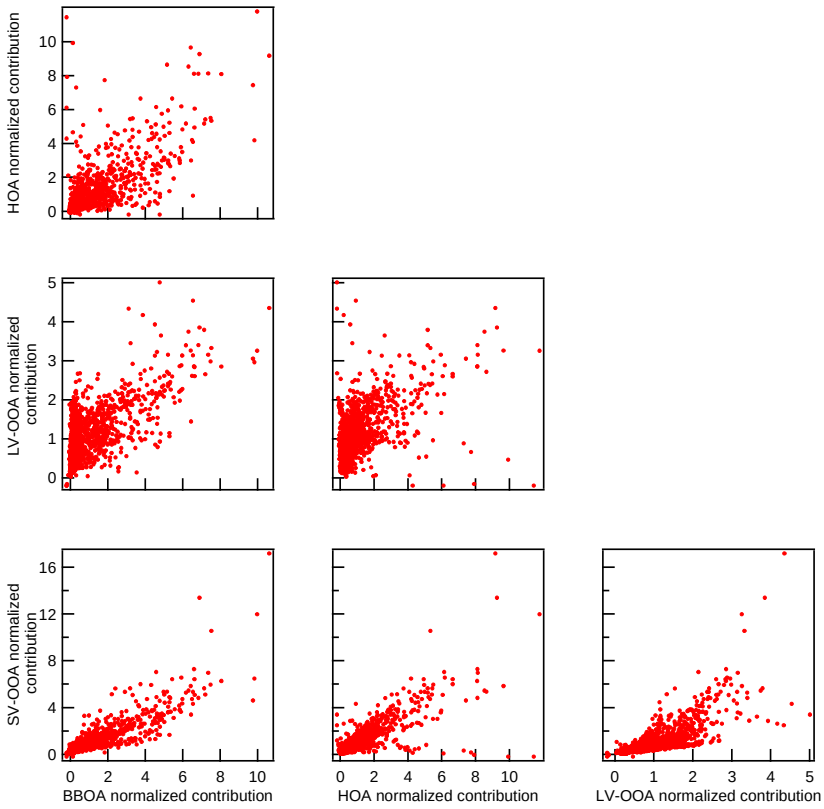

Figure 3-24. G-space plot for the four-factor solution. Figure is reproduced under Creative Commons Attribution 3.0, originally published in Brown et al., 2012.

The plot of HOA and LV-OOA has sufficient points at each axis so that there is no consistent edge away from the axes, but a subset of points shows a consistent ratio of 2.4 between HOA and LV-OOA. These points occur under all conditions throughout the study. In the five-factor solution (not shown) this is still evident, and there is more of an edge in the G-space plot. In the six-factor solution (not shown) this group of points is not as prominent, as the mass of LV-OOA under these high-mass conditions is now associated with night OA II. This suggests that the night OA factors may be informative, even if it is not clear what their sources are.

To ascertain whether the solution changes or whether these edges can be rotated to the y- and x-axes, rotation using Fpeak was performed. PMF runs were conducted with Fpeak values at increments of 2 between 8 and –8 for a total of eight runs. In general, minimal change was seen in the factor profile, contributions, and G-space plots; *Q* increased by less than 0.1% for the runs with the highest Fpeak value and by even less under other Fpeak values. Since there is little change in the solution with Fpeak-induced rotations, the base solution appears to be rotationally unique. The oblique edges in the G-space plots may be due to co-dependence among factors, or modeling errors, such as variation in true source profiles during the monitoring campaign.

The four-factor solution was further explored with ME-2 rotational tools available in EPA PMF. In each scenario, fragment ratios in factor profiles were pulled toward source profile ratios. In one scenario, the ratio of *m/z* 43/44 in the SV-OOA factor (6.75) was pulled toward the *m/z* 43/44 ratio in the 5-hour aged diesel exhaust profile (1.34). In another scenario, the *m/z* 57/55 and 41/43 ratios in HOA (0.78 and 0.80) were pulled to the ratios in the diesel exhaust profile (1.03 and 0.69, respectively). The BBOA factor ratio of *m/z* 60/91 was pulled to the chestnut smolder profile ratio (1.96 to 7.20). Lastly, 157 points along an apparent edge in the SV-OOA versus LV-OOA G-space plot were pulled in an attempt to force additional independence between these factors. Seeing how the solutions change, in terms of factor profiles, *dQ*, and G-space plots, can help us understand the stability of the original solutions. Different maximum *dQ* values were allowed for each combination; 1% and 3% of *Q*(robust) were calculated, and these values were used for the maximum *dQ* allowed for a given pull. In the G-space pull, each point was allowed a *dQ* of 0.2%, for a total *dQ* of 31%.

The results from these pulls are summarized in Table 3-2 and Figure 3-25. Since results were similar with *dQ* values of 1% and 3%, only the *dQ* of 1% are shown, except for the BBOA

pull, where both are provided as an example. In general, most pulls resulted in only minor changes in the HOA and LV-OOA factor profiles and contributions. For example, when the HOA factor was pulled toward the diesel exhaust profile, the correlation between the two increased by only 0.02. In all pulls, the correlation between BBOA and the chestnut smolder profile improved (e.g., correlation improved from 0.79 to 0.88 with the BBOA pull). However this was often at the expense of the SV-OOA profile, where the amount of *m/z* 44 was much lower compared to the base solution, and in some pulls, was actually zero. While LV-OOA and HOA did not vary much between these pulled solutions, the changes in SV-OOA and BBOA profiles and contributions suggest some rotational freedom in these two factors. LV-OOA and HOA factors are similar across many studies, but the SV-OOA and BBOA factors vary among studies, and within this study under different pulling scenarios, because these factor profiles represent semi-fresh factors that are likely changing minute-to-minute in the atmosphere. Overall, the pulling results indicate that the base solution is likely at a global *Q* minima, and that there is little rotational freedom in the unpulled, base solution, in particular regarding the contributions of SV-OOA and BBOA.

With the G-space pull, 157 points along an edge in the LV-OOA/SV-OOA scatter plot were pulled to reduce LV-OOA to zero. LV-OOA concentrations on these points were successfully reduced towards zero, so that the edge was less well defined. This resulted in a *dQ* of 9%, but an improvement in the comparison of the BBOA profile to the chestnut smolder profile (r^2 from 0.79 to 0.93) and in the SV-OOA to aged diesel profile comparison (r^2 from 0.69 to 0.72). The SV-OOA *m/z* 43/44 ratio also decreased from 4.4 to 2.9, which is similar to the ratio of other studies summarized in Ng et al (Ng et al., 2010). HOA and BBOA contributions increased, while LV-OOA and SV-OOA contributions decreased. Even though Q increased by

9%, these results are useful to show that contribution pulls based on the G-space plots helped improve the factor profiles, and to show what may be the bounds in the base solution results.

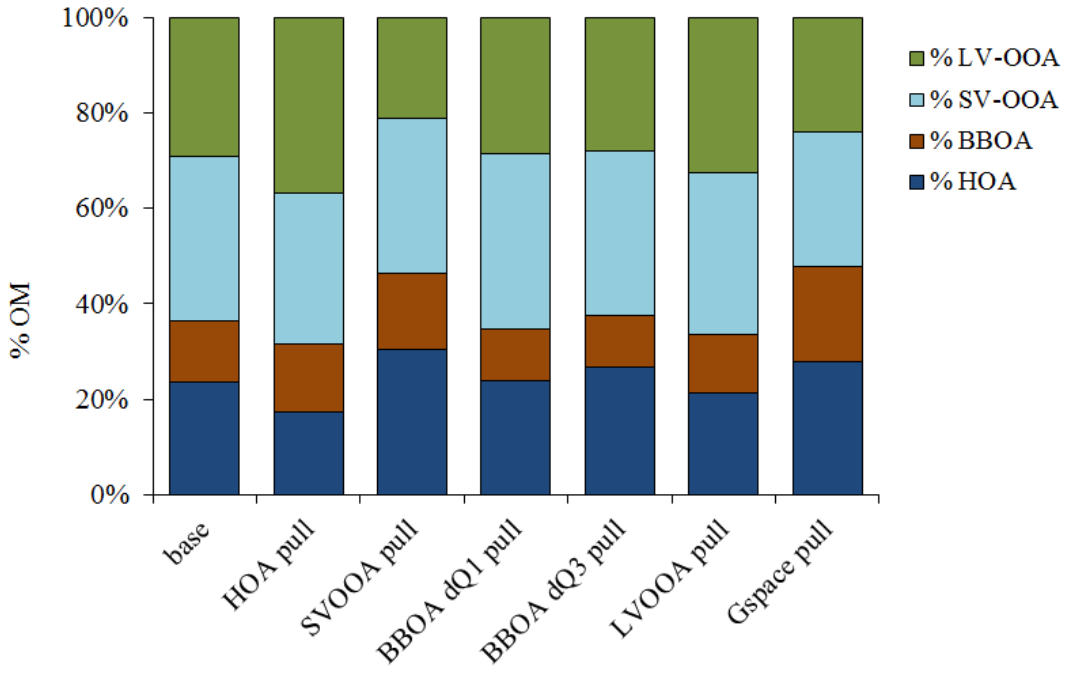

Figure 3-25. Attribution of OM with four factors for base run (base); ratio of *m/z* 41/43 in the HOA profile pulled toward the diesel exhaust profile (HOA pull); ratio of *m/z* 43/44 in the SV-OOA profile pulled toward the 5-hour aged diesel profile (SVOOA pull); ratio of *m/z* 60/91 in the BBOA profile pulled toward the oak-flame source profile with different dQ values (BBOA dQ 1 and 3 pull); *m/z* 44 in LV-OOA profile pulled up maximally (LVOOA pull); and edge points on the HOA/LV-OOA G-space plot pulled down to the y- and x-axes (G space pull). Figure is reproduced under Creative Commons Attribution 3.0, originally published in Brown et al., 2012.

Table 3-2. Summary of pulls on the four-factor solutions, all with a maximum allowed *dQ* of 1%, except for one iteration with BBOA to Chestnut smolder (dQ=3%), and except for the edge points pull, which had a total allowed *dQ* of 31%, or 0.2% per point with a total of 157 points.

Pull	SV-OOA to Aged Diesel	HOA to Diesel	BBOA to Chestnut Smolder (*dQ*=1%)	BBOA to Chestnut Smolder (*dQ*=3%)	Edge points on SV-OOA vs. LV-OOA
Target	Ratio *m/z* 43/44 from 6.75 to 1.34	Ratio *m/z* 57/55 from 0.78 to 1.03 and ratio *m/z* 41/13 from 0.80 to 0.69	Ratio *m/z* 60/91 from 1.96 to 7.20	Ratio *m/z* 60/91 from 1.96 to 7.20	157 points pulled to axis
Change in target values?	Yes	Yes	Yes	Yes	Yes
dQ	0.1%	0.5%	0.4%	1.3%	8.8%
Improved G-space plot?	Worse LV-OOA vs. SV-OOA plot	No change	No change	No change	No change but for forced points
LV-OOA vs Pittsburgh OOA	Declined r^2 from 0.99 to 0.93	No change	No change	No change	No change
HOA vs Diesel	No change	Slightly better	No change	No change	No change
BBOA vs Chestnut smolder	Slightly better; excl. *m/z* 44	Improved r^2 from 0.79 to 0.87	Improved r^2 from 0.79 to 0.88	Improved r^2 from 0.79 to 0.86	Improved r^2 from 0.79 to 0.93
SV-OOA vs Aged Diesel	Improved r^2 from 0.62 to 0.69	Slightly worse r^2 from 0.62 to 0.57	Worse r^2 0.62 to 0.56, due to *m/z* 44 = 0	Worse r^2 0.62 to 0.56, due to *m/z* 44 = 0	Improved r^2 from 0.69 to 0.72
Other Changes of Note	0 *m/z* 44 in BBOA factor; unreasonable result	Large decrease in *m/z* 44 in SV-OOA, resulting in 43/44 ratio of 21, higher than HOA ratio of 10	In SV-OOA *m/z* 44 = 0; unreasonable result	In SV-OOA *m/z* 44 = 0; in BBOA *m/z* 55 = 0; unreasonable result	SV-OOA *m/z* 43/44 ratio changed from 4.4 to 2.9

3.5 Interpretation and Limitations of Factor Analysis Results

Evaluating solutions with different numbers of factors, comparing profiles to source profiles, examining temporal trends, and exploring rotational ambiguity with the rotational tools available in ME-2 can lead to a greater understanding of the AMS data set. In general, all the factors were consistent under multiple scenarios, suggesting high confidence in their apportionment. Increasing the number of factors from four helped to better characterize the solution space, but the additional "night OA" factors are not easily attributable to known sources. Oblique edges were present in G-space plots, suggesting that the obtained rotation may not be the most plausible one. Since solutions found by pulling the profiles or using Fpeak retained these oblique edges, there appears to be little rotational freedom in the base solution and it can be judged as reasonable.

The Q/Q_{exp} ratios for most fragments were around unity (i.e., between 0.8 and 1.3), indicating that the obtained Q values were approximately equal to the expected values, and the Q/Q_{exp} values for each sample date/time were also reasonable (Figure 3-26). Large Q/Q_{exp} values in the time series occurred during sudden 2-minute spikes in OM concentration and during extremely low concentration periods, meaning the PMF solution does not explain the OM very well during these periods. Some fragments had Q/Q_{exp} ratios below 0.5, indicating that computed Q values were significantly smaller than the expected Q values. This discrepancy is most likely due to the global uncertainty (s_{ij} increase of 10%); since the Q/Q_{exp} ratios for some *m/z* were fairly low, the 10% value may be too high for these *m/z* but appropriate for many other fragments. The Q/Q_{exp} ratios were between 1.3 and 2 for several *m/z*, indicating that the average residuals are between 11 and 14% of x_{ij} for these *m/z*, since Q depends quadratically on the average size of the residuals. The Q contributions drop sharply above *m/z*=198, as most of these

fragments had low S/N ratios and were downweighted. The large residuals may indicate that the PMF solution does not fully characterize these fragments; fragments with high Q/Q_{exp} include *m/z* = [44, 60, 73, 85, 86, 111, 112, 113, 114, 123, 124, 125, 126, 137, 138, 140, 141, 154, 155, 156]. Inaccurate subtraction of the inorganic component from x_{ij} before PMF analysis is a possibility, though many of the fragments with high Q/Q_{exp} do not have an inorganic component. More likely, the large residuals are due to the variation of factor profiles with time and/or to the presence of an occasional, spurious, or localized source(s).

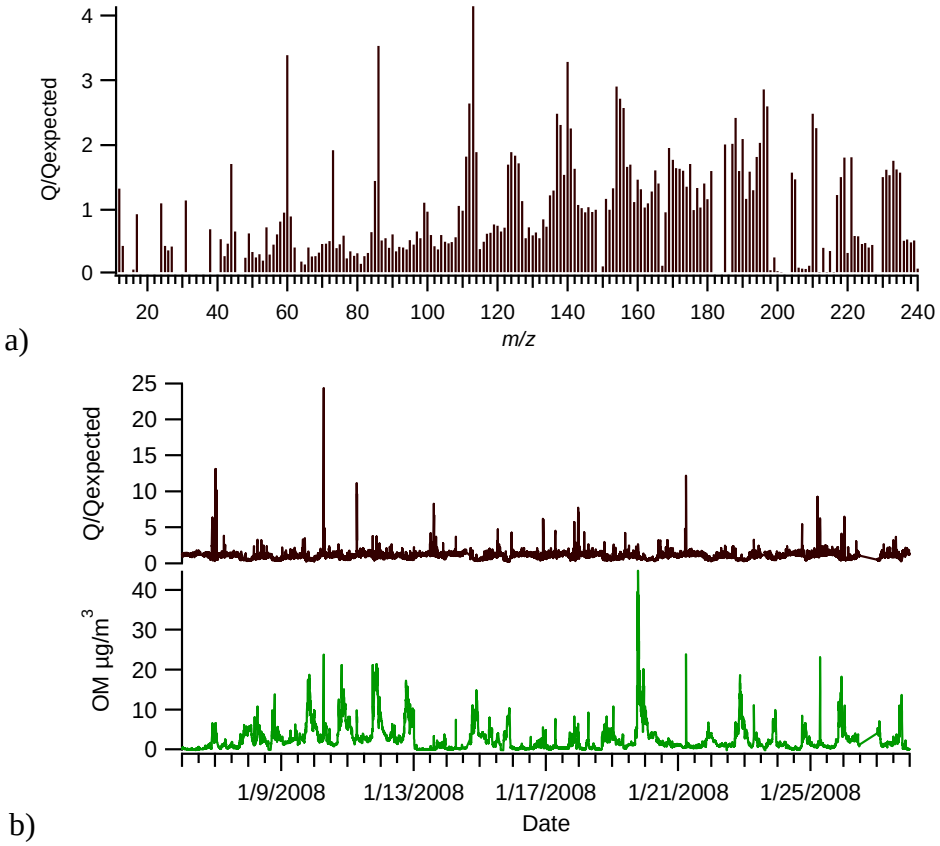

Figure 3-26. $Q/Q_{(expected)}$ a) by fragment for the four-factor solution (the highest $Q/Q_{(expected)}$ values are for *m/z* 113, 86, 60, and 140, all of which are greater than 3), and b) by date/time, along with OM (µg/m^3) values (tick marks with the date indicate midnight on that date). Figures are reproduced under Creative Commons Attribution 3.0, originally published in Brown et al., 2012.

While factors in the four-factor solution are similar to those observed elsewhere, the apportionment of mass among them is different from that seen in other studies. This difference

is expected because a number of the previous studies occurred in the summer and/or in environments with a higher amount of oxidized aerosol than the present study. Previous studies in Los Angeles, Pittsburgh, rural British Columbia, and elsewhere have typically found that at least one-third of the OM was attributable to LV-OOA, originally termed OOA I (Allan et al., 2003a; Ulbrich et al., 2009a; Docherty et al., 2008; Jimenez et al., 2009; Sun et al., 2009). The lower amount of LV-OOA observed during the wintertime Las Vegas study could be due to less transported/aged aerosol, lower biogenic emissions, and/or less overall atmospheric oxidation compared to summertime. In Zurich, a wintertime study found 52% to 57% of the OM to be LV-OOA (Lanz et al., 2008), 69% of which originated from non-fossil sources such as wood burning. In Las Vegas, there is a much lower concentration of BBOA than in Zurich, leading to a smaller concentration of LV-OOA from non-fossil sources and a smaller concentration of LV-OOA overall.

3.6 Summary

EPA PMF v4.0, with its new rotational tools, was successfully applied to a near-road, high time resolution AMS data set. HOA was a quarter of the OM (24%), and higher under downwind conditions (about 40%). In addition to this local, primary OA, there was a highly oxidized background of OA (LV-OOA) that, on average, constituted 29% of the OM, and a less oxidized, semi-volatile fraction that accounted for 34% of the OM. During the evening hours, biomass burning (BBOA) was also seen, likely from the surrounding residential area. Rotational tools allowed for additional analysis of the PMF solution space, increasing our confidence in the results.

4. Elemental Analyses of Organic Aerosol

4.1 Chapter Summary

Understanding the organic matter/organic carbon (OM/OC) ratio in ambient aerosol is critical to achieve aerosol mass closure in routine particulate matter (PM) measurements, to assess the sources of and the degree of chemical processing organic aerosol particles have undergone, and to relate ambient pollutant concentrations to health effects. Of particular interest is how the OM/OC ratio varies in the urban environment, where strong spatial and temporal gradients in source emissions are common. We provide results of near-roadway high-time-resolution OM concentration and OM/OC ratio observations during January 2008 at Fyfe Elementary School in Las Vegas, Nevada, 18 meters from the US 95 freeway soundwall, measured with an Aerodyne High Resolution Time-of-Flight Aerosol Mass Spectrometer (HR-AMS). The average OM/OC ratio was 1.54 (±0.20 standard deviation), typical of environments with a low amount of secondary aerosol formation. The 2-minute average OM/OC ratios varied between 1.17 and 2.67, and daily average OM/OC ratios varied between 1.44 and 1.73. The ratios were highest during periods of low OM concentrations and generally low during periods of high OM concentrations. OM/OC ratios were low (1.52 ±0.14 on average) during the morning rush hour (average OM = 2.4 $\mu g/m^3$) when vehicular emissions dominate this near-road measurement site. The ratios were slightly lower (1.46 ± 0.10) in the evening (average OM=6.3 $\mu g/m^3$), when a combination of vehicular and fresh residential biomass burning emissions was typically present during a period characterized by strong atmospheric stability. The hourly averaged OM/OC ratio peaked at 1.66 at midday. OM concentrations were similar, regardless of whether the monitoring site was downwind or upwind of the adjacent freeway throughout the

day, though they were higher during stagnant conditions (wind speed < 0.5 m/s). The OM/OC ratio generally varied more with time of day than with wind direction and speed.

4.2 Daily Patterns of OM/OC Ratio

Daily averaged OM/OC ratios varied between 1.44 and 1.73, with an average of 1.54, while daily concentration averages of OM were between 1.1 and 6.6 $\mu g/m^3$. Generally the OM/OC ratio was low when OM was high; this occurred when stagnant conditions led to a build-up of OM concentrations (Figure 4-1). The lower OM/OC ratios are consistent with more fresh, primary aerosol, while the higher values mean more oxygen, hydrogen, and/or nitrogen is associated with the organic aerosol, likely from atmospheric processing. Higher OM concentrations are also expected to cause increased partitioning of the semi-volatile, less oxidized material to the particle phase (Sage et al., 2008; Robinson et al., 2007), leading to lower OM/OC ratios. No clear relationship of OM/OC with temperature was evident in the data set, even though temperature plays a role in gas/particle partitioning and can, therefore, influence the ambient OM concentration. Hourly averaged temperature ranged between -1.6 to 15.5 degrees C. On a daily average basis, higher wind speeds were associated with higher OM/OC ratios. When the urban area is well ventilated we expect more oxidized, aged, regional aerosol to comprise a greater proportion of the OM. This relationship is clearer when examining hourly averages (discussed later). For the observed daily average OM/OC ratio range of 1.44 to 1.73, if OC is measured and OM calculated with the traditionally assumed urban OM/OC ratio of 1.4, then the estimate of OM could be biased low by up to 17%.

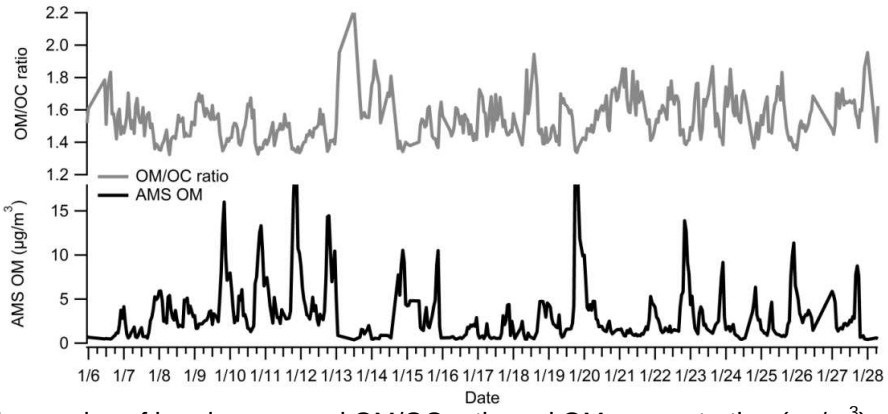

Figure 4-1. Time series of hourly averaged OM/OC ratio and OM concentration (µg/m^3).

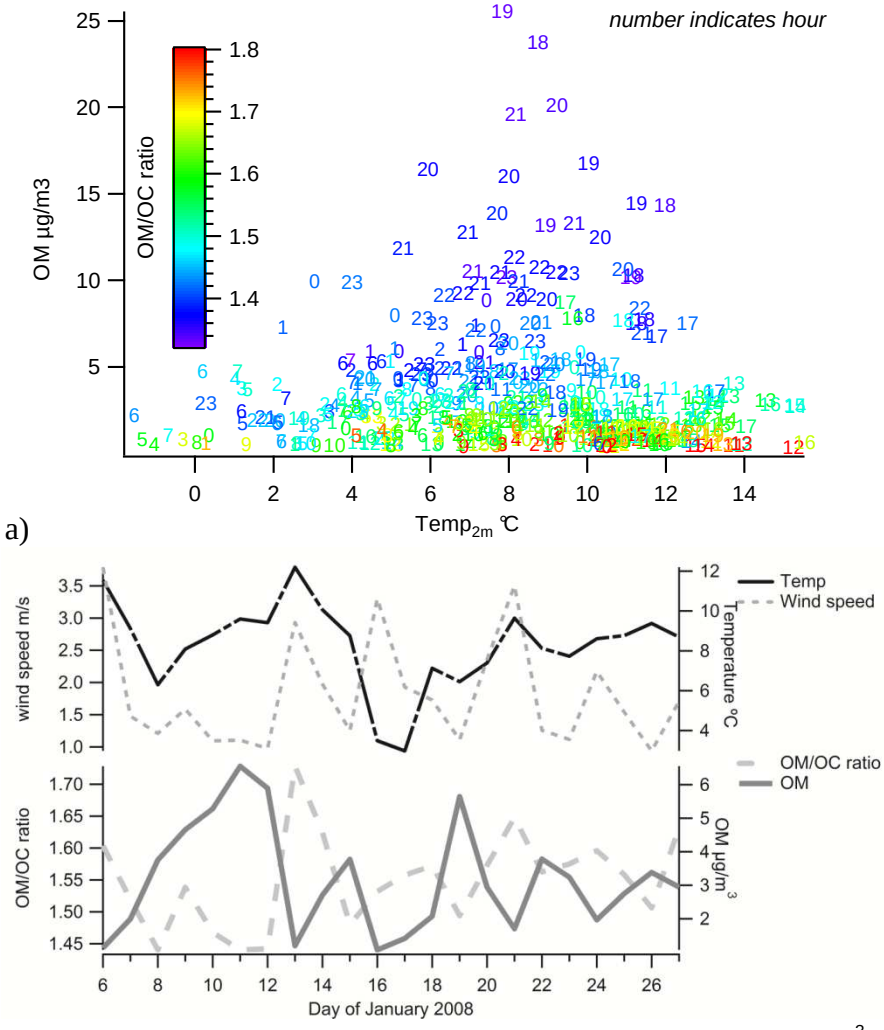

Figure 4-2. Relationship of OM/OC, OM with temperature: a) hourly averaged OM (µg/m^3) and temperature (℃) colored by OM/OC ratio, with numbe rs indicating hour of day; and b) average daily OM/OC ratio, OM concentration (µg/m^3), temperature (℃) and wind speed (m/s).

4.3 Diurnal Patterns of OM/OC and Elemental Ratios

Concentrations of OM were highest in the evening hours when wind speeds were low, atmospheric stability was relatively high, and a combination of local primary emissions (including residential biomass burning) occurred (Brown et al., 2012). A secondary OM peak typically occurred during the morning rush hour; Figure 4-3 summarizes the average diurnal variability of OM, OM/OC, BC, CO, wind speed, temperature, and small vehicle volume during the study. Large-vehicle volume (not shown) peaked in the midday and was low overnight. Traffic volume peaked in the morning and evening hours, with speeds averaging between 55 and 65 mph. For comparison, BC and CO had similar concentration peaks in the morning and in the evening.

The AMS-derived OM/OC ratio was on average higher in the midday (1.67) and at 0300 LST (1.70) than in the morning (1.55 at 0600 LST) and evening (1.47 at 2100 LST). The low ratio in the morning hours corresponded with the morning rush hour and typically low wind speeds. Under these conditions and time of day, the predominant source of organic aerosol is likely fresh emissions from the freeway and the larger urban area, with a low amount of SOA. The OM/OC ratio of 1.54 is indicative of fresh aerosol, and in particular of fresh vehicle emissions (Chirico et al., 2010; Reff A. et al., 2009). The increasing OM/OC ratio during the day is consistent with aerosol aging and SOA production.

Between 1500 LST and 1700 LST, the OM/OC ratio rapidly drops from 1.67 to 1.50, then remains low until the minimum of 1.47 at 2100 LST. During this time, average OM goes from a minimum of 1.3 $\mu g/m^3$ at 1500 LST to 3.3 $\mu g/m^3$ at 1700 LST, reaching a peak of 5.9 $\mu g/m^3$ at 2100 LST, as a combination of vehicular emissions from the evening rush hour and

residential biomass burning contribute OM while wind speeds decrease and atmospheric stability increases (Brown et al., 2012).

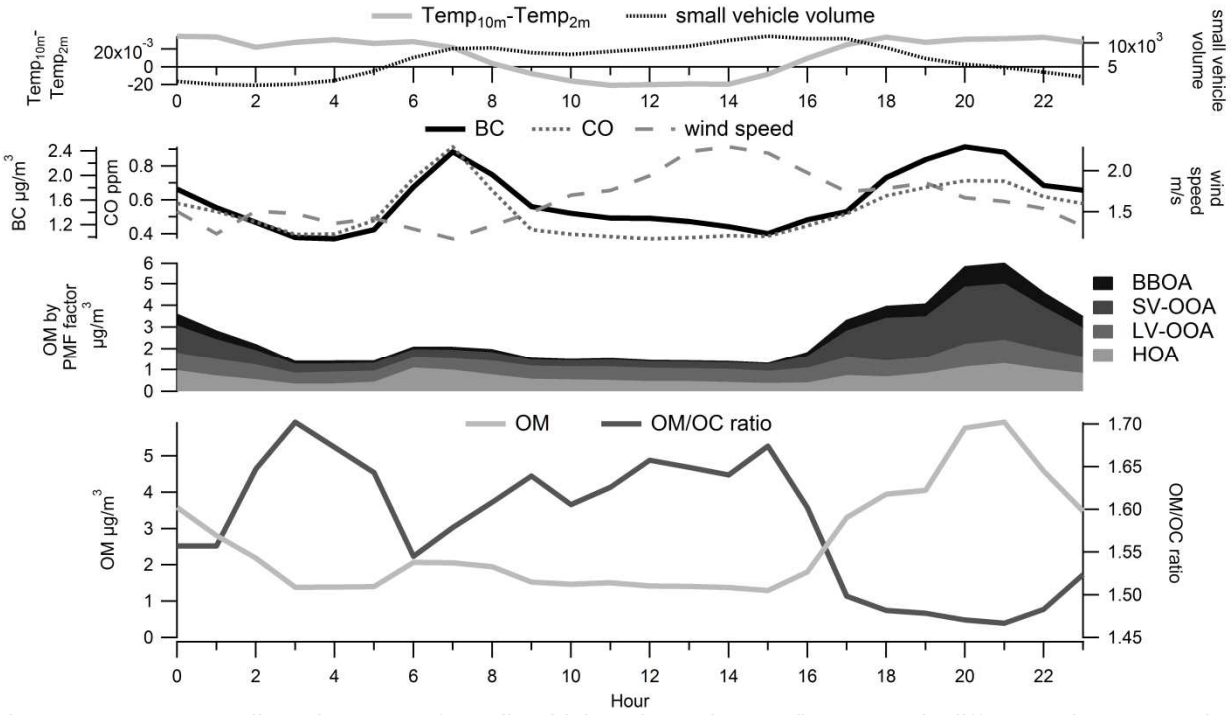

Figure 4-3. Average diurnal pattern of small-vehicle volume (counts/hour*1000), difference in 10 m and 2 m temperature (positive values indicate a stronger ground-level temperature inversion), BC (µg/m^3), CO (ppm), wind speed (m/s), average concentration by hour and PMF factor (µg/m^3), OM (µg/m^3), and OM/OC ratio at Fyfe during January 5-28, 2008, by hour (LST).

While examination of diurnal averages is valuable, the aggregation of many data points to calculate the averages may mask additional features in the data. In particular, there are differences in OM/OC ratios both with time of day and with OM concentration. Figure 4-4a shows the OM/OC ratio vs. OM concentration for four times of day: morning rush hour (0500-0900 LST), midday (0900-1700 LST), evening (1700-2300 LST), and overnight (2300-0500 LST). At all times of day, OM/OC is lower and the range of values decreases when OM concentrations are higher, as also seen in Figure 4-4b. The observed relationship between OM/OC and OM might result from greater gas-to-particle partitioning of more volatile organic compounds when OM is present at higher concentration (Robinson et al., 2007; Lipsky and

Robinson, 2006). Cappa and Jimenez (2010) determined that biomass burning organic aerosol (BBOA) and primary, hydrocarbon-like organic aerosol (HOA) have the greatest potential for aerosol formation because the semi-volatile material associated with BBOA and HOA is most likely to move to the particle phase under high OM, low temperature conditions. This semi-volatile material has a relatively low OM/OC ratio and can move into the particle phase under these high OM conditions without first undergoing extensive oxidation. Chan et al. (2010) also demonstrated that OM/OC decreases with increased OM concentrations, though they ascribed this trend to different source mixtures as well as increased partitioning at their site, near Toronto.

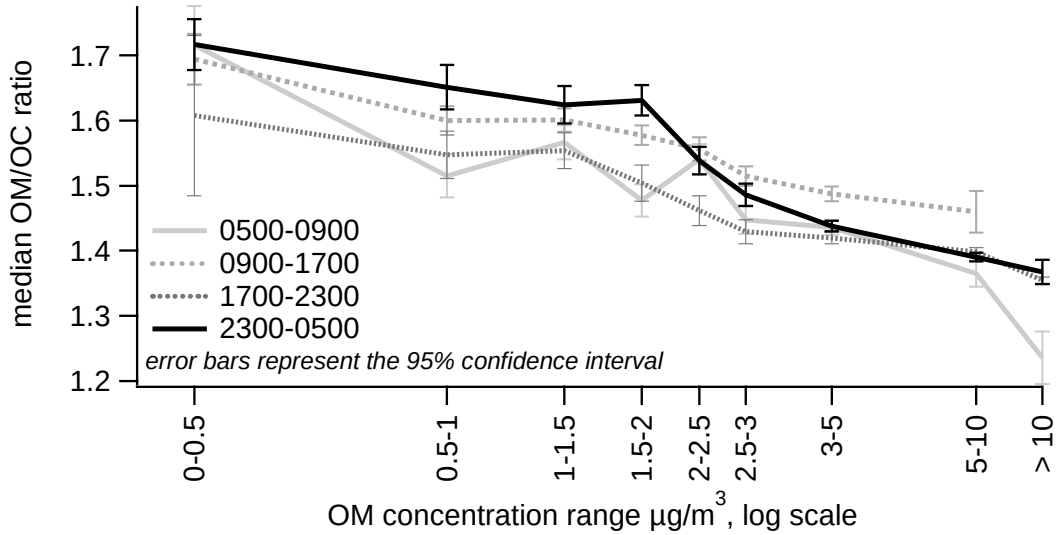

a)

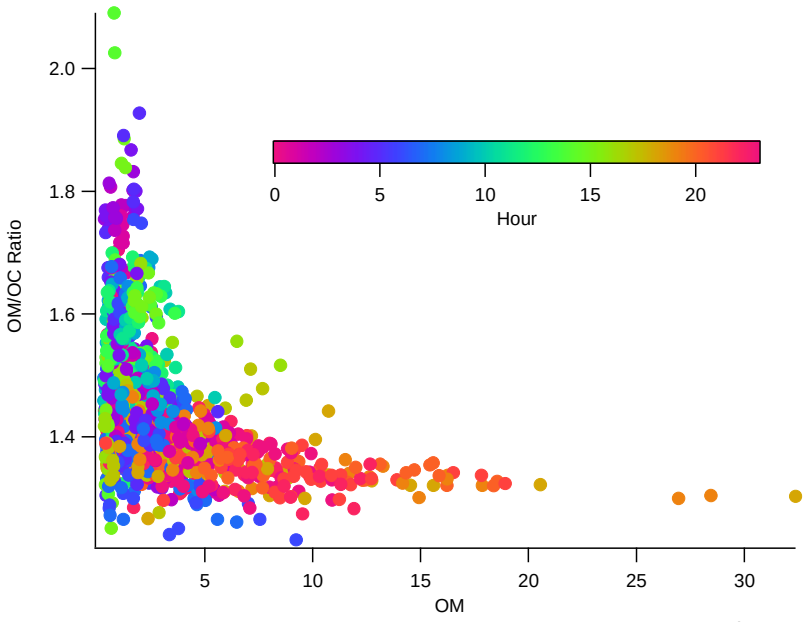

b)

Figure 4-4. (a) median OM/OC ratio by OM concentration (µg/m^3) bin and time of day, with 95% confidence interval, with log scale on x-axis; and (b) hourly averages of OM/OC ratio and OM concentrations (µg/m^3) colored by hour. Originally published in Brown et al., 2013.

The diurnal variations of the Las Vegas OM/OC ratio are largely driven by changes in O/C ratio, and to a lesser degree, H/C ratio. Figure 4-5 shows the diurnal pattern of O/C and H/C, and Figure 4-6 shows a scatter plot of H/C versus O/C for hourly averages, also known as a van Krevelen diagram (Heald et al., 2010). H/C is highest in the morning and evening (overall average 1.75), while O/C is highest in the middle of the day (overall average 0.30). On the H/C versus O/C scatter plot, starting in the lower right corner at 0300 LST, average H/C is at its lowest and O/C at its highest. As the morning commute (and associated fresh vehicle emissions) begins, there is a slow increase in H/C and decrease in O/C; at 0600 LST, when the morning commute is nearing its peak, there is a sharp increase in H/C and decrease in O/C. Starting at 0800, H/C slowly decreases and O/C slowly increases until 1600 LST. During this midday period, mixing heights increase, temperatures rise, and increased atmospheric oxidation occurs, leading to lower OM concentrations and higher O/C. As OM is diluted and temperatures

increase, more organic matter can partition to the gas phase; the species partitioning to the gas phase are expected to have lower O/C ratios than the species remaining in the particle phase, further increasing the O/C ratio of the particle phase.

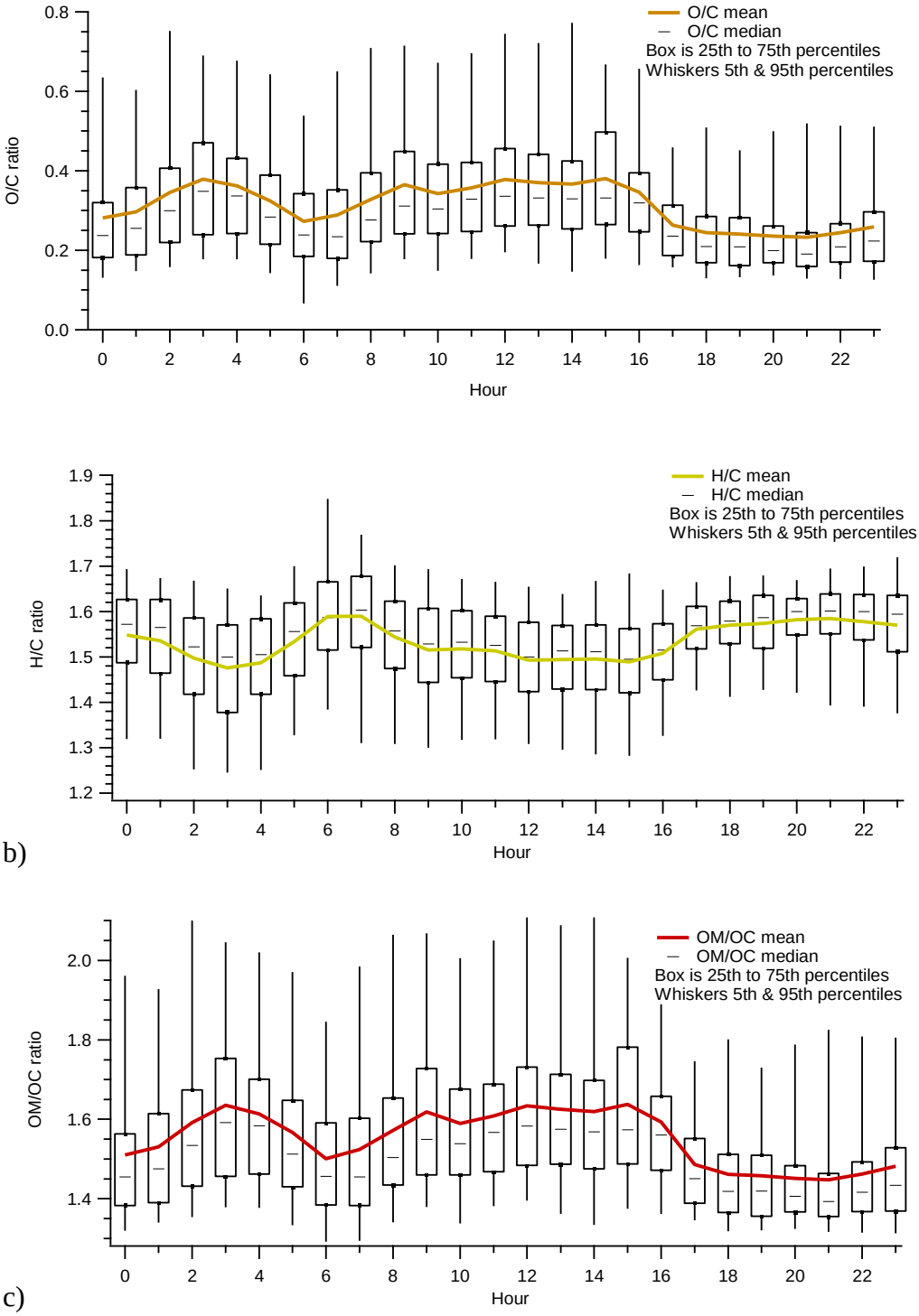

Figure 4-5. Diurnal pattern in January 2008 of a) O/C ratio; b) H/C ratio; and c) OM/OC ratio. Boxes show the interquartile range, whiskers the 5th and 95th percentiles, dashes the median, and solid colored line the mean.

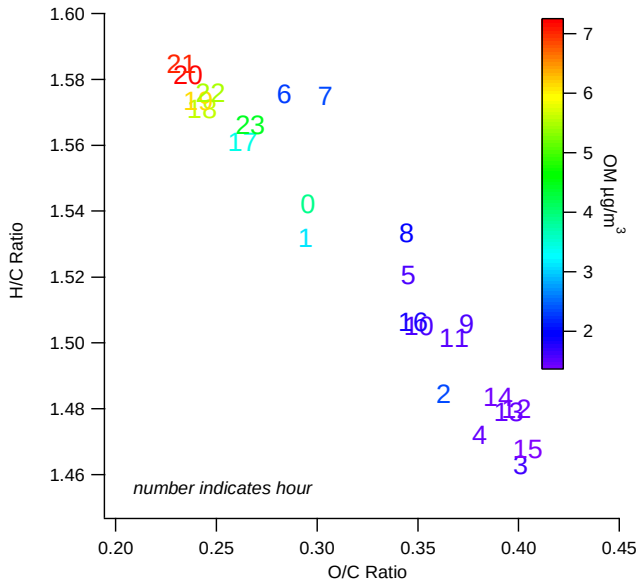

Figure 4-6. H/C vs O/C ratio averaged by hour during all hours of January 2008, colored by OM concentration; each number indicates the hour (LST).

By 1700 LST, the evening commute has begun and atmospheric stability increases, leading to a large increase in H/C and a decrease in O/C. Over the next 6 hours, OM peaks, H/C remains high (evening average of 1.58) and O/C remains relatively low (evening average of 0.24). During the evening, in addition to fresh vehicle emissions, residential biomass burning contributes to OM, as seen via analysis of the data with positive matrix factorization (PMF) (Brown et al., 2012). As OM increases and temperature decreases in the evening, more organic compounds can partition to the particle phase, further increasing OM and the H/C ratio. By 2300 LST, the emissions associated with the evening commute and residential biomass burning have decreased, leading to a slow decrease in OM, a decrease in H/C, and an increase in O/C throughout the night. A number of studies (Donahue et al., 2012; Kroll et al., 2011; Jimenez et al., 2009; Aiken et al., 2008) have demonstrated that direct, primary emissions typically have O/C of 0-0.17; heavily oxidized organic aerosols have O/C of 0.67-1; semi-volatile organic aerosols have O/C between 0.33 and 0.67; and biomass burning organic aerosols have a very

wide range of 0.07-0.42. Thus, a combination of mobile source and residential biomass burning emissions, in addition to oxidized background organic aerosol, can easily result in the observed O/C and OM/OC ratios at this Las Vegas site.

4.4 Additional H/C versus O/C Ratio Analyses

Figure 4-7 summarizes the van Krevelen diagrams for all 2-minute data measured during January 2008. H/C and O/C span a wide range. At lower OM concentrations, O/C is high and H/C is low, indicating that the OA is well oxidized. When OM is high, H/C is also high and O/C relatively low, indicating that high OM concentrations occur when fresh emissions (high H/C) are a large source of OM. These high OM concentrations typically occur in the evening (Figure 4-7b). High H/C with low O/C also occurs in the morning, but OM concentrations are not as high as in the evening.

Figure 4-8 shows Van Krevelen diagrams where data points are colored by the fraction of OM coming from different PMF factors: HOA, LV-OOA, SV-OOA and BBOA. At high H/C and low O/C, HOA is highest, while at high O/C LV-OOA is highest. BBOA by mass is highest in the evening when H/C is high and O/C is low, and points of high BBOA fraction occur along the lower edge of the data range. SV-OOA is highest when H/C is high across a range of O/C values.

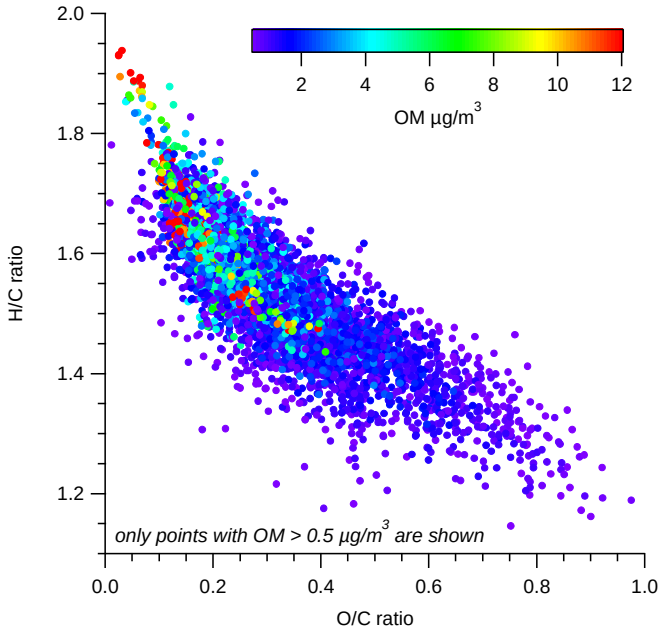

a)

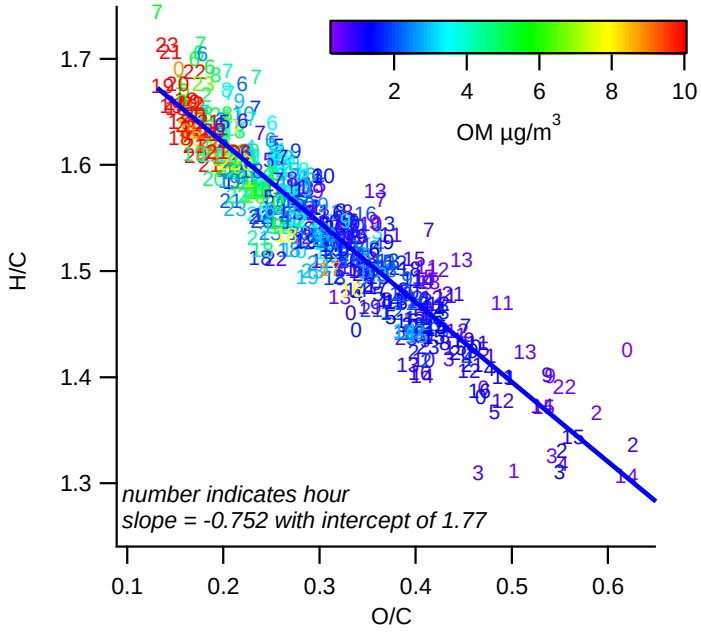

b)

Figure 4-7. H/C vs O/C when OM > 0.5 µg/m^3 for a) all 2-minute data, colored by OM concentration, and b) hourly averages, colored by OM concentration and with numbers indicating hour of the day.

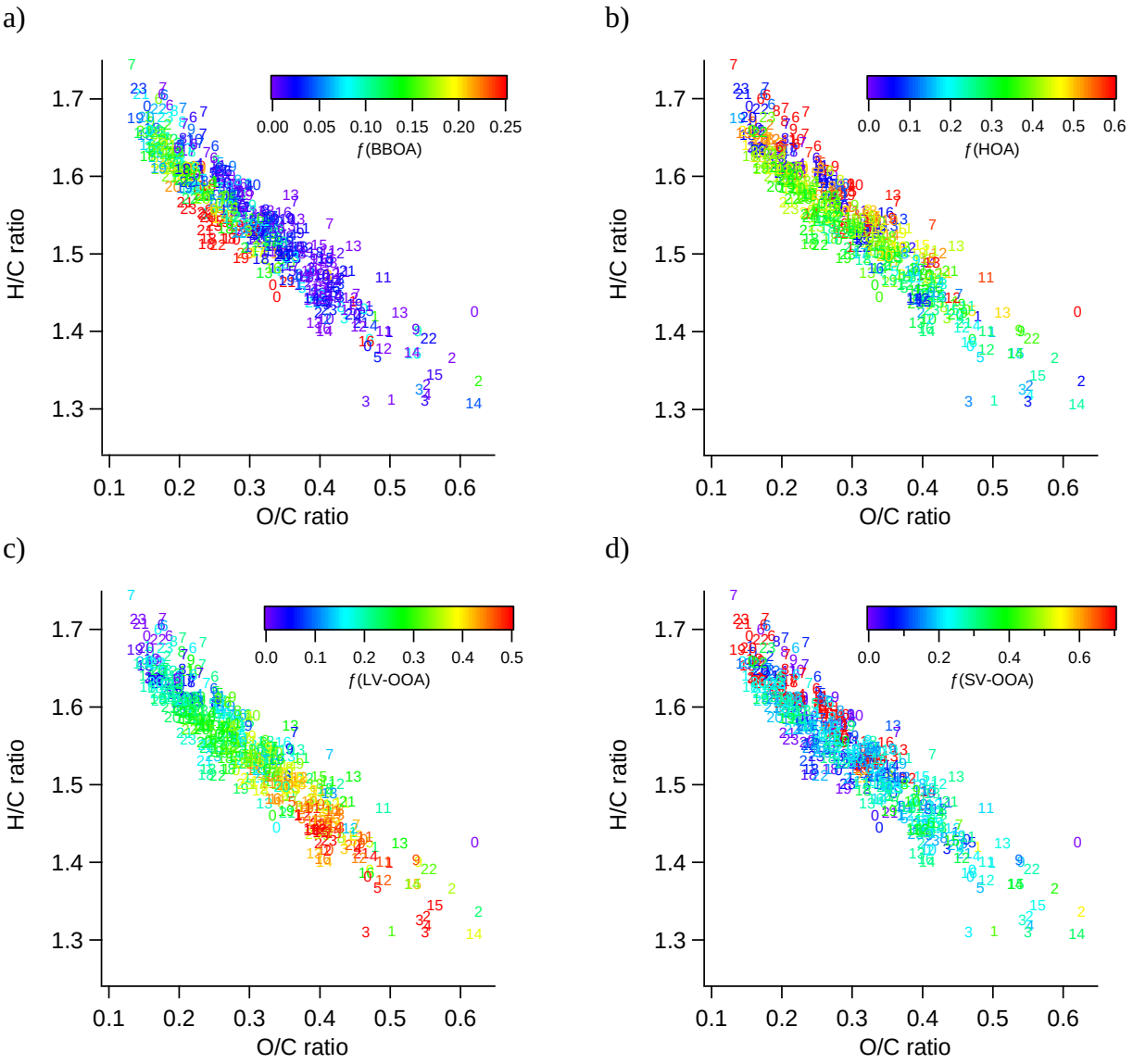

Figure 4-8. H/C vs O/C ratio by fraction of OM from: a) HOA; b) BBOA; c) LV-OOA; and d) SV-OOA; numbers indicate hour of day.

4.5 Variations by Wind Speed and Direction (Upwind/Downwind)

We also examined how the OM/OC ratio and OM and BC concentrations vary with changes in wind speed and wind direction (i.e., whether the monitoring site is upwind or downwind of the adjacent freeway). OM and BC were higher during low wind periods. Figure 4-9 shows the relationship of hourly OM with wind speed and OM/OC ratio: once winds are

greater than 2 m/s, OM is nearly always below 5 µg/m^3, and the OM/OC ratio is generally greater than 1.6. With low wind speeds, OM is high, and the OM/OC ratio is quite low, averaging 1.4.

BC has a pattern similar to OM, with much higher concentrations when wind speeds are less than 2 m/s. With higher wind speeds and greater ventilation, aged/oxidized regional aerosol makes up a larger proportion of the OM. Note that lower OM concentrations may lead to the less-oxidized material partitioning into the gas phase, reinforcing a higher OM/OC ratio. The opposite is true when higher OM concentrations lead to more semi-volatile, less oxidized material partitioning into the particle phase.

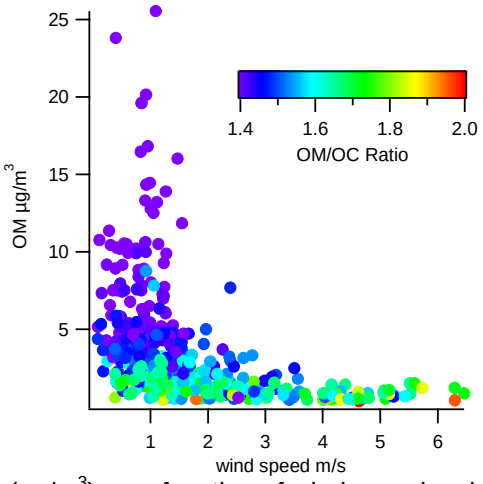

Figure 4-9. OM concentrations (µg/m^3) as a function of wind speed, colored by OM/OC ratio.

There was little trend in H/C and O/C with wind speed or direction, except that low wind speeds are associated with high OM concentrations, and thus higher H/C and lower O/C. Figure 4-10 shows van Krevelen diagrams colored by wind speed and direction. As seen with OM/OC ratio, there was no statistically significant difference in the H/C to O/C relationship during upwind versus downwind conditions. Rather, wind speed and time of day were more important than wind direction.

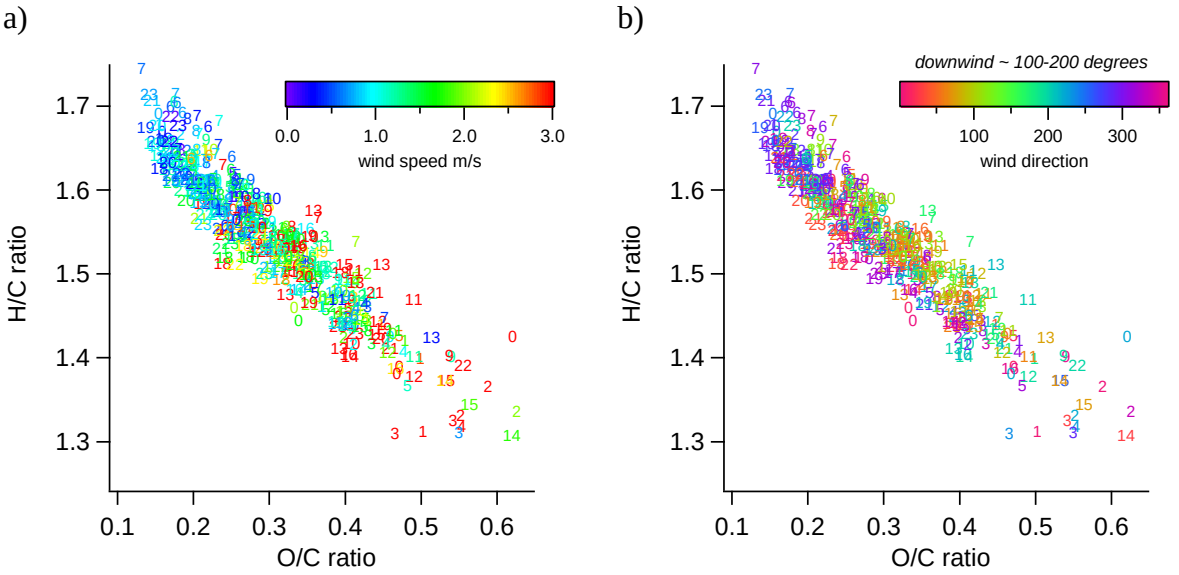

Figure 4-10. H/C vs O/C ratio by a) wind speed, and b) wind direction. In panel b, green indicates the direction when the monitoring site is downwind of the freeway, which mostly occurred during midday. In both plots, numbers indicate hour of day.

Since concentrations vary significantly by time of day, we compared values during upwind, downwind, and stagnant conditions, grouped into five times of day (Figure 4-11): overnight (0000-0600), morning (0600-0900), midday (0900-1600), evening (1600-2100), and late evening (2100-0000). During all time periods, OM is consistently higher during stagnant conditions. The OM/OC ratio is broadly similar under all upwind/downwind/stagnant regimes for a given time period. During the morning rush hour, when OM/OC on average dips to 1.51, there is no statistical difference in the OM/OC ratio at the 95% confidence level between upwind, downwind, or stagnant conditions. In the midday, OM is higher and OM/OC lower during downwind conditions compared to upwind conditions; this is the time of day when winds blow generally perpendicular to the freeway, so it is the time of the most direct influence of fresh freeway emissions at the site. During the 1600-2100 and 2100-0000 LST periods, OM/OC is similar regardless of wind direction, with a median value between 1.41 and 1.45. During the

overnight period before the morning rush hour, OM/OC is the most variable, especially during downwind conditions.

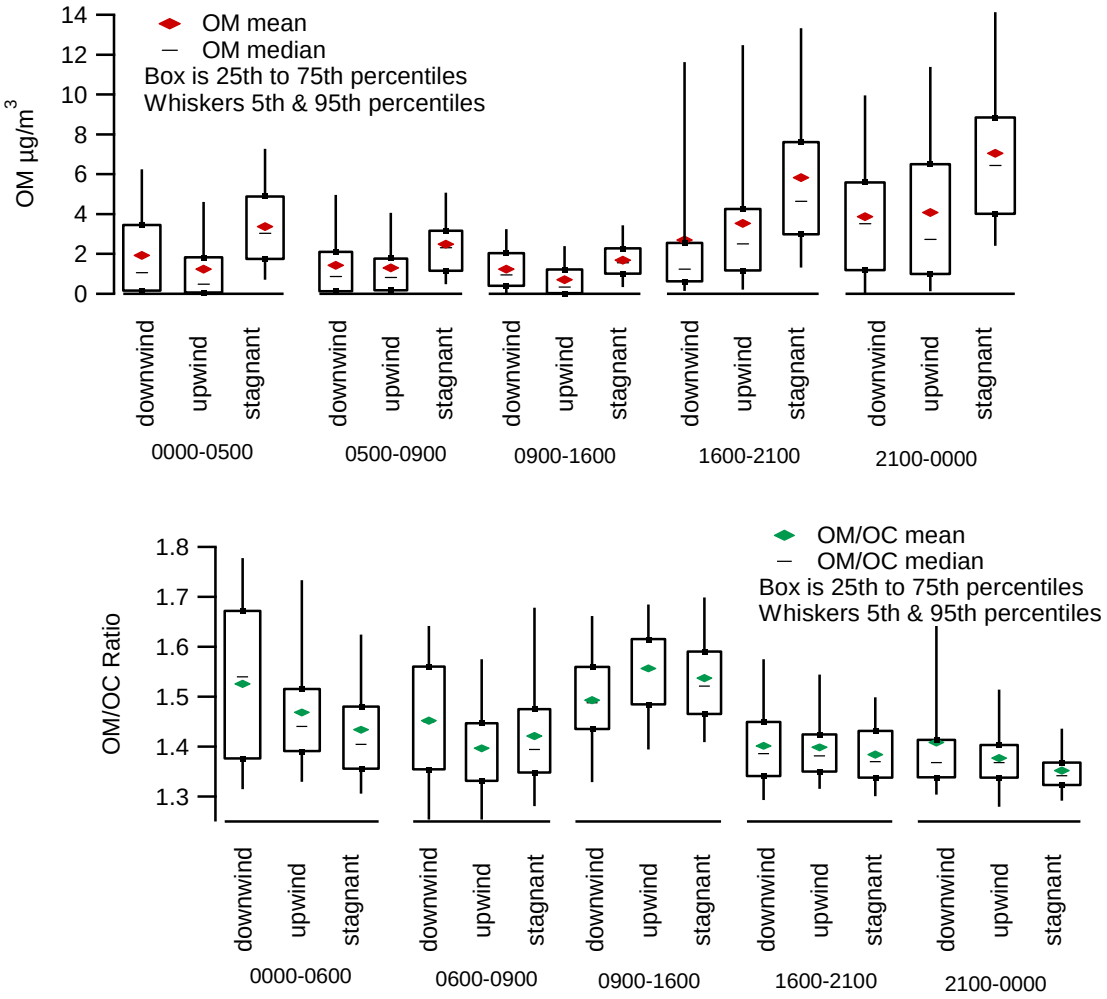

Figure 4-11. Values by time of day bin during downwind, upwind, and stagnant (wind speed < 0.5 m/s) conditions for (top) OM concentrations and (bottom) OM/OC ratio. Top figure is reproduced under Creative Commons Attribution 3.0, originally published in Brown et al., 2012.

4.6 Discussion

The average OM/OC ratio of 1.54 presented here is on the low end of historic ambient measurements but well within the range of 1.3-2.3 found in numerous ambient studies; moreover, it is consistent with the close proximity of the sampling location to a freeway and with limited wintertime photochemistry. Studies that found values on the higher end of this range

took place in locations and/or times of year with more photochemistry and thus higher OM/OC. For example, Mexico City and Riverside summertime average OM/OC ratios were around 1.8 (Williams et al., 2010; Aiken et al., 2008), and the ratio can be even higher at rural sites, such as 2.3 in rural British Columbia (Sun et al., 2009), and 1.9 at rural Midwestern sites (Bae et al., 2006). The average ratio of 1.54 is typical of relatively fresh vehicle or other emissions, such as those generated in laboratory settings (Chirico et al., 2010; Mohr et al., 2009). In Las Vegas during the summertime, the OM/OC ratio would likely be higher, as increased photochemistry would lead to higher oxygen content and higher OM/OC ratios.

The day-to-day variability in the OM/OC ratio is quite large, suggesting that using a fixed OM/OC value in PM mass closure calculations, even one that changes seasonally, may be insufficient to achieve accurate mass closure on individual days. In national scale networks like CSN and IMPROVE, neither OM/OC nor OM is measured; rather, an assumed OM/OC ratio must be employed to estimate the OM from OC measurements, or the OM/OC ratio may be imputed, e.g., by assuming that any $PM_{2.5}$ mass unaccounted for is due to the unmeasured O, H, and N associated with the OC. Since OC often accounts for one-third to one-half of the average $PM_{2.5}$ mass (Hand et al., 2011), the use of a fixed OM/OC ratio is likely the largest uncertainty in trying to achieve mass closure. Even with semi-continuous measurements, such as those from the Sunset OCEC analyzer, OM/OC cannot be determined. Health studies that rely on OC measurements may under- or over-estimate exposure to OM, and converting OC to OM with a fixed OM/OC ratio represents a significant source of uncertainty.

As seen in Figure 4-4, OM/OC decreases with increasing OM concentrations. This is especially evident in the evening, when mobile source emissions are at a peak, wind speeds are low, and atmospheric stability is increased. The low OM/OC at higher OM is likely due to a

combination of fresh particulate and semi-volatile emissions accompanied by the movement of some semi-volatile material into the particle phase as OM concentrations increase. The low OM/OC ratio at high OM concentrations indicates that there may be a large effect from gas-to-particle partitioning of relatively fresh, less oxidized material, since if emissions were first oxidized before partitioning into the particulate phase, the evening OM/OC ratio would likely be higher than the observed 1.4. Robinson (2007) and others have demonstrated that as particle concentrations increase, semi-volatile material is more likely to move into the particle phase. Here, this mechanism may lead to a rapid rise in OM and corresponding decrease in OM/OC ratio in the evening, as fresh, less-oxidized material partitions into the particle phase without first undergoing extensive oxidation.

4.7 Chapter Conclusions

The wintertime diurnal and daily variations in OM/OC ratio in Las Vegas were determined using an HR-AMS. HR-AMS measurements correlated well with measurements made by a Sunset OC analyzer. We found that the OM/OC ratio was on average 1.54 (± 0.20 standard deviation), and the daily average varied between 1.44 and 1.73. OM/OC was generally lowest, approximately 1.4, during the morning and evening hours when OM was highest. A combination of peak emissions and stable atmospheric conditions in the evening may lead to increasing OM and, as more volatile material partitions into the particle phase, decreasing OM/OC. The diurnal variation of the OM/OC ratio suggests it is a combination of regional, oxidized background aerosol with a high OM/OC ratio (i.e., OM/OC ratio of 2 or higher), dominant during the daytime, which is then combined with fresh, low OM/OC ratio emissions (i.e., with OM/OC ratio of 1.2 to 1.5) in the morning and evening. Day-to-day variability in the fine particle OM/OC ratio is quite large, suggesting that using a fixed OM/OC value in PM mass

closure calculations, even one that changes seasonally, may be insufficient to achieve accurate mass closure on individual days. Health studies that rely on OC measurements may under- or over-estimate exposure to OM, and converting OC to OM with a fixed OM/OC ratio represents a significant source of uncertainty; thus, air quality managers may not have sufficient information about the importance of OM contributions to $PM_{2.5}$ to make optimal regulatory decisions.

5. Particle Size Analyses

5.1 Chapter Summary

Observations of the particle size distribution by mass during our study were analyzed to understand how the organic size distribution is different than the distribution of inorganic species, and how the organic size distribution varies with time of day and meteorology. OM had a very broad average size distribution, indicating a mixture of fresh, less oxidized smaller particles and more aged, oxidized particles. In contrast, the inorganic species like nitrate had mass clearly associated with larger particles only, i.e., vacuum aerodynamic diameter (d_{va}) of 500 nm. There was only modest difference in OM size distribution by time of day or upwind/downwind/stagnant conditions, though the larger size particles (e.g., greater than 200 nm) were enhanced in heavily oxidized fragments like *m/z* 44. Time series analysis revealed OM was well distributed between 100 and 400 nm d_{va} during the evenings when OM was highest. These analyses support the chemical analyses shown in earlier chapters, which suggest that primary, less oxidized particles and biomass burning are a large fraction of the OM.

5.2 Average Size Distribution by Species

Over the course of the study, OM had on average a very broad size distribution (Figure 5-1), while inorganic species, ammonium, sulfate, and nitrate, all had a sharper size distribution, with peaks at 400-500 nm d_{va}. Ammonium nitrate and ammonium sulfate are formed as a result of the reaction of gaseous ammonia with sulfuric and nitric acids, oxidation products of SO_2 and NO_x. Their large particle sizes observed here suggest that these products likely formed by gas-to-particle partitioning onto the surface of pre-existing aerosol particles or, perhaps, droplet processing. OM exhibited a large particle size range. Larger particles may result from

condensation of organic gases onto existing particles, coagulation of smaller particles, or oxidation in atmospheric droplets via aqueous reactions. Smaller particles may reflect fresh particle formation from emissions or new particle formation from oxidized VOCs. This combination of pathways and mixture of fresh and aged particles likely leads to the observed broad size distribution.

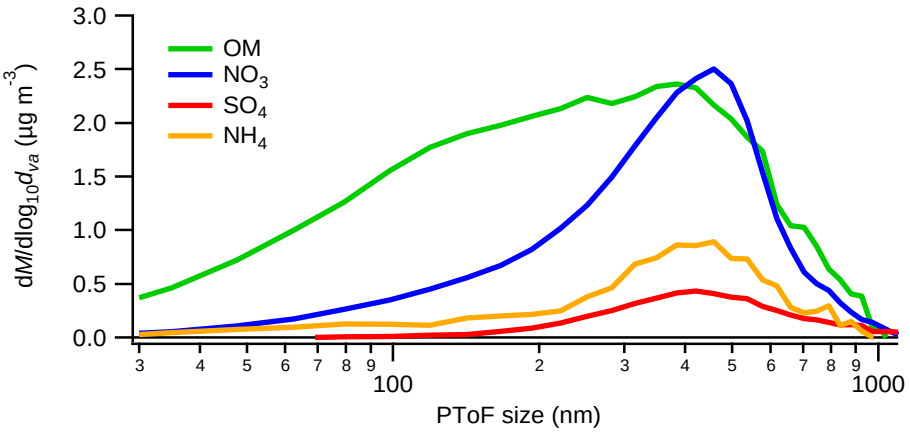

Figure 5-1. Size distribution ($dM/d\log_{10}d_{va}$) of OM, nitrate, sulfate and ammonium by vacuum aerodynamic particle diameter (d_{va}) during January 2008.

5.3 Characterization of OM Size Distribution and Composition

As seen in Figure 5-1, the average size distribution of OM is quite broad, in contrast to the inorganic species. In Figure 5-2, the average OM mass spectra for particles with d_{va} less than 100 nm, between 100 nm to 300 nm, 300 nm to 600 nm and greater than 600 nm are shown. In addition, the ratio between *m/z* 43 and *m/z* 57 with *m/z* 44 (43/44 ratio, 57/44 ratio) is also shown; these ratios can be used to understand the relative portion of HOA-type aerosol (represented by *m/z* 57) or SV-OOA type aerosol (*m/z* 43) to LV-OOA-type aerosol (represented by m/z 44). There is little variability in the average spectra among each size bin. However, there is some variation in the 43/44 ratio, with a lower ratio in the largest 2 size bins (1.35 for

600-1000 nm, and 2.11 for 300-600 nm) compared to smaller particles sizes (range of 2.42-2.61). This is consistent with the idea that more oxidized particles, enhanced in m/z 44, are more aged and associated with larger particles, leading to a lower 43/44 ratio in the particles with d_{va} greater than 300 nm, and in particular those greater than 600 nm.

By examining the size distributions of *m/z* fragments that are examples of the range of organic aerosol we can better understand the type of aerosol that may be important in different size ranges. For fresh, primary HOA-type aerosol, *m/z* 57 can be used; for HOA and SV-OOA, *m/z* 43 can be used; for heavily oxidized OOA-type aerosol, *m/z 44* can be used; and for BBOA, *m/z* 60 can be used. Differences between *m/z* are better seen in Figure 5-3, which shows the size distribution of these four fragments over the whole study. Similar to OM, *m/z* 43, 57 and 60 all have broad size distributions, generally with most mass between 200 to 400 nm d_{va}, though with some modest mass even below 100 nm. In contrast, *m/z* 44 has a peak between 300 to 500 nm d_{va}, more similar to the secondary inorganic species. These results indicate that smaller size particles are not only freshly emitted particles, but are a mixture of fresh, HOA-type organic species mixed with more aged, oxidized species.

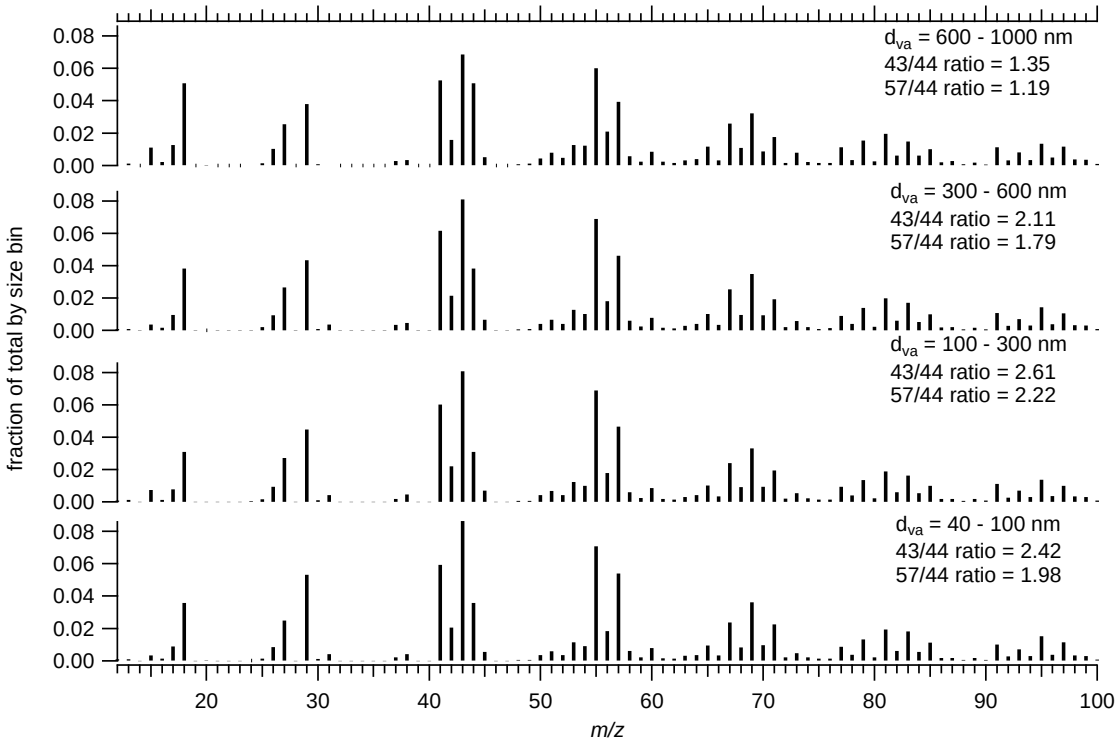

Figure 5-2. Average mass spectra of OM and ratios of *m/z* 43 to 44 and 57 to 44 for particles of d_{va}: 40 to 100 nm, between 100 nm to 300 nm, 300 nm to 600 nm and greater than 600 nm.

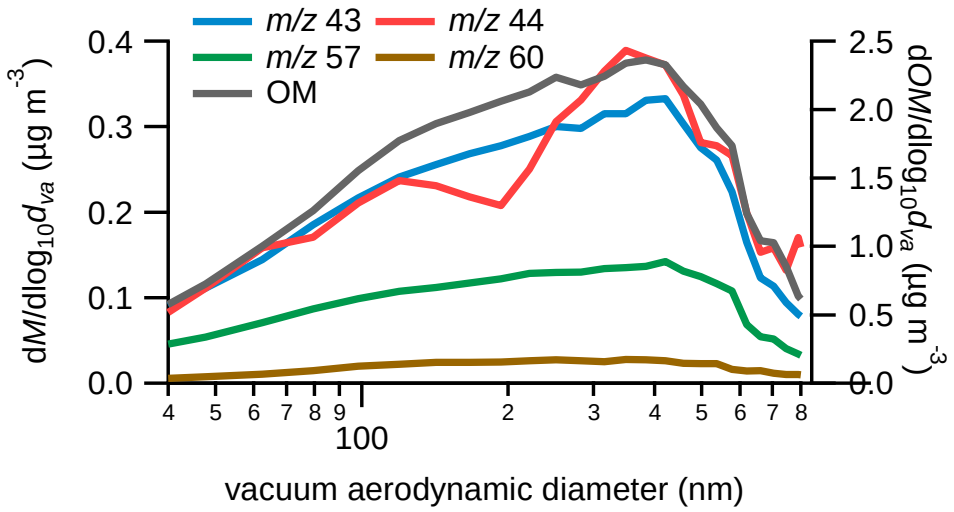

Figure 5-3. Size distribution of *m/z* 43, 44, 57 and 60 (primary y-axis) and OM (secondary y-axis).

5.4 Diurnal changes in OM particle size distribution and composition

5.4.1 Variations in OM Mass Spectra by Size and Time of Day

Because there was little difference between mass spectra among the four size bins in Figure 5-2, we separated the data into two size bins, at 200 nm d_{va}. Looking at Figure 5-1, above

200 nm d_{va} is where the majority of the mass of the inorganic species resides, possibly indicating this size range is where the more processed aerosol are, whereas fresher, organic-dominated particles are less than 200 nm d_{va}. Particles less than 200 nm d_{va} would also account for the majority of particle number. Figures 5-4 through 5-6 step through organic mass spectra for particles greater than and less than 200 nm d_{va}, on average and for the morning, midday and evening. There is little difference between the smaller and larger diameter spectra in the evening, with the difference between spectra for every *m/z* less than 0.01. In the morning and midday the major difference between the smaller and larger diameter spectra is fraction of signal from *m/z* 44 (and *m/z* that are directly proportional to *m/z* 44 such as 28). In midday, *m/z* 44 is 7% of the signal in the larger size particles, and is 5% of the signal in the smaller particles. In the morning, *m/z* 44 is 5% of the signal in the larger particle spectrum and 3% in the smaller particle spectrum. These differences are small, though do suggest the smaller particles have less mass from heavily oxidized organic aerosol compared to the larger particles.

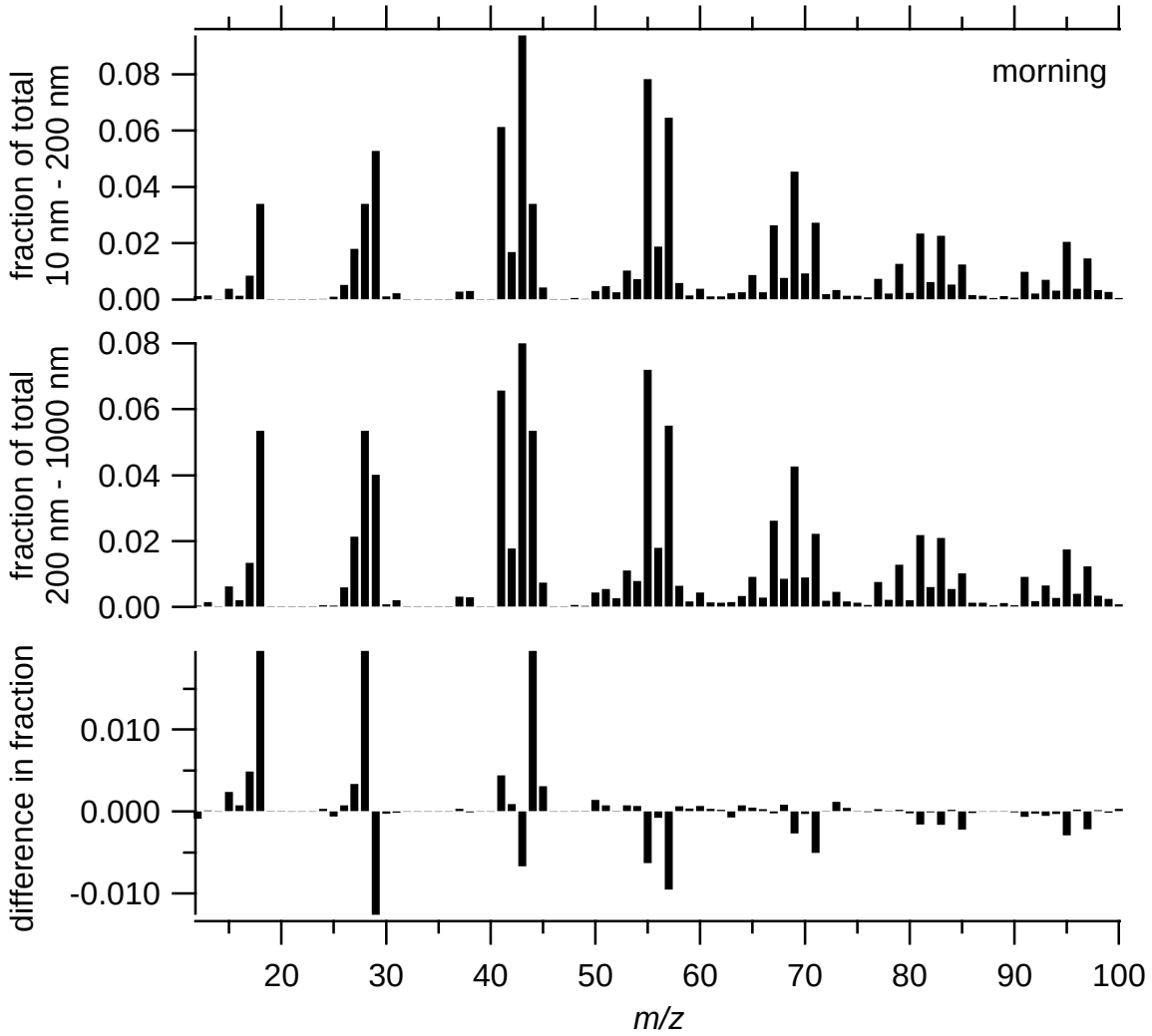

Figure 5-4. Average organic mass spectra (fraction of signal by *m/z*) during morning (0500-0900 LST) for (top) particles less than 200 nm d_{va}, (middle) particles greater than 200 nm d_{va}, and (bottom) the difference between the top and middle spectra.

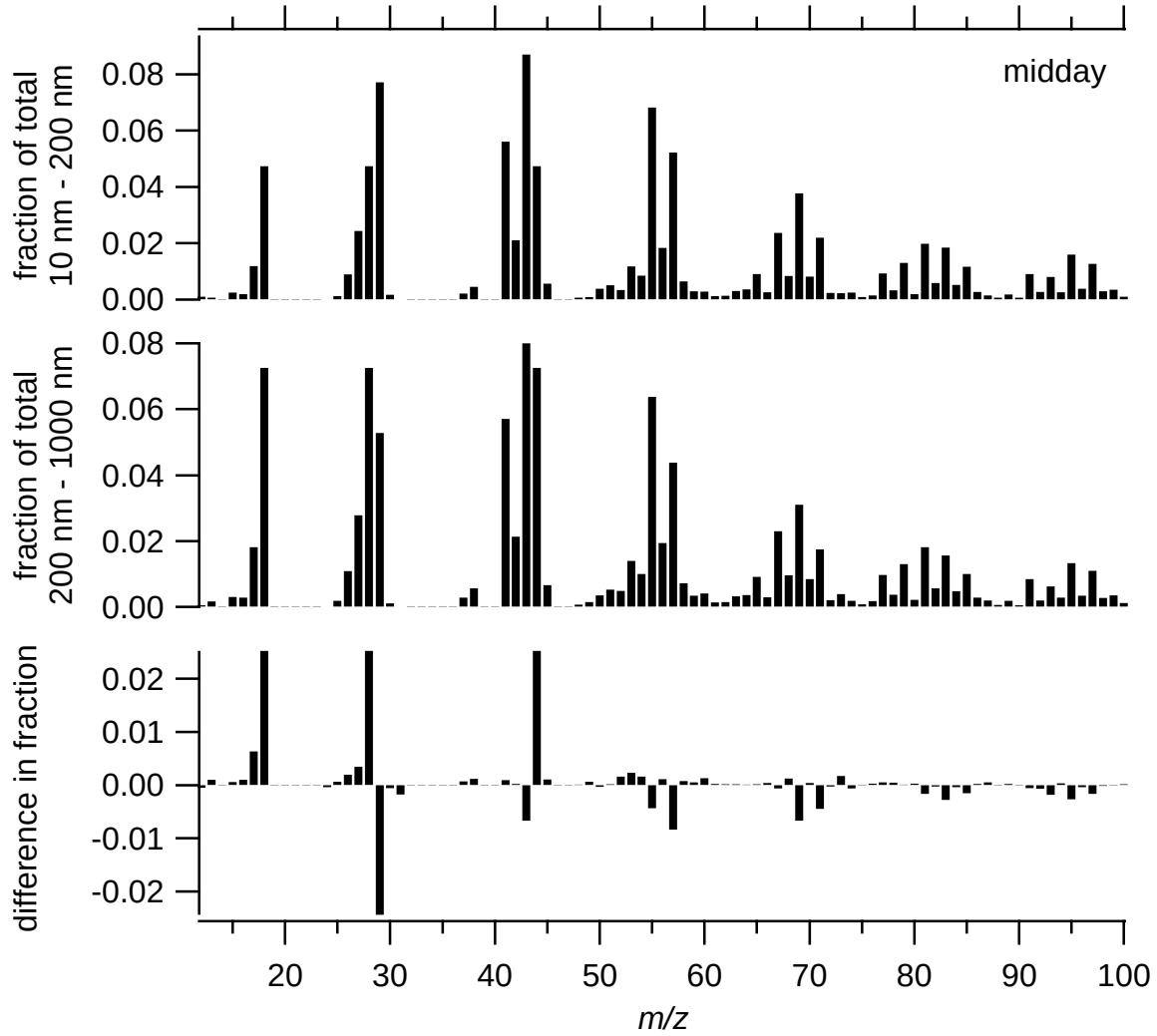

Figure 5-5. Average organic mass spectra (fraction of signal by *m/z*) during midday (1100-1500 LST) for (top) particles less than 200 nm d_{va}, (middle) particles greater than 200 nm d_{va}, and (bottom) the difference between the top and middle spectra.

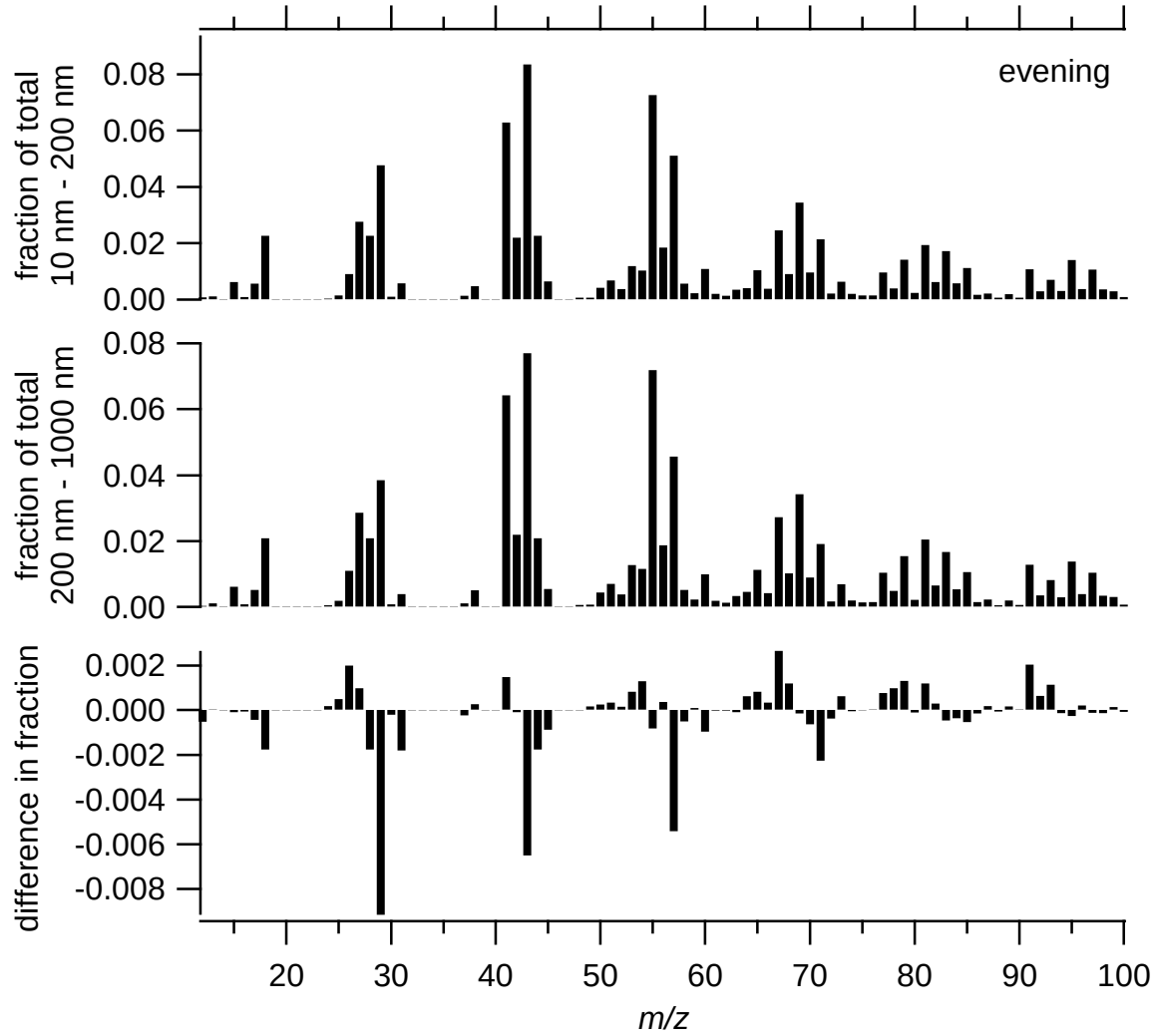

Figure 5-6. Average organic mass spectra (fraction of signal by *m/z*) during evening (1700-2100 LST) for (top) particles less than 200 nm d_{va}, (middle) particles greater than 200 nm d_{va}, and (bottom) the difference between the top and middle spectra.

5.4.2 Changes in OM Size Distribution by Time of Day

The OM size distribution was typically broad throughout the day, even as OM concentrations changed. Figure 5-7 summarizes the average OM size distribution in morning, midday and evening; the average concentration by hour is also shown. The size distribution of the inorganic species remained relatively constant throughout the day, i.e., the overall average is representative of the entire study, so the distribution by time of day for these species is not shown.

During morning, midday and evening OM has an average broad size distribution. In the evening, there is relatively more mass in smaller particles less than 200 nm d_{va} compared to other times of day. This broader size distribution with similar mass from 100 nm d_{va} particles and from 400 nm d_{va} particles in the evening indicates the presence of smaller, fresh/less oxidized particles compared to other times of day. This result is consistent with the low OM/OC, low O/C and high H/C ratios observed in the evening. With higher OM, low inversion layers and low wind speed in the evening, smaller, fresh particles may be forming during the evening, leading to the broad size distribution.

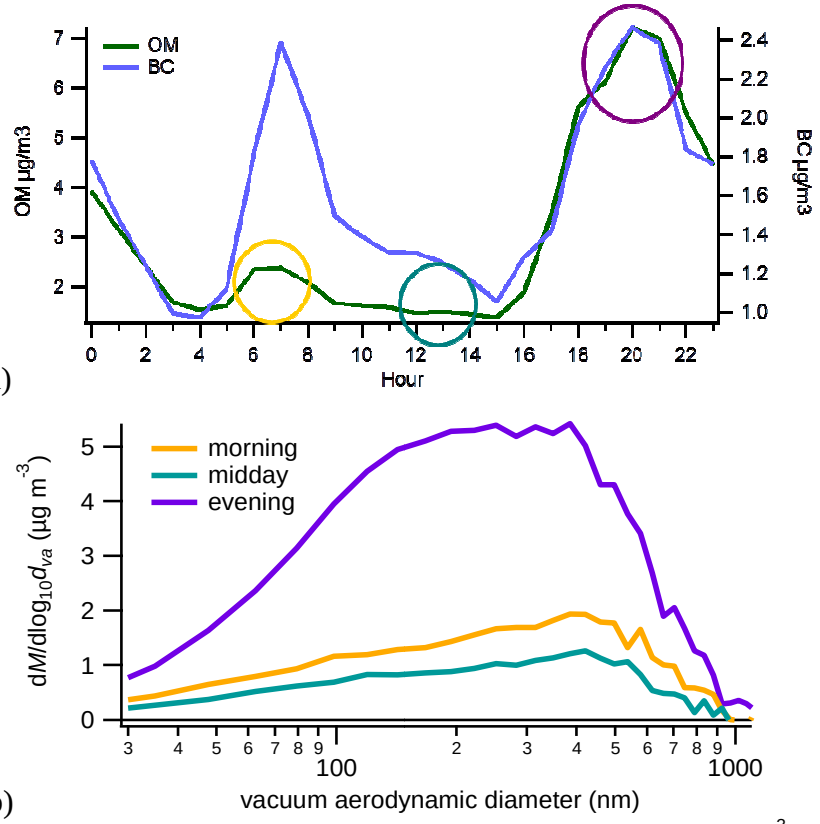

Figure 5-7. a) average concentration by hour for OM and BC (µg/m^3), with circles indicating the time of day (morning, midday and evening); b) size distribution (dM/dlog$_{10}$d$_{va}$) of OM for morning (0600-0900), midday (1100-1500) and evening (1700-2200).

Differences in the size distribution of example *m/z* further demonstrate the importance of fresh, small particles in the morning and evening. Figure 5-8 shows *m/z* 43, 44, 57 and 60 for morning (0500-0900 LST), midday (1200-1500 LST) and evening (1800-2100 LST). At all

times, *m/z* 44 has a peak around 300-400 nm, and in the evening it also has a secondary peak around 100 nm. *m/z* 57 and *m/z* 43 also have a peak around 300-400 nm, but have a wider distribution down to the smaller size range, especially in evening when the amount of mass is similar between 100 to 400 nm. *m/z* 60 is only evident in the evening, and it also has a wide size distribution, similar to *m/z* 57.

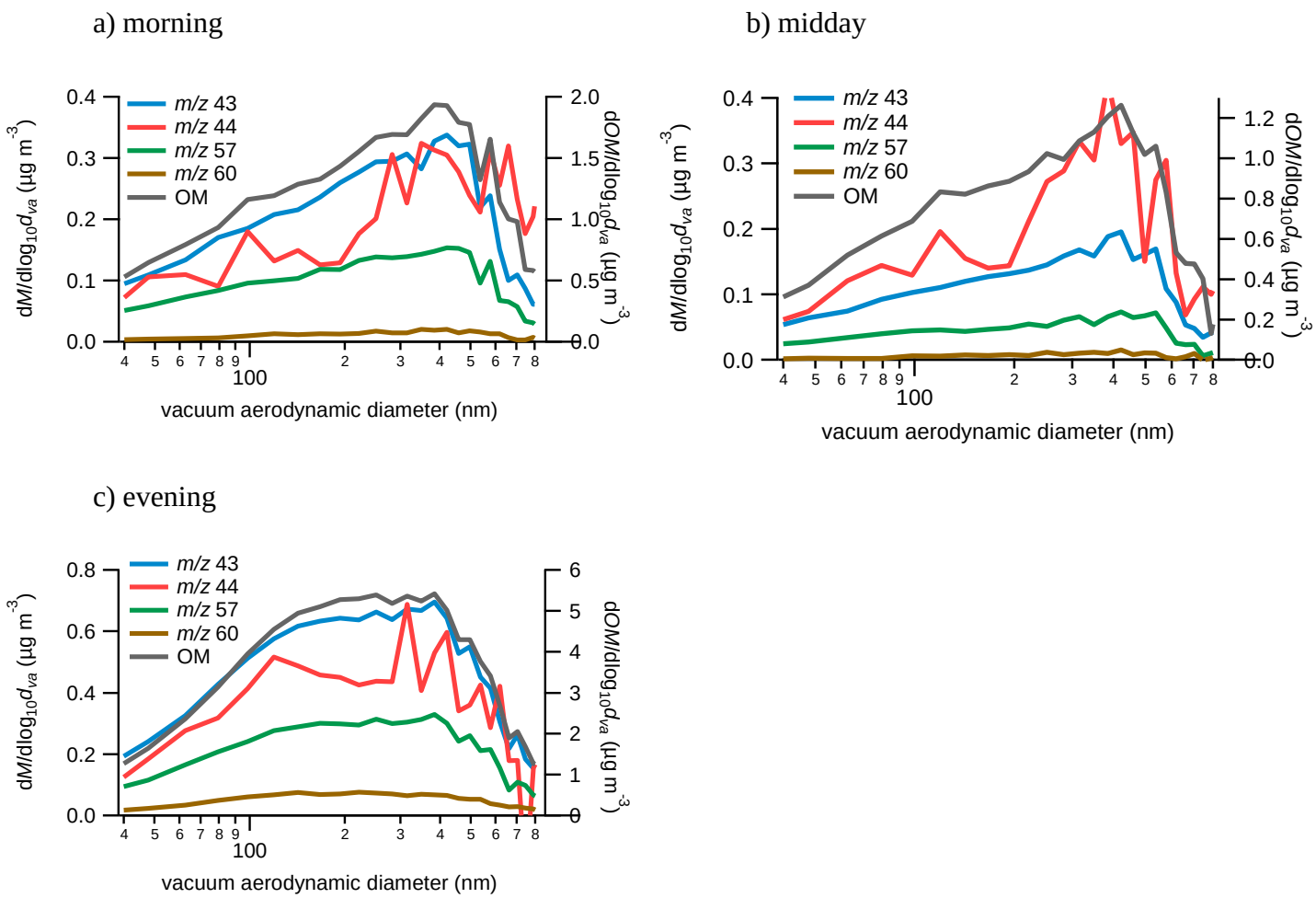

Figure 5-8. Size distributions of *m/z* 43, 44, 57 and 60 during: a) 0500-0900 LST; b) 1200-1500 LST; and c) 1800-2100 LST.

Next, the differences in OM size distribution during upwind, downwind and stagnant conditions, by time of day, were examined (Figure 5-9). At all times concentrations are higher during stagnant conditions than upwind or downwind conditions. Under stagnant conditions, there appears to be slightly more mass from smaller size particles, e.g., less than 200 nm, compared to upwind or downwind conditions. During midday and 0000 LST there is slightly more mass from these smaller particles during downwind conditions compared to upwind conditions as well, possibly due to influence from emissions on the freeway. This effect is not noticeable during the morning or evening, possibly because concentrations are higher from both upwind and downwind conditions in these times; a similar lack of difference between upwind and downwind conditions during morning and evening is also seen for OM and OM/OC.

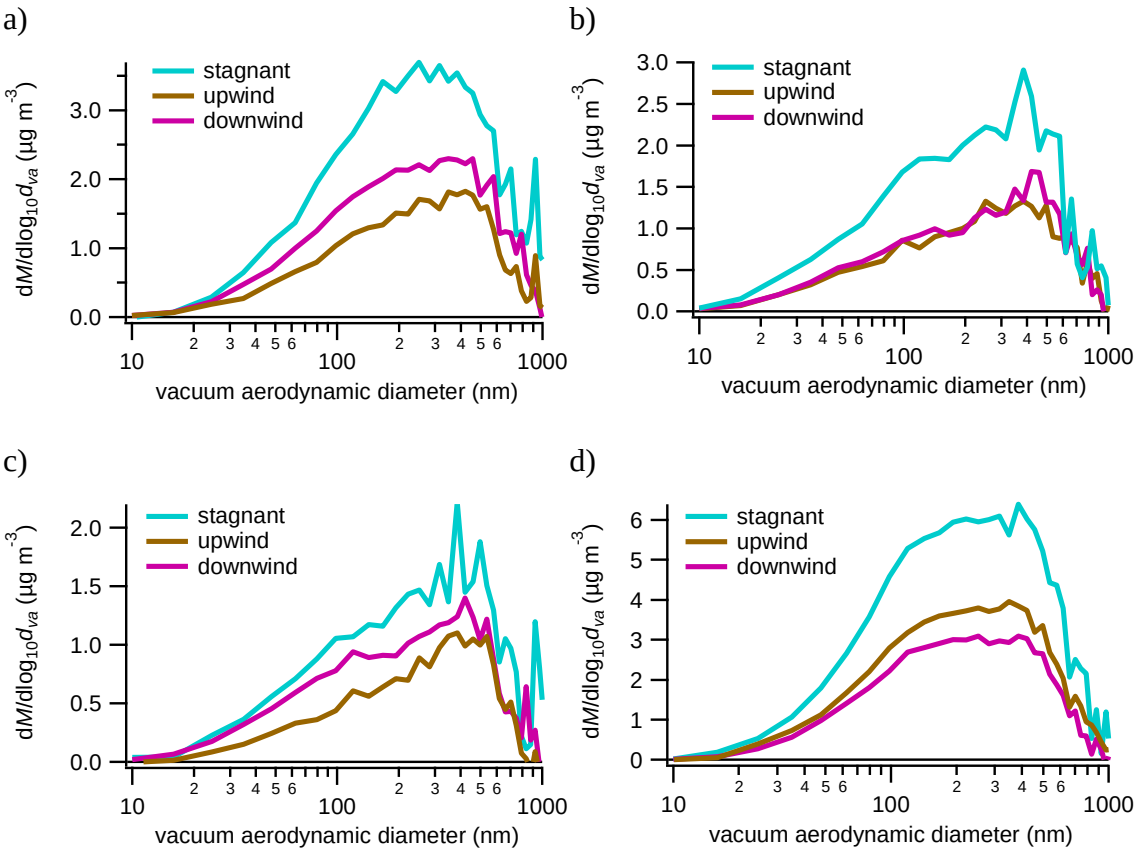

Figure 5-9. OM size distribution during stagnant, upwind and downwind conditions for a) 2200-0500 LST; b) 0500-0900 LST; c) 0900-1700 LST; and d) 1700-2200 LST.

5.5 Time Series Analysis of OM Size Distribution

OM followed a typical pattern of high evening concentrations, a secondary peak in the early morning, and low concentrations other times of day. During all times of day, the OM distribution was fairly broad, though in the evening there was more mass from smaller particles than in other times of day. Figures 5-10 through 5-12 show time series of the OM size distribution for multi-day periods where hourly average OM concentrations were greater than 5 $\mu g/m^3$ during multiple days.

In general, OM and m/z 60 vary together during the evenings, when concentrations are highest. On evenings with hourly OM concentrations greater than 10 $\mu g/m^3$ after a rapid increase in OM (e.g., January 9, 11, 19, and 22, etc), OM mass is predominantly in the 100 nm to 500 nm range. Evenings where the increase is slower or concentrations are lower, such as January 10, 12, 23, and 25, concentrations are shifted slightly, with more mass in particles in 200 -500 nm range. In both sets of evenings there is still modest OM even below 100 nm. While there is not a clear picture of a shifting size distribution during the evening, i.e., of smaller particles growing into larger particles, mass in particles less than 100 nm occurs when OM and *m/z* 60 concentrations are at their highest. Once OM begins to decrease around midnight, OM remains predominantly in the 100-500 nm range, but there is little mass in particles with d_{va} less than 100 nm. January 9 and 11 are good examples of this process. These results further suggest that the particles with d_{va} less than 100 nm are due to extremely fresh emissions, as there is little mass in these particles once fresh emissions from biomass burning and mobile sources decrease in the 2300-0100 LST time frame.

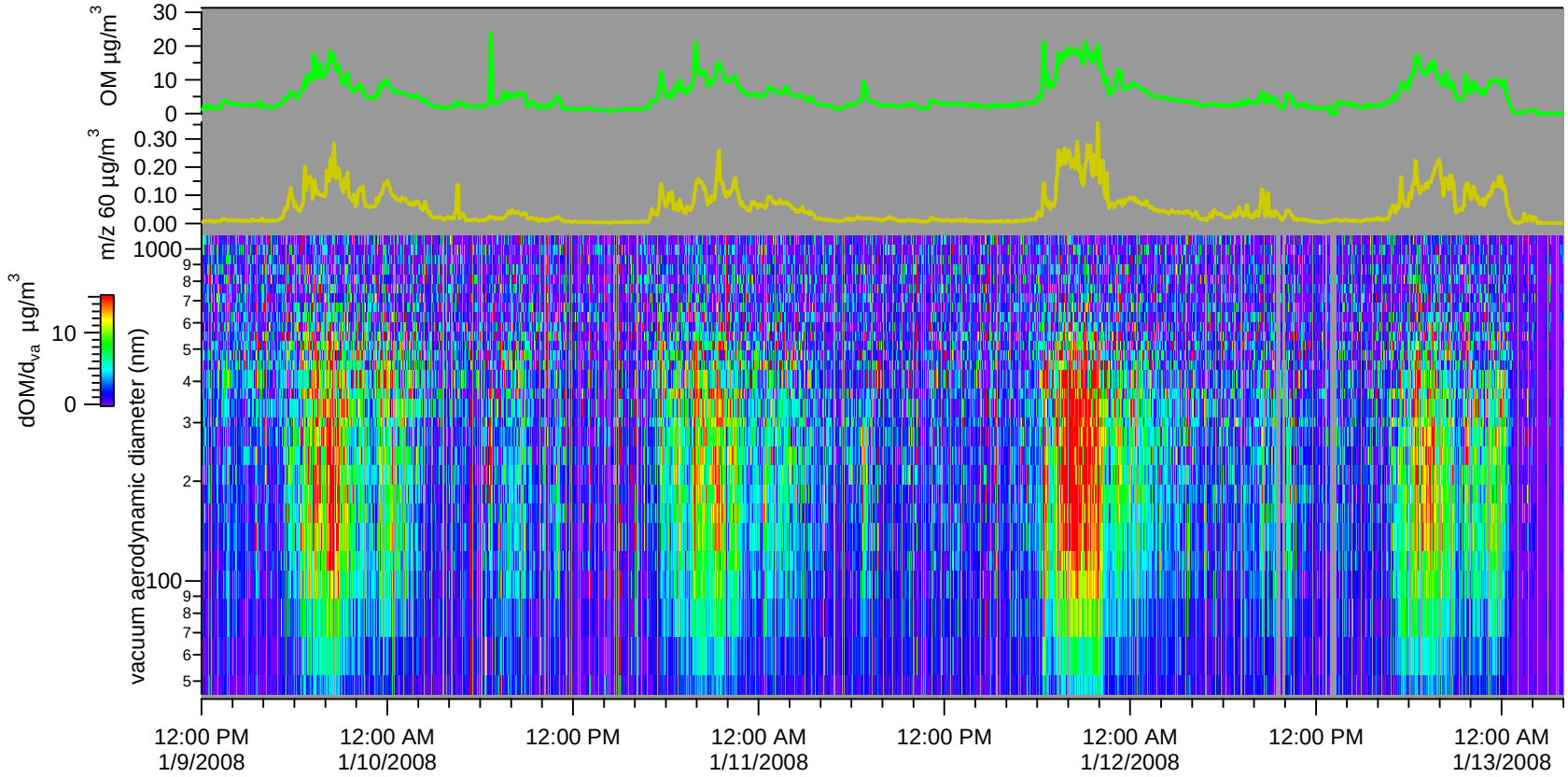

Figure 5-10. Time series contour plot of dOM/d_{va} by size during January 9-13 2008, with OM and *m/z* 60 concentrations µg/m^3.

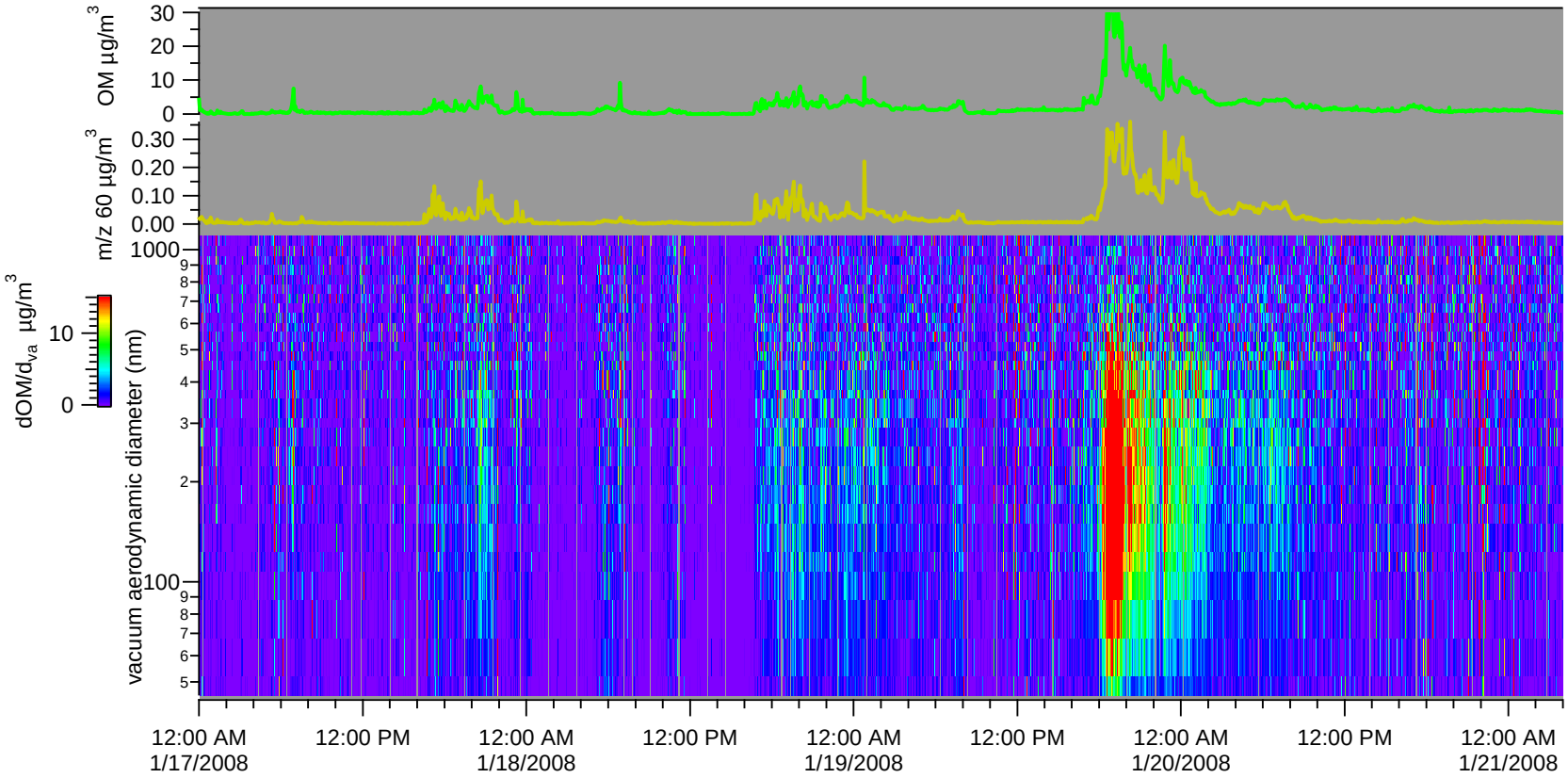

Figure 5-11. Time series contour plot of dOM/d_{va} by size during January 17-21, with OM and *m/z* 60 concentrations in µg/m^3.

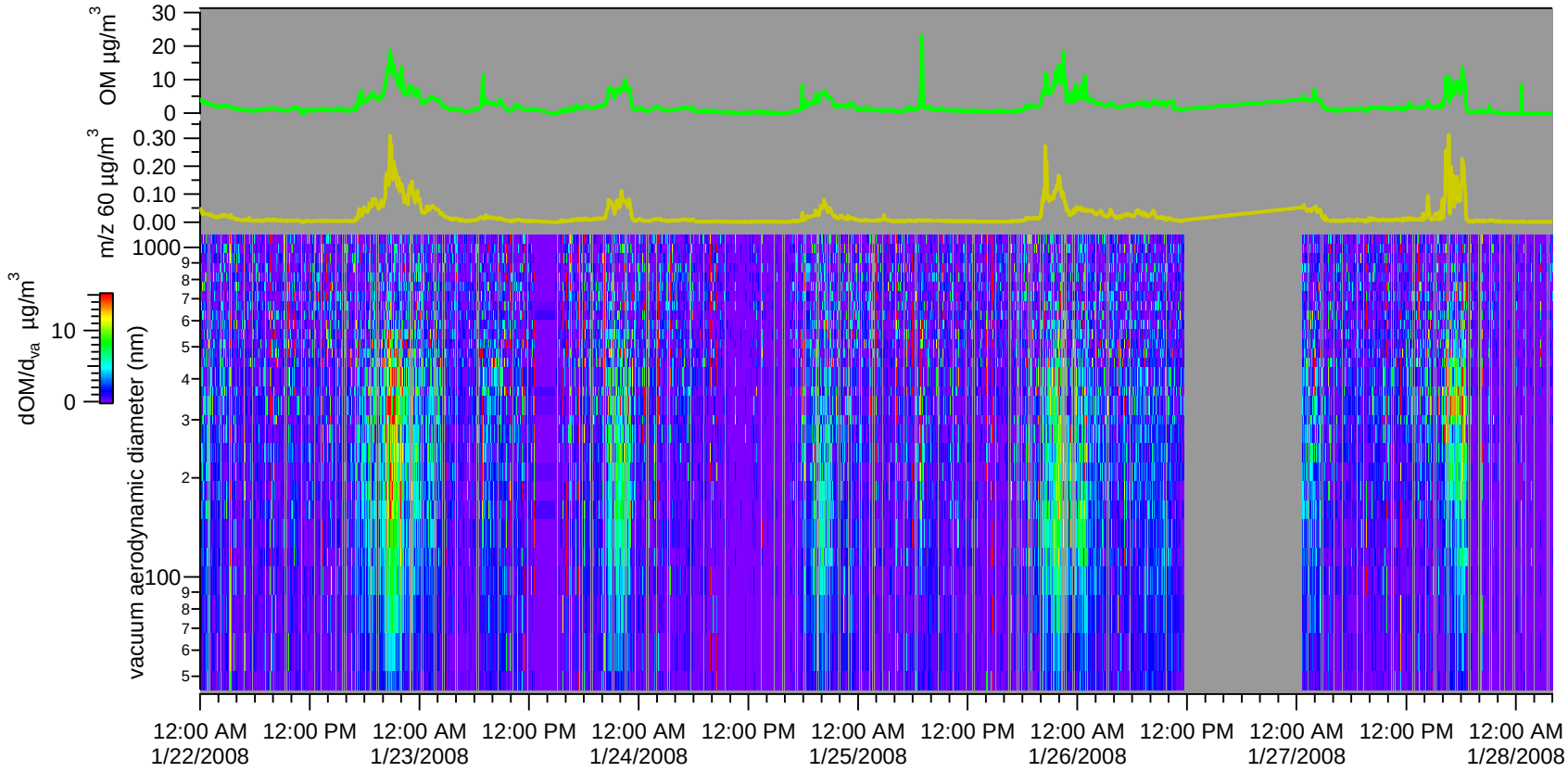

Figure 5-12. Time series contour plot of dOM/d_{va} by size during January 22-28, with OM and m/z 60 concentrations µg/m^3.

Figure 5-13 shows the OM size distribution when the fraction of OM from each PMF factor is relatively high: when LV-OOA is greater than 60% of the OM, (N=646, OM average = 0.71 $\mu g/m^3$), when HOA was greater than 55% (N=128, OM average = 4.11 $\mu g/m^3$), when SV-OOA was greater than 60% (N=167, OM average = 5.42 $\mu g/m^3$), and when BBOA was greater than 35% (N=105, OM average = 3.12 $\mu g/m^3$). Sufficient points were available with a threshold of 60% for LV-OOA and SV-OOA, but a lower threshold was used for HOA and BBOA in order to include more samples in the analysis. The OM size distribution under high HOA conditions peaks at around 250 nm d_{va}, while the size distribution during high LV-OOA conditions peaks at between 385-460 nm d_{va}. The high HOA conditions typically occur in the morning and evening under calmer winds (average wind speed = 1.5 m/s), when fresh emissions are the main source of particles and OM is high. High LV-OOA conditions occur when wind speeds are high (average wind speed = 2.75 m/s), when regional, oxidized aerosol are the main influence on OM; OM is also lower during these periods. High BBOA conditions result in a size distribution that looks like a combination of HOA and LV-OOA, with peaks between 300-400 nm d_{va}.

When SV-OOA is high, there is a broad OM distribution between 150 nm and 320 nm, peaking around 250 nm d_{va}. It is initially surprising that the size distribution during high HOA conditions has more mass from larger particles compared to high SV-OOA conditions, since HOA is typical of fresh emissions, while SV-OOA characterizes slightly aged conditions. However, 66% of the high HOA conditions are between 0600-0800 LST, when fresh HOA-type particles are emitted and combined with larger, aged particles "leftover" overnight, thus resulting in a size distribution that accounts for both the smaller, fresh particles and the larger processed particles. High SV-OOA conditions occur in the evening (49% during 1700-2000 LST, 64% during 1700-2200 LST), when OM is much higher than at any other point in the day. During

these times the amount of fresh and slightly aged OM dwarfs the amount of mass from large, oxidized particles, resulting in a broad size distribution. It may be that the PMF factors cannot characterize the evening time period well, when concentrations quickly rise and OM composition quickly moves from a more-oxidized regime to a fresh, less oxidized regime. As discussed in Chapter 3, when more factors are used in PMF, the additional factors are found only in the evening, and devolve the SV-OOA factor into factors that are apparent in the early and later evening.

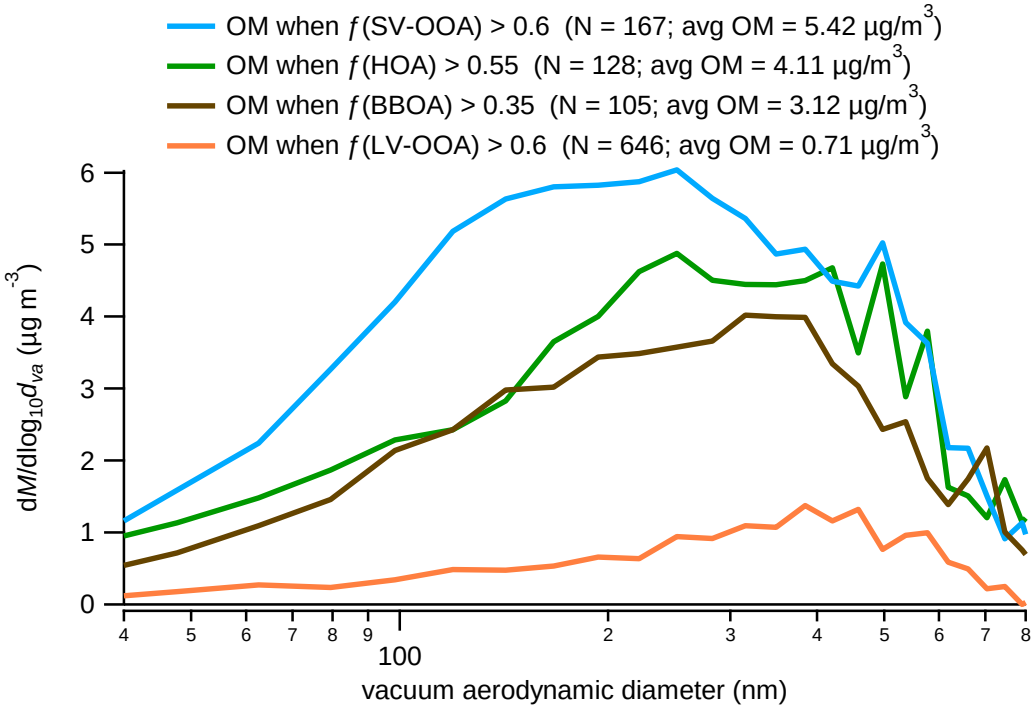

Figure 5-13. OM size distribution when the fraction of PMF factors is high: when HOA is >55%; (green trace); when LV-OOA is >60% (orange trace); when SV-OOA is > 60% (blue trace); and when BBOA is > 35% (brown trace).

5.6 Case Study: Three example mornings

OM concentrations increased during the morning rush hour, although concentrations were on average lower than evening concentrations. The relatively low peak during the morning is somewhat surprising, since during the morning rush hour there is a peak in vehicle emissions. However, the morning rush hour occurred when the ground-level inversion layer typically began to break (see Figure 4-3), while the evening rush hour occurred just as the inversion layer began, so increased mixing during the morning rush hour may help explain these differences. Earlier figures show the size distribution during the morning overall and by wind direction/speed. As an example case study, Figure 5-14 shows the OM size distribution during three consecutive mornings on January 10 through January 13, paired with the time series of OM and other parameters. In these examples, we can see that the average morning distribution seen earlier is quite representative, though with some morning-to-morning variability. On the mornings of January 10 and 12 there is more mass in the larger diameter particles, while on the morning of January 11 the distribution is centered at 200 nm d_s. During these mornings, OM has a small rise in concentration, as do CO and BC. Wind speeds are light, less than 2 m/s, and only on the first of these three mornings is the monitoring site downwind of the freeway. This is the morning with the highest concentrations, though still modest compared to evening levels. The 10 m – 2 m temperature difference becomes non-negative between 0800 and 0900, indicating the break-up of the overnight inversion layer. The combination of this break-up and decrease in emissions as the morning rush hour wanes leads to lower concentrations by 0900-1000 LST.

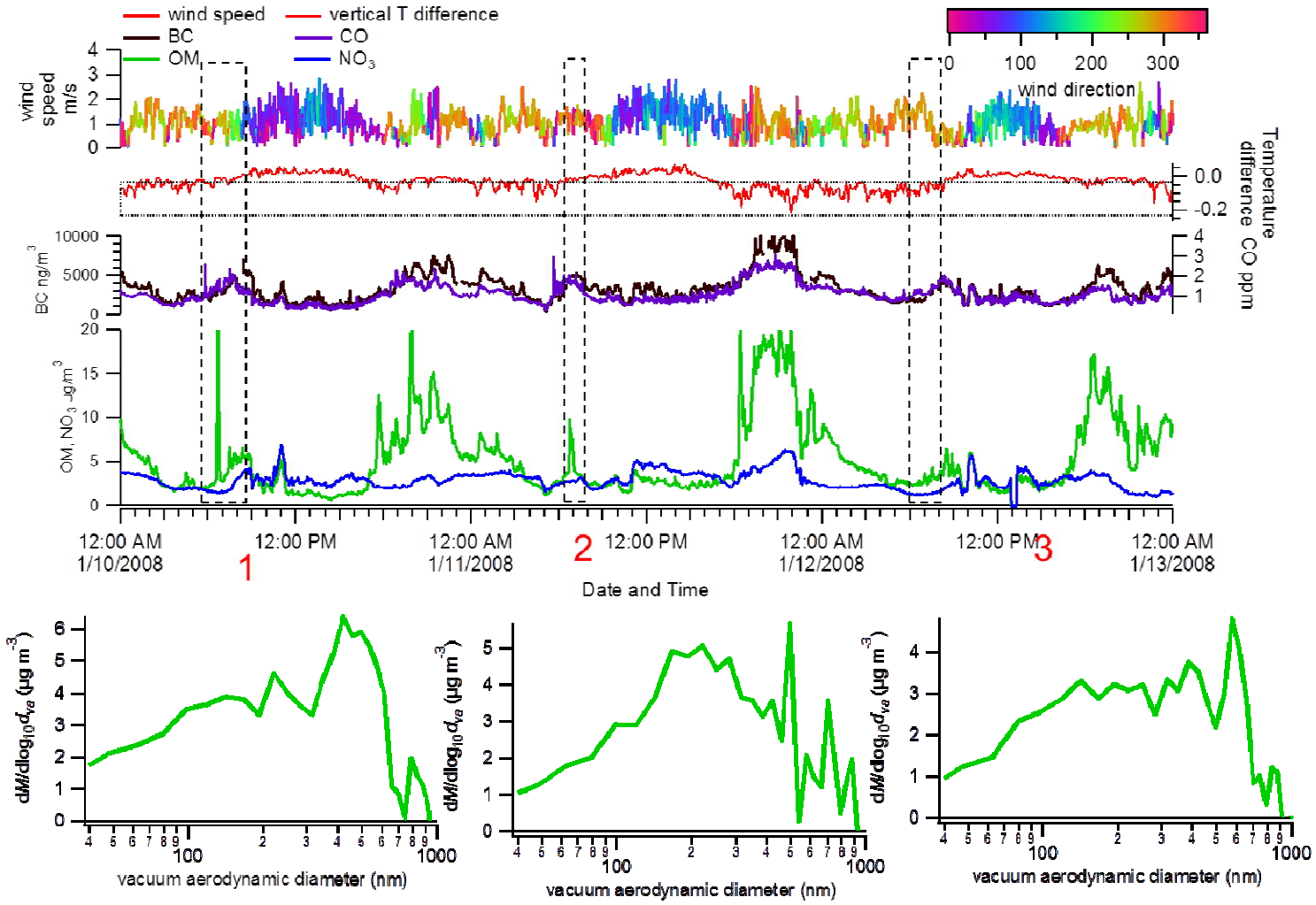

Figure 5-14. Time series of wind speed, direction, 10 m – 2 m vertical temperature difference, BC, CO, OM and NO_3, with OM size distributions of OM for the morning of January 10, 11 and 12.

5.7 Case Study: Hourly Progression of January 10 evening

As an additional case study, the changes of the OM size distribution during a typical evening, January 10, were also examined; Figure 5-15 shows a time series of OM and other species, along with the 2-hour averaged OM size distribution for 1700-1900, 1900-2100, 2100-2300 and 2300-0300 LST. OM increased from 1.9 $\mu g/m^3$ at 1600 LST to 13.3 $\mu g/m^3$ at 2100 LST (hourly averages), then slowly decreased overnight until 0500 LST the next day. During the first two hours the size distribution is broad but with the most mass around 400 nm d_{va}. During the next four hours OM is high and the mass size distribution is shifted to smaller particles between 100 to 400 nm. After the evening rush hour, from 2300 to 0300 LST, OM declines slowly and has a size distribution centered between 200 to 300 nm d_{va}. This example suggests a large influx of small particles during the evening rush hour, when residential biomass burning also occurs.

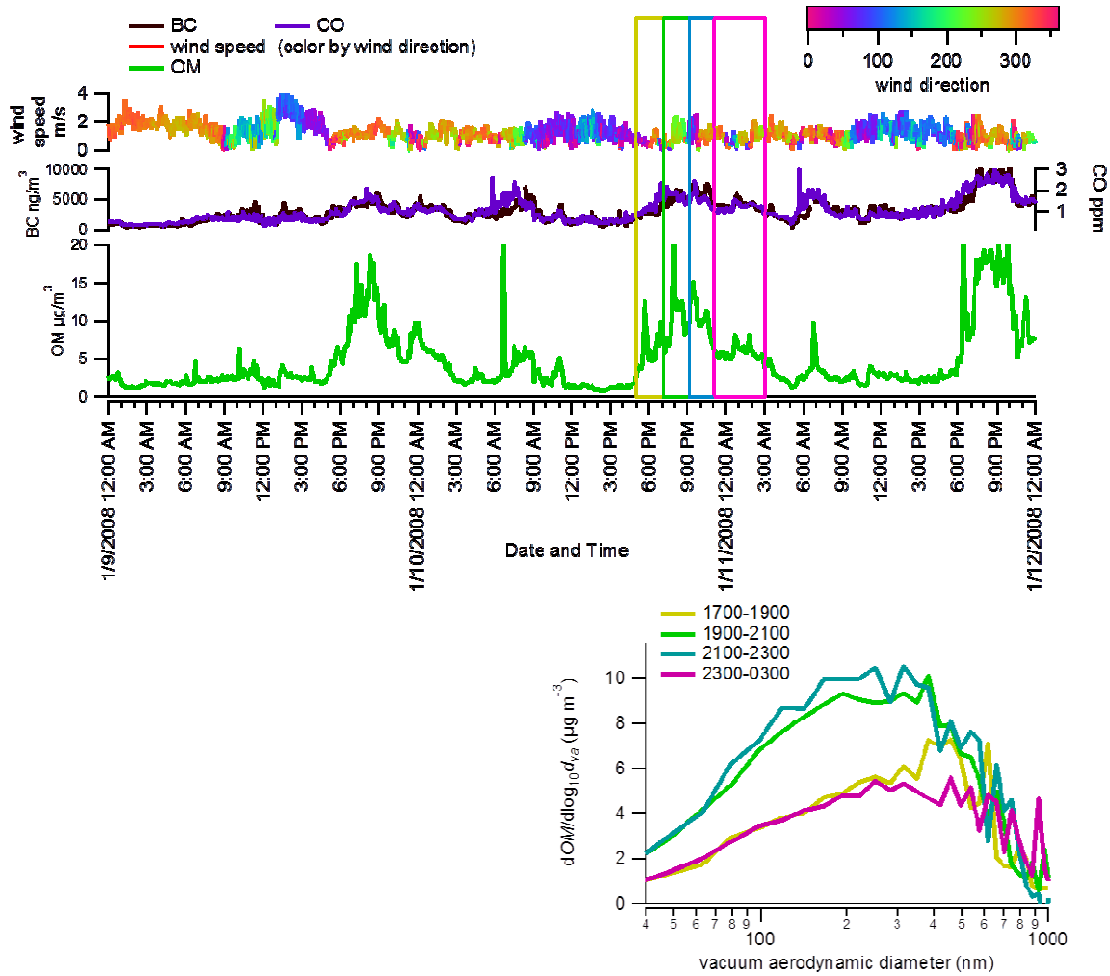

Figure 5-15. Time series of wind speed, direction, 10 m – 2 m vertical temperature difference, BC, CO, OM and NO_3, with OM size distributions of OM for the evening of January 10 during 1700-1900, 1900-2100, 2100-2300 and 2300-0300 LST.

5.8 Additional Analyses

Additional analyses of particle size data were performed but were generally not fruitful, and are only briefly summarized here. One analysis was to evaluate if the PAH content of smaller and larger particles differ. Slowik et al (Slowik et al., 2004) showed that soot particles could be classified into two general types: 1) particles with d_{va} less than 100 nm that are high in BC but low in PAH content; and 2) particles with d_{va} around 400 nm that are high in PAH content and lower in BC content. BC data were not available by particle size, so we are unable to evaluate BC content directly. In addition no particle number distribution data were collected,

so we are unable to identify periods when sub-100 nm d_{va} particles were dominant; if we could, we could perhaps evaluate case studies when smaller particles were in high concentration. Using the AMS data, we calculated the fraction of OM from PAH for multiple size bins, averaged over the entire study period: less than 100 nm, 100-300 nm, 300-600 nm, and greater than 600 nm d_{va}. The PAH fraction was between 2.9-3.5% of total OM for all size bins, so results were inconclusive. With either BC data by size or particle number distribution data we may have been better to able to evaluate different soot types proposed, but were not able to here.

In addition, the nitrate size distributions during the one high nitrate concentration period of January 8 -10 were investigated. However, nitrate consistently had the same size distribution as shown in Figure 5-1, with a peak around 450 nm, shown in a time series in Figure 5-16. The relatively invariable size distribution is indicative of aged, processed particles, as expected for nitrate. Nitrate concentrations were low during the rest of the study. In addition, Figure 5-17 shows the size distribution of sulfate, which was extremely low during the study. Sulfate is consistently found in larger particles throughout the study, since sulfate is likely in aged and well processed particles.

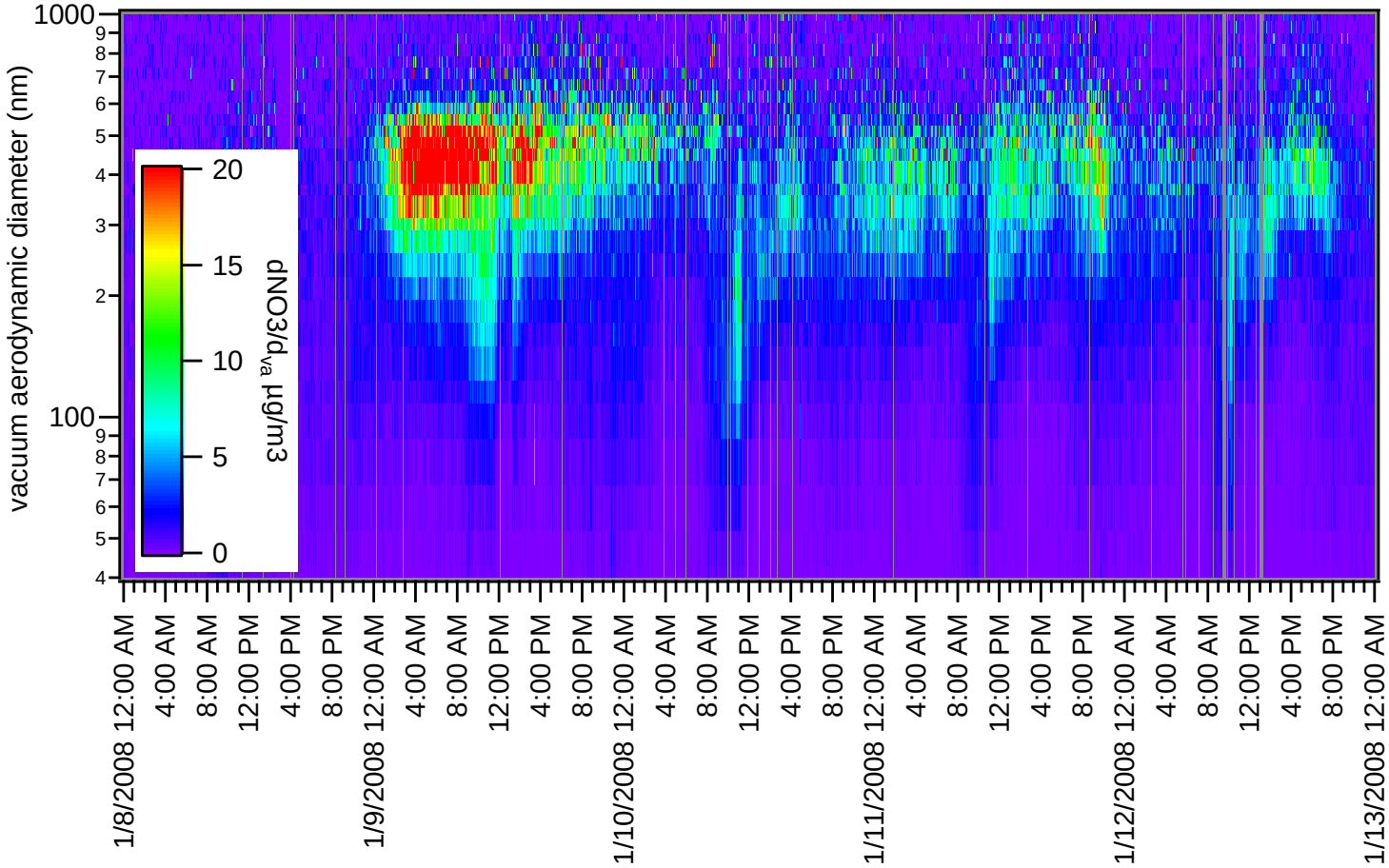

Figure 5-16. Time series contour plot of dNO_3/d_{va} by size during January 9-13 2008.

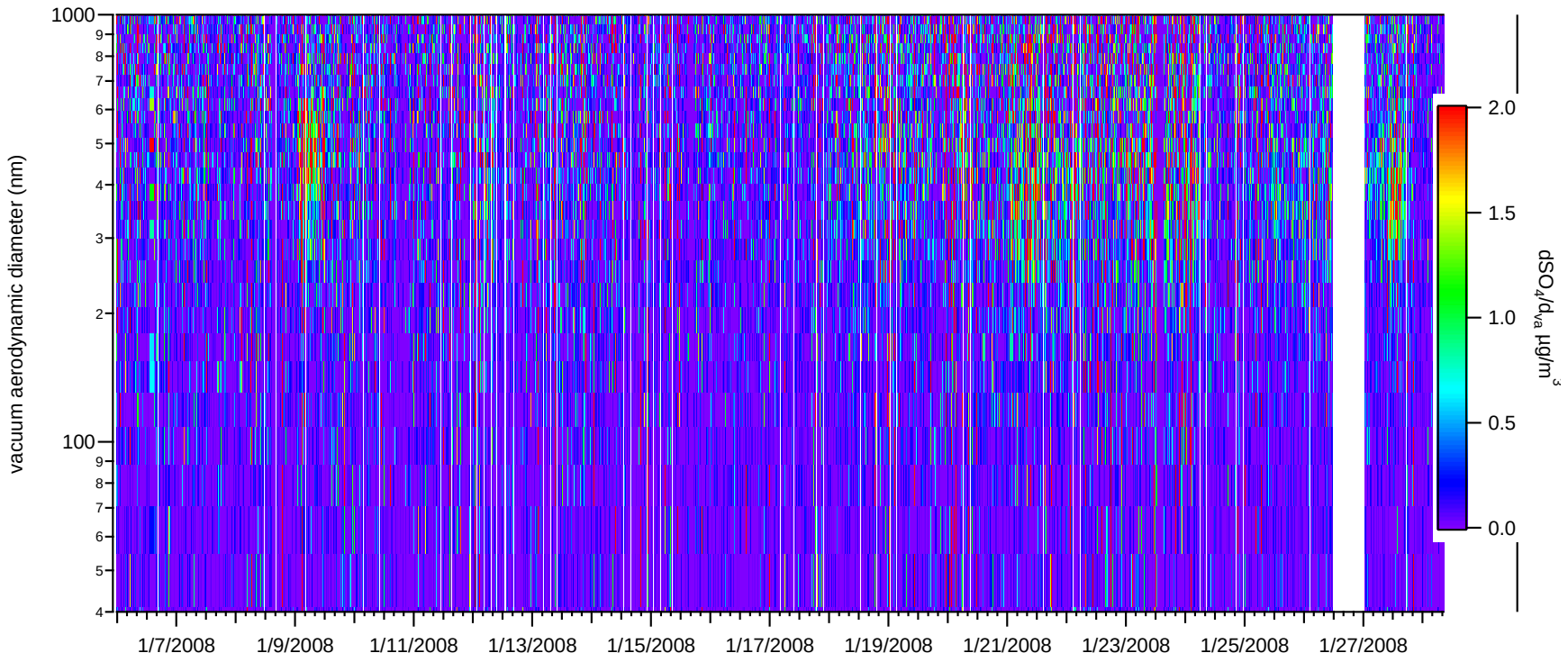

Figure 5-17. Time series contour plot of dSO_4/d_{va} by size during January 5-28 2008.

6. The Importance of Urban-Scale Sources: Residential Biomass Burning

6.1 Chapter Summary

The impact of residential biomass burning in Las Vegas on carbonaceous aerosol concentrations was evident through a number of measurements made at Fyfe Elementary School in winter 2007/2008. During January 2008, detailed high time resolution measurements of organic matter (OM) were made with an Aerodyne High Resolution Aerosol Mass Spectrometer (HR-AMS), including a biomass burning tracer, the fragment $C_2H_4O_2^+$ at *m/z* 60 which is derived from levoglucosan and other anhydrosugars produced from combustion of cellulose and hemi-cellulose. Hourly concentrations of water soluble potassium (K^+), another indicator of biomass burning, were measured with a particle into liquid system with ion chromatography (PILS-IC). Measurements of levoglucosan via gas chromatography-mass spectroscopy from 12-hour overnight quartz fiber filters were also made. On average, 12% of the OM, and 25% of OM during the nighttime, was apportioned to biomass burning via PMF analysis of AMS data. Using source profiles and levoglucosan data, on average 33% of the OM was attributed to biomass burning in the nighttime, when OM reached its peak. Levoglucosan and AMS $C_2H_4O_2^+$ were strongly correlated (r^2=0.92). K^+ correlated well with $C_2H_4O_2^+$ (r^2=0.86) during the evening (1800-2200 LST), with a ratio to $C_2H_4O_2^+$ on average at 1.4, but overnight the correlation slowly decreased and the ratio increased, so that by midday the correlation approached zero, and the ratio reached a peak, possibly due to loss of $C_2H_4O_2^+$, but not K^+, by aging processes. While K^+ may be an indicator of BB, it is not necessarily a good tracer for source apportionment alone, as contributions of non-BB sources to K^+ appear to be significant and can change day to day.

Aethalometer measurements of BC were done at Fyfe and an urban background site during June 2007-June 2008. Using the difference between UV and BC channels from the Aethalometer for apportioning BC from biomass burning, we found that BB was on average 5% of the BC, and 7% during the evening; BCbb was only evident in the wintertime. There was only a modest correlation (r^2=0.40 to 0.60) of BCbb and of UV-BC difference with $C_2H_4O_2^+$ and with levoglucosan. The much lower contribution to BC compared to OM, and the low correlation with $C_2H_4O_2^+$, may be due to the heavy influence of fossil fuel combustion emissions on a nearby freeway.

6.2 Ambient Concentrations of Biomass Burning Markers

Concentrations of organic matter, black carbon, and biomass burning indicators (levoglucosan, $C_2H_4O_2^+$, K^+, and UV-BC difference) varied widely from day to day during January 2008, typically reaching a peak in the early evening (i.e., 1900 through 2100 LST). Figure 6-1 shows a time series for these species during January 2008. OM on average was 3.3 $\mu g/m^3$, while BC was 1.8 $\mu g/m^3$. Other aerosol and gaseous species were also measured, and are summarized elsewhere (Brown et al., 2012); in January 2008, OM and BC comprised 74% of the PM_1 mass measured via the AMS and aethalometer, excluding metals and crustal material which were not measured. At a nearby urban CSN site (4701 Mitchell St, AQS ID 32-003-0020) OM and EC were 68% of the total measured species in January 2008, based on 24-hour filter data. BC at Fyfe is higher than typical for urban sites, since the monitoring site is located next to the US 95 freeway. For comparison, in January 2008 BC concentrations at the Hancock urban site, more than 2 km from a freeway, were less than 1 $\mu g/m^3$, and 24-hour filter EC at the CSN site averaged 0.8 $\mu g/m^3$. The OM concentrations are not particularly high for an urban area, and are typical of OM concentrations found in prior Las Vegas studies. This average is similar to the

average OM concentrations based on 24-hour filter data collected on 5 days in January 2008 at an urban CSN site in Las Vegas, where the non-blank corrected average OC was 2.8 $\mu g/m^3$. Using a standard blank correction of 1 $\mu g/m^3$ (Chow et al., 2010; Frank, 2010), this results in 1.8 $\mu g/m^3$. Using an average OM/OC ratio of 1.54 (Brown et al., 2013), this translates to an OM level of 2.8 $\mu g/m^3$, which is close to our AMS-OM average of 3.3 $\mu g/m^3$. $C_2H_4O_2^+$ concentrations averaged 0.018 $\mu g/m^3$, and between 1800-0000 LST were nearly three times higher at 0.040 $\mu g/m^3$. PILS K^+ concentrations were, on average, 0.033 $\mu g/m^3$, and levoglucosan concentrations during the 12-hr overnight samples averaged 0.14 $\mu g/m^3$. For comparison, the CSN site concentrations of elemental potassium during the same time frame were 0.03 $\mu g/m^3$ across five measurement days.

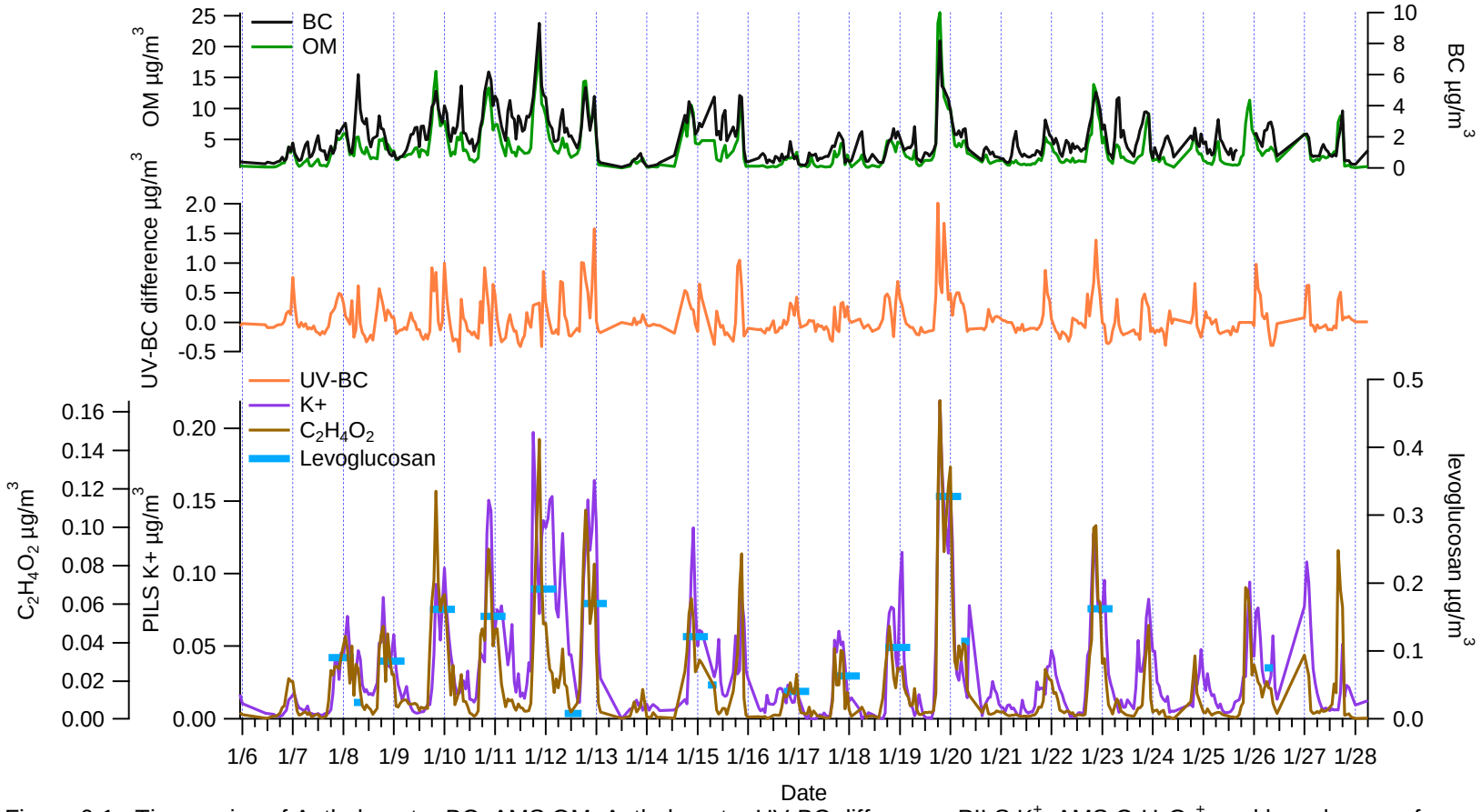

Figure 6-1. Time series of Aethalometer BC, AMS OM, Aethalometer UV-BC difference, PILS K^+, AMS $C_2H_4O_2^+$, and levoglucosan from quartz fiber filters at Fyfe during January 2008 (all units µg/m^3).

Figure 6-2 summarizes the typical diurnal pattern of the semi-continuous measurements. BC concentrations were similar in the morning and evening, associated with the rush hour commute times. OM had a minor peak in the morning, and was on average three times higher in the evening than in the morning. $C_2H_4O_2^+$, K^+, and UV-BC difference all show a very similar average diurnal pattern. K^+ concentrations decrease more slowly than $C_2H_4O_2^+$ after midnight, possibly suggesting that $C_2H_4O_2^+$ is being lost due to other mechanisms than those affecting the conservative species K^+, such as partitioning from particle to gas phase or atmospheric reactions. K^+, $C_2H_4O_2^+$, and UV-BC difference are all at a minimum in the midday, when emissions of residential biomass burning are low, wind speeds and dispersion are higher, and OM is lower.

OM has a similar pattern as these BB indicators, while BC has a different pattern; concentrations of BC reach similar average maxima in the morning and evening. The diurnal pattern of BC indicates that mobile source emissions related to rush hour traffic are likely the most important source of BC. With low concentrations in the midday and a steep rise in concentrations in the evening, the diurnal OM pattern is likely due to a mix of fresh emissions in the morning and evening with the rush hour and other activities, plus an additional evening source of biomass burning. This was further demonstrated with PMF analyses on the AMS data (Brown et al., 2012), which showed that fresh, hydrocarbon-like organic aerosol (HOA) was present in the morning and evening, and that additional semi-volatile oxidized organic aerosol (SV-OOA) and biomass burning organic aerosol (BBOA) were evident in the evening peak.

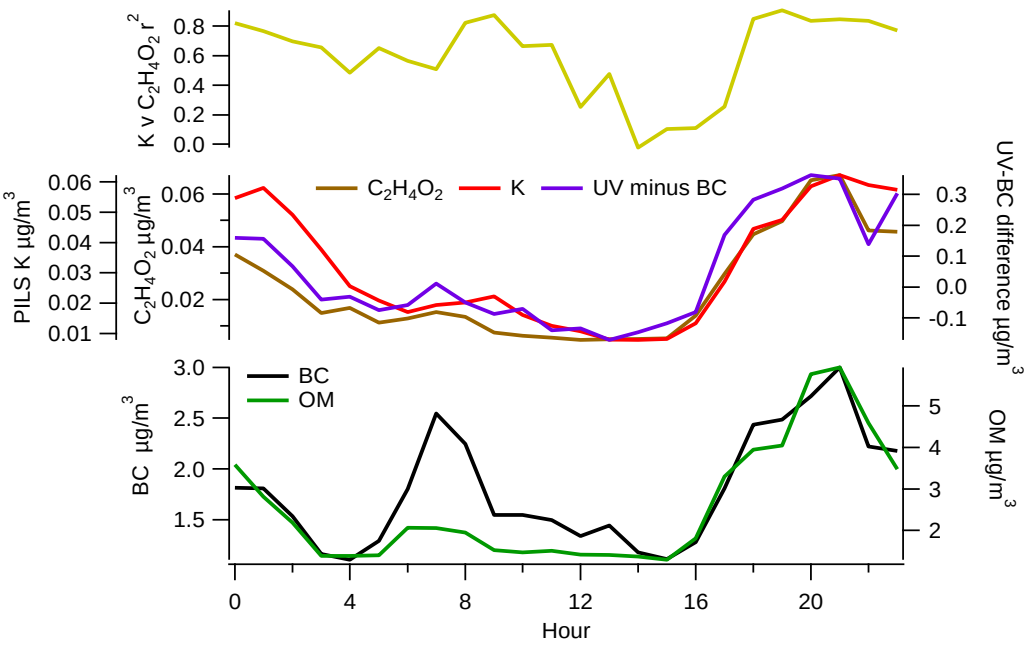

Figure 6-2. Average concentration by hour for Aethalometer BC, AMS OM, UV-BC difference, PILS K^+, and AMS $C_2H_4O_2^+$ (all units µg/m^3), plus correlation (r^2) by hour of PILS K^+ versus AMS $C_2H_4O_2^+$.

6.3 Comparison Among Biomass Burning Markers

6.3.1 Comparisons with Levoglucosan

There was a range in how well the potential biomass burning indicators correlated with each other. Filter-based levoglucosan was available only for a subset of times during the study, at varying intervals. Correlations of levoglucosan with other measurements are summarized here (Figure 6-3), while correlation among semi-continuous measurements from other instruments is discussed in the next section (6.3.2).

Levoglucosan concentrations measured from filters had high correlations with AMS $C_2H_4O_2^+$, with an r^2=0.92. This is expected since $C_2H_4O_2^+$ is a fragment from levoglucosan and other co-emitted anhydrous sugars; pure levoglucosan introduced into an AMS yields a suite of ions that has $C_2H_4O_2^+$ as 13%-14% of the total ion fragment pattern (Lee et al., 2010). Unlike

$C_2H_4O_2^+$, there was only a moderate correlation of PILS K^+ (r^2=0.66) or UV-BC difference (r^2=0.53) with levoglucosan; no correlation was seen between levoglucosan and BC (r^2=0.16). The lower correlations are perhaps not surprising, as both BC and K^+ have other non-biomass burning sources, and levoglucosan may be depleted during the 12-hour sampling period via atmospheric reactions or phase partitioning to the gas phase, while BC and K^+ would not undergo similar processes. BC and K^+ are emitted primarily during flaming combustion, while levoglucosan more during smoldering combustion(Lee et al., 2010), which may also cause the lower correlation. The very low correlation with BC is likely because next to a roadway BC is predominantly from mobile sources, rather than biomass burning. The modest correlation of levoglucosan with UV-BC difference, in the context of no correlation with BC, indicates that the UV-BC difference can be indicative of biomass burning aerosol, even when total BC is overwhelmingly from traffic-related sources.

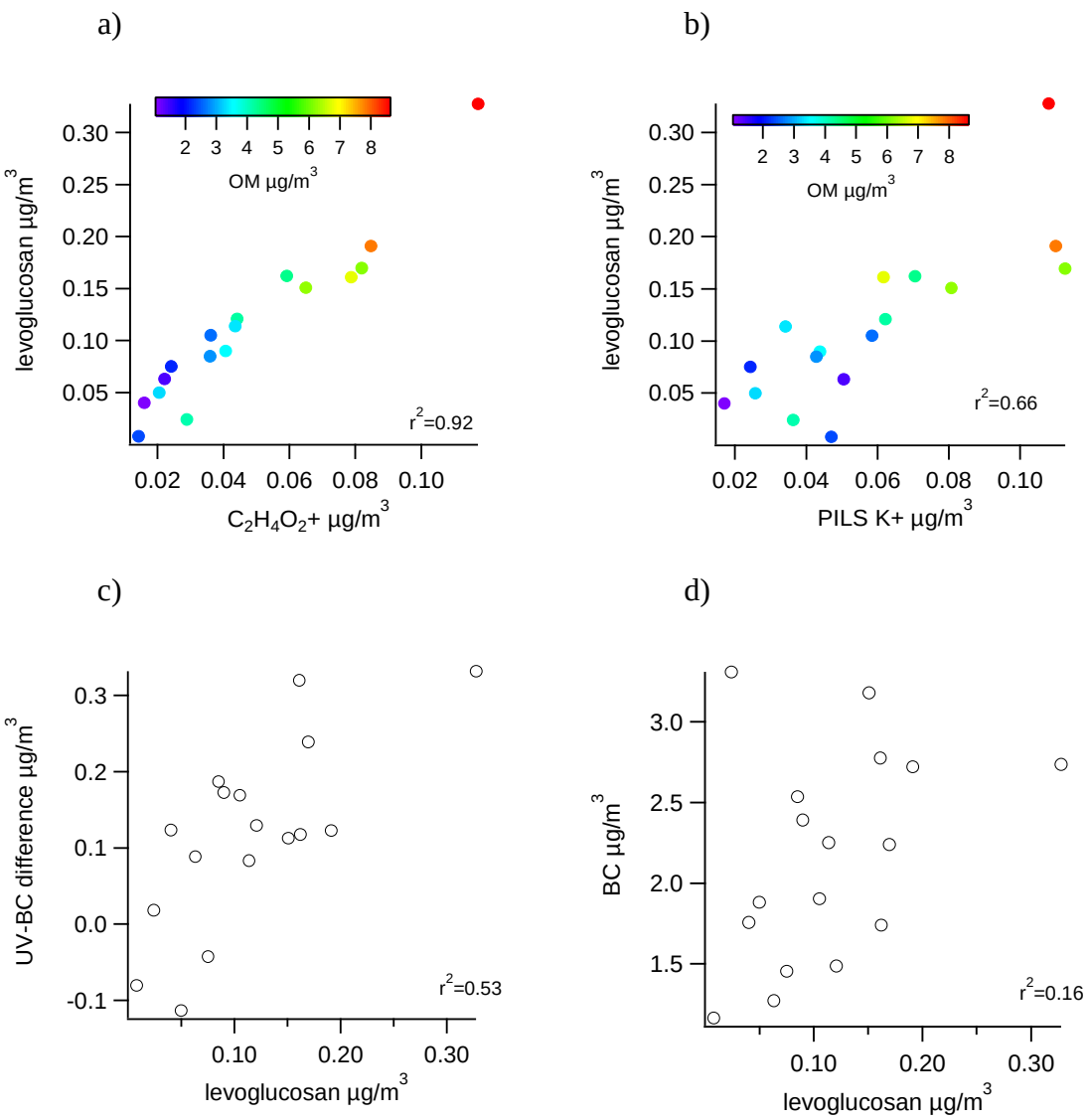

Figure 6-3. Scatter plots of levoglucosan concentrations µg/m^3 with a) AMS $C_2H_4O_2^+$ (µg/m^3), b) PILS K^+ (µg/m^3), c) UV-BC difference (µg/m^3), and d) BC (µg/m^3).

6.3.2 Correlation Among Semi-continuous Biomass Burning Markers

While there are a limited number of multi-hour samples with levoglucosan, the high correlation between levoglucosan and $C_2H_4O_2^+$ confirms that $C_2H_4O_2^+$ is an excellent tracer for levoglucosan and biomass burning emissions, so we next examined correlations of hourly averaged $C_2H_4O_2^+$ concentrations with K^+ and UV-BC difference values, as well as with BC. As

indicated by similar diurnal patterns, the measurements of biomass burning indicators were somewhat correlated, with some differences between species and time of day. The overall correlation coefficient (r^2) between K^+ and $C_2H_4O_2^+$ was 0.56, but if the concentrations for each hour of the day are examined separately, there is a large range in this correlation coefficient (Figure 6-2). Between 1800 and 0000 LST, when fresh biomass burning emissions are most likely, the correlation coefficient between K^+ and $C_2H_4O_2^+$ was 0.84, and then slowly decreased through the morning until 1200 through 1600 LST, when the correlation coefficient was 0.19.

UV-BC difference had only a modest correlation with $C_2H_4O_2^+$, of r^2=0.43, similar to the comparison of UV-BC difference with levoglucosan. When comparing BC versus $C_2H_4O_2^+$ there is a good correlation during the evening (r^2=0.80), during the period of strong residential wood combustion, and only a modest one in the morning (r^2=0.35) There was a poor correlation between K^+ and both BC and UV-BC difference. Overall these results suggest that either K^+ and UV-BC difference are only modestly good indicators of biomass burning here in Las Vegas next to a roadway, and/or that there are other sources of K^+ and BC at the monitoring site. It is clearly plausible that the majority of BC is from traffic-related emissions, which may complicate the relationship between UV-BC difference and levoglucosan or $C_2H_4O_2^+$. For K^+, the modest correlation with levoglucosan or $C_2H_4O_2^+$ may be due to differences in emissions of these species during flaming and smoldering processes, or of minor sources of K^+ confounding the relationship.

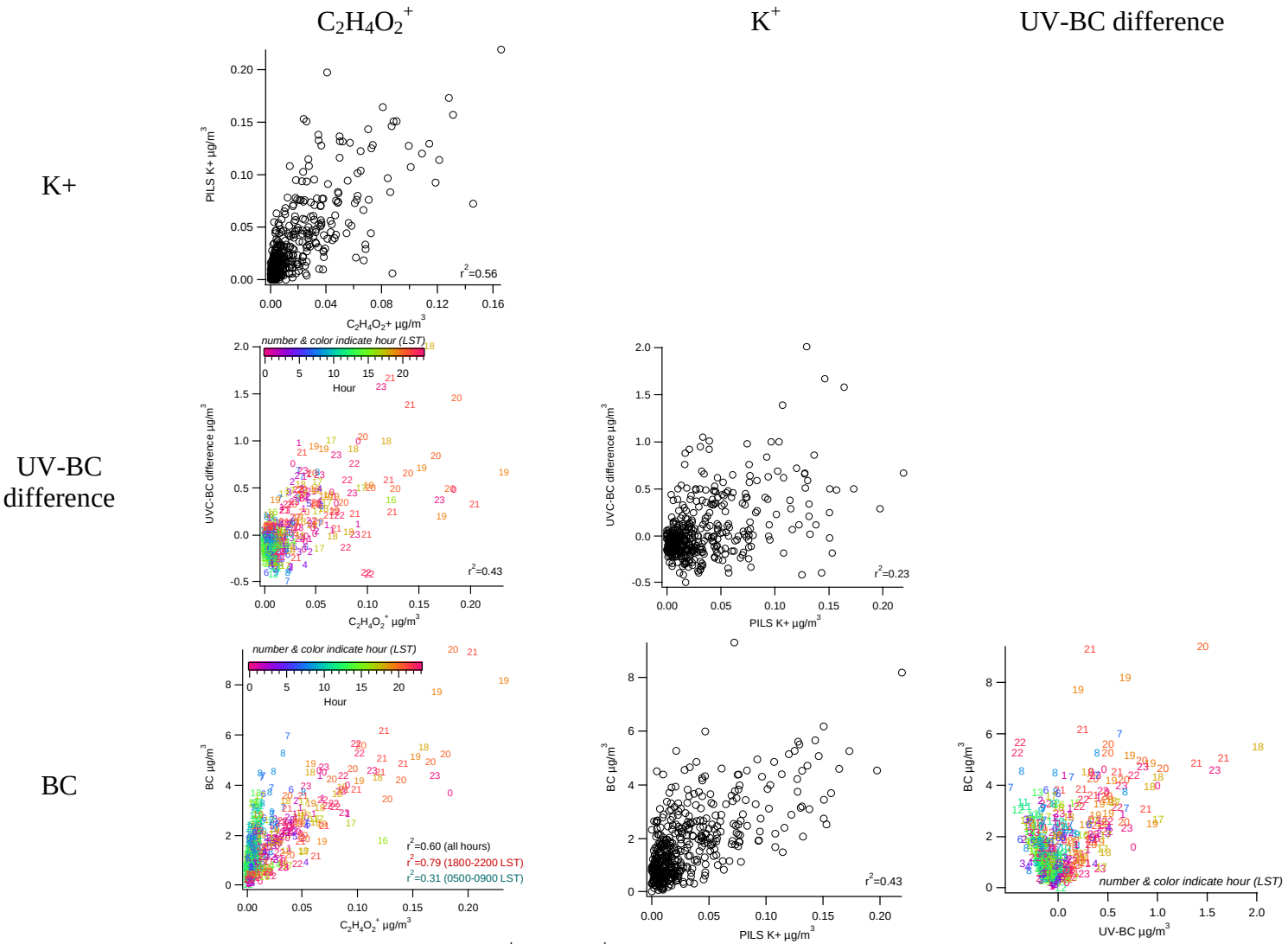

Figure 6-4. Scatter plots of hourly average $C_2H_4O_2^+$, PILS K^+, UV-BC difference and BC concentrations; on select graphs, colors and numbers indicate hour of day LST, and all units are µg/m^3.

6.3.3 Urban Background Levels of *m/z* 60 and $C_2H_4O_2^+$

There is a clear, strong relationship of levoglucosan with *m/z* 60 and $C_2H_4O_2^+$. However, there can be contributions to *m/z* 60 and $C_2H_4O_2^+$ from non-biomass burning sources, like organic acids (Cubison et al., 2011). Cubison et al 2011 (Cubison et al., 2011) suggested that there is a background level of *m/z* 60, so that even when biomass burning is null there will still be some small concentration of *m/z* 60. This background *m/z* 60 can be seen when evaluating the fraction of OM from *m/z* 60 versus the fraction from *m/z* 44 (Figure 6-5). There is a background of *m/z* 60 evident during the morning and midday hours of 0.4 % of the OM; during the evening the fraction of mass from *m/z* 44 is much lower and the fraction from *m/z* 60 is much higher. In figure 6-5b, we can see how the day progresses, with the morning have a low *m/z* 44 fraction and *m/z* 60 fraction, followed by a midday increase in *m/z* 44 fraction, then in the evening an increase in *m/z* 60 fraction and decrease of *m/z* 44 fraction. This further shows the important contribution of biomass burning during the evening only, while mobile source emissions contribute to OM in throughout the day.

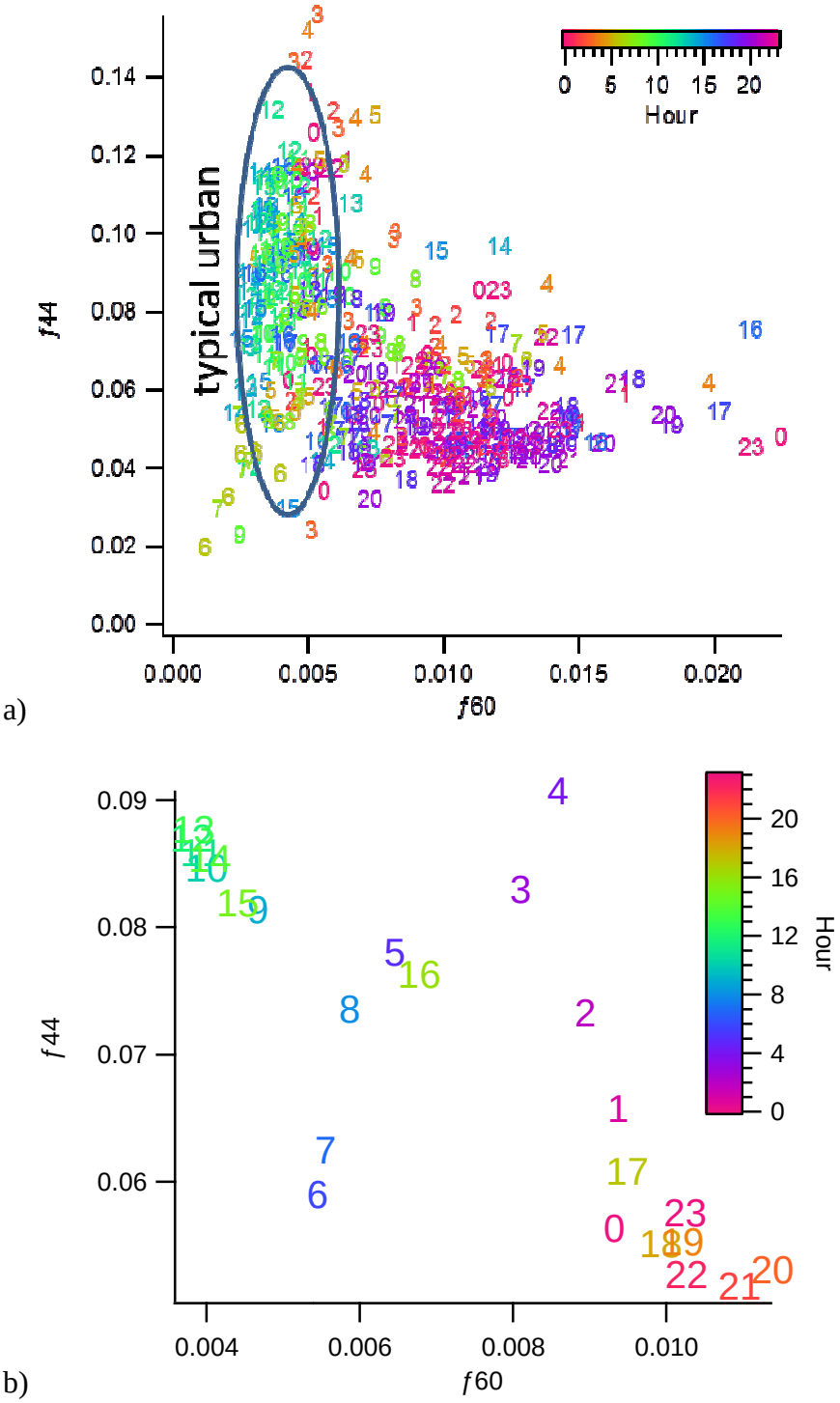

Figure 6-5. Scatter plot of the fraction of OM from *m/z* 44 and *m/z* 60, with color and numbers indicating hour of the day, for: a) all data (hourly averages); and b) hourly averages by hour during the study.

6.3.4 Ambient Ratios of Biomass Burning Markers and Comparison to Source Profiles

We also compared the ratios between species in ambient measurements to ratios found in source profiles. Figure 6-6 shows the diurnal variation of the correlation and ratio of $C_2H_4O_2^+$ and K^+. In an open flame experiment, Lee et al found a $C_2H_4O_2^+$/levoglucosan ratio of around 0.14 for numerous flaming and smoldering experiments with multiple biomass fuels (Lee et al., 2010). The average $C_2H_4O_2^+$/levoglucosan ratio in the 12-hour overnight samples in our study was 0.28. Other molecules such as acids or other oxidized species can also contribute to $C_2H_4O_2^+$. With the 12 hour sample time and abundance of other urban sources, it is possible that additional secondary products contributed to $C_2H_4O_2^+$ concentrations, leading to a higher $C_2H_4O_2^+$/levoglucosan ratio here compared to laboratory studies. The K^+/levoglucosan ratio for the 12-hour sample periods averages 0.52. Puxbaum et al., summarize source profile ratios, and report the K^+/levoglucosan ratio for a mixture of European sites with 24 hour filter samples, and after determining soluble, non-sea salt K concentrations (Puxbaum et al., 2007). The value of 0.52 here is in the range found at the European sites, where the average ratio across sites ranged between 0.2-2.1. Source profiles from Fine et al., and Schauer et al., however, report K/levoglucosan ratios of 0.1-0.2(Fine et al., 2004a; Schauer and Cass, 2000). Thus it appears that there may be additional non-biomass burning sources of K that are contributing to the concentrations in this study and in Puxbaum et al., 2007, and/or that levoglucosan is aging faster than K over the course of multiple hours required for sampling. Differences in fuel type between what is used in Las Vegas and in these studies, as well as differences in the amount of flaming versus smoldering burning emissions may also play a role.

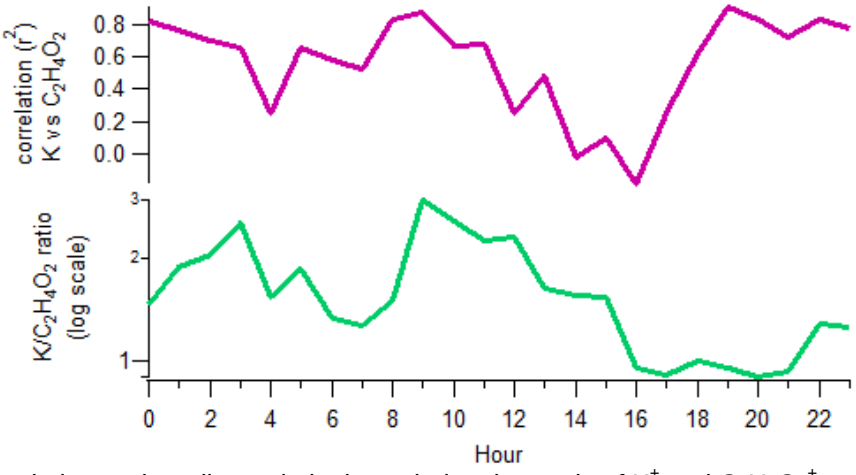

Figure 6-6. Correlation and median ratio by hour during the study of K^+ and $C_2H_4O_2^+$.

6.4 Biomass Burning Apportionment via Multiple Methods

With the suite of biomass burning tracers observed here, there are multiple methods available to apportion the contribution of biomass burning to OM: 1) PMF-AMS, where PMF is applied to the AMS data to determine contributing factors, including BBOA (Lanz et al., 2007; Ulbrich et al., 2009a); 2) use a AMS $(C_2H_4O_2^+*OM)^{-1}$ ratio reported in laboratory source experiments for biomass burning fuels, and estimate the amount of OM from BBOA; and 3) use a $(\text{levoglucosan/OC})^{-1}$ ratio as reported in filter-based source profiles, then based on the levoglucosan concentrations estimate the amount of OC, and using an assumed OM/OC ratio, estimate BBOA contribution to OM. Since methods 2 and 3 rely on source profiles, these methods should estimate primary emissions, if the source profiles represent only primary emissions. The PMF factor approach in method 1 may include primary and some amount of secondary aerosol formation associated with BBOA. However, the PMF method could underestimate secondary OA from biomass burning in the obtained BBOA factor if the secondary OA is chemically more similar to the SV-OOA or LV-OOA than to primary BBOA. Since SV-OOA concentrations observed here are typically concurrent with and higher than

BBOA, secondary OA associated with biomass burning emissions may not be fully captured in the BBOA factor. With only three PMF factors, i.e, with no SV-OOA factor, BBOA is higher than when four factors are used; it may be that with three factors more of the secondary OA associated with biomass burning is contained in the BBOA factor. Table 6-1 summarizes the fraction of OM apportioned via each method. Reported in Brown et al and in an earlier chapter are the results from the PMF-AMS method, where using unit mass resolution AMS data and the EPA PMF program, on average 12% of the OM was attributable to biomass burning organic aerosol (BBOA). During overnight periods BBOA was on average 26% of the OM.

A number of studies have reported a range of $OM/C_2H_4O_2^+$ ratios from source experiments. Lee et al report a value of 34.5 for the $OM/C_2H_4O_2^+$ ratio generated in biomass burning experiments (Lee et al., 2010). Alfarra et al used a combination of PMF and ^{14}C analyses to determine a similar ratio for OM to *m/z* 60, equal to 36, for wintertime wood combustion in Zurich, and suggested use of this ratio as a conservative estimate for apportioning BBOA (Alfarra et al., 2007). Using the ratio of 34.5, on average BBOA is estimated as 15% of the OM, similar to but slightly higher than the PMF-AMS results. When using just three factors, BBOA is on average 15% of the OM, matching the estimate for this method. For overnight periods, 32% of the OM is BBOA via this method, again similar to the 26% estimate from PMF-AMS. Since the PMF-AMS method results in BBOA estimates that are lower than using source profiles, secondary BBOA appears not to be captured in the PMF factor; it likely is contained instead in the SV-OOA factor.

Fine et al. report an OC/levoglucosan ratio of 7.35 for residential biomass burning emissions, used here to apportion BB OC based on our filter levoglucosan measurements (Fine et al., 2002a). Recent studies have reported a wider range of levoglucosan/OC emission ratios

depending on biomass fuel type and burn conditions (Sullivan et al., 2008; Puxbaum et al., 2007; Minguillon et al., 2011). The 7.35 value is representative of fireplace combustion of hardwoods, which is likely appropriate for the Las Vegas area. Schmidl et al developed a similar factor for Austrian fuels of 7.1 based on test burns in a tiled stove (Schmidl et al., 2008). Puxbaum et al. suggest an OM/OC conversion factor of 1.4 based on their calculations from the data reported in Fine et al . During the wintertime evening in Las Vegas, when biomass burning is most prevalent, the average OM/OC ratio is 1.46 (Chapter 4), so a value of 1.4 for biomass burning appears reasonable. This yields a conversion of biomass burning OM equal to levoglucosan*7.35*1.4. Using this conversion, 33% of the OM is from biomass burning during the overnight periods. This range matches well with the 32% apportioned via the $C_2H_4O_2^+$/OM ratios, and is slightly higher than the 26% apportioned via PMF-AMS.

Apportionment of BBOA by these different methods is summarized in Table 6-1, and the fraction of OM by each method for periods with levoglucosan data is shown in Figure 6-7. Figure 6-8 shows how the PMF-BBOA compares with levoglucosan measurements and levoglucosan-BBOA apportionment. All but the highest levoglucosan concentration data points fall about the 1:1 line between PMF-BBOA and levoglucosan-BBOA in Figure 6-8, and on most evenings the three apportionment methods yield a similar result.

The sample with the highest disagreement between methods was the night of January 19, where levoglucosan-BBOA is 1.6 times higher than PMF-BBOA and 1.4 times higher than $C_2H_4O_2^+$-BBOA. As seen in Figure 6-1, this was not only the evening of the highest levoglucosan and *m/z* 60 concentrations but also OM. It may be that PMF is under predicting the amount of BBOA since the OM concentration and possibly composition is quickly changing, or that the AMS is missing some BBOA in the very small (less than 50 nm) or very large (greater

than 700 nm) diameter particles where transmission is low. The $Q/Q_{expected}$ ratio and scaled residuals from PMF during this evening are low, indicating a good fit, but during this evening SV-OOA is also very high, so it's likely that some of mass assigned by PMF as SV-OOA is actually BBOA. Since a constant profile is needed in PMF, differences in the BBOA composition between evenings means a "typical" or average profile is found, and when there are deviations from this profile mass appears to be apportioned to SV-OOA. However, as the results are consistent for all the other data points, our conclusion is that the three BBOA methods compare rather well most of the time.

Table 6-1. Fraction of OM apportioned during 12 overnight (1700-0500 LST) periods, January evenings, and over all hours, via PMF-AMS, $C_2H_4O_2^+$/OM ratios, and levoglucosan. Apportionment by levoglucosan is only available for the 12 overnight filter sample periods.

Sample range	fOM from BB via levoglucosan	fOM from BB via PMF-AMS (BBOA)	fOM from BB via $C_2H_4O_2^+$/OM ratios
12 12-hour overnight periods	33%	26%	32%
All evenings (1800-2300 LST)	n/a	15%	21%
All hours	n/a	9%	14%

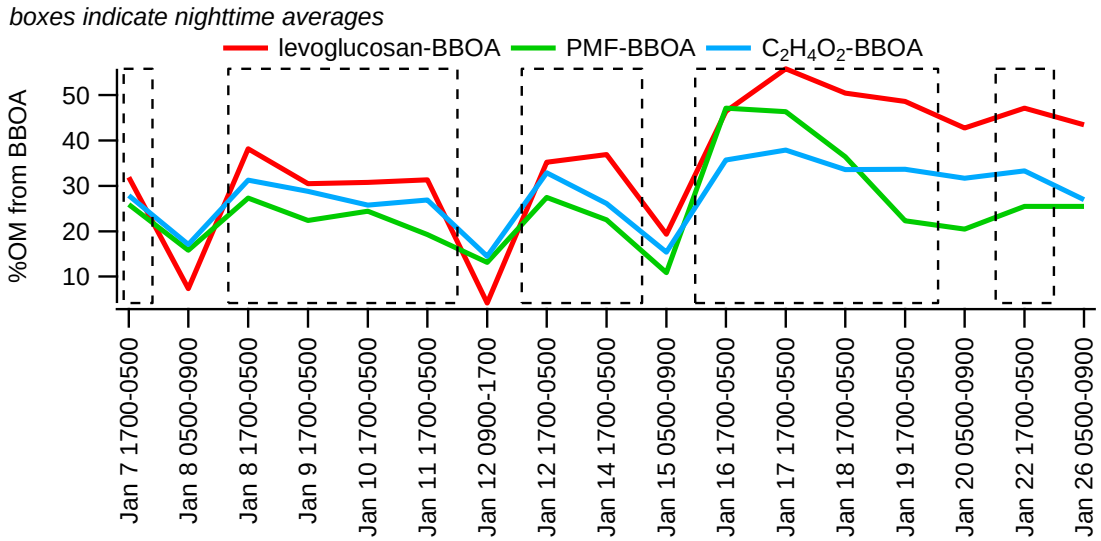

Figure 6-7. Percentage of OM apportioned by three methods for each time period where levoglucosan was quantified; boxes indicate nighttime averages (1700-0500 LST).

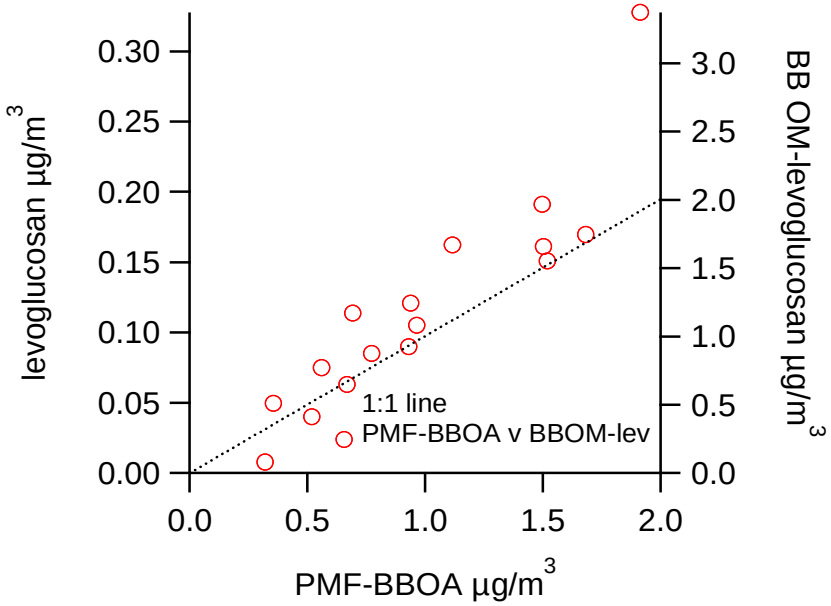

Figure 6-8. Comparison of PMF-BBOA concentrations versus levoglucosan (primary y-axis) and BB OM by levoglucosan (secondary y-axis); all units µg/m^3.

7. Conclusions and Recommendations

7.1 Conclusions

With multiple high-time resolution measurements we have investigated the variability and sources of aerosol next to a major freeway during winter in Las Vegas, Nevada. Using data gathered via a HR-AMS and Aethalometer we can understand the composition of the aerosol. OM averaged 3.3 $\mu g/m^3$ during the January intensive campaign and was typically highest during the evening hours (i.e., 1900 through 2100 LST) with a secondary peak in the morning (i.e., 0600-0900 LST, during rush hour commute). Temporal patterns for both sulfate and nitrate differed from the temporal pattern for OM. Sulfate concentrations were extremely low throughout the study, and nitrate concentrations were episodic but were also on average very low (less than 1 $\mu g/m^3$). In contrast to the inorganic species, BC had a median concentration of 1.24 $\mu g/m^3$, which was more than twice as high as nitrate, an order of magnitude higher than sulfate, and a third of OM. BC is more than twice as high at this site compared to a site 2 km away in the urban center but away from freeways (Hancock Elementary School), where BC was, on average, 0.5 $\mu g/m^3$. OM comprised on average 48% of the measured aerosol, and was the focus of much of our analyses.

Black carbon followed the typical diurnal traffic patterns with peaks in concentration during the morning and evening rush hours. The coincident patterns indicate that next to the freeway a large fraction of the BC is from vehicular emissions on the freeway and in the local area. Unlike BC, OM peaked in the evening, with a secondary peak in the morning. Using PMF, the OM was deconstructed into its main components, which revealed that the HOA component behaved similar to BC and traffic patterns, with peaks of similar magnitude in the

morning and evening. In the evening, there was additional OM from SV-OOA and BBOA, leading to higher OM concentrations compared to the morning, when SV-OOA was low and BBOA minimal.

The change in OM mixture throughout the day was reflected in the diurnal changes of its elemental composition. H/C ratio was highest, and O/C and OM/OC ratios lowest, during the evening when OM concentrations were highest. Thus, during the highest concentration periods, it appears that the OM is mostly primary in origin, i.e., not very oxidized (low O/C and OM/OC). The average OM/OC ratio was 1.54 (±0.20 standard deviation), typical of environments with a low amount of secondary organic aerosol formation. This ratio is dependent on the mix of emissions impacting a monitoring site, dispersion, atmospheric oxidation, and gas/particle partitioning. The OM/OC ratio is highest in the midday, when dispersion increases and atmospheric oxidation processes are highest. In the evening, a combination of fresh emissions and gas-to-particle partitioning under stable conditions appears to rapidly drive OM up and the OM/OC ratio down.

BC exhibited typical upwind/downwind patterns, where concentrations are much higher when the monitoring site is downwind compared to when it is upwind of the freeway. However, there was no significant difference in OM between upwind and downwind concentrations on average. While BC is primary emissions, and thus dependent on the relationship between the monitoring site and source locations, OM is a constantly changing mixture of primary and secondary aerosol, meaning it is less variant to changes in wind direction. The size distribution of OM was similar between upwind and downwind conditions as well, but under stagnant conditions, there was relatively more mass from smaller, fresh particles (those with vacuum aerodynamic diameter of less than 100 nm) compared to during upwind or downwind conditions.

These size distribution results further show the influence of fresh emissions during low wind speed conditions, and the complex nature of OM.

Given the sampling location next to a twelve-lane freeway, urban-scale biomass burning was found to be a surprising source of substantial OM. Multiple methods were used to quantify the impact of BBOA on OM, using HR-AMS data as well as levoglucosan data from filters, and confirmed by PILS K^+ measurements. On average, BBOA was 9%-14% of the OM, but only was present during the evening hours, when OM was highest. During the overnight period between 1700 and 0500 LST, BBOA contributed between 26%-33% of the OM (range from different analysis/measurement techniques).

Overall this suite of measurements and analyses yielded a comprehensive look into near-roadway aerosol, and in particular, how OM is different than more commonly measured species such as BC. While BC is a primary emission and does not react or form in the atmosphere, OM is a combination of primary emissions and secondarily produced aerosol, which can vary throughout the day as atmospheric conditions change.

7.2 Recommendations

Based on the analyses presented here, there are a number of recommendations that would further explore the data collected as part of this study, enhance future near-road field studies, and better understand receptor modeling results, discussed below.

Potential additional steps with measurements from current study:

- Perform chemical analyses on additional, archived filters from this study for levoglucosan, hopanes, PAH and other organic species to develop a complete time series of these compounds. Then apply CMB, PMF or other apportionment

methods to determine the impact of biomass burning, vehicular emissions and other sources on OM.

- Analyze Sunset OC/EC ratio data to compare with typical ratios from vehicular (car and truck) and biomass burning emissions, as well as to crudely estimate primary and secondary OC using OC/EC ratios.
- Use dispersion models to model CO and BC from roadway emissions at Fyfe Elementary, and compare to observed CO and BC concentrations to understand if models such as the American Meteorological Society/Environmental Protection Agency Regulatory Model Improvement Committee (AERMIC) Dispersion Model (AERMOD) can correctly predict near-road aerosol concentrations. Utilizing the BC results, predictions could also be made of OC, assuming a range of OC/BC ratios based on observations.

In future near-roadway studies:

- Conduct a study at Fyfe Elementary similar to this one, but in summer, to understand how the influence of mobile source emissions may change in summertime, when temperatures are very high, boundary layer heights are higher, inversions are rare, and secondary organic aerosol may be the largest component of OM.
- Include aerosol size instrumentation to gain a broader view of particle size distribution variations, particularly for particles with diameter less than 50 nm, which are typically high next to a roadway and are not quantifiable by the HR-

AMS. This could be done simply with a total particle counter (e.g., condensation particle counter), where total particle number is dominated by ultrafine particles, with a scanning mobility particle size (SMPS) instrument where the number of particles in multiple size bins can be determined, or with a micro-orifice uniform deposit impactor (MOUDI) instrument where different size particles are impacted on a series of impaction substrates to be later analyzed for OC/EC/organics or metals and ions.

- Include VOC and/or SVOC measurements, to understand the contribution of mobile sources and other sources to the VOC/SVOC mixture, which can be used to help interpret the changes in OM with changes in meteorology and time of day. Recent work (Xie et al., 2013) has suggested that including such measurements can help elucidate sources of OA, and potentially better identify contributions from mobile sources, etc.

Refinement of receptor modeling methods

- New algorithms are becoming available in EPA PMF to understand uncertainty in PMF factors and to better understand the robustness of solutions. These algorithms could be used to better understand the quality of the PMF solutions found here, and help indicate which solutions (3, 4, or 5 factors) are most robust.

- Utilize other receptor models such as Unmix and CMB to evaluate the HR-AMS data. Unmix relies on "edges" between species, as observed in scatter plots, to determine factors. Unmix may be better able to resolve BBOA, SV-OOA and other factors separate from HOA and LV-OOA. CMB requires known source profiles; with CMB, cooking OA, which was not found here, and a spectrum of

BBOA and SV-OOA source profiles, which are variable among sites and OA conditions, could be used to determine the best fit. If separate diesel exhaust and gasoline exhaust source profiles are available, these could be used to potentially quantify gas/diesel contributions to OM.

7.3 Implications

Residential biomass burning is a significant and underrepresented source of PM. Despite being next to a major freeway in a city with little tradition of residential biomass burning for home heating, biomass burning was an important source of PM in the wintertime. This source is minimal in the national emission inventory for Las Vegas, and as other sources are better controlled and decrease in emissions over time, residential biomass burning will be more important to understand, characterize and potentially control.

PM next to roadways is predominantly organic and unlikely to be well modeled by existing tools

EPA requires a hotspot analysis for PM for any freeway project in a $PM_{2.5}$ non-attainment or maintenance area. Modeling tools for PM hot spot analyses such as AERMOD and CAL3QHCR are not well adapted to model rapid formation of secondary OM next to a roadway, rather they focus only on primary emissions such as BC; therefore, they are likely to underestimate the amount of near-road PM. If modeling results are compared to ambient measurements, modeling for most roadways may be inadequate to understand and predict near-road PM concentrations.

Exposure to high concentrations of near-roadway aerosol can be highly variable

While there are clear health effects associated with living, working and attending school next to major freeways, this work shows that concentrations and thus exposure to near-roadway aerosol is highly variable, both in terms of composition and in concentration. Health studies examining aggregate near-road concentrations, such as annual or seasonal averages, may miss links between short-term exposure to different levels and composition of near-road PM, e.g., times when OM and PAHs are high but BC low, or times when O/C ratio is high, etc.

8. References

Abu-Allaban M., Gillies J.A., and Gertler A.W. (2003) Application of a multi-lag regression approach to determine on-road PM_{10} and $PM_{2.5}$ emission rates. *Atmos. Environ.*, 37, 5157-5164, (37), Dec.

Adonis M.I., Riquelme R.M., Martinez V.D., Gil L., Rios C., Rodriguez L., and Rodriquez E.M. (2003) PAHs and mutagenicity of inhalable and respirable diesel particulate matter in Santiago, Chile. *Polycyclic Aromatic Compounds*, 23, 495-514.

Aiken A.C., DeCarlo P., and Jimenez J.L. (2007) Elemental analysis of organic species with electron ionization high-resolution mass spectrometry. *Analytical Chemistry (Washington)*, 79, 8350-8358, doi: 10.1021/ac071150w (21).

Aiken A.C., DeCarlo P., Kroll J.H., Worsnop D.R., Huffman J.A., Docherty K.S., Ulbrich I.M., Mohr C., Kimmel J.R., Sueper D., Sun Y., Zhang Q., Trimborn A., Northway M., Ziemann P.J., Canagaratna M.R., Onasch T.B., Alfarra M.R., Prévôt A.S.H., Dommen J., Duplissy J., Metzger A., Baltensperger U., and Jimenez J.L. (2008) O/C and OM/OC ratios of primary, secondary, and ambient organic aerosols with high-resolution time-of-flight aerosol mass spectrometry. *Environ. Sci. Technol.*, 42, 4478-4485, doi: 10.1021/es703009q (12).

Aiken A.C., Salcedo D., Cubison M.J., Huffman J.A., DeCarlo P.F., Ulbrich I.M., Docherty K.S., Sueper D., Kimmel J.R., Worsnop D.R., Trimborn A., Northway M., Stone E.A., Schauer J.J., Volkamer R., Fortner E., Foy B.d., Wang J., Laskin A., Shutthanandan V., Zheng J., Zhang R., Gaffney J., Marley N., Paredes-Miranda G., Arnott W.P., Molina L.T., Sosa G., and Jimenez J.L. (2009) Mexico City aerosol analysis during MILAGRO using high resolution aerosol mass spectrometry at the urban supersite (T0). Part 1: fine particle composition and organic source apportionment. *Atmos. Chem. Phys.*, 9, 6633-6653, doi: 10.5194/acp-9-6633-2009 (17). Available at http://www.atmos-chem-phys.net/9/6633/2009/acp-9-6633-2009.pdf.

Aiken A.C., de Foy B., Wiedinmyer C., DeCarlo P.F., Ulbrich I.M., Wehrli M.N., Szidat S., Prévôt A.S.H., Noda J., Wacker L., Volkamer R., Fortner E., Wang J., Laskin A., Shutthanandan V., Zheng J., Zhang R., Paredes-Miranda G., Arnott W.P., Molina L.T., Sosa G., Querol X., and Jimenez J.L. (2010) Mexico city aerosol analysis during MILAGRO using high resolution aerosol mass spectrometry at the urban supersite (T0). Part 2: analysis of the biomass burning contribution and the non-fossil carbon fraction. *Atmos. Chem. Phys.*, 10, 5315-5341, doi: 10.5194/acp-10-5315-2010 (12). Available at http://www.atmos-chem-phys.net/10/5315/2010/acp-10-5315-2010.pdf.

Alfarra M.R., Coe H., Allan J.D., Bower K.N., Boudries H., Canagaratna M.R., Jimenez J.L., Jayne J.T., Garforth A.A., Li S.-M., and Worsnop D.R. (2004) Characterization of urban and rural organic particulate in the Lower Fraser Valley using two Aerodyne aerosol mass spectrometers. *Atmos. Environ.*, 38, 5745-5758, doi: 10.1016/j.atmosenv.2004.01.054.

Alfarra M.R., Paulsen D., Gysel M., Garforth A.A., Dommen J., Prévôt A.S.H., Worsnop D.R., Baltensperger U., and Coe H. (2006) A mass spectrometric study of secondary organic

aerosols formed from the photooxidation of anthropogenic and biogenic precursors in a reaction chamber. *Atmos. Chem. Phys.*, 6, 5279-5293.

Alfarra M.R., Prévôt A.S.H., Szidat S., Sandradewi J., Weimer S., Lanz V.A., Schreiber D., Mohr M., and Baltensperger U. (2007) Identification of the mass spectral signature of organic aerosols from wood burning emissions. *Environ. Sci. Technol.*, 41, 5770-5777, doi: 10.1021/es062289b.

Allan J.D., Alfarra M.R., Bower K.N., Williams P.I., Gallagher M.W., Jimenez J.L., McDonald A.G., Nemitz E., Canagaratna M.R., Jayne J.T., Coe H., and Worsnop D.R. (2003a) Quantitative sampling using an Aerodyne aerosol mass spectrometer - 2. Measurements of fine particulate chemical composition in two U.K. cities. *Journal of Geophysical Research-Atmospheres*, 108, (D3), Feb 4.

Allan J.D., Jimenez J.L., Williams P.I., Alfarra M.R., Bower K.N., Jayne J.T., Coe H., and Worsnop D.R. (2003b) Quantitative sampling using an Aerodyne aerosol mass spectrometer - 1. Techniques of data interpretation and error analysis. *Journal of Geophysical Research-Atmospheres*, 108, (D3), Feb 4.

Allan J.D., Delia A.E., Coe H., Bower K.N., Alfarra M.R., Jimenez J.L., Middlebrook A.M., Drewnick F., Onasch T.B., Canagaratna M.R., Jayne J.T., and Worsnopf D.R. (2004) A generalised method for the extraction of chemically resolved mass spectra from Aerodyne aerosol mass spectrometer data. *Journal of Aerosol Science*, 35, 909-922, (7), Jul.

Allan J.D., Williams P.I., Morgan W.T., Martin C.L., Flynn M.J., Lee J., Nemitz E., Phillips G.J., Gallagher M.W., and Coe H. (2010) Contributions from transport, solid fuel burning and cooking to primary organic aerosols in two UK cities. *Atmos. Chem. Phys.*, 10, 647-668, doi: 10.5194/acp-10-647-2010.

Allen G.A., Miller P.J., Rector L.J., Brauer M., and Su J.G. (2011) Characterization of valley winter woodsmoke concentrations in Northern NY using highly time-resolved measurements. *Aerosol and Air Quality Research*, 11, 519-530, doi: 10.4209/aaqr.2011.03.0031. Available at http://aaqr.org/VOL11_No5_October2011/6_AAQR-11-03-OA-0031_519-530.pdf.

Bae M.S., Schauer J.J., DeMinter J.T., and Turner J.R. (2004a) Hourly and daily patterns of particle-phase organic and elemental carbon concentrations in the urban atmosphere. *J. Air Waste Manage.*, 54, 823-833, (7), Jul.

Bae M.S., Schauer J.J., DeMinter J.T., Turner J.R., Smith D., and Cary R.A. (2004b) Validation of a semi-continuous instrument for elemental carbon and organic carbon using a thermal-optical method. *Atmos. Environ.*, 38, 2885-2893, (18), Jun.

Bae M.S., Schauer J.J., and Turner J.R. (2006) Estimation of the monthly average ratios of organic mass to organic carbon for fine particulate matter at an urban site. *Aerosol Science & Technology*, 40, 1123-1139, September.

Baldauf R., Thoma E., Hays M., Shores R., Kinsey J.S., Gullet B., Kimbrough S., Isakov V., Long T., Snow R., Khlystov A., Weinstein J., Chen F.-L., Seila R., Olson D., Gilmour I., Cho S.-H., Watkins N., Rowley P., and Bang J. (2008) Traffic and meteorological

impacts on near-road air quality: summary of methods and trends from the Raleigh near-road study. *J. Air Waste Manage.*, 58, 865-878, July.

Barregard L., Sallsten G., Andersson L., Almstrand A.-C., Gustafson P., M. Andersson, and Olin A.-C. (2007) Experimental exposure to wood smoke: effects on airway inflammation and oxidative stress. *Occup. Environ. Med.*, 65, 319-324, doi: 10.1136/oem.2006.032458.

Bauer J.J., Yu X.-Y., Cary R., Laulainen N., and Berkowitz C. (2009) Characterization of the sunset semi-continuous carbon aerosol analyzer. *J. Air Waste Manage.*, 59, 826-833, doi: 10.3155/1047-3289.59.7.826 (7).

Bergauff M.A., Ward T.J., Noonan C.W., and Palmer C.P. (2009) The effect of a woodstove changeout on ambient levels of $PM_{2.5}$ and chemical tracers for woodsmoke in Libby, Montana. *Atmos. Environ.*, 43, 2938-2943, doi: 10.1016/j.atmosenv.2009.02.055 (18). Available at http://dx.doi.org/10.1016/j.atmosenv.2009.02.055.

Brown S.G., Frankel A., Raffuse S.M., Roberts P.T., Hafner H.R., and Anderson D.J. (2007) Source apportionment of fine particulate matter in Phoenix, Arizona, using positive matrix factorization. *J. Air Waste Manage.*, 57, 741-752, doi: 10.3155/1047-3289.57.6.741.

Brown S.G., Lee T., Norris G.A., Roberts P.T., Collett J.L., Jr., Paatero P., and Worsnop D.R. (2012) Receptor modeling of near-roadway aerosol mass spectrometer data in Las Vegas, Nevada, with EPA PMF. *Atmospheric Chemistry and Physics*, 12, 309-325, doi: 10.5194/acp-12-309-2012. Available at http://www.atmos-chem-phys.net/12/309/2012/.

Brown S.G., Lee T.L., Roberts P.T., and Collett Jr. J.L. (2013) Variations in the OM/OC ratio of urban organic aerosol next to a major roadway. *J. Air Waste Manage.*, 63, 1422-1433, doi: 10.1080/10962247.2013.826602 (12), December. Available at http://www.tandfonline.com/doi/full/10.1080/10962247.2013.826602#.UrIEQfTu3H4.

Brunekreef B., Janssen N.A., de Hartog J., Harssema H., Knape M., and van Vliet P. (1997) Air pollution from truck traffic and lung function in children living near motorways. *Epidemiology*, 8, 298-303, (3).

Canagaratna M.R., Jayne J.T., Ghertner D.A., Herndon S., Shi Q., Jimenez J.L., Silva P.J., Williams P., Lanni T., Drewnick F., Demerjian K.L., Kolb C.E., and Worsnop D.R. (2004) Chase studies of particulate emissions from in-use New York City vehicles. *Aerosol Science and Technology*, 38, 555-573, (6), Jun.

Canagaratna M.R., Jayne J.T., Jimenez J.L., Allan J.D., Alfarra M.R., Zhang Q., Onasch T.B., Drewnick F., Coe H., Middlebrook A., Delia A., Williams L.R., Trimborn A.M., Northway M.J., DeCarlo P.F., Kolb C.E., Davidovits P., and Worsnop D.R. (2007) Chemical and microphysical characterization of ambient aerosols with the aerodyne aerosol mass spectrometer. *Mass Spectrometry Reviews*, 26, 185-222, doi: 10.1002/mas.20115 (2). Available at http://onlinelibrary.wiley.com/doi/10.1002/mas.20115/abstract.

Canagaratna M.R., Onasch T.B., Wood E.C., Herndon S.C., Jayne J.T., Cross E.S., Miake-Lye R.C., Kolb C.E., and Worsnop D.R. (2010) Evolution of vehicle exhaust particles in the atmosphere. *J. Air Waste Manage.*, 60, doi: 10.3155/1047-3289.60.10.1192 (10).

Cappa C.D. and Jimenez J.L. (2010) Quantitative estimates of the volatility of ambient organic aerosol. *Atmos. Chem. Phys.*, 10, 5409-5424, doi: 10.5194/acp-10-5409-2010. Available at http://www.atmos-chem-phys.net/10/5409/2010/acp-10-5409-2010.html.

Chan T.W., Huang L., Leaitch W.R., Sharma S., Brook J.R., Slowik J.G., Abbatt J.P.D., Brickell P.C., Liggio J., Li S.-M., and Moosmuller H. (2010) Observations of OM/OC and specific attenuation coefficients (SAC) in ambient fine PM at a rural site in central Ontario, Canada. *Atmos. Chem. Phys.*, 10, 2393-2411. Available at www.atmos-chem-phys.net/10/2393/2010.

Chirico R., DeCarlo P.F., Heringa M.F., Tritscher T., Richter R., Prévôt A.S.H., Dommen J., Weingartner E., Wehrle G., Gysel M., Laborde M., and Baltensperger U. (2010) Impact of aftertreatment devices on primary emissions and secondary organic aerosol formation potential from in-use diesel vehicles: results from smog chamber experiments. *Atmos. Chem. Phys.*, 10, 11545-11563, doi: 10.5194/acp-10-11545-2010.

Chow J.C., Watson J.G., Crow D., Lowenthal D.H., and Merrifield T. (2001) Comparison of IMPROVE and NIOSH carbon measurements. *Aerosol Science and Technology*, 34, 23-34.

Chow J.C., Watson J.G., Chen L.-W.A., Rice J., and Frank N.H. (2010) Quantification of $PM_{2.5}$ organic carbon sampling artifacts in US networks. *Atmos. Chem. Phys.*, 10, 5223-5239, doi: 10.5194/acp-10-5223-2010. Available at http://www.atmos-chem-phys.net/10/5223/2010/.

Cubison M.J., Ortega A.M., Hayes P.L., Farmer D.K., Day D., Lechner M.J., Brune W.H., Apel E., Diskin G.S., Fisher J.A., Fuelberg H.E., Hecobian A., Knapp D.J., Mikoviny T., Riemer D., Sachse G.W., Sessions W., Weber R.J., Weinheimer A.J., Wisthaler A., and Jimenez J.L. (2011) Effects of aging on organic aerosol from open biomass burning smoke in aircraft and laboratory studies. *Atmos. Chem. Phys.*, 11, 12049-12064, doi: 10.5194/acp-11-12049-2011

Available at http://www.atmos-chem-phys.net/11/12049/2011/acp-11-12049-2011.pdf.

de Gouw J.A., Middlebrook A.M., Warneke C., Goldan P.D., Kuster W.C., Roberts J.M., Fehsenfeld F.C., Worsnop D.R., Canagaratna M.R., Pszenny A.A.P., Keene W.C., Marchewka M., Bertman S.B., and Bates T.S. (2005) Budget of organic carbon in a polluted atmosphere: Results from the New England Air Quality Study in 2002. *Journal of Geophysical Research*, 110, D16305, doi:16310.11029/12004JD005623.

de Gouw J.A., Brock C.A., Atlas E.L., Bates T.S., Rehsenfeld F.C., Goldan P.D., Holloway J.S., Kuster W.C., Lerner B.M., Matthew B.M., Middlebrook A.M., Onasch T.B., Peltier R.E., Quinn P.K., Senff C.J., Stohl A., Sullivan A.P., Trainer M., Warneke C., Weber R.J., and Williams E.J. (2008) Sources of particulate matter in the northeastern United States in summer: direct emissions and secondary formation of organic matter in urban plumes. *Journal of Geophysical Research*, 113, 1-19, doi: 10.1029/2007JD009243 (D08301).

DeCarlo P., Slowik J.G., Worsnop D.R., Davidovits P., and Jimenez J.L. (2004) Particle morphology and density characterization by combined mobility and aerodynamic diameter measurements. Part 1: theory, aerosol science and technology. *Aerosol Science and Technology*, 38, 1185-1205, doi: 10.1080/027868290903907.

DeCarlo P., Kimmel J.R., Trimborn A., Northway M., Jayne J.T., Aiken A.C., Gonin M., Fuhrer K., Horvath T., Docherty K.S., Worsnop D.R., and Jimenez J.L. (2006) Field-deployable, high-resolution, time-of-flight aerosol mass spectrometer. *Analytical Chemistry (Washington)*, 78, 8281-8289, doi: 10.1021/ac061249n (24).

Docherty K.S., Stone E.A., Ulbrich I.M., DeCarlo P., Snyder D.C., Schauer J.J., Peltier R.E., Weber R.J., Murphy S.M., Seinfeld J.H., Grover B.D., Eatough D.J., and Jimenez J.L. (2008) Apportionment of primary and secondary organic aerosols in Southern California during the 2005 Study of Organic Aerosols in Riverside (SOAR-1). *Environ. Sci. Technol.*, 42, 7655-7662, doi: 10.1021/es8008166 (20).

Docherty K.S., Aiken A.C., Huffman J.A., Ulbrich I.M., DeCarlo P.F., Sueper D., Worsnop D.R., Snyder D.C., Peltier R.E., Weber R.J., Grover B.D., Eatough D.J., Williams B.J., Goldstein A.H., Ziemann P.J., and Jimenez J.L. (2011) The 2005 study of organic aerosols at Riverside (SOAR-1): instrumental intercomparisons and fine particle composition. *Atmos. Chem. Phys.*, 11, 12387-12420, doi: 10.5194/acp-11-12387-2011 (23). Available at http://www.atmos-chem-phys.net/11/12387/2011/acp-11-12387-2011.pdf.

Dockery D.W., Pope C.A., Xu X.P., Spengler J.D., Ware J.H., Fay M.E., Ferris B.G., and Speizer F.E. (1993) An association between air pollution and mortality in six U.S. cities. *New Engl. J. Med.*, 329, 1753-1759, December 9.

Dockery D.W. and Stone P.H. (2007) Cardiovascular risks from fine particulate air pollution. *New Engl. J. Med.*, 356, 511-513, February. Available at http://content.nejm.org/cgi/content/extract/356/5/511.

Donahue N.M., Kroll J.H., Pandis S.N., and Robinson A.L. (2012) A two-dimensional volatility basis set – Part 2: Diagnostics of organic-aerosol evolution. *Atmos. Chem. Phys.*, 12, 615-634, doi: 10.5194/acp-12-615-2012.

Drewnick F., Jayne J.T., Canagaratna M., Worsnop D.R., and Demerjian K.L. (2004a) Measurement of ambient aerosol composition during the PMTACS-NY 2001 using an aerosol mass spectrometer. Part II: Chemically speciated mass distributions. *Aerosol Science and Technology*, 38, 104-117.

Drewnick F., Schwab J.J., Jayne J.T., Canagaratna M., Worsnop D.R., and Demerjian K.L. (2004b) Measurement of ambient aerosol composition during the PMTACS-NY 2001 using an aerosol mass spectrometer. Part I: Mass concentrations. *Aerosol Science & Technology*, 38, 92-103, (Suppl 1).

Drewnick F., Hings S.S., DeCarlo P., Jayne J.T., Gonin M., Fuhrer K., Weimer S., Jimenez J.L., Demerjian K.L., Borrmann S., and Worsnop D.R. (2005) A new time-of-flight aerosol mass spectrometer (TOF-AMS)—instrument description and first field deployment. *Aerosol Science & Technology*, 39, 637-658, doi: 10.1080/02786820500182040.

Dzepina K., Arey J., Marr L.C., Worsnop D.R., Salcedo D., Q. Z., Onasch T.B., Molina L.T., Molina M.J., and Jimenez J.L. (2007) Detection of particle-phase polycyclic aromatic hydrocarbons in Mexico City using an aerosol mass spectrometer. *International Journal of Mass Spectrometry*, 263, 152-170, doi: 10.1016/j.ijms.2007.01.010.

Edwards J., Walters S., and Griffiths R.K. (1994) Hospital admissions for asthma in preschool children: relationship to major roads in Birmingham, United Kingdom. *Arch. Environ. Health*, 49, 223-227, Jul-Aug.

Engel-Cox J.A. and Weber S.A. (2007) Compilation and assessment of recent positive matrix factorization and UNMIX receptor model studies on fine particulate matter source apportionment for the eastern United States. *J. Air Waste Manage.*, 57, 1307-1316 doi: 10.3155-1047-3289.57.11.1307 (11), November.

Engling G., Herckes P., Kreidenweis S.M., Malm W.C., and Collett J.L., Jr. (2006) Composition of the Fine Organic Aerosol in Yosemite National Park During the 2002 Yosemite Aerosol Characterization Study. *Atmos. Environ.*, 40, 2959-2972.

Fine P.M., Cass G.R., and Simoneit B.R.T. (2001) Chemical characterization of fine particle emissions from fireplace combustion of woods grown in the northeastern United States. *Environ. Sci. Technol.*, 35, 2665-2675, (13).

Fine P.M., Cass G.R., and Simoneit B.R.T. (2002a) Organic compounds in biomass smoke from residential wood combustion: emissions characterization at a continental scale. *Journal of Geophysical Research-Atmospheres*, 107, (D21), Nov.

Fine P.M., Cass G.R., and Simoneit B.R.T. (2002b) Chemical characterization of fine particle emissions from the fireplace combustion of woods grown in the southern United States. *Environ. Sci. Technol.*, 36, 1442-1451, (7), Apr 1.

Fine P.M., Cass G.R., and Simoneit B.R.T. (2004a) Chemical characterization of fine particle emissions from the fireplace combustion of wood types grown in the Midwestern and Western United States. *Environmental Engineering Science*, 21, 387-409, (3), May-Jun.

Fine P.M., Shen S., and Sioutas C. (2004b) Inferring the sources of fine and ultrafine particulate matter at downwind receptor sites in the Los Angeles basin using multiple continuous measurements. *Aerosol Science and Technology*, 38, 182-195.

Finkelstein M.M., Jerrett M., and Sears M.R. (2004) Traffic air pollution and mortality rate advancement periods. *Am. J. Epidemiol.*, 160, 173-177, Jul.

Flowers L., Rieth S.H., Cogliano V.J., Foureman G.L., Hertzberg R., Hofmann E.L., Murphy D.L., Nesnow S., and Schoeny R.S. (2002) Health assessment of polycyclic aromatic hydrocarbon mixtures: current practices and future directions. *Polycyclic Aromatic Compounds*, 22, 811-821.

Frank N. (2010): Urban EC and OC trends using CSN, IMPROVE, SEARCH EC & OC, "BC" & OCMmb via FRM PM2.5: *IMPROVE Carbon Workshop, Columbia Gorge, WA, October 27*.

Fraser M.P., Kleeman M.J., Schauer J.J., and Cass G.R. (2000) Modeling the atmospheric concentrations of individual gas-phase and particle-phase organic compounds. *Environ. Sci. Technol.*, 34, 1302-1312, (7), Apr 1.

Freeman L., Stiefer P.S., and Weir B.R. (1992) Carcinogenic risk and residential wood smoke. Report by Systems Applications International, San Rafael, CA, SYSAPP-91/148.

Fruin S., Westerdahl D., Sax T., Sioutas C., and Fine P.M. (2008) Measurements and predictors of on-road ultrafine particle concentrations and associated pollutants in Los Angeles. *Atmos. Environ.*, 42, 207-219, doi: 10.1016/j.atmosenv.2007.09.057.

Gilardoni S., Liu S., Takahama S., Russell L.M., Allan J.D., Steinbrecher R., Jimenez J.L., DeCarlo P.F., Dunlea E.J., and Baumgardner D. (2009) Characterization of organic ambient aerosol during MIRAGE 2006 on three platforms. *Atmospheric Chemistry and Physics*, 9, 5417-5432, (15). Available at http://www.atmos-chem-phys.net/9/5417/2009/acp-9-5417-2009.pdf.

Green M.C., Chow J.C., Hecobian A., Etyemezian V., Kuhns H., and Watson J.G. (2002) Las Vegas Valley visibility and $PM_{2.5}$ study. Final Report prepared for the Clark County Department of Air Quality Management, Las Vegas, NV, by the Desert Research Institute, Las Vegas, NV, May.

Green R.S., Smorodinsky S., Kim J.J., McLaughlin R., and Ostro B. (2004) Proximity of California public schools to busy roads. *Environ. Health Persp.*, 112, 61-66, (1), January.

Grieshop A.P., Lipsky E.M., Pekney N.J., Takahama S., and Robinson A.L. (2006) Fine particle emission factors from vehicles in a highway tunnel: effects of fleet composition and season. *Atmos. Environ.*, 40, 287-298.

Gundel L.A., Lane D.A., and Schauer J.J. (1999) Optimizing measurements of semi-volatile organic compounds from mission sources, environmental chambers and the atmosphere. *Abstracts of Papers of the American Chemical Society*, 217, U733-U734, Mar 21.

Hand J.L., Copeland S.A., Day D.E., Dillner A.M., Indresand H., Malm W.C., McDade C.E., Moore C.T., Pitchford M.L., Schichtel B.A., and Watson J.G. (2011) Spatial and seasonal patterns and temporal variability of haze and its constituents in the United States: IMPROVE Report V. June. Available at http://vista.cira.colostate.edu/improve/publications/reports/2011/2011.htm.

Hansen A.D.A. (1998) The Aethalometer™. Instument guide prepared by the Magee Scientific Company, Berkeley, CA.

Hansen A.D.A. (2002) The Aethalometer™ - real-time aerosol analysis for measuring carbonaceous aerosol species. Prepared by Magee Scientific Company, Berkeley, CA.

Hays M.D., Smith N.D., and Dong Y.J. (2004) Nature of unresolved complex mixture in size-distributed emissions from residential wood combustion as measured by thermal desorption-gas chromatography-mass spectrometry. *Journal of Geophysical Research-Atmospheres*, 109, (D16), Jun 25.

Heald C.L., Kroll J.H., Jimenez J.L., Docherty K.S., DeCarlo P.F., Aiken A.C., Chen Q., Martin S.T., Farmer D.K., and Artaxo P. (2010) A simplified description of the evolution of organic aerosol composition in the atmosphere. *Geophysical Research Letters*, 37, doi: 10.1029/2010GL042737 (L08803). Available at http://www.agu.org/pubs/crossref/2010/2010GL042737.shtml.

Hennigan C.J., Miracolo M.A., Engelhart G.J., May A.A., Presto A.A., Lee T., Sullivan A.P., McMeeking G.R., Coe H., Wold C.E., Hao W.-M., Gilman J.B., Kuster W.C., de Gouw J., Schichtel B.A., Collett J.L., Jr., Kreidenweis S.M., and Robinson A.L. (2011) Chemical and physical transformations of organic aerosol from the photo-oxidation of

open biomass burning emissions in an environmental chamber. *Atmospheric Chemistry and Physics*, 11, 7669-7686, August 1.

Heringa M.F., DeCarlo P.F., Chirico R., Tritscher T., Dommen J., Weingartner E., Richter R., Wehrle G., Prévôt A.S.H., and Baltensperger U. (2011) Investigations of primary and secondary particulate matter of different wood combustion appliances with a high-resolution time-of-flight aerosol mass spectrometer. *Atmos. Chem. Phys.*, 11, 5945-5957, doi: 10.5194/acp-11-5945-2011. Available at http://www.atmos-chem-phys.net/11/5945/2011/acp-11-5945-2011.pdf.

Hiura T.S., Li N., Kaplan R., Horwitz M., Seagrave J.C., and Nel A.E. (2000) The role of a mitochondrial pathway in the induction of apoptosis by chemicals extracted from diesel exhaust particles. *J. Immunol.*, 165, 2703-2711.

Hoek G., Brunekreef B., Goldbohm S., Fischer P., and van den Brandt P.A. (2002) Association between mortality and indicators of traffic-related air pollution in the Netherlands: a cohort study. *Lancet*, 360, 1203-1209.

Huffman J.A., Docherty K.S., Mohr C., Cubison M., Ulbrich I.M., Ziemann P.J., Onasch T.B., and Jimenez J.L. (2009) Chemically-resolved volatility measurements of organic aerosol from different sources. *Environ. Sci. Technol.*, 43, 5351-5357, doi: 10.1021/es803539d.

Jayne J.T., Leard D.C., Zhang X.F., Davidovits P., Smith K.A., Kolb C.E., and Worsnop D.R. (2000) Development of an aerosol mass spectrometer for size and composition analysis of submicron particles. *Aerosol Science & Technology*, 33, 49-70, (1-2).

Jeong C.H., Hopke P.K., Kim E., and Lee D.W. (2004) The comparison between thermal-optical transmittance elemental carbon and Aethalometer black carbon measured at multiple monitoring sites. *Atmos. Environ.*, 38, 5193-5204, (31), October 2004.

Jimenez J.L., Jayne J.T., Shi Q., Kolb C.E., Worsnop D.R., Yourshaw I., Seinfeld J.H., Flagan R.C., Zhang X.F., Smith K.A., Morris J.W., and Davidovits P. (2003) Ambient aerosol sampling using the Aerodyne Aerosol Mass Spectrometer. *Journal of Geophysical Research-Atmospheres*, 108, (D7), Apr 15.

Jimenez J.L., Canagaratna M.R., Donahue N.M., Prévôt A.S.H., Zhang Q., Kroll J.H., DeCarlo P.F., Allan J.D., Coe H., Ng N.L., Aiken A.C., Docherty K.S., Ulbrich I.M., Grieshop A.P., Robinson A.L., Duplissy J., Smith J.D., Wilson K.R., Lanz V.A., Hueglin C., Sun Y.L., Tian J., Laaksonen A., Raatikainen T., Rautiainen J., Vaattovaara P., Ehn M., Kulmala M., Tomlinson J.M., Collins D.R., Cubison M.J., Dunlea E.J., Huffman J.A., Onasch T.B., Alfarra M.R., Williams P.I., Bower K., Kondo Y., Schneider J., Drewnick F., Borrmann S., Weimer S., Demerjian K., Salcedo D., Cottrell L., Griffin R., Takami A., Miyoshi T., Hatakeyama S., Shimono A., Sun J.Y., Zhang Y.M., Dzepina K., Kimmel J.R., Sueper D., Jayne J.T., Herndon S.C., Trimborn A.M., Williams L.R., Wood E.C., Middlebrook A.M., Kolb C.E., Baltensperger U., and Worsnop D.R. (2009) Evolution of organic aerosols in the atmosphere. *Science*, 326, 1525-1529, doi: 10.1126/science.1180353, December 11.

Ke L., Liu W., Want Y., Russell A.G., Edgerton E.S., and Zheng M. (2008) Comparison of $PM_{2.5}$ source apportionment using positive matrix factorization and molecular marker-based chemical mass balance. *Science of the Total Environment*, 394, 290-302.

Kim E., Larson T.V., Hopke P.K., Slaughter C., Sheppard L.E., and Claiborn C. (2003) Source identification of $PM_{2.5}$ in an arid northwest U.S. city by positive matrix factorization. *Atmospheric Research*, 66, 291-305, (4), May-Jun.

Kim E. and Hopke P.K. (2007) Source identifications of airborne fine particles using positive matrix factorization and U.S. Environmental Protection Agency positive matrix factorization. *J. Air Waste Manage.*, 57, 811-819, doi: 10.3155-1047-3289.57.7.811 (7), July.

Kim J.J., Smorodinsky S., Lipsett M., Singer B.C., Hodgson A.T., and Ostro B. (2004) Traffic-related air pollution near busy roads: the East Bay Children's Respiratory Health Study. *Am. J. Resp. Crit. Care*, 170, 520-526, (5), Sep 1.

Kirchstetter T.W., Harley R.A., Kreisberg N.M., Stolzenburg M.R., and Hering S.V. (1999) On-road measurement of fine particle and nitrogen oxide emissions from light- and heavy-duty motor vehicles. *Atmos. Environ.*, 33, 2955-2968.

Kirchstetter T.W., Novakov T., and Hobbs P.V. (2004) Evidence that spectral light absorption by aerosols emitted from biomass burning and motor vehicles is different due to organic carbon. *J. Geophys. Res*, 109, doi: 10.1029/2004JD004999 (D21208).

Kittelson D.B., Watts W.F., Johnson J.P., Remerowki M.L., Ische E.E., Oberdorster G., Gelein R.A., Elder A., Hopke P.K., Kim E., Zhao W., Zhou L., and Jeong C.H. (2004) On-road exposure to highway aerosols. 1. Aerosol and gas measurements. *Inhalation Toxicology*, 16, 31-39.

Kleindienst T.E., Jaoui M., Lewandowski M., Offenberg J.H., Lewis C.W., Bhave P.V., and Edney E.O. (2007) Estimates of the contributions of biogenic and anthropogenic hydrocarbons to secondary organic aerosol at a southeastern US location. *Atmos. Environ.*, 41, 8288-8300, (37), December.

Kroll J.H., Donahue N.M., Jimenez J.L., Kessler S.H., Canagaratna M.R., Wilson K.R., Altieri K.E., R.Mazzoleni L., Wozniak A.S., Bluhm H., Mysak E.R., Smith J.D., Kolb C.E., and Worsnop D.R. (2011) Carbon oxidation state as a metric for describing the chemistry of atmospheric organic aerosol. *Nature Chemistry*, 3, 133-139, doi: 10.1038/NCHEM.948.

Kunzli N., Kaiser R., Medina S., Studnicka M., Chanel O., and Filliger P. (2000) Public-health impact of outdoor and traffic-related air pollution: a European assessment. *Lancet*, 356, 795-801.

Lanz V.A., Alfarra M.R., Baltensperger U., Buchmann B., Hueglin C., and Prévôt A.S.H. (2007) Source apportionment of submicron organic aerosols at an urban site by factor analytical modelling of aerosol mass spectra. *Atmos. Chem. Phys.*, 7, 1503-1522.

Lanz V.A., Alfarra M.R., Baltensperger U., Buchmann B., Hueglin C., Szidat S., Wehrli M.N., Wacker L., Weimer S., Caseiro A., Puxbaum H., and Prévôt A.S.H. (2008) Source attribution of submicron organic aerosols during wintertime inversions by advanced factor analysis of aerosol mass spectra. *Environ. Sci.Technol.*, 42, 214-220, doi: 10.1021/es0707207 (1).

Lanz V.A., Prévôt A.S.H., Alfarra M.R., Weimer S., Mohr C., DeCarlo P.F., Gianini M.F.D., Hueglin C., Schneider J., Favez O., D'Anna B., George C., and Baltensperger U. (2010) Characterization of aerosol chemical composition with aerosol mass spectrometry in

Central Europe: an overview. *Atmos. Chem. Phys.*, 10, 10453-10471, doi: 10.5194/acp-10-10453-2010, November 8.

Larsen R.K. and Baker J.E. (2003) Source apportionment of polycyclic aromatic hydrocarbons in the urban atmosphere: a comparison of three methods. *Environ. Sci. Technol.*, 37, 1873-1881, (9), May 1.

Lee T., Sullivan A.P., Mack L., Jimenez J.L., Kreidenweis S.M., Onasch T.B., Worsnop D.R., Malm W., Wold C.E., Hao W.M., and Jeffrey L. Collett J. (2010) Chemical smoke marker emissions during flaming and smoldering phases of laboratory open burning of wildland fuels. *Aerosol Science & Technology*, 44, i-v, doi: 10.1080/02786826.2010.499884 (9).

Li N., Sioutas S., Cho A., Schmitz D., Misra C., Sempf J., Wang M., Oberly T., Froines J., and Nel A.E. (2003) Ultrafine particulate pollutants induce oxidative stress and mitochondrial damage. *Environ. Health Persp.*, 111, 455-460.

Lighty J.S., Veranth J.M., and Sarofim A.F. (2000) Combustion aerosols: factors governing their size and composition and implications to human health. *J. Air Waste Manage.*, 50, 1565-1618, (9), September.

Lipsky E.M. and Robinson A.L. (2006) Effects of dilution on fine particle mass and partitioning of semivolatile organics in diesel exhaust and wood smoke. *Environ. Sci. Technol.*, 40, 155-162.

Liu W., Wang Y., Russell A., and Edgerton E.S. (2005) Atmospheric aerosol over two urban-rural pairs in the southeastern United States: chemical composition and possible sources. *Atmos. Environ.*, 39, 4453-4470.

Lobscheid A.B. and McKone T.E. (2004) Constraining uncertainties about the sources and magnitude of polycyclic aromatic hydrocarbon (PAH) levels in ambient air: the state of Minnesota as a case study. *Atmos. Environ.*, 38.

Malm W.C., Sisler J.F., Huffman D., Eldred R.A., and Cahill T.A. (1994) Spatial and seasonal trends in particulate concentration and optical extinction in the United States. *Journal of Geophysical Research*, 99, 1347-1370, (D1).

Maria S.F., Russell L.M., Turpin B.J., Porcja R.J., Campos T.L., Weber R.J., and Huebert B.J. (2003) Source signatures of carbon monoxide and organic functional groups in Asian Pacific Regional Aerosol Characterization Experiment (ACE-Asia) submicron aerosol types. *J. Geophys. Res*, 108, 8637, doi: 10.1029/2003JD003703 (D23). Available at http://aerosol.ucsd.edu/papers/Maria2003jgr.pdf.

Matthew B.M., Middlebrook A.M., and Onasch T.B. (2008) Collection efficiencies in an Aerodyne aerosol mass spectrometer as a function of particle phase for laboratory generated aerosols. *Aerosol Science & Technology*, 42, 884-898, doi: 10.1080/02786820802356797.

Mauderly J.L. (1994) Toxicological and epidemiological evidence for health risks from inhaled engine emissions. *Environ. Health Persp.*, 102, 165-171.

McCarthy M.C., Ludwig J.F., Brown S.G., Vaughn D.L., and Roberts P.T. (2013) Filtration effectiveness of HVAC systems at near-roadway schools. *Indoor Air*, 23, 196-207, doi:

10.1111/ina.12015 (3), January 25. Available at http://onlinelibrary.wiley.com/doi/10.1111/ina.12015/abstract.

McDonald J.D., Harrod K.S., Seagrave J., Seilkop S.K., and Mauderly J.L. (2004) Effects of low sulfur fuel and a catalyzed particle trap on the composition and toxicity of diesel emissions. *Environ. Health Persp.*, 112, 1307-1312, (13).

Middlebrook A.M., Bahreini R., Jimenez J.L., and Canagaratna M.R. (2012) Evaluation of composition-dependent collection efficiencies for the Aerodyne aerosol mass spectrometer using field data. *Aerosol Science and Technology*, 46, 258-271, doi: 10.1080/02786826.2011.620041 (3), September 28. Available at http://www.tandfonline.com/doi/abs/10.1080/02786826.2011.620041#.Udw6VflZd_4 and http://cires.colorado.edu/~jjose/Papers/2011_AST_Middlebrook_CE.pdf.

Miguel A.H., Kirchstetter T.W., Harley R.A., and Hering S.V. (1998) On-road emissions of particulate polycyclic aromatic hydrocarbons and black carbon from gasoline and diesel vehicles. *Environ. Sci. Technol.*, 32, 450-455, (4), Feb 15.

Minguillon M.C., Arhami M., Schauer J.J., and Sioutas C. (2008) Seasonal and spatial variations of sources of fine and quasi-ultrafine particulate matter in neighborhoods near the Los Angeles-Long Beach harbor. *Atmos. Environ.*, 42, 7317-7328.

Minguillon M.C., Perron N., Querol X., Szidat S., Fahrni S.M., Alastuey A., Jimenez J.L., Mohr C., Ortega A.M., Day D.A., Lanz V.A., Wacker L., Reche C., Cusack M., Amato F., Kiss G., Hoffer A., Decesari S., Moretti F., Hillamo R., Teinila K., Seco R., Penuelas J., Metzger A., Schallhart S., Muller M., Hansel A., Burkhart J.F., Baltensperger U., and Prévôt A.S.H. (2011) Fossil versus contemporary sources of fine elemental and organic carbonaceous particulate matter during the DAURE campaign in Northeast Spain. *Atmos. Chem. Phys.*, 11, 12067-12084, doi: 10.5194/acp-11-12067-2011. Available at http://www.atmos-chem-phys.net/11/12067/2011/acp-11-12067-2011.pdf.

Mohr C., Huffman J.A., Cubison M., Aiken A.C., Docherty K.S., Kimmel J.R., Ulbrich I.M., Hannigan M., and Jimenez J.L. (2009) Characterization of primary organic aerosol emissions from meat cooking, trash burning, and motor vehicles with high-resolution aerosol mass spectrometry and comparison with ambient and chamber observations. *Environ. Sci. Technol.*, 43, 2443-2449, doi: 10.1021/es8011518 (7).

Naeher L.P., Brauer M., Lipsett M., Zelikoff J.T., Simpson C.D., Koenig J.Q., and Smith K.R. (2007) Woodsmoke health effects: a review. *Inhalation Toxicology*, 19, 67-106, doi: 10.1080/08958370600985875.

Ng N.L., Canagaratna M.R., Zhang Q., Jimenez J.L., Tian J., Ulbrich I.M., Kroll J.H., Docherty K.S., Chhabra P.S., Bahreini R., Murphy S.M., Seinfeld J.H., Hildebrandt L., Donahue N.M., DeCarlo P.F., Lanz V.A., Prévôt A.S.H., Dinar E., Rudich Y., and Worsnop D.R. (2010) Organic aerosol components observed in Northern Hemispheric datasets from Aerosol Mass Spectrometry. *Atmos. Chem. Phys.*, 10, 4625-4641, doi: 10.5194/acp-10-4625-2010.

Ng N.L., Canagaratna M.R., Jimenez J.L., Zhang Q., Ulbrich I.M., and Worsnop D.R. (2011) Real-time methods for estimating organic component mass concentrations from aerosol mass spectrometer data. *Environ Sci Technol*, 45, 910-916, doi: 10.1021/es102951k (3), December 27. Available at http://pubs.acs.org/doi/abs/10.1021/es102951k.

Nitta H., Sato T., Nakai S., Maeda K., Aoki S., and Ono M. (1993) Respiratory health associated with exposure to automobile exhaust. 1. Results of cross-sectional studies in 1979, 1982, and 1983. *Arch. Environ. Health*, 48, 53-58, Jan-Feb.

Norris G., Vedantham R., Wade K.S., Brown S.G., Prouty J.D., and Foley C. (2008) EPA positive matrix factorization (PMF) 3.0 fundamentals and user guide. Prepared for the U.S. Environmental Protection Agency, Washington, D.C., by the National Exposure Research Laboratory, Research Triangle Park; Sonoma Technology, Inc., Petaluma, CA; and Lockheed Martin Systems Engineering Center, Arlington, VA, EP-D-05-004; STI-907045.05-3347-UG, October.

Norris G., Vedantham R., Wade K., Zahn P., Brown S., Paatero P., Eberly S., and Foley C. (2009) Guidance document for PMF applications with the Multilinear Engine. Prepared for the U.S. Environmental Protection Agency, Research Triangle Park, NC, by the National Exposure Research Laboratory, Research Triangle Park, NC; Sonoma Technology, Inc., Petaluma, CA; University of Helsinki, Helsinki, Finland; Geometric Tools, Inc., Phoenix, AZ; and Lockheed Martin, Systems Engineering Center, Arlington, VA, EPA 600/R-09/032, April.

Ntziachristos L., Ning Z., Geller M.D., and Sioutas C. (2007) Particle concentration and characteristics near a major freeway with heavy-duty diesel traffic. *Environ. Sci. Technol.*, 41, 2223-2230, doi: 10.1021/es062590s (7).

Oja V. and Suuberg E.M. (1999) Vapor pressures and enthalpies of sublimation of d-glucose, d-xylose, cellobiose, and levoglucosan. *J. Chem Eng. Data*, 44, 26-29.

Olson D.A., Vedantham R., Norris G.A., Brown S.G., and Roberts P. (2012) Determining source impacts near roadways using wind regression and organic source markers. *Atmos. Environ.*, 47, 261-268, doi: 10.1016/j.atmosenv.2011.11.003, February. Available at http://www.sciencedirect.com/awma/article/pii/S1352231011011654.

Orsini D.A., Ma Y.L., Sullivan A., Sierau B., Baumann K., and Weber R.J. (2003) Refinements to the particle-into-liquid sampler (PILS) for ground and airborne measurements of water soluble aerosol composition. *Atmospheric Environment*, 37, 1243-1259, (9-10), Mar. Available at <Go to ISI>://000181777100011.

Paatero P. and Tapper U. (1994) Positive matrix factorization: a non-negative factor model with optimal utilization of error estimates of data values. *Environmetrics*, 5, 111-126.

Paatero P. (1997) Least squares formulation of robust non-negative factor analysis. *Chemometrics and Intelligent Laboratory Systems*, 37, 23-35.

Paatero P., Hopke P.K., Song X.H., and Ramadan Z. (2002) Understanding and controlling rotations in factor analytic models. *Chemometrics and Intelligent Laboratory Systems*, 60, 253-264.

Paatero P. and Hopke P.K. (2003) Discarding or downweighting high-noise variables in factor analytic models. *Analytica Chimica Acta*, 490, 277-289.

Paatero P. (2007) End user's guide to multilinear engine applications. February.

Paatero P. and Hopke P.K. (2008) Rotational tools for factor analytic models.

Park S.S., Hansen A.D.A., and Cho S.Y. (2010) Measurement of real time black carbon for investigating spot loading effects of Aethalometer data. *Atmos. Environ.*, 44, 1449-1455, doi: 10.1016/j.atmosenv.2010.01.025.

Phuleria H.C., Sheesley R.J., Schauer J.J., Fine P.M., and Sioutas C. (2007) Roadside measurements of size-segregated particulate organic compounds near gasoline and diesel-dominated freeways in Los Angeles, CA. *Atmos. Environ.*, 41, 4653-4671, doi: 10.1016/j.atmosenv.2007.03.031.

Poirot R. (1998) Tracers of opportunity: Potassium. Available at <http://capita.wustl.edu/PMFine/Workgroup/SourceAttribution/Reports/In-progress/potass/Kcover.htm>.

Poirot R.L., Wishinski P.R., Hopke P.K., and Polissar A.V. (2001) Comparative application of multiple receptor methods to identify aerosol sources in northern Vermont. *Environ. Sci. Technol.*, 35, 4622-4636, (23), November.

Polidori A., Turpin B., Lim H.-J., Totten L., and Davidson C. (2004): Polarity and molecular weight/carbon weight of the Pittsburgh organic aerosol: *23rd American Association for Aerosol Research Annual Conference, Atlanta, GA, October 4-8*.

Polidori A., Turpin B.J., Davidson C.I., Rodenburg L.A., and Maimone F. (2008) Organic PM2.5: fractionation by polarity, FTIR spectroscopy, and OM/OC ratio for the Pittsburgh aerosol. *Aerosol Science & Technology*, 42, 233-246, doi: 10.1080/02786820801958767 (3). Available at http://dx.doi.org/10.1080/02786820801958767.

Puxbaum H., Caseiro A., Sanchez-Ochoa A., Kasper-Giebl A., Claeys M., Gelencser A., Legrand M., Preunkert S., and Pio C. (2007) Levoglucosan levels at background sites in Europe for assessing the impact of biomass combustion on the European aerosol background. *J. Geophys. Res*, 112, doi: 10.1029/2006JD008114 (D23S05).

Rattigan O.V., Felton H.D., Bae M.-S., Schwab J.J., and Demerjian K.L. (2010) Multi-year hourly PM2.5 carbon measurements in New York: diurnal, day of week and seasonal patterns. *Atmos. Environ.*, 44, 2043-2053, doi: 10.1016/j.atmosenv.2010.01.019, January.

Reff A., Eberly S.I., and Bhave P.V. (2007) Receptor modeling of ambient particulate matter data using positive matrix factorization: review of existing methods. *J. Air Waste Manage.*, 57, 146-154.

Reff A., Bhave P.V., Simon H., Pace T.G., Pouliot G.A., Mobley J.D., and Houyoux M. (2009) Emissions inventory of $PM_{2.5}$ trace elements across the United States. *Environ. Sci. Technol.*, 43, 5790-5796, (15). Available at http://www.ncbi.nlm.nih.gov/pubmed/19731678.

Reynolds P., Von Behren J., Gunier R.B., Goldberg D.E., and Hertz A. (2004) Residential exposure to traffic in California and childhood cancer. *Epidemiology*, 15, 6-12, Jan.

Riddle S.G., Robert M.A., Jakober C.A., Hannigan M.P., and Kleeman M.J. (2008) Size-resolved source apportionment of airborne particle mass in a roadside environment. *Environ. Sci. Technol.*, 42, 6580-6586, doi: 10.1021/es702827h (17).

Roberts P.T., McCarthy M.C., and Brown S.G. (2008): Characteristics of mobile-source air toxics (MSATs) at three schools next to U.S. 95 in Las Vegas, Nevada: *Air & Waste*

Management Association's 101st Annual Conference & Exhibition, Portland, OR, June 25.

Roberts P.T., Brown S.G., McCarthy M.C., DeWinter J.L., and Vaughn D.L. (2010) Mobile source air toxics (MSATs) at three schools next to U.S. 95 in Las Vegas, Nevada. Final report prepared for the Nevada Department of Transportation, Las Vegas, NV, by Sonoma Technology, Inc., Petaluma, CA, STI-906034-3509-FR2, May.

Robinson A.L., Donahue N.M., Shrivastava M.K., Weitkamp E.A., Sage A.M., Grieshop A.P., Lane T.E., Pierce J.R., and Pandis S.N. (2007) Rethinking organic aerosols: semivolatile emissions and photochemical aging. *Science*, 315, 1259.

Robinson A.L., Grieshop A.P., Donahue N.M., and Hunt S.W. (2010) Updating the conceptual model for fine particle mass emissions from combustion systems. *J. Air Waste Manage.*, 60, 1204-1222, doi: 10.3155/1047-3289.60.10.1204 (October).

Rogge W.F., Mazurek M.A., Hildemann L.M., Cass G.R., and Simoneit B.R.T. (1993) Quantification of Urban Organic Aerosols at a Molecular-Level - Identification, Abundance and Seasonal-Variation. *Atmospheric Environment Part a-General Topics*, 27, 1309-1330, (8), Jun.

Russell L.M. (2003) Aerosol organic-mass-to-organic-carbon ratio measurements. *Environ. Sci. Technol.*, 37, 2982-2987, (13), Jul 1.

Sage A.M., Weitkamp E.A., Robinson A.L., and Donahue N.M. (2008) Evolving mass spectra of the oxidized component of organic aerosol: results from aerosol mass spectrometer analyses of aged diesel emissions. *Atmos. Chem. Phys.*, 8, 1139-1152.

Sandradewi J., Prévôt A.S.H., Alfarra M.R., Szidat S., Wehrli M.N., Ruff M., Weimer S., Lanz V.A., Weingartner E., Perron N., Caseiro A., Kasper-Giebl A., Puxbaum H., Wacker L., and Baltensperger U. (2008) Comparison of several wood smoke markers and source apportionment methods for wood burning particulate mass. *Atmos. Chem. Phys. Discuss.*, 8, 8091-8118, doi: 10.5194/acpd-8-8091-2008 (2). Available at www.atmos-chem-phys-discuss.net/8/8091/2008/.

Sandradewi J., Prévôt A.S.H., Weingartner E., Schmidhauser R., Gysel M., and Baltensperger U. (2008) A study of wood burning and traffic aerosols in an Alpine valley using a multi-wavelength Aethalometer. *Atmos. Environ.*, 42, 101-112, (1). Available at http://www.sciencedirect.com/science/article/pii/S1352231007008072.

Sardar S.B., Fine P.M., Yoon H., and Sioutas C. (2004) Associations between particle number and gaseous co-pollutant concentrations in the Los Angeles basin. *J. Air Waste Manage.*, 54, 992-1005, (8), Aug.

Schauer J.J., Rogge W.F., Hildemann L.M., Mazurek M.A., Cass G.R., and Simoneit B.R.T. (1996) Source apportionment of airborne particulate matter using organic compounds as tracers. *Atmos. Environ.*, 30, 3837-3855, (22).

Schauer J.J., Kleeman M.J., Cass G.R., and Simoneit B.R.T. (1999a) Measurement of emissions from air pollution sources. 2. C_1 through C_{30} organic compounds from medium duty diesel trucks. *Environ. Sci. Technol.*, 33, 1578-1587, (10), May 15.

Schauer J.J., Kleeman M.J., Cass G.R., and Simoneit B.R.T. (1999b) Measurement of emissions from air pollution sources. 1. C_1 through C_{29} organic compounds from meat charbroiling. *Environ. Sci. Technol.*, 33, 1566-1577.

Schauer J.J. and Cass G.R. (2000) Source apportionment of wintertime gas-phase and particle-phase air pollutants using organic compounds as tracers. *Environ. Sci. Technol.*, 34, 1821-1832, (9).

Schauer J.J., Kleeman M.J., Cass G.R., and Simoneit B.R.T. (2001) Measurement of emissions from air pollution sources. 3. C_1 through C_{29} organic compounds from fireplace combustion of wood. *Environ. Sci. Technol.*, 35, 1716-1728, (9), May 1.

Schauer J.J., Fraser M.P., Cass G.R., and Simoneit B.R.T. (2002a) Source reconciliation of atmospheric gas-phase and particle-phase pollutants during a severe photochemical smog episode. *Environ. Sci. Technol.*, 36, 3806-3814, (17).

Schauer J.J., Kleeman M.J., Cass G.R., and Simoneit B.R.T. (2002b) Measurement of emissions from air pollution sources. 5. C-1-C-32 organic compounds from gasoline-powered motor vehicles. *Environ. Sci. Technol.*, 36, 1169-1180, (6), Mar 15.

Schmidl C., Marr I.L., Caseiro A., Kotianova P., Berner A., Bauer H., Kasper-Giebl A., and Puxbaum H. (2008) Chemical characterisation of fine particle emissions from wood stove combustion of common woods growing in mid-European Alpine regions. *Atmos. Environ.*, 42, 126-141, doi: 10.1016/j.atmosenv.2007.09.028.

Schneider J., Weimer S., Drewnick F., Borrmann S., Helas G., Gwaze P., Schmid O., Andreae M.O., and Kirchner U. (2006) Mass spectrometric analysis and aerodynamic properties of various types of combustion-related aerosol particles. *Int. J. Mass Spec.*, 258, 37-49, doi: 10.1016/j.ijms.2006.07.008 (1-3).

Schweitzer L. and Valenzuela A. (2004) Environmental injustice and transportation: The claims and the evidence. *Journal of Planning Literature*, 18, 383-398, (4), May.

Seagrave J., McDonald J.D., Bedrick E., Edgerton E.S., Gigliotti A.P., Jansen J.J., Ke L., Naeher L.P., Seilkop S.K., Zheng M., and Mauderly J.L. (2006) Lung toxicity of ambient particulate matter from southeastern U.S. sites with different contributing sources: relationships between composition and effects. *Environ. Health Persp.*, 114, 1387-1393, (9).

Sheesley R.J., Schauer J.J., Meiritz M., DeMinter J.T., Bae M.S., and Turner J.R. (2007) Daily variation in particle-phase source tracers in an urban atmosphere. *Aerosol Science & Technology*, 41, 981-993, (11). Available at <http://dx.doi.org/10.1080/02786820701644277>.

Simon H., Bhave P.V., Swall J.L., Frank N.H., and Malm W.C. (2011) Determining the spatial and seasonal variability in OM/OC ratios across the US using multiple regression. *Atmospheric Chemistry and Physics*, 11, 2933-2949, doi: 10.5194/acp-11-2933-2011. Available at http://www.atmos-chem-phys.net/11/2933/2011/acp-11-2933-2011.html.

Simoneit B.R.T., Schauer J.J., Nolte C.G., Oros D.R., Elias V.O., Fraser M.P., Rogge W.F., and Cass G.R. (1999) Levoglucosan, a tracer for cellulose in biomass burning and atmospheric particles. *Atmos. Environ.*, 33, 173-182.

Simoneit B.R.T. (2002) Biomass burning - a review of organic tracers for smoke from incomplete combustion. *Applied Geochemistry*, 17, 129-162.

Sin D.W.M., Fung W.H., Choi Y.Y., Lam C.H., and Wong Y.C. (2004) Measurement of carbonaceous aerosols: validation of a thermal gravimetric method and its comparison with a thermal optical transmittance method. *Microchemical Journal*, 77, 63-70, (1), May.

Slowik J.G., Stainken K., Davidovits P., Williams L.R., Jayne J.T., Kolb C.E., Worsnop D.R., Rudich Y., DeCarlo P.F., and Jimenez J.L. (2004) Particle morphology and density characterization by combined mobility and aerodynamic diameter measurements. Part 2: application to combustion-generated soot aerosols as a function of fuel equivalence ratio. *Aerosol Science and Technology*, 38, 1206-1222, doi: 10.1080/027868290903916. Available at http://cires.colorado.edu/~jjose/Papers/Slowik_AST_2004_Published.pdf.

Sorooshian A., Brechtel F.J., Ma Y.L., Weber R.J., Corless A., Flagan R.C., and Seinfeld J.H. (2006) Modeling and characterization of a particle-into-liquid sampler (PILS). *Aerosol Science and Technology*, 40, 396-409, doi: 10.1080/02786820600632282 (6), June. Available at http://www.tandfonline.com/doi/abs/10.1080/02786820600632282#preview.

Sullivan A.P., Holden A.S., Patterson L.A., McMeeking G.R., Kreidenweis S.M., Malm W.C., Hao W.M., Wold C.E., and Collett J.L., Jr. (2008) A method for smoke marker measurements and its potential application for determining the contribution of biomass burning from wildfires and prescribed fires to ambient $PM_{2.5}$ organic carbon. *J. Geophys. Res.*, 113, D22302, doi: 10.1029/2008jd010216, November. Available at http://dx.doi.org/10.1029/2008JD010216.

Sun Y., Zhang Q., MacDonald A.M., Hayden K., Li S.M., Liggio J., Liu P.S.K., Anlauf K.G., Leaitch W.R., Steffen A., Cubison M., Worsnop D.R., van Donkelaar A., and Martin R.V. (2009) Size-resolved aerosol chemistry on Whistler Mountain, Canada with a high-resolution aerosol mass spectrometer during INTEX-B. *Atmos. Chem. Phys.*, 9, 3095-3111.

Takegawa N., Miyazaki Y., Kondo Y., Komazaki Y., Miyakawa T., Jimenez J.L., Jayne J.T., Worsnop D.R., Allan J.D., and Weber R.J. (2005) Characterization of an Aerodyne Aerosol Mass Spectrometer (AMS): intercomparison with other aerosol instruments. *Aerosol Science & Technology*, 39, 760-770, doi: 10.1080/02786820500243404.

Takegawa N., Miyakawa T., Kawamura K., and Kondo Y. (2007) Contribution of selected dicarboxylic and omega-oxocarboxylic acids in ambient aerosol to the m/z 44 signal of an aerodyne aerosol mass spectrometer. *Aerosol Science and Technology*, 41, 418-437, doi: 10.1080/02786820701203215 (4), April. Available at http://www.tandfonline.com/doi/abs/10.1080/02786820701203215.

Takegawa N., Miyakawa T., Watanabe M., Kondo Y., Miyazaki Y., Han S., Zhao Y., van Pinxteren D., Bruggemann E., Gnauk T., Herrmann H., Xiao R., Deng Z., Hu M., Zhu T., and Zhang Y. (2009) Performance of an Aerodyne aerosol mass spectrometer (AMS) during intensive campaigns in China in the summer of 2006. *Aerosol Science and Technology*, 43, 189-204, doi: 10.1080/02786820802582251 (3), February 9. Available at http://dx.doi.org/10.1080/02786820802582251.

Tkacik D.S., Presto A.A., Donahue N.M., and Robinson A.L. (2012) Secondary organic aerosol formation from intermediate-volatility organic compounds: cyclic, linear, and branched alkanes. *Environ. Sci. Technol.*, 46, 8773-8781, doi: 10.1021/es301112c.

Travis C.C., Etnier E.L., and Meyer H.R. (1985) Health risks of residential wood heat. *Environ Manage*, 9, 209-215, doi: 10.1007%2fBF01867077 (3). Available at http://www.springerlink.com/content/kvh30u27872566w2/?MUD=MP.

Turlington J.M., Olson D.A., Stockburger L., and McDow S.R. (2010) Trueness, precision, and detectability for sampling and analysis of organic species in airborne particulate matter. *Analytical and Bioanalytical Chemistry*, 397, 2451-2463. Available at http://www.mendeley.com/research/trueness-precision-detectability-sampling-analysis-organic-species-airborne-particulate-matter-7/.

Turpin B.J. and Lim H.-J. (2001) Species contribution to $PM_{2.5}$ mass concentrations: revisiting common assumptions for estimating organic mass. *Aerosol Science and Technology*, 35, 602-610, (10), July.

Ulbrich I.M., Canagaratna M.R., Zhang Q., Worsnop D.R., and Jimenez J.L. (2009a) Interpretation of organic components from Positive Matrix Factorization of aerosol mass spectrometric data. *Atmos. Chem. Phys.*, 9, 2891-2918.

Ulbrich I.M., Lechner M., and Jimenez J.L. (2009b) AMS spectral database (unit mass resolution). Jimenez Group, University of Colorado, Boulder, CO. Available at http://cires.colorado.edu/jimenez-group/AMSsd/.

Volkamer R., Jimenez J.L., Martini F.S., Dzepina K., Zhang Q., Salcedo D., Molina L.T., Worsnop D.R., and Molina M.J. (2006) Secondary organic aerosol formation from anthropogenic air pollution: rapid and higher than expected. *Geophys. Res. Lett.*, 33, doi: 10.1029/2006GL026899 (L17811). Available at http://www.agu.org/pubs/crossref/2006/2006GL026899.shtml.

Wang Y., Hopke P.K., and Utell M.J. (2011) Urban-scale spatial-temporal variability of black carbon and winter residential wood combustion particles. *Aerosol and Air Quality Research*, 11, 473-481, doi: 10.4029/aaqr.2011.01.0005. Available at http://aaqr.org/VOL11_No5_October2011/1_AAQR-11-01-OA-0005_473-481.pdf.

Ward T. and Noonan C. (2008) Results of a residential indoor $PM_{2.5}$ sampling program before and after a woodstove changeout. *Indoor Air*, 18, 408-415, doi: 10.1111/j.1600-0668.2008.00541.x (5). Available at http://onlinelibrary.wiley.com/doi/10.1111/j.1600-0668.2008.00541.x/abstract.

Watson J.G., Barber P.W., Chang M.C.O., Chow J.C., Etyemezian V.R., Green M.C., Keislar R.E., Kuhns H.D., Mazzoleni C., Moosmüller H., Nicolic D., and Whitaker C.E. (2007) Southern Nevada air quality study. Final Report prepared for the U.S. Department of Transportation, Washington, DC, by Desert Research Institute, Reno, NV, FTA-NV-26-7003-2006.01, February.

Weber R., Orsini D., Duan Y., Baumann K., Kiang C.S., Chameides W., Lee Y.N., Brechtel F., Klotz P., Jongejan P., ten Brink H., Slanina J., Boring C.B., Genfa Z., Dasgupta P., Hering S., Stolzenburg M., Dutcher D.D., Edgerton E., Hartsell B., Solomon P., and Tanner R. (2003) Intercomparison of near real time monitors of $PM_{2.5}$ nitrate and sulfate

at the US Environmental Protection Agency Atlanta Supersite. *Journal of Geophysical Research-Atmospheres*, 108, 8421, doi:8410.1029/2001JD001220, (D7), Jan 29. Available at <Go to ISI>://000182898300001.

Weber R.J., Orsini D., Daun Y., Lee Y.N., Klotz P.J., and Brechtel F. (2001) A particle-into-liquid collector for rapid measurement of aerosol bulk chemical composition. *Aerosol Science and Technology*, 35, 718-727, (3), Sep. Available at <Go to ISI>://000171020000003.

Weimer S., Alfarra M.R., Schreiber D., Mohr M., Prévôt A.S.H., and Baltensperger U. (2008) Organic aerosol mass spectral signatures from wood-burning emissions: influence of burning conditions and wood type. *Journal of Geophysical Research (Atmospheres)*, 113, D10304, (doi: 10.1029/2007JD009309).

Weingartner E., Burtscher H., and Baltensperger U. (1997) Hygroscopic properties of carbon and diesel soot particles. *Atmos. Environ.*, 31, 2311-2327, (15).

White W.H. and Roberts P.T. (1977) On the nature and origin of visibility-reducing aerosols in the Los Angeles Air Basin. *Atmos. Environ.*, 11, 803-812.

Williams B.J., Goldstein A.H., Kreisberg N.M., Hering S.V., Worsnop D.R., Ulbrich I.M., Docherty K.S., and Jimenez J.L. (2010) Major components of atmospheric organic aerosol in southern California as determined by hourly measurements of source marker compounds. *Atmos. Chem. Phys.*, 10, 11577-11603, doi: 10.5194/acp-10-11577-2010.

Wu Y.-C. and Batterman S.A. (2006) Proximity of schools in Detroit, Michigan to automobile and truck traffic. *Journal of Exposure Science and Environmental Epidemiology*, 16, 457-470, doi: 10.1038/sj.jes.7500484, April 19.

Xie M., Barsanti K.C., Hannigan M.P., Dutton S.J., and Vedal S. (2013) Positive matrix factorization of $PM_{2.5}$: eliminating the effects of gas/particle partitioning of semivolatile organic compounds. *Atmos. Chem. Phys.*, 13, 7381-7393, doi: 10.5194/acp-13-7381-2013 (15). Available at http://www.atmos-chem-phys.net/13/7381/2013/.

Zhang Q., Stanier C.O., Canagaratna M.R., Jayne J.T., Worsnop D.R., Pandis S.N., and Jimenez J.L. (2004a) Insights into the chemistry of new particle formation and growth events in Pittsburgh based on aerosol mass spectrometry. *Environ. Sci. Technol.*, 38, 4797-4809, (18), Sep 15.

Zhang Q., Alfarra M.R., Worsnop D.R., Allan J.D., Coe H., Canagaratna M.R., and Jimenez J.L. (2005a) Deconvolution and quantification of hydrocarbon-like and oxygenated organic aerosols based on aerosol mass spectrometry. *Environ. Sci. Technol.*, 39, 4938-4952, doi: 10.1021/es048568l.

Zhang Q., Worsnop D.R., Canagaratna M.R., and Jimenez J.L. (2005b) Hydrocarbon-like and oxygenated organic aerosols in Pittsburgh: insights into sources and processes of organic aerosols. *Atmos. Chem. Phys.*, 5, 3289-3311.

Zhang Q., Jimenez J.L., Canagaratna M.R., Ulbrich I.M., Ng N.L., Worsnop D.R., and Sun Y. (2011) Understanding atmospheric organic aerosols via factor analysis of aerosol mass spectrometry: a review. *Anal. Bioanal. Chem.*, doi: 10.1007/s00216-011-5355-y (October).

Zhang X., Smith K.A., Worsnop D.R., Jimenez J.L., Jayne J.T., Kolb C.E., Morris J., and Davido P. (2004b) Numerical characterization of particle beam collimation: part II integrated aerodynamic-lens-nozzle system. *Aerosol Science and Technology*, 38, 619-638, doi: 10.1080/02786820490479833. Available at http://128.138.136.5/jimenez/Papers/XZhang_Lens_Part2.pdf.

Zhang X., Hecobian A., Zheng M., Frank N.H., and Weber R.J. (2010) Biomass burning impact on $PM_{2.5}$ over the southeastern US during 2007: integrating chemically speciated FRM filter measurements, MODIS fire counts and PMF analysis. *Atmos. Chem. Phys.*, 10, 6839-6853, doi: 10.5194/acp-10-6839-2010. Available at www.atmos-chem-phys.net/10/6839/2010/.

Zheng M., Cass G.R., Schauer J.J., and Edgerton E.S. (2002) Source apportionment of $PM_{2.5}$ in the southeastern United States using solvent-extractable organic compounds as tracers. *Environ. Sci. Technol.*, 36, 2361-2371.

Zheng M., Cass G.R., Ke L., Wang F., Schauer J.J., Edgerton E.S., and Russell A.G. (2007) Source apportionment of daily fine particulate matter at Jefferson Street, Atlanta, GA, during summer and winter. *J. Air and Waste Manag. Assoc.*, 57, 228-242, (2), February.

Zhu Y., Hinds W.C., Kim S., Shen S., and Sioutas C. (2002a) Study of ultrafine particles near a major highway with heavy-duty diesel traffic. *Atmos. Environ.*, 36, 4323-4335, (27), 2002/9. Available at http://www.sciencedirect.com/science/article/B6VH3-46MBTBP-5/2/1cfd97e9d1d1d605fbdcd5844cc7c4d6.

Zhu Y.F., Hinds W.C., Kim S., and Sioutas C. (2002b) Concentration and size distribution of ultrafine particles near a major highway. *J. Air Waste Manage.*, 52, 1032-1042, (9), September.

Zielinska B., Sagebiel J., Arnott W.P., Rogers C.F., Kelly K.E., Wagner D.A., Lighty J.S., Sarofim A.F., and Palmer G. (2004a) Phase and size distribution of polycyclic aromatic hydrocarbons in diesel and gasoline vehicle emissions. *Environ. Sci. Technol.*, 38, 2557-2567, (9), May 1.

Zielinska B., Sagebiel J., McDonald J.D., Whitney K., and Lawson D.R. (2004b) Emission rates and comparative chemical composition from selected in-use diesel and gasoline-fueled vehicles. *J. Air Waste Manage.*, 54, 1138-1150.

Appendix A
HR-AMS Data Processing Steps

Mass calibrations against background *m/z* were done using the "SQ_mz_cal" panel in Squirrel. Fragments due to background gases like Ar, O_2 and N_2, plus fragments from tungsten (atomic symbol W) or phthalates which are found in the AMS, provide a stable set of background ions to use to ensure that the peaks from the mass spectrometer are assigned to the correct *m/z*. In the calibration panel, we select fragments that are from the background species that are evident when the AMS is operating in "closed" mode, i.e., when there is no aerosol being analyzed by the MS. Usually at least four peaks are used, including one peak at a higher *m/z* above 90. Here, we used CH+ (*m/z* 13), O2+ (m/z 32), Ar (*m/z* 40), C5H2+ (*m/z* 50), and $C8H5O_3$+ (*m/*z 149), and tested the fits of all the other available fitting fragments as well. We first test the fit on individual runs (i.e., 2-minute averages); Figure A-1 shows the fit for an example run (#30559). Once fits are reasonable for a handful of example runs, we next process all runs. Figure A-2 shows a summary of the fit between DAQ and our manual calibration; nearly all runs have a fit ratio (DAQ/Squirrel) within 0.05, indicating a stable calibration. Evident in the figure are some runs where the fits are well beyond +/- 0.05. These runs were "blacklisted" and excluded from any analysis, as the calibrations were insufficient.

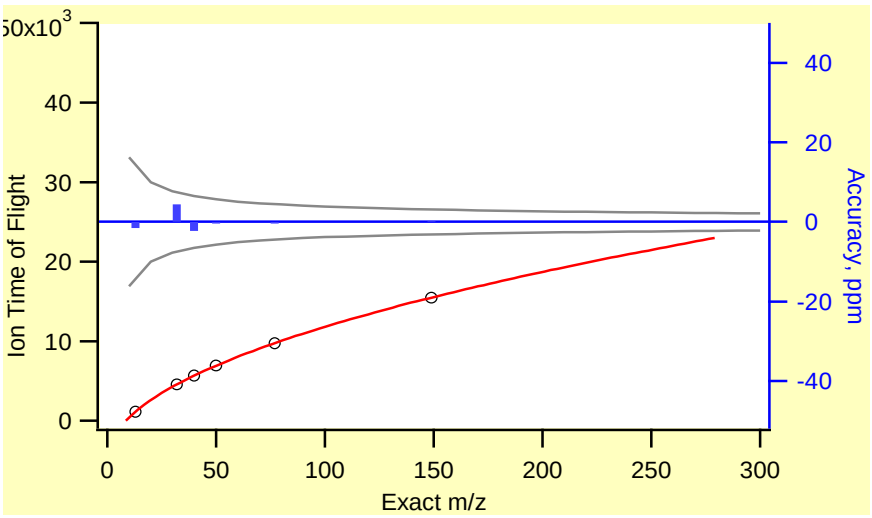

a)

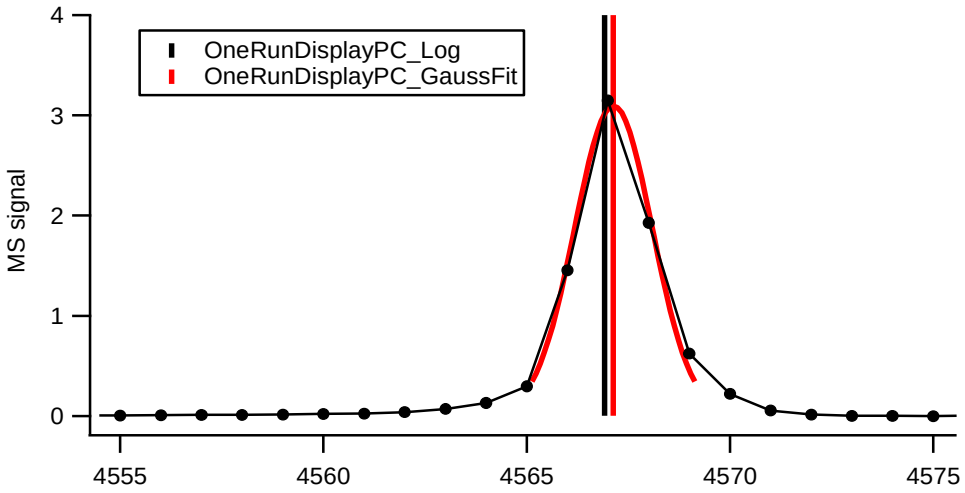

b)

Figure A-1. a) Calibration for example run using CH+ (*m/z* 13), O2+ (m/z 32), Ar (*m/z* 40), C5H2+ (*m/z* 50), and $C8H5O_3$+ (*m/z* 149); the red line shows the ion time of flight fit so that each *m/z* can be correctly found; the accuracy is the comparison of this post-processing fit to the in-field calibrations; and b) raw data (black) for O2+ ion and Gaussian peak shape fits (red). The goal is to have the red line in the middle of the red Gaussian fit; the red and black vertical lines may not necessarily line up, depending on the initial m/z calibration used in the field and DAQ.

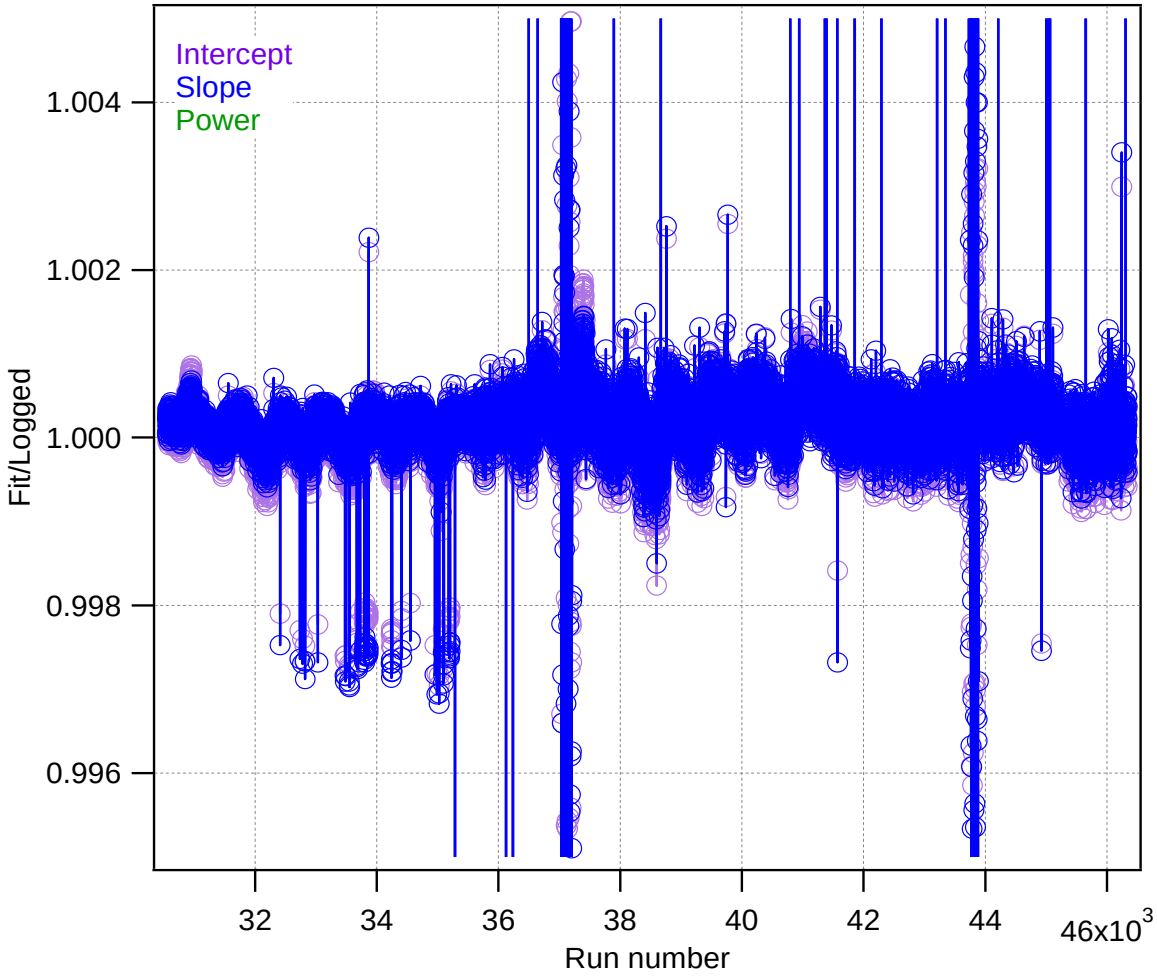

Figure A-2. Ratio of DAQ/Squirrel calibration by run number. Values beyond +/- 0.005 (0.5%) were excluded from analysis.

To correctly quantify each *m/z* peak area, the baseline of the MS signal during open and closed modes needs to be determined. As part of the post-processing, the baseline was checked for 10 v-mode runs every third day, to ensure there was no sudden change in the baseline during the monitoring campaign. We found that the baseline did not change noticeably during the study. As seen in Figure A-3, the baseline was large for the *m/z* originating from gaseous species, such as *m/z* 15 and 28 from N_2, which is typical. The correction for the baseline was effective, as indicated by the green line centered on 0, which is the difference between the open and closed modes and after baseline correction.

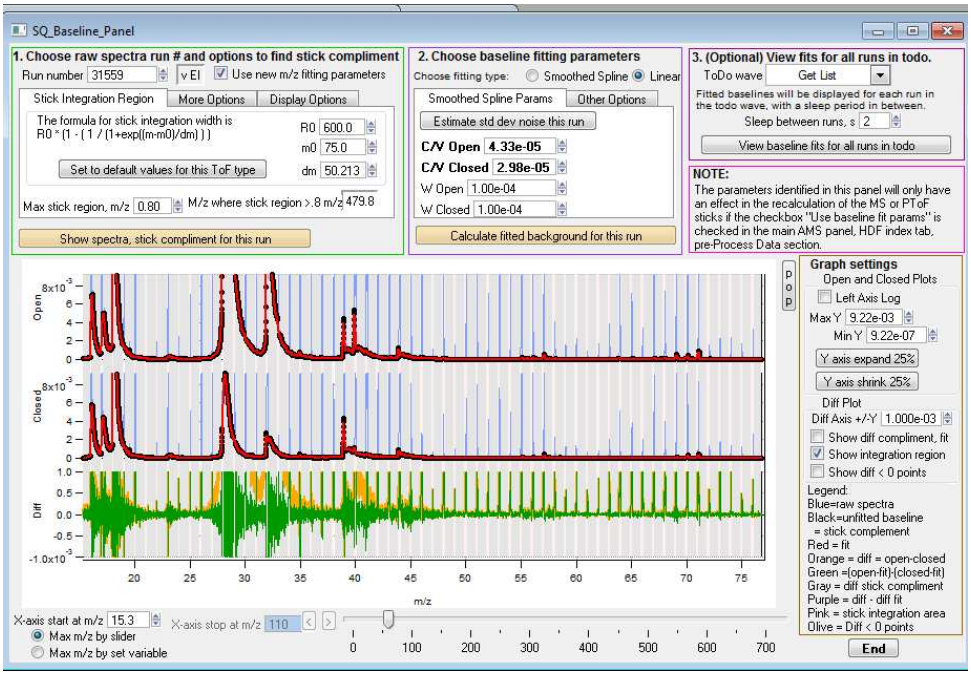

Figure A-3. Baseline diagnostic panel for example run. The red line is the baseline fit, which should follow the black line, which is the measured baseline. The alternating grey and pink areas are the areas where there is peak integration (pink) and no integration (grey) The blue lines are signal at given *m/z*. The orange and green show the difference between the open and closed mass spectra without baseline correction (orange) and with baseline correction (green); the green should be centered about 0 to indicate correct baseline subtraction.

A standard fragmentation table (frag table), as described in Allen et al. (Allan et al., 2004), was used to account for interference of gaseous species such as nitrogen and oxygen, and to ensure correct allocation of the UMR signal among aerosol species such as nitrate, ammonium, and organics. For example, the signal at *m/z* 64 could be from SO_2^+ ion (from a sulfate aerosol) or from organic fragments (e.g., $C_5H_4^+$). At this *m/z* the organic fraction is calculated based on the signal at the *m/*z where an alkyl group (CH_2^+) is subtracted or added to the *m/z* 64 ion (in this case *m/z* 50 and 78), since organic aerosol are usually comprised of long chain hydrocarbons and the vaporization/ionization scheme used in the AMS results in a series of C_nH_{2n+1} fragments. Since inorganic species like sulfate, nitrate and ammonium have characteristic fragmentation patterns, and only occur at a handful of *m/*z, these patterns can be taken into account and the mass at each *m/*z from other species, namely organic aerosol, can be

determined for the *m/*z that have both an inorganic and organic component. Other *m/z* may have only organic signals, so the full signal is assigned to organics. As part of the fragmentation pattern, there is a correction for CO_2 gas. Often this correction is fairly stable throughout a field study, though may need to be modified in chamber or laboratory experiments where CO_2 is produced at levels greater than is typical in the ambient atmosphere. We used a default CO_2 gas concentration of 370 ppm. We can examine if this assumed concentration is correct by comparing the mass at *m/z* 43, which is entirely organic, and *m/z* 44; if the CO_2 gas correction is not correct, there will be a bias evident, i.e., the data will not trend through the origin. As seen in Figure A-4, the data do trend through the origin, so no change to the CO_2 correction was made. Another check of the corrections and frag table is to examine the measured ammonium compared to the amount of ammonium predicted by the measured sulfate and nitrate, assuming all sulfate and nitrate are associated with ammonium (i.e., NH_4NO_3 and $(NH_4)_2SO_4$). As seen in Figure A-5, predicted and measured ammonium agree extremely well, with the exception of one outlier, suggesting the corrections and frag table settings are correct.

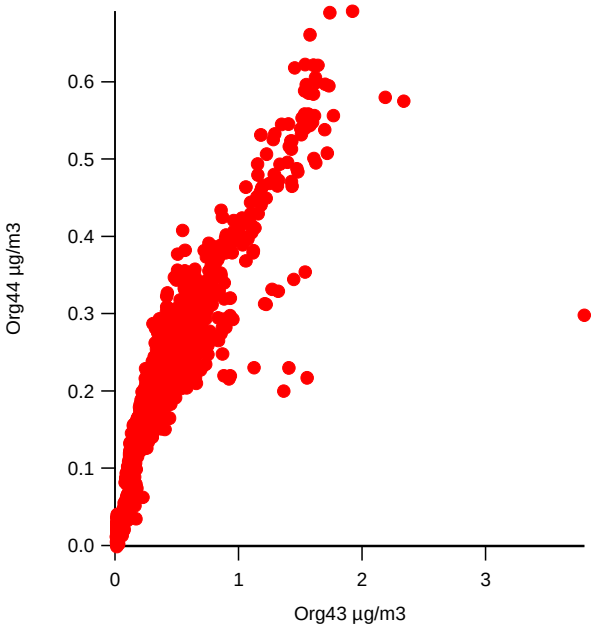

a)

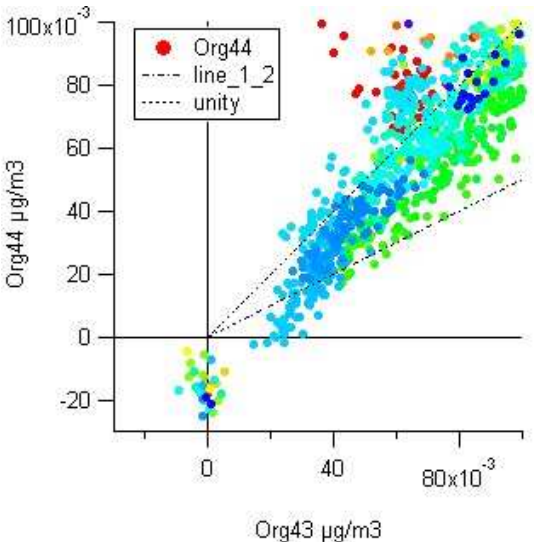

b)

Figure A-4. Concentrations of *m/z* 43 and 44 for a) our study, and b) example data showing an incorrect offset for CO_2 (from http://cires.colorado.edu/jimenez-group/wiki/index.php/Field_Data_Analysis_Guide)

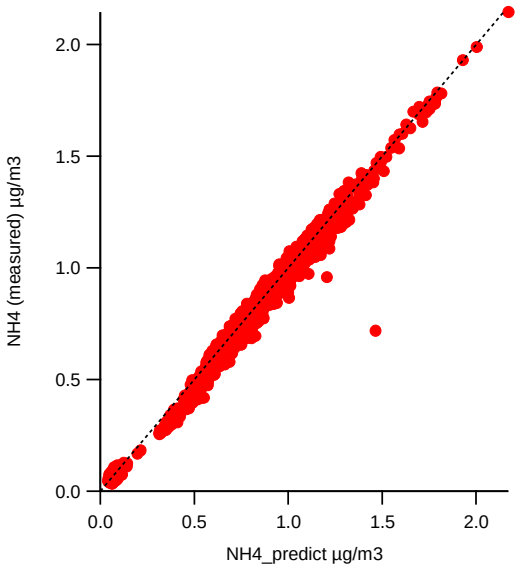

Figure A-5. Measured ammonium compared to predicted ammonium based on sulfate and nitrate concentrations and assuming neutralization of sulfate and nitrate by ammonium. The line represents the 1:1 line.

Particle size data were processed using the "ptof corrections" tab available in Squirrel. When in PToF mode, the aerosol beam is chopped, and particles that make it through the chopper enter a particle time of flight (PToF) region, where larger particles take longer to travel through than smaller particles. The time it takes to travel through the PToF region for selected size particles is determined with particles of known diameter, as described earlier. As part of the post-processing, a baseline of the time it takes before particles make it through the PToF region needs to be determined. To do this we examine individual runs to find the time it takes before aerosol signal is found, and the time at which there are no more particles being transmitted through the AMS. Before particles make it through the PToF region, we are only measuring gaseous species like CO_2. Figure A-6 shows the PToF corrections dashboard. Here we select a series of individual runs and high mass *m/z* such as *m/z* 57, 43 or 44, and examine the time it takes in the PToF chamber when we typically see signal. In our dataset, particles traveled through the PToF region in between 1000 and 4500 µs, consistent with calibration values performed in the field.

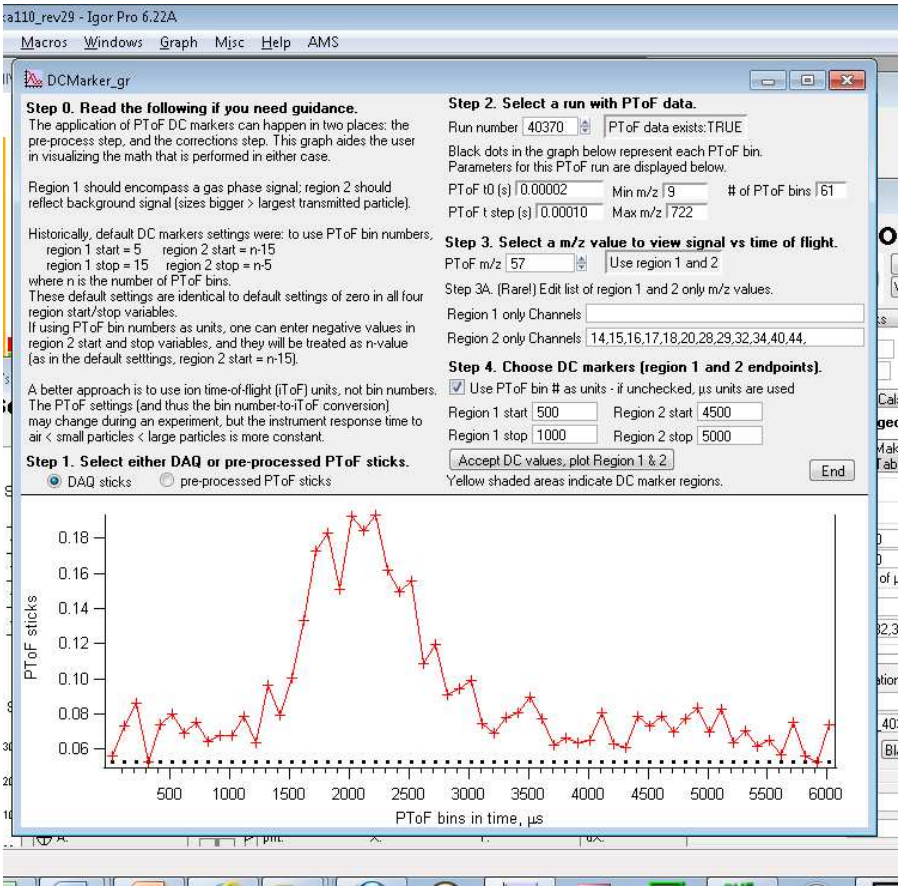

Figure A-6. PToF corrections dashboard. The plot is showing the amount of signal at *m/z* 57 by time in PToF chamber (µs) for an example run 40370.

High resolution (HR) data were processed with the "PIKA" module provided by CU Boulder and Aerodyne, version 1.10, following procedures laid out in the HR data analysis guide wiki (http://cires.colorado.edu/jimenez-group/wiki/index.php/High_Resolution_ToF-AMS_Analysis_Guide), conceptually shown in Figure A-7. Via PIKA, individual unit mass resolution (UMR) m/z can be deconvolved into ions of higher resolution, e.g., from *m/z* 43 to the ions $C_3H_7^+$ (mass 43.05478) and $C_2H_3O^+$ (mass 43.01839), using a Gaussian fit for each HR ion peak width and shape. Only ions up to *m/z* 100 were determined, since above this threshold it is difficult to separate out ions within a given UMR *m/z* since the number of ions per m/z is much higher than for *m/z* less than 100. Since more than 95% of the organic signal is typically included in ions less than *m/z* 100, this has little effect on determining OM via HR ions. In

PIKA, m/z calibration and baseline from Squirrel were used, and were well fit, as described above. Next, peak width and shape were determined. Similar to m/z calibration, the Gaussian fits for selected calibration ions were generated to develop a relationship between peak width and m/z. CH^+, OH^+, H_2O^+, C_2H^+, N_2^+, O_2^+, Ar^+, SO^+, $C_4H_2^+$, SO^+, and $C_6H_5^+$ gave the best fitting statistics for peak width. The summary of the fit across the entire dataset for V mode for a subset of these calibration fragments is shown in Figure A-8. The time series was inspected to identify any problematic runs, which may occur when usually-negligible peaks are abundant and overwhelm the signal of neighboring ions, or under fast data acquisition mode (i.e., less than 1 minute), of which the latter is not applicable here; no runs were excluded with this inspection. Figure A-8b shows a time series for the peak width using one fitting fragment, O_2^+, for a subset of the study. Next, peak shape was determined using O_2^+ and CH^+. The goal is to use the fitting ions to develop a smooth peak shape, which PIKA will then use as the shape for all ion peaks. Figure A-9 shows the peak shape using the five fitting fragments, i.e., an overlay of each fragments' normalized peak shape. While the tails are slightly larger than the perfect Gaussian fit, this is not unusual, and the tails are smooth, indicating a good shape.

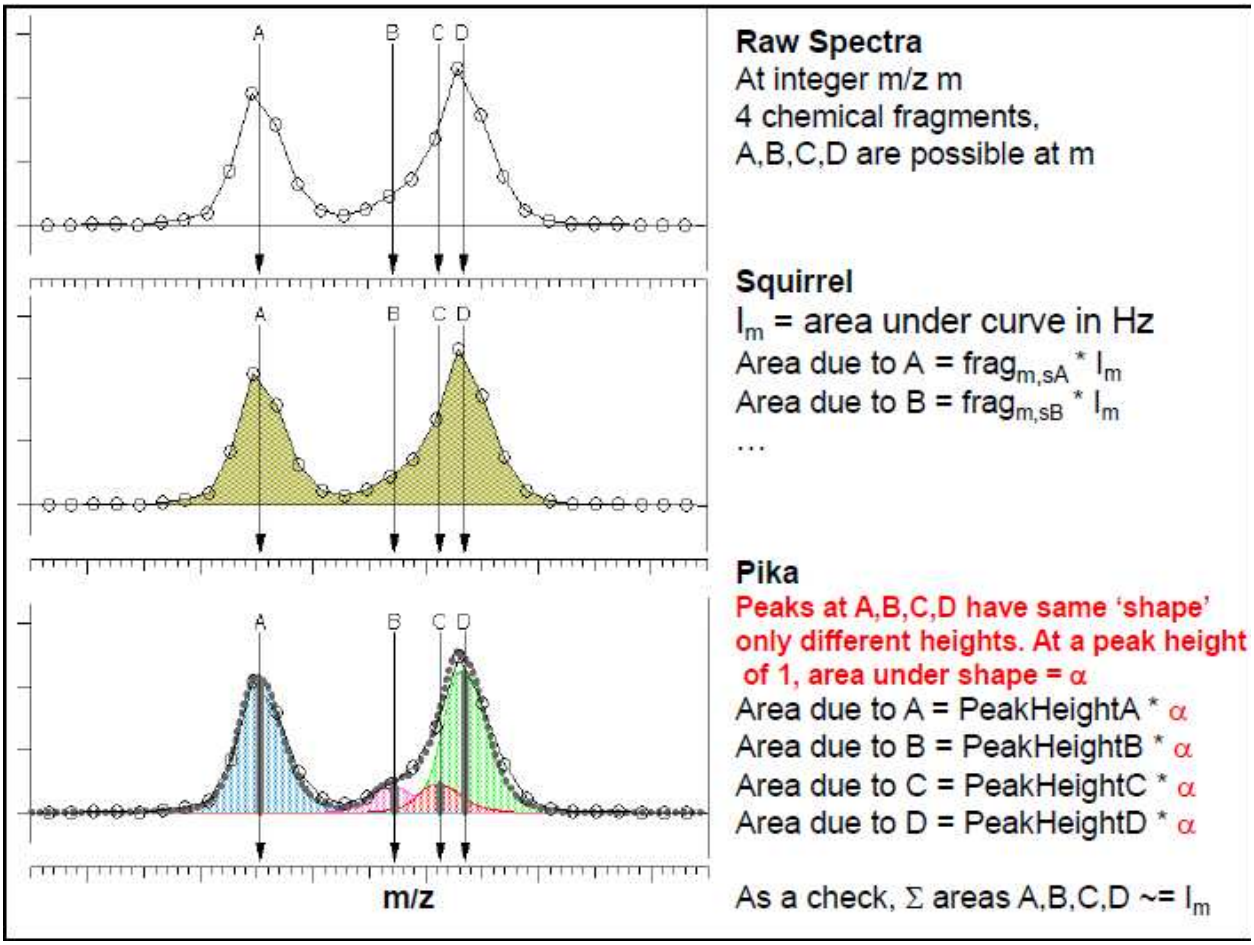

Figure A-7. Example process of identifying UMR m/z in Squirrel, and then breaking down each UMR m/z into individual HR ions. From "Squirrel and Pika Analysis Comparison", Donna Sueper, 2010 AMS User's Meeting; http://cires.colorado.edu/jimenez-group/UsrMtgs/UsersMtg11/2010UsersMtgSquirrelPikaCompar.pdf.

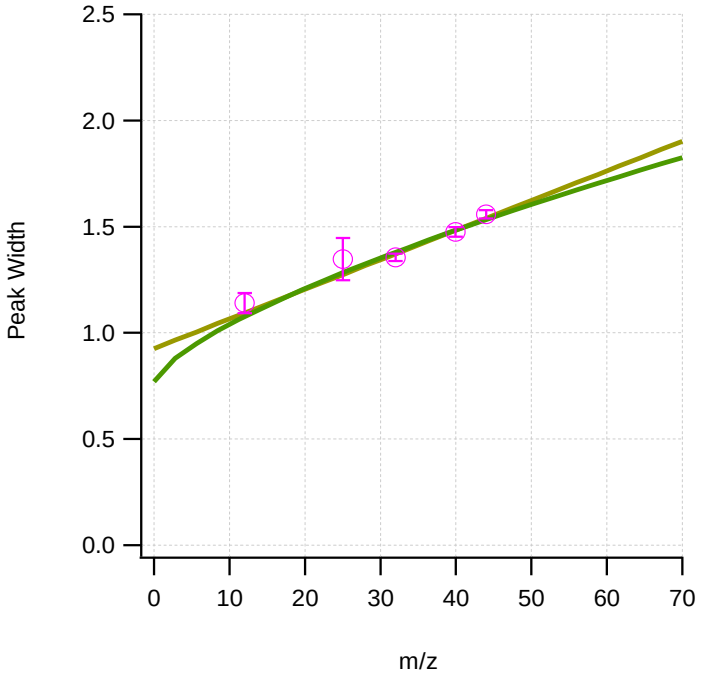

a)

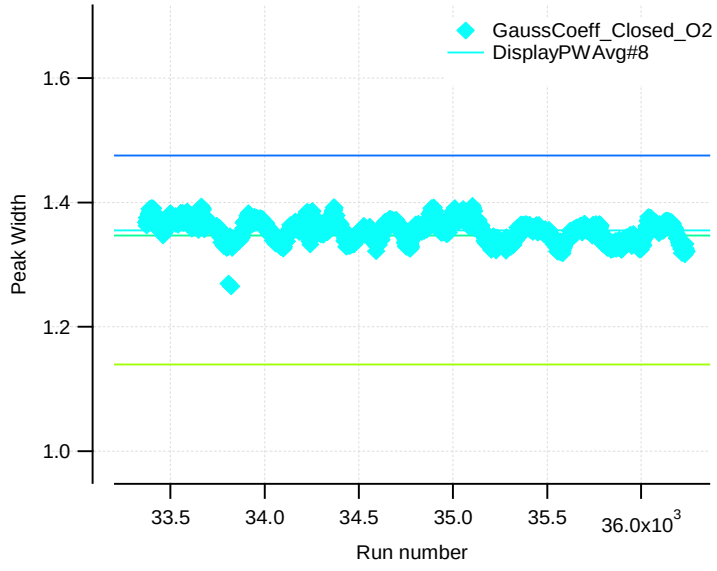

b)

Figure A-8. a) Peak width versus m/z for selected best fit fragments for entire data set in V mode, along with linear fit (yellow/green) and power fit (green); a linear fit was used, and the error bars indicate the standard deviation; b) time series of peak width fit for O_2^+ fitting fragment for example 4 days (January 10-13).

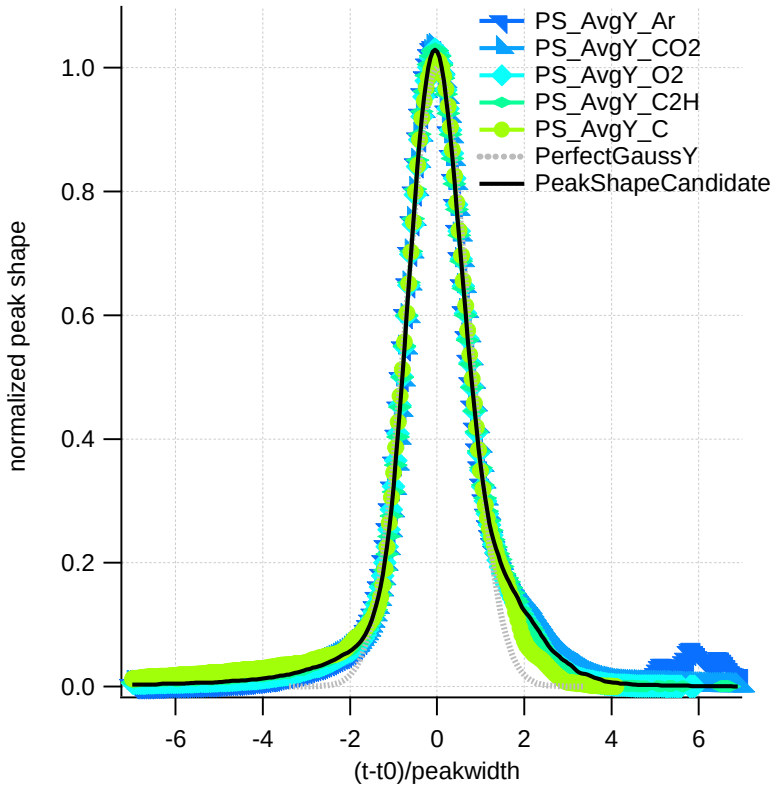

Figure A-9. Peak shape of fitting fragments (Ar^+, CO_2^+, O_2^+, C_2H^+, C^+) for V mode data.

Next, the ion fits for key m/z were examined visually for a handful of samples, i.e., two samples each day, for the difference between the open and closed signals. The key *m/z* included: 28, 32, 39, 43, 44, 55, 57, 60, 73, 80, 81, 90, 95, 96, though other *m/z* were also examined. The default list of fitting ions was used initially, with only a few modifications. The default list includes the typical HR ions found in the ambient environment; adding additional ions may help improve the fits of each series of peaks, but these additional ions may not actually be present in detectable quantifies, so including them in the fitting is often not appropriate. Peak shape was assessed by examining the left side of *m/z* 48 and 64, which do not have any ions to their left, and by examining the right side of *m/z* 41, which has no ion to the right. The peak shape appeared to be a good fit for these three examples (two of which are shown in Figure A-10). For the key *m/z*, the residual between the fit peaks and the signal in the open-closed spectrum were

examined, with the goal of +/- 5% for each fitted peak. Following recommendations of best practices for HR analysis, a conservative approach was used, where an ion was included in the fit only if the residuals were greatly improved by its addition. Organic nitrogen species often have little or no signal, but their inclusion can improve residuals. Two examples showing the improvement in fit when including these trace ions are shown in Figures A-11 and A-12, for *m/z* 59 and 72 when $C_3H_9N^+$ and $C_3H_6NO^+$ are included and excluded, respectively. The inclusion of these ions improves residuals, and visual inspection over multiple runs indicates this signal is real, so these ions were included in the fits for all runs.

The fits over all runs and m/z were assessed by examining the time series and mass spectra of individual "families" of HR ions, e.g., family CH are all ions with C and H, family CHO are all ions with C, H and O, etc. Examples of mass spectra and time series are shown in figures A-13 and A-14. The mass spectra by family is consistent with what was seen with UMR data, and shows a relatively high amount of family CH, again consistent with less oxidized aerosol at the monitoring site location during the winter. In addition, the HR and UMR mass for OM by sample was compared, in order to understand if the two methods were consistent. As shown in Figure A-15, there was excellent agreement between HR- and UMR-resolved OM. Lastly, elemental ratios were calculated for OM, using the W mode data for samples where OM was greater than 0.3 $\mu g/m^3$ and the ratios specified in Aiken et al 2007(Aiken et al., 2007).

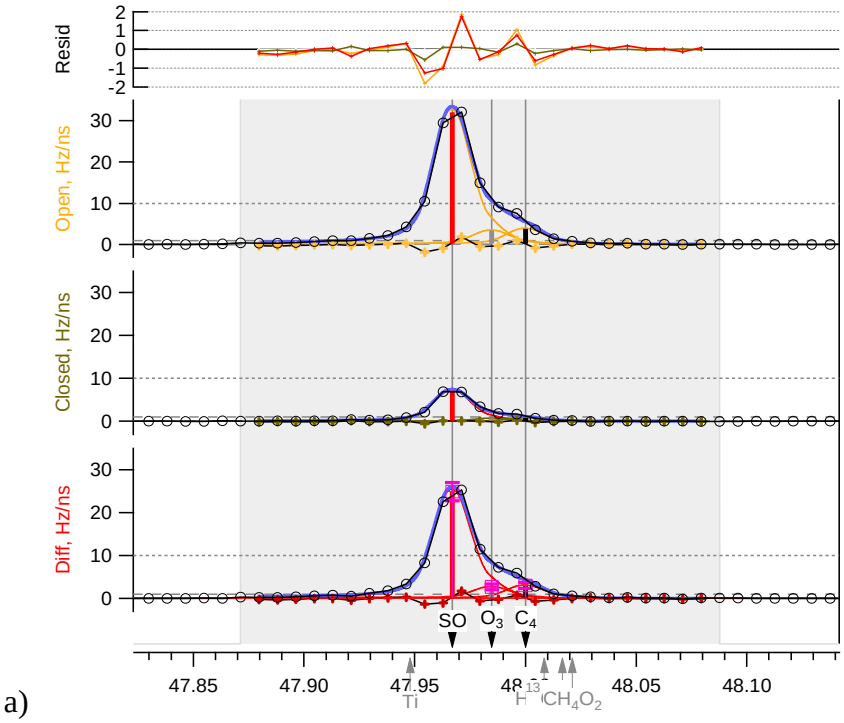

a)

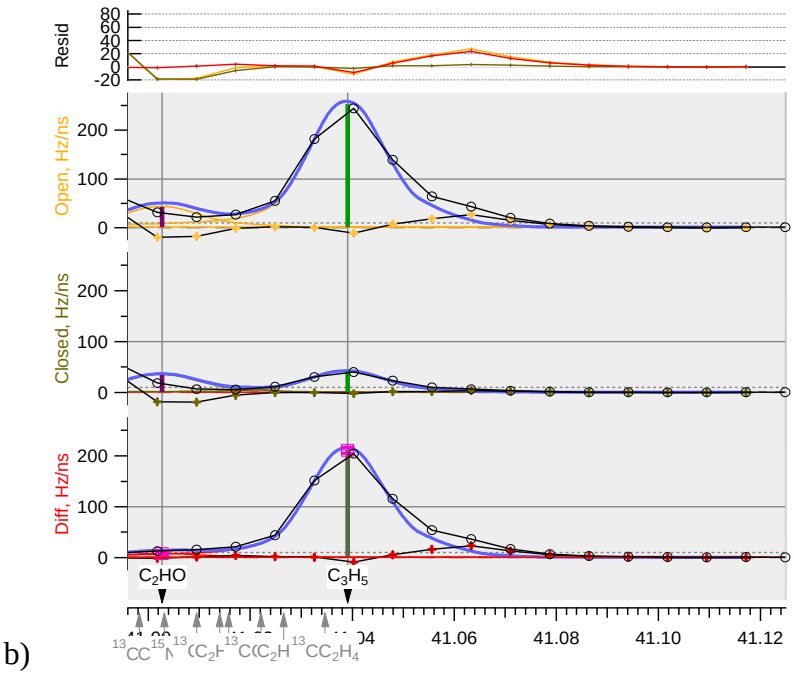

b)

Figure A-10. Peak fitting of open, closed and open-closed spectrum for example run of a) *m/z* 48 and b) *m/z* 41. The green or pink vertical lines indicate the exact mass of the ion along the x-axis, the black line and circles show the raw data, the orange line the open spectrum fits and residuals, the brown line the closed spectrum fits and residuals, and the pink lines the difference spectrum fits and residuals; black ions (e.g., $C_3H_5^+$) indicate fit ions, and the grey ions indicate ions that were not included in the fit.

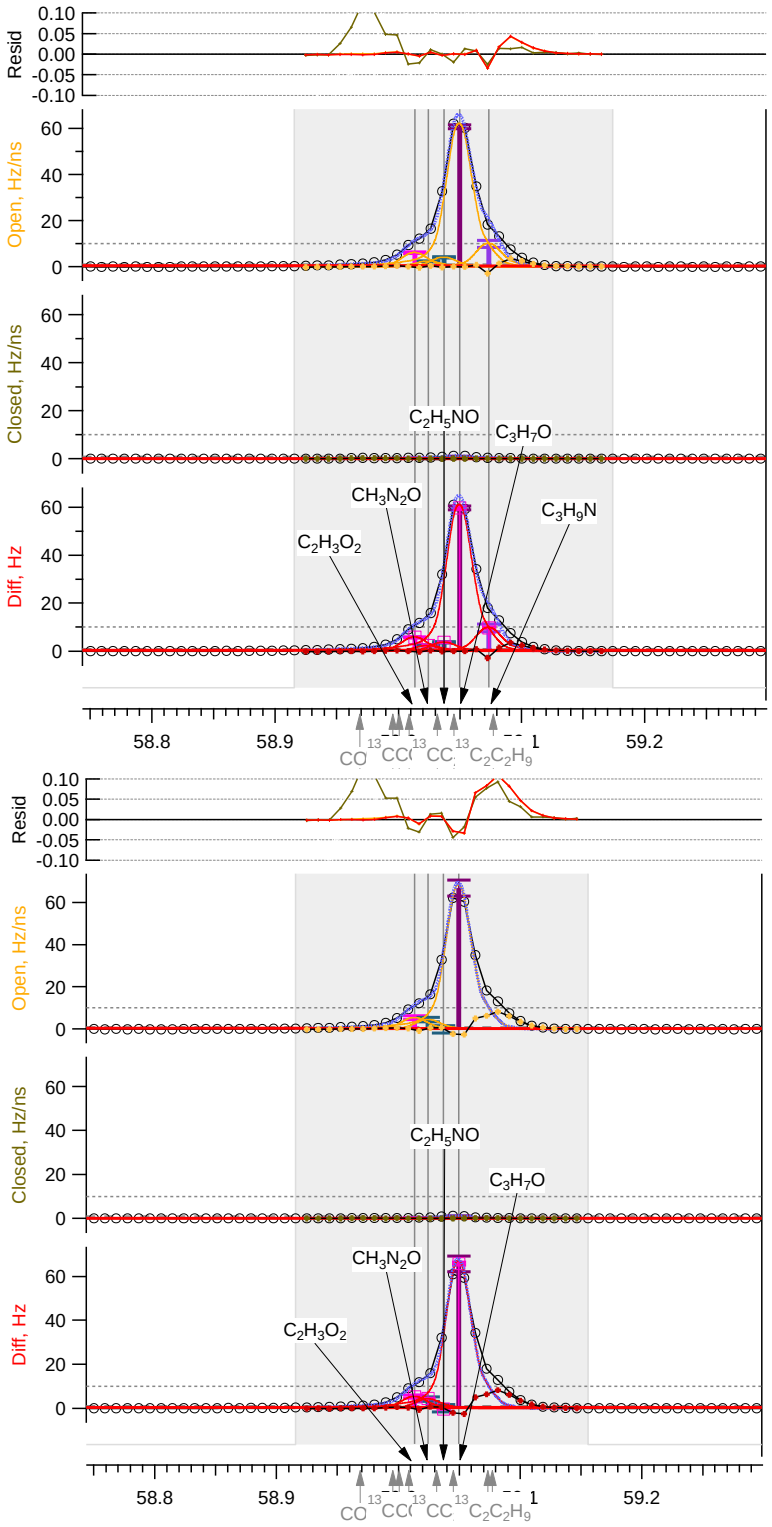

Figure A-11. Fits for example run for *m/z* 59 with $C_3H_3N^+$ included (top) and excluded (bottom).

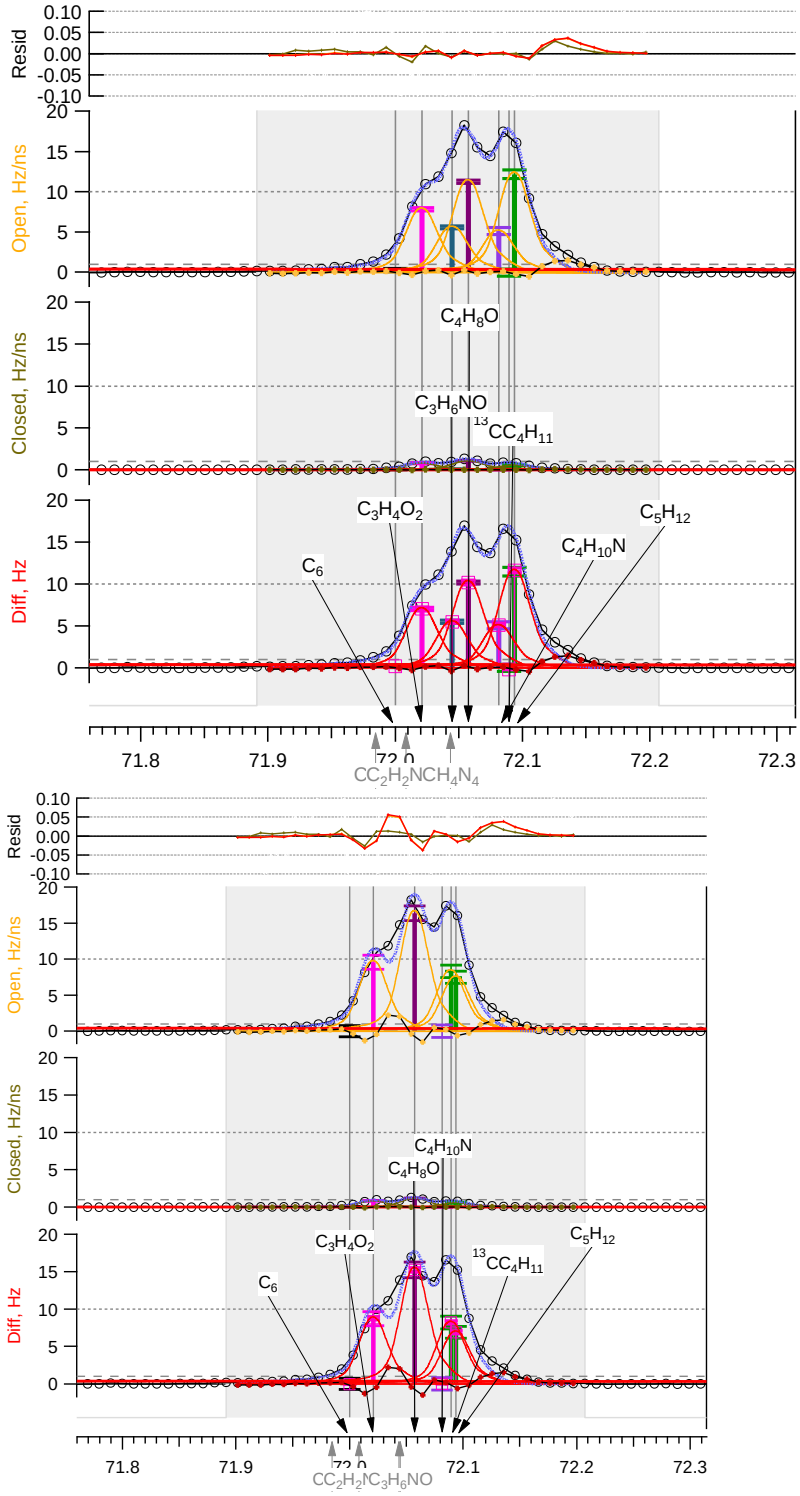

Figure A-12. Fits for example run for *m/z* 72 with $C_3H_6NO^+$ included (top) and excluded (bottom).

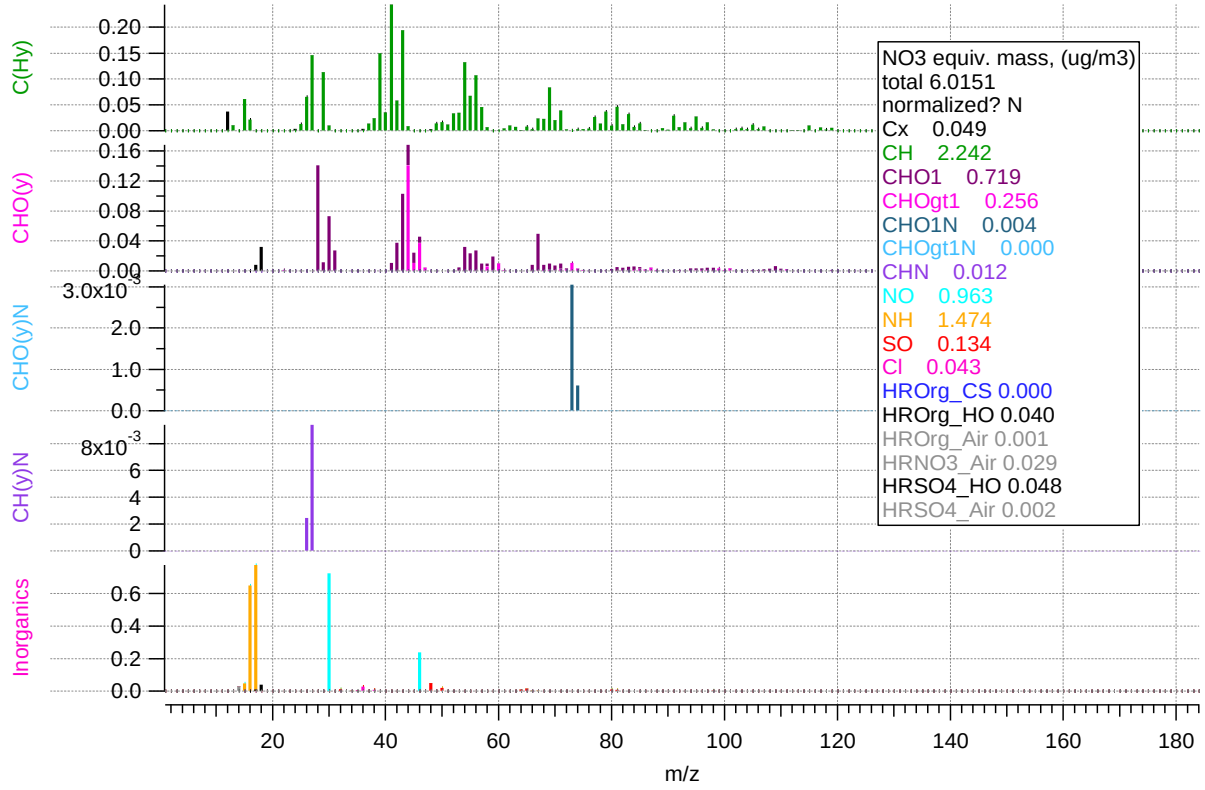

Figure A-13. Mass spectra by HR family for entire study; note y-axis differences for each graph, particularly that organic nitrogen species are more than an order of magnitude lower than the typically more abundance CH and CHO families.

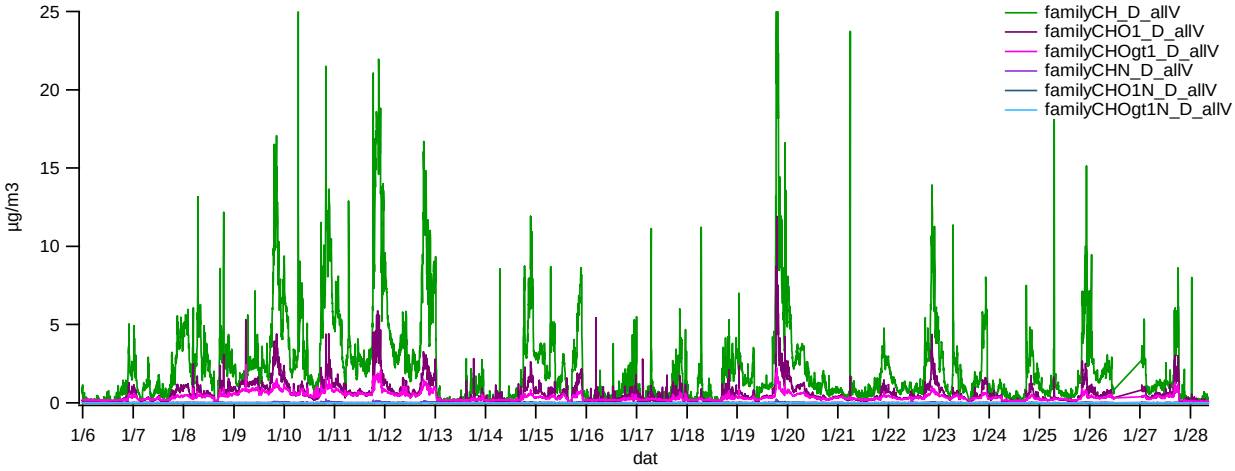

Figure A-14. Time series of HR organic families.

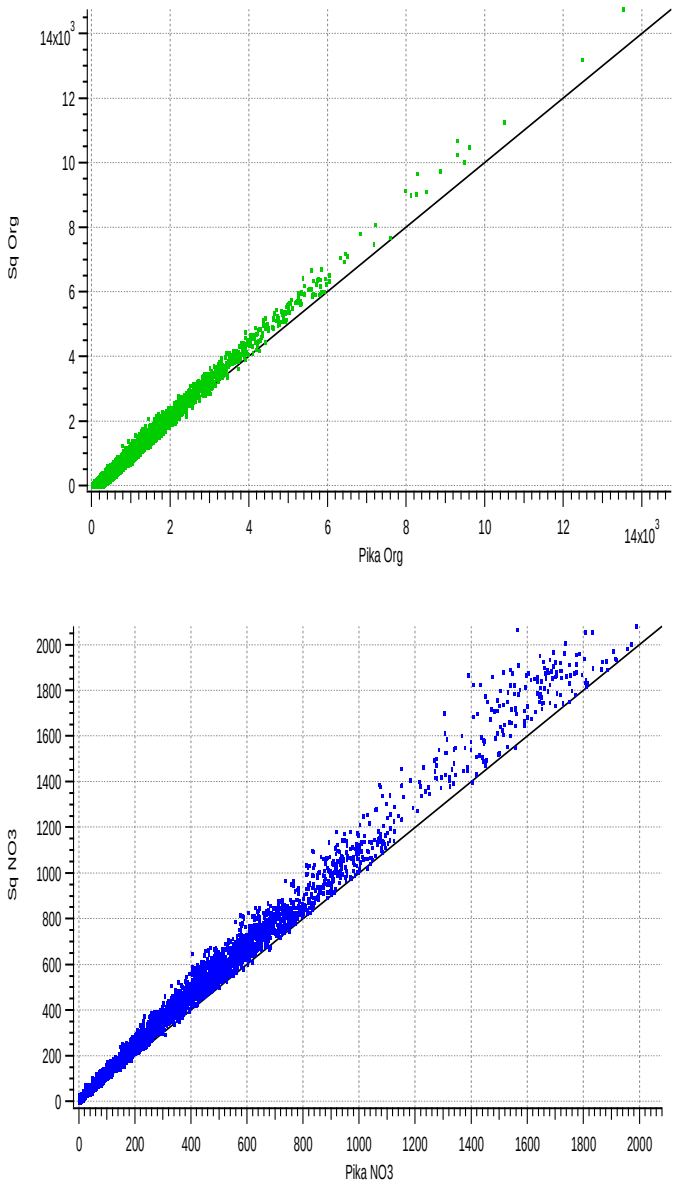

Figure A-15. Comparison of UMR (y-axis) and HR (x-axis) concentrations for a) OM and b) nitrate.

Appendix B
PAH Analyses

PAH data were collected via three methods: 1) from the HR-AMS, at 2-minute resolution; 2) from the PAS instrument, at 5-minute resolution, starting January 15, 2008; and 3) from GC-MS analysis of extracts from quartz fiber filters collected at various times during January 2008. Table B-1 summarizes these measurements. Each method measures PAH in a different manner. With the HR-AMS, total PAH are calculated based on work in Dzepina et al., 2007, who used a number of PAH standards to develop a fragmentation table for calculating PAH, while comparing the mass spectra to NIST standards. In the PAS, aerosol are exposed to UV light, causing PAH on the aerosol surface to photoemit electrons, which are translated into a concentration based on manufacturer specifications. Quartz fiber filters were taken and analyzed by GC-MS as described in Section 2.6 and elsewhere (Olson et al., 2012).

In Mexico City, Dzepina et al. report a range of agreement between the three methods used here. They report an r^2 of 0.39 between PPAH and APAH, but better agreement between APAH and FPAH for specific PAH types, e.g, PAH with molecular weight (MW) 226 + 228 had an r^2=0.99, and for MW 276+278 an r^2=0.80.

Here, we compare how PPAH, APAH, and individual FPAHs compare among each other and with BC and AMS PMF factors. First, using the continuous measurements for the period between January 15th and January 28th, when PPAH and APAH measurements were both available. PPAH had a similar pattern to BC (r^2=0.86), while APAH was more similar to OM (r^2=0.79). Figure B-1 shows a time series of these measurements, and scatter plots of the PAH measurements versus BC and OM. As shown in Figure B-2, there is modest agreement between PPAH and APAH measurements (r^2=0.49), which was better than in Mexico City (Dzepina et al., 2007). Figure B-3 and Tables B-1 and B-2 show scatter plots and correlations of these two PAH measurements with AMS PMF factors as well as BC and OM. PPAH is extremely well

correlated with BC, but not with other measurements, while APAH has a modest correlation (r=0.62) with BBOA. Somewhat surprisingly, neither PAH measurement has a good correlation with HOA, despite PAH being from primary emissions, similar to in concept what HOA represents. While PPAH is tightly correlated with BC, also a primary emission, PPAH appears to be a good measurement of true primary emissions, as denoted by BC, while APAH may have some influence from secondary products.

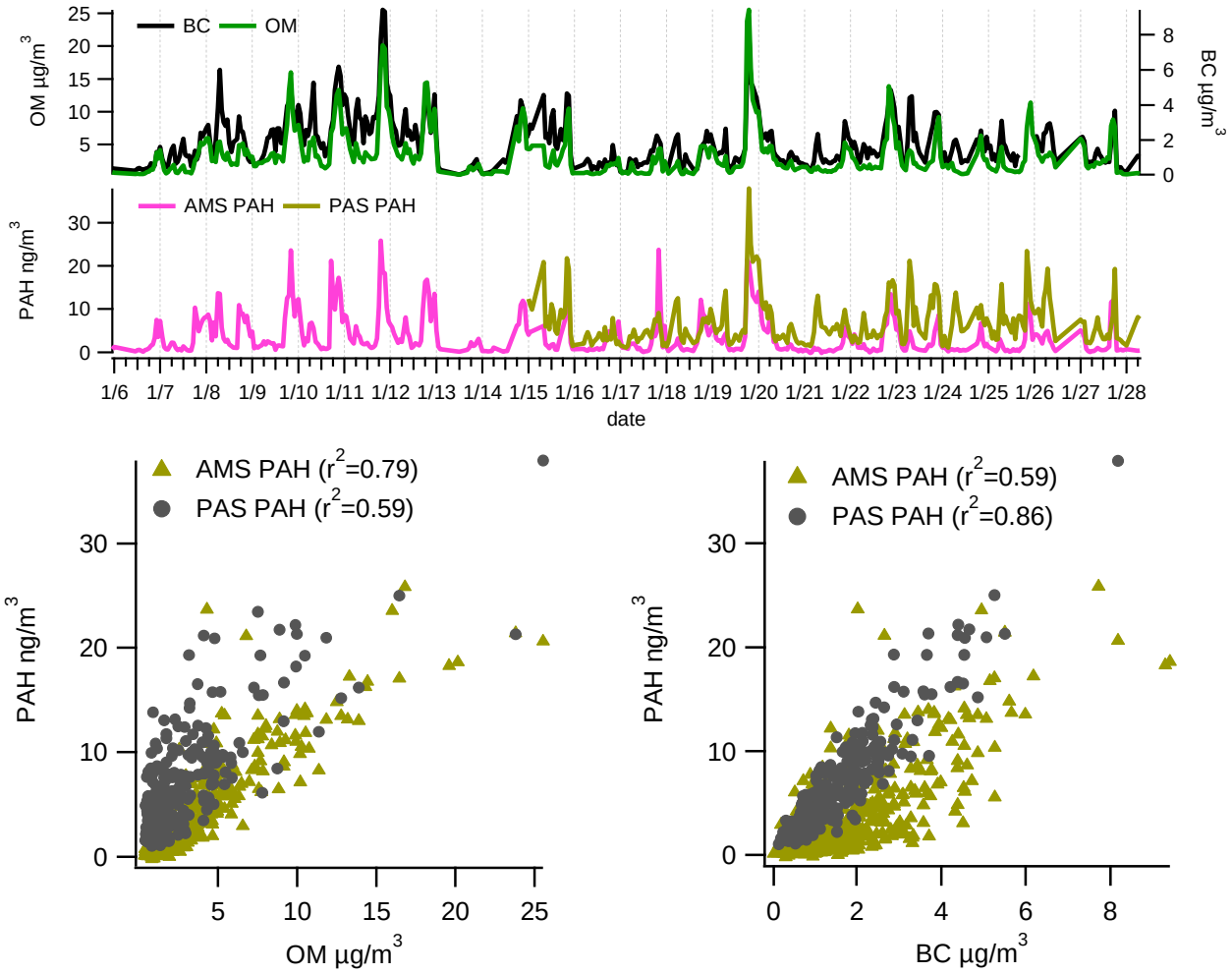

Figure B-1. (top) time series of hourly PPAH, APAH, BC, and OM concentrations, and (bottom) PAH concentrations against OM and BC concentrations.

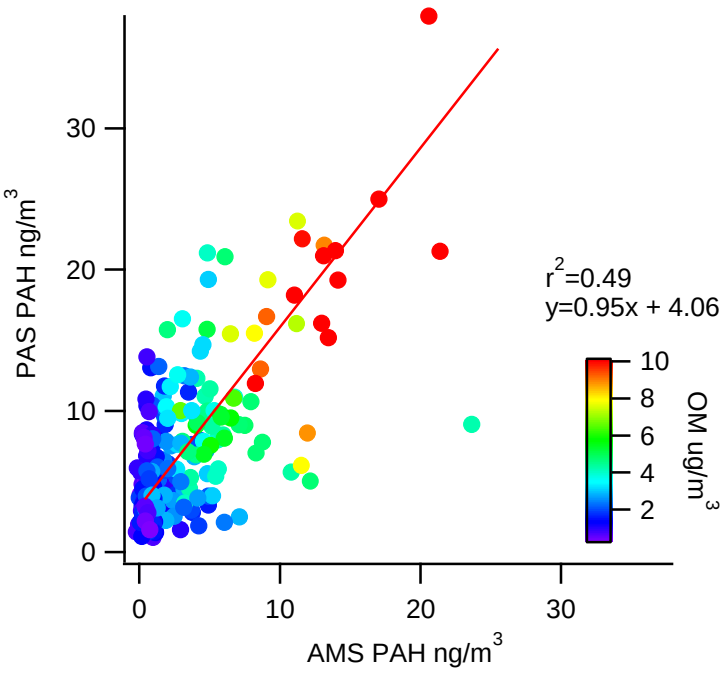

Figure B-2 Scatter plot of hourly averaged PPAH and APAH measurements, colored by OM concentrations.

Table B-1. Correlations (r) between hourly measurements of PMF factors (SV-OOA, HOA, BBOA, LV-OOA), OM, BC, APAH and PPAH during January 15 -28 2008; colors indicate high (red) to low (green) correlations.

	SV-OOA	HOA	BBOA	LV-OOA	OM	BC	PAS PAH	AMS PAH
SV-OOA	1.00							
HOA	-0.52	1.00						
BBOA	-0.42	-0.07	1.00					
LV-OOA	0.21	-0.72	-0.40	1.00				
OM	-0.07	0.00	0.36	-0.24	1.00			
BC	-0.18	0.19	0.25	-0.29	0.85	1.00		
PAS PAH	-0.12	0.27	0.18	-0.37	0.77	0.93	1.00	
AMS PAH	-0.21	0.04	0.62	-0.38	0.87	0.74	0.68	1.00

Table B-2. Correlations (r) between hourly measurements of PMF factors (SV-OOA, HOA, BBOA, LV-OOA), OM, BC, and APAH during January 6 -28 2008; colors indicate high (red) to low (green) correlations.

	SV-OOA	HOA	BBOA	LV-OOA	OM	BC	AMS PAH
SV-OOA	1.00						
HOA	-0.82	1.00					
BBOA	-0.32	0.11	1.00				
LV-OOA	-0.50	0.06	-0.21	1.00			
OM	0.27	-0.18	0.28	-0.43	1.00		
BC	0.34	-0.15	0.12	-0.51	0.87	1.00	
AMS PAH	0.16	-0.11	0.51	-0.49	0.89	0.77	1.00

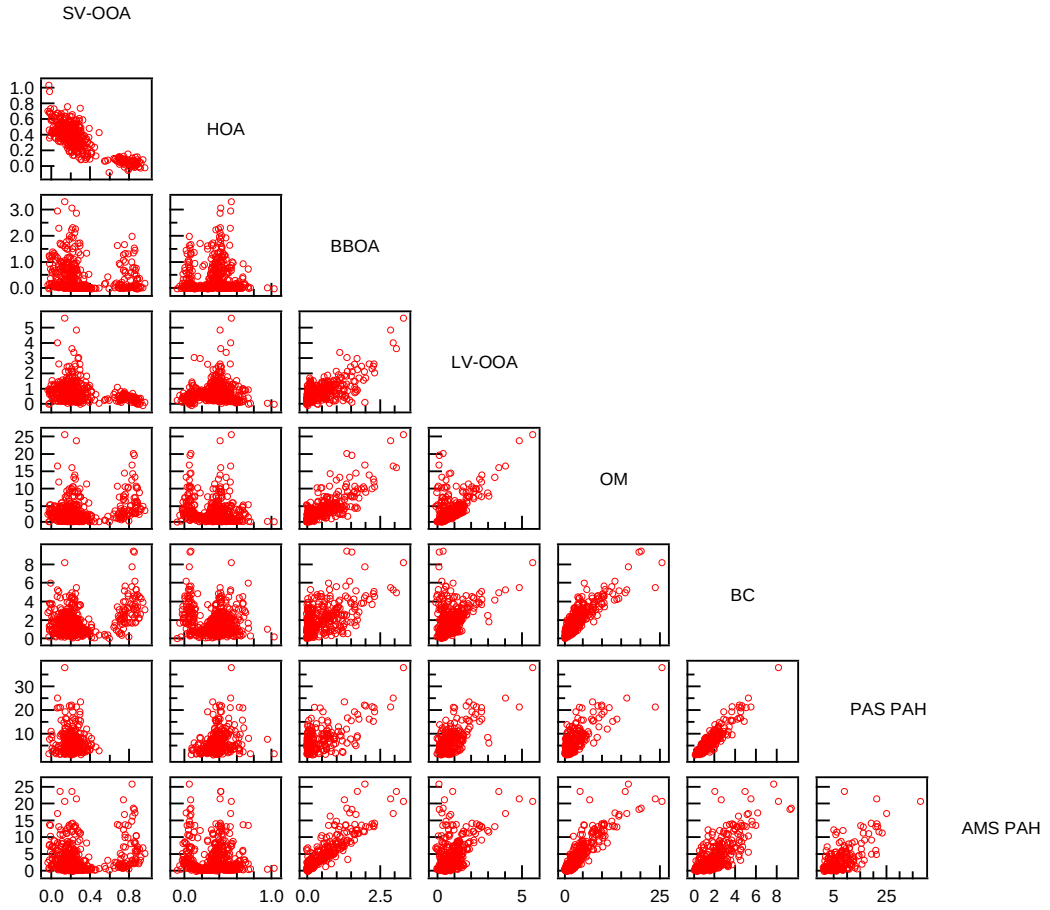

Figure B-3. Scatter plot matrix of hourly measurements of PMF factors (SV-OOA, HOA, BBOA, LV-OOA), OM, BC, APAH and PPAH during January 15 -28 2008.

Next, measurements of PPAH, APAH and FPAH were compared for the intervals where filters were analyzed. Individual PAH concentrations by sample are shown in Table B-3 and Olson et al., 2012. Of the 26 filter samples, 17 had both coincident PPAH and APAH measurements, while an additional 9 filter samples had coincident APAH measurements.

Neither PPAH nor APAH measurements compared well with the sum of total measured FPAH or of total measured hopanes, as shown in the scatter plot matrix in Figure B-4 and correlation matrix in Table B-4. APAH had a high correlation with chrysene (r=0.80) and modest correlation with benzo(b)fluoranthene (r=0.69) and benzo(e)pyrene (r=0.66). PPAH did not have a correlation higher than 0.48 with any individual FPAH.

Lastly, APAH and PPAH measurements were compared with levoglucosan, to identify if evenings with high wood smoke concentrations were also high in PAH. Figure B-5 shows a modest correlation between APAH and levoglucosan values (r^2=0.38), with generally high APAH values with higher levoglucosan. Driving the correlation low are daytime periods when APAH concentrations are relatively high but levoglucosan is not, plus one outlier nighttime point when OM concentrations were very low (less than 1.5 $\mu g/m^3$). Without the 5 daytime points and one outlier point, the correlation is much higher (r^2=0.65). A modest relationship between APAH and BBOA is also seen in Table B-2 and Figure B-3, showing that biomass burning is a source of PAH, but is not the main source, even in the evening.

Results indicate that PPAH measurements are more closely related to BC concentrations than OM, APAH or specific FPAHs, while APAH are closely related to chysene concentrations. PAH measurements correlated modestly with hopanes and levoglucosan, indicating PAH are from a mix of mobile, biomass burning and potentially other urban sources.

Table B-3. Concentrations of FPAH by sample (ng/m^3), originally reported in Olson et al., 2012.

Sample day	Sample Hours (LST)	norhopane	hopane	homohopane	pyrene	chrysene	benzo(b_fluoranthene	benzo(k)fluoranthene	benzo(e)pyrene	benzo(a)pyrene	perylene	Indeno(1,2,3-cd)pyrene	benzo(g,h,i)perylene	coronene	Sum FPAH	Sum hopanes
5-Jan	1700-0500	21.5	12.9	14.9	4.4	8.8	12.4	6.7	7.8	7.1	5.4	8	10.9	9.2	80.7	49.3
6-Jan	900-1100	20.1	21.8	11.8	10.2	4.9	18.1	25.2	10.8	25.5	0	13.3	6.9	25.9	140.8	53.7
7-Jan	1100-1700	33.9	20.4	23.3	37.4	8.5	11.5	9.8	7.6	12.2	10.5	7.8	11.1	2.2	118.6	77.6
8-Jan	900-1100	77.9	48.2	54.7	63	28.6	42.1	31.9	27.3	42.1	32.3	29.3	41.2	16	353.8	180.8
9-Jan	1100-1700	19.4	13.9	13.2	40.6	10.9	13.3	11.4	8.5	12.7	10.6	7.7	10.8	0.7	127.2	46.5
10-Jan	1100-1700	17.5	13.3	11.3	59.4	11.8	13.3	10.1	8.5	12.2	10.5	7.4	9.2	0	142.4	42.1
11-Jan	1100-1700	71.4	41.7	51	57.4	20.8	22.8	12.6	15	18.4	11.9	14.3	26.6	5	204.8	164.1
12-Jan	1100-1700	17.1	12.7	11.5	70.8	12.9	17	12.5	10.7	14.3	10.8	9.4	15.1	0.9	174.4	41.3
14-Jan	1100-1700	38.4	23.7	26.9	65.2	9.8	10.9	9.7	7.3	11.6	10.6	6.5	7	0	138.6	89
16-Jan	500-900	74.4	46.3	56	24	11.2	17.4	14.9	11.4	16.3	15.4	12.6	15.6	8	146.8	176.7
16-Jan	900-1100	22.3	24.4	14.6	14.8	4.9	18.1	25.1	11	26.1	29.5	0	6.9	5.5	141.9	61.3
18-Jan	900-1100	53.6	39.8	36.1	21	14.4	26.3	27.9	16.4	30.3	0	18.7	17	9.1	181.1	129.5
19-Jan	1100-1700	35.8	22.5	26.9	19	27.3	36.9	12.1	24.3	29.1	13.3	30.7	55.2	26	273.9	85.2
20-Jan	900-1100	54.9	36	38.7	27.6	29.6	42.7	31.1	23.5	36.3	30.9	0	25.7	14	261.4	129.6
20-Jan	0500-0500	31.8	23.6	26.6	14.3	14.2	16.6	6.1	10.4	9.3	3.8	11.1	17.6	8.9	112.3	82
21-Jan	500-900	72.6	28.4	53.8	28.9	23.9	29.1	21.1	19	25.6	17	21.3	33.9	14.2	234	154.8
21-Jan	900-1100	33.4	29.9	21.7	20.7	11	22.7	26.4	13.9	28.2	29.8	15.8	13	5.9	187.4	85
21-Jan	0500-0500	49.4	27.4	41.9	28.6	31.8	35	12.2	20.2	26.8	6.7	22.6	26.2	16.6	226.7	118.7
22-Jan	1100-1700	22	15.1	14	59.1	7.9	9.7	9.1	6.2	10.3	10.2	0	4.6	0	117.1	51.1
23-Jan	900-1100	55.5	40.5	38.1	33.5	18.9	30.5	28.5	19.3	32.6	30.7	21.3	24.9	11.5	251.7	134.1
23-Jan	1700-0500	35.1	20.3	28	15.8	31	37.2	13.8	23.5	22.2	8.2	23.7	35.8	19.2	230.4	83.4
24-Jan	500-900	54.2	33.4	37.2	25.2	19.3	24.3	17	15.7	23	16.5	17.2	27.3	10.7	196.2	124.8
24-Jan	900-1100	28.9	35.2	18.1	14.1	10.4	23.3	26.6	14.6	28.2	0	0	14.2	4.9	136.3	82.2
25-Jan	900-1100	73	45.8	47.5	23.7	17.3	27.9	28.4	18.1	30.8	31.2	19.6	20.6	12.5	230.1	166.3
26-Jan	900-1100	80.4	52.2	56.4	23.3	27.7	42.6	31.6	26.2	37.7	31.3	30.2	34.2	18.3	303.1	189
27-Jan	900-1100	32.3	26.5	20	18.8	16.6	27.7	27.8	16.5	31.5	30.3	18.6	16.7	5.7	210.2	78.8

Table B-4. Correlation matrix of FPAHs, BC, OM, APAH, PPAH, and AMS PMF factors during the 26 sampling intervals with FPAH data; colors indicate high (red) to low (green) correlations.

	NORHOPANE	HOPANE	HOMOHOPANE	PYRENE	CHRYSENE	BENZO(B)FLUORANTHENE	BENZO(K)FLUORANTHENE	BENZO(E)PYRENE	BENZO(A)PYRENE	PERYLENE	INDENO(123CD)PYRENE	BENZO(ghi)PERYLENE	CORONENE	SUMFILTERPAH	SUMHOPANES	BC	OM	AMS PAH	PAS PAH	HOA	BBOA	SVOOA
NORHOPANE	1.00																					
HOPANE	0.89	1.00																				
HOMOHOPANE	0.99	0.84	1.00																			
PYRENE	0.03	-0.10	0.02	1.00																		
CHRYSENE	0.58	0.41	0.64	0.00	1.00																	
BENZO(B)FLUORANTHENE	0.60	0.59	0.61	-0.21	0.89	1.00																
BENZO(K)FLUORANTHENE	0.45	0.68	0.36	-0.25	0.24	0.61	1.00															
BENZO(E)PYRENE	0.63	0.61	0.64	-0.18	0.89	0.99	0.59	1.00														
BENZO(A)PYRENE	0.55	0.70	0.50	-0.23	0.57	0.86	0.90	0.85	1.00													
PERYLENE	0.46	0.49	0.39	0.05	0.31	0.48	0.62	0.48	0.61	1.00												
INDENO(123CD)PYRENE	0.56	0.44	0.58	-0.12	0.67	0.67	0.27	0.73	0.54	0.27	1.00											
BENZO(ghi)PERYLENE	0.56	0.41	0.60	-0.09	0.87	0.82	0.21	0.87	0.56	0.28	0.79	1.00										
CORONENE	0.35	0.31	0.38	-0.50	0.59	0.70	0.34	0.71	0.57	0.09	0.67	0.69	1.00									
SUM FPAH	0.68	0.62	0.67	0.09	0.84	0.92	0.60	0.94	0.84	0.61	0.75	0.83	0.59	1.00								
SUM HOPANES	0.99	0.93	0.98	0.00	0.57	0.62	0.49	0.65	0.59	0.46	0.55	0.55	0.36	0.68	1.00							
BC	0.39	0.28	0.38	0.54	0.46	0.34	0.14	0.38	0.24	0.23	0.41	0.40	0.09	0.53	0.37	1.00						
OM	0.17	0.06	0.20	0.35	0.61	0.47	0.05	0.47	0.21	0.19	0.41	0.46	0.26	0.53	0.16	0.81	1.00					
AMS PAH	0.25	0.12	0.30	0.36	0.68	0.55	0.05	0.55	0.26	0.16	0.36	0.51	0.23	0.57	0.24	0.69	0.83	1.00				
PAS PAH	0.40	0.23	0.35	0.02	0.32	0.26	0.18	0.33	0.22	0.15	0.48	0.32	0.19	0.39	0.36	0.82	0.32	0.12	1.00			
HOA	0.42	0.35	0.43	0.05	0.56	0.60	0.36	0.62	0.49	0.34	0.47	0.54	0.50	0.63	0.42	0.51	0.51	0.71	0.32	1.00		
BBOA	0.11	0.01	0.18	-0.16	0.68	0.58	0.03	0.54	0.24	-0.02	0.33	0.44	0.56	0.40	0.11	0.22	0.57	0.78	-0.02	0.62	1.00	
SVOOA	-0.10	-0.16	-0.09	0.46	0.10	-0.07	-0.25	-0.07	-0.21	-0.16	-0.03	0.02	-0.24	0.01	-0.12	0.50	0.57	0.33	0.25	-0.33	-0.01	1.00
LV-OOA	0.14	0.07	0.16	0.11	0.56	0.50	0.16	0.48	0.30	0.29	0.43	0.42	0.34	0.51	0.13	0.57	0.83	0.64	0.24	0.66	0.57	0.11

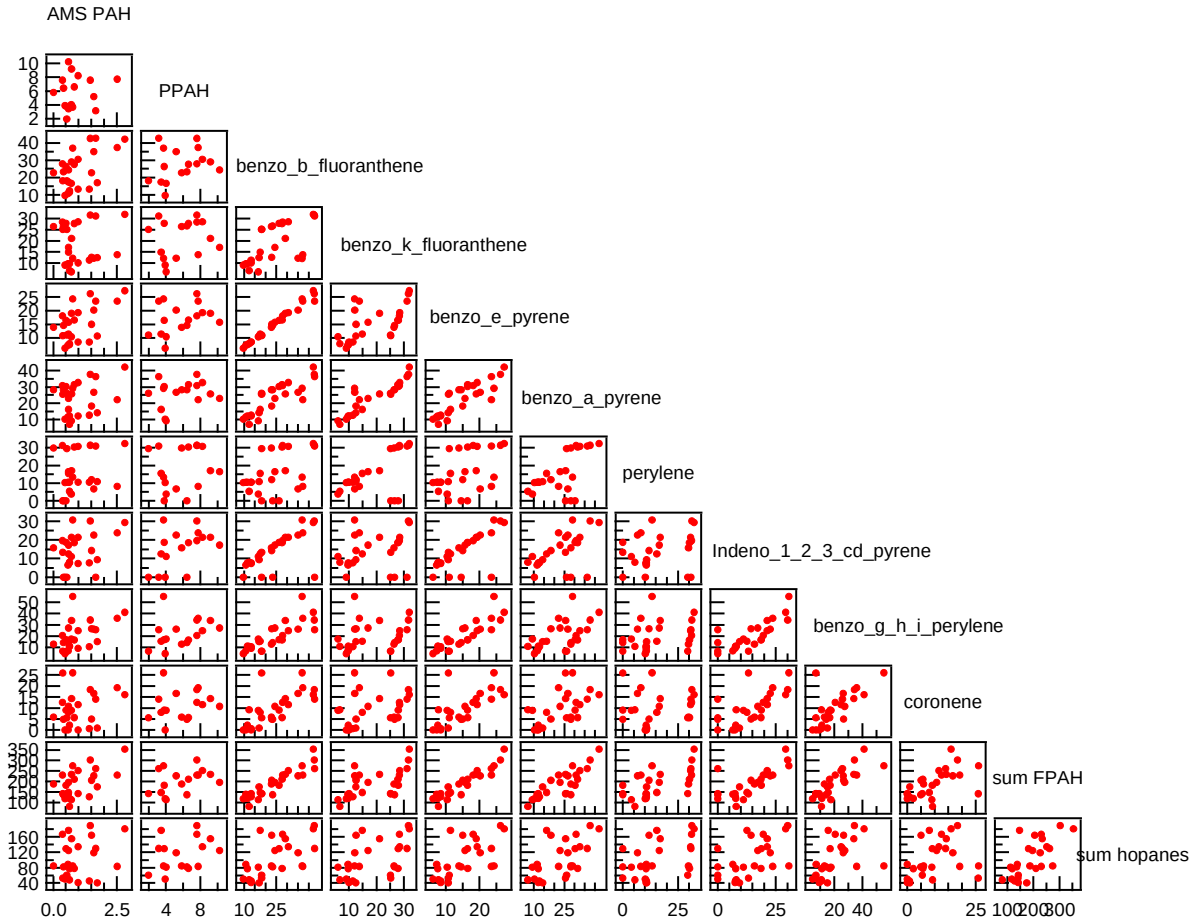

Figure B-4. Scatter plot matrix of filter PAH measurements with APAH and PPAH.

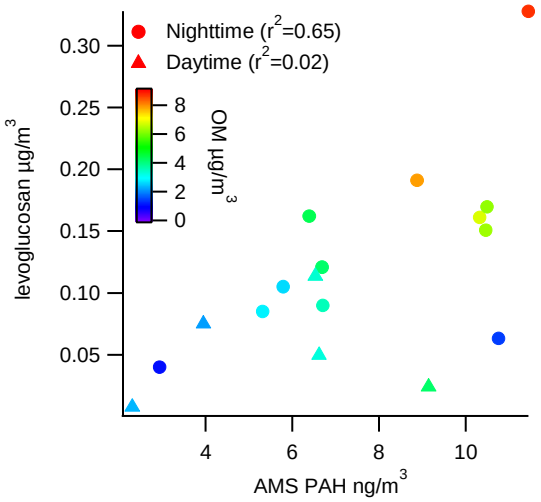

Figure B-5. Scatter plot of levoglucosan and APAH concentrations during day (triangles) and night (circles), colored by OM concentrations.